Tholeiitic magmatism in the Belingwe greenstone belt, Zimbabwe

Chris Brake

Thesis submitted for the degree of Doctor of Philosophy
The University of Edinburgh
1996

DECLARATION

This thesis has been composed by me, and all the work is my own.

CONTENTS

ABSTRACT

The Belingwe greenstone belt in southern Zimbabwe contains one of the most well preserved Archaean volcanic successions in the world. The komatiites in this succession have been studied in great detail, but the associated basalts have received much less attention. A detailed study of these basalts in the Zeederbergs Formation has revealed the existence of a previously unrecognised lava type which has important implications for the petrogenesis of the suite.

The Zeederbergs Formation and the underlying Reliance Formation form the 2.7 Ga Ngezi Group volcanics, which are underlain by thin, generally shallow water sediments of the Manjeri Formation. These in turn rest unconformably on 3.6 Ga and 2.9 Ga granitoid gneisses in the east and on older (2.9 Ga) greenstones in the west.

The nature of the basal contact of the Ngezi Group volcanics on the sediments of the Manjeri Formation has been the subject of recent controversy, and is interpreted here as conformable. The type section of the Zeederbergs Formation in the Ngezi River is logged and described in detail for the first time. Combined with correlation of geochemical marker horizons in other sections this has led to a re-evaluation of the vertical thicknesses of the Zeederbergs Formation - estimated here to be approximately 3km. Study of the geochemical stratigraphy has revealed a horizon of basalts with low Zr/Nb and high CaO/Al_2O_3 compared to the rest of the formation. The basalts in this horizon are called Type II (as opposed to the Type I basalts which make up the majority of the formation).

Examination of the petrography of the Zeederbergs Formation basalts has revealed that no subdivision into different rock types on petrographic grounds is practical. The lavas are generally fine grained, sparsely phyric and altered to hydrated low greenschist assemblages. The 'spheroids' in the lavas are considered in some detail, and are thought to represent products of spherulitic devitrification.

A detailed study of alteration and element mobility suggests that a series of simple screens can be applied to the dataset to remove heavily altered samples. Further, the mobility of individual elements during alteration can be assessed. The HFSE and REE are thought to have been reasonably immobile. There is good evidence for silicification and bulk SiO_2 mobility within the Zeederbergs Formation, and the possibility of correcting for this using theoretical fractionation trends is investigated.

The geochemical differences between the Type I and Type II lavas are examined in detail. Their major element chemistry is similar, with the exception of the much lower Al_2O_3 contents in the Type II lavas. The Type II lavas show higher abundances of nearly all incompatible trace elements, show distinctly LREE enriched REE patterns, and have lower initial ε_{Nd} values.

It is clear that the Type I and Type II lavas cannot be directly genetically related. The parent liquids for the Type I lavas are similar to those seen in the Reliance Formation. The only lavas which could have been parent liquids for the Type II lavas would be similar to the Al-depleted komatiites seen in Barberton. The Type II lavas have also seen much more crustal contamination during their evolution than the Type I lavas.

ACKNOWLEDGEMENTS

This project was supported by the Natural Environment Research Council and supervised by Dr. Godfrey Fitton.

I would like to thank a number of people for their help and support:

In **Edinburgh**: My supervisor, Godfrey Fitton, for his help and tolerance, and Dodie James for being an invaluable sanity marker! This work was helped by discussions with others in the 'basalt' group and beyond; Clive, Ray, Bjorn, Mike, Ian, Simon & Nic. A jovial office atmosphere was provided by Neil, Cliff, Karen & Coleen. Thank you to all the staff and technicians at the Department of Geology and Geophysics. Many thanks to all my friends in Edinburgh (too numerous to mention) without whom this project would probably have been possible, but the rest of my time wouldn't have been nearly as much fun !

In **SURRC, East Kilbride**: Many thanks to Rob Ellam, Graham Rogers, Anne and Vinnie.

Elsewhere in the **UK**: Thanks to Mike Cheadle, Mike Bickle, Dan McKenzie and Euan Nisbet for useful discussions.

In **Zimbabwe**: I am indebted to a number of people for making my time in Zimbabwe both productive and enjoyable. Kevin Walsh was an invaluable companion in Harare and Belingwe, and there is no doubt this really *wouldn't* have been possible without him. Many thanks to all the staff and technicians at University of Zimbabwe. Progress was an excellent camp guard and part-time field assistant. A big thank you to Tony & Rona Martin and Tony & Charlotte Rauch for looking after Morag and I in Harare and Belingwe respectively.

Finally, a **huge** thank you to Morag Hunter, for being the best person I could wish to share two field seasons in Zimbabwe with. Thanks Mo !

LIST OF CONTENTS

LIST OF TABLES

LIST OF FIGURES

LIST OF PLATES

LIST OF APPENDICES

1

INTRODUCTION AND THEORETICAL BACKGROUND

1.1 Introduction

The aim of this thesis is to examine the basaltic rocks associated with the ultramafic komatiite suite in the Belingwe greenstone belt, Zimbabwe. The rocks of the ultramafic, komatiite-bearing Reliance Formation have been heavily studied (e.g. Scholey, 1992; Bickle and Nisbet, 1993, and references therein), but the overlying, more voluminous, mainly mafic rocks of the Zeederbergs Formation have received little attention. By studying these rocks, which are closely associated with the komatiites, it is hoped that some new light may be shed on the petrogenesis of the entire suite.

The rationale behind this study will be discussed in the context of the history of work on komatiites, and of the evolution of ideas about their petrogenesis. This chapter is a brief summary of work discussed by Scholey (1992) and Cattell and Taylor (1990)

1.2 Archaean basic magmas

Basic magmas in the Archaean can be easily divided into 3 groups: komatiites, basaltic komatiites and basalts.

1.2.1 Komatiites

The term komatiite was introduced by Viljoen and Viljoen (1969a) to describe ultramafic lavas from the Barberton greenstone belt of South Africa. The atypical nature of these komatiites led to some debate over an exact geochemical definition, which is documented in Arndt and Nisbet (1982a, b). Their definition, now generally accepted, of a komatiite is a volcanic rock with more than 18 wt% MgO, derived from a liquid with more than 18 wt% MgO. A common diagnostic feature of many komatiites is the presence of olivine spinifex texture. This is formed by very rapid

crystallisation of olivine from a supersaturated liquid, and is a clear indicator of an extrusive origin. Olivine is the only common phenocryst phase in komatiites.

The exact MgO content of the primary liquids for komatiites is very important in considering their petrogenesis, but is very difficult to determine accurately. Aphyric tops to komatiite flows are almost always altered, and spinifex zones may contain some cumulate olivine (Bickle, 1982; Cattell and Arndt, 1987). Many early papers on komatiites paid a great deal of attention to CaO/Al_2O_3. This is because the first type komatiites from Barberton had high CaO/Al_2O_3, and this was included in early definitions. It subsequently became clear that such komatiites are atypical, and most komatiites have CaO/Al_2O_3 values between 0.8 and 1. This has led to a subdivision of komatiites into Al-depleted ($CaO/Al_2O_3>1$, $Al_2O_3/TiO_2<14$) or 'Barberton type' komatiites and Al-undepleted ($CaO/Al_2O_3<1$, $Al_2O_3/TiO_2>18$) or 'Munro type' komatiites.

The concentrations of incompatible and partially compatible elements in komatiites reflect this division into Al-depleted and undepleted types. Al-depleted komatiites also have low concentrations of V, Sc Y and the HREE (Nesbitt and Sun, 1976; Sun and Nesbitt 1978; Nesbitt *et al.* 1979; Jahn *et al.* 1982; Smith and Erlank, 1982; Gruau *et al.* 1987). Possible explanations for the depleted nature of these komatiites are discussed at greater length in §7.7.2.

1.2.2 Tholeiitic basalts

The most common occurrence of tholeiitic basalts in the Archaean is as pillowed lava flows. Massive and weakly layered flows are reasonably common, but volcaniclastic material is rare. The tholeiitic flows generally lack the compositional layering found in their high-magnesium basalt and komatiite counterparts. They are usually only sparsely porphyritic, containing olivine, plagioclase and augite microphenocrysts in rapidly cooled lavas, and usually only clinopyroxenes in the more phyric lavas.

In their major element composition, Archaean tholeiites are broadly similar to modern low-K tholeiites. The most significant feature is the relatively high Fe content (and correspondingly high Mn content) at a given MgO. These high Fe and Mg contents at, say, a given Al content compared to modern basalts leads to the crystallisation sequence: olivine (+ chromite), (Cr-bearing) augite, augite + plagioclase, augite + plagioclase + Fe-Ti oxide. The late crystallisation of plagioclase leads to lower concentrations of TiO_2 and other incompatible elements at a given

mg# compared to modern basalts. Most Archaean tholeiitic basalts have unfractionated REE distributions, with overall concentrations about ten times chondrite in the less evolved samples.

1.2.3 High-magnesium basalts

Many Archaean mafic–ultramafic volcanic sequences contain a suite of Mg- and Si-rich basalts with characteristic pyroxene spinifex textures, often known as high-magnesium basalts. Several other names have been used to describe the same rocks (eg. komatiitic basalt), and it is important to note that the use of a particular name does not imply any genetic link between these lavas and the associated komatiites. The most characteristic feature of these flows is the occurrence of a coarse acicular (spinifex) pyroxene, although this is not always present. The flows often show extreme compositional and textural layering, with cumulate bases, upper spinifex zones and aphyric flow tops.

High-magnesium basalts were erupted with MgO contents of between 7 and 15%, though *in situ* layering may result in parts of individual flows having much higher, or lower, values. There is no general chemical discriminant which can be universally applied to distinguish these high-magnesium basalts from tholeiites, though some have been proposed (e.g. Arndt *et al.* 1977). In general they tend to be Si-rich and Al-poor when compared to tholeiitic basalts at a similar mg#. Whilst high-magnesium basalts do show a division into Al-depleted and undepleted suites, the boundary is blurred by the compatibility of V and Sc in clinopyroxene during fractionation, and the resulting increases in Ti/V and Ti/Sc. A notable feature of many high-magnesium basalts is a marked enrichment in the LREE and Zr, giving rise to low Ti/Zr (Sun and Nesbitt, 1978; Arndt and Jenner, 1986; Barley, 1986; Cattell, 1987). The degree of this enrichment does not vary systematically with the degree of fractionation within a suite, but it does vary significantly from one suite to another.

1.3 Petrogenesis

1.3.1 Komatiites

Ideas about komatiite genesis have continuously evolved over the last 20 years, as more data becomes available, and as understanding of the melting process has developed. Models for producing komatiites can broadly be divided into two groups:

those which require large degrees of melting at shallow depths and those which require lower degrees of melting at much greater depths.

The large degree melting idea is reasonably simple: induce >50% melting of the mantle and then extract and erupt the resulting liquid as a komatiite flow. Unfortunately we know that melt will tend to escape from the source long before 50% melt is produced, and commonly before even 5% is produced (McKenzie, 1985). The large degree melting models have incorporated various schemes to overcome this difficulty.

There have been several models which involve more than one stage of melting, with the komatiites being the product of the last melting episode. Since the residue of each melting episode is more refractory and Mg-rich, the amount of melting required to produce a komatiitic liquid is reduced. The prior melting events may be unrelated earlier events (Weaver and Tarney, 1979) or an earlier part of the same event (Arndt, 1977). Whilst it is clear that most komatiites have been derived from previously depleted mantle (the marked LREE depletion leaves little room for doubt) it is unlikely that the mantle source could be so refractory as to produce low percentage (<5%) melts of komatiite composition.

The driving force which separates liquid and solid during melting is gravity, buoyant liquids being driven upward relative to dense residual solid. With increasing pressure this density contrast declines (particularly for olivine, which is relatively incompressible). Theoretical and experimental work indicates that olivine may be less dense than silicate liquids at high pressures, and therefore any liquid within an olivine-dominated residue would not tend to rise, or might even sink (Nisbet and Walker, 1982; Agee and Walker, 1988). Clearly, if this liquid–solid separation is prevented, then komatiite liquids may be produced. This debate centres around the question of whether or not olivine is denser than the natural liquid compositions at the appropriate mantle depths, a controversial question (Herzberg, 1987).

The observation that low percentage mantle melts become increasingly magnesian with increasing pressure has produced several komatiite-generation models which appeal to lower degrees of melting at greater depths (Takahashi and Scarfe, 1985; Herzberg and O'Hara, 1985; Herzberg and Ohtani, 1988). High pressure experiments have shown that at 50kb initial melts are komatiitic (Takahashi and Scarfe, 1985). These models overcome many of the problems of komatiite genesis mentioned above,

as large degree melting is no longer required. But the inferred trace element compositions for such deep (>150km) melts are far removed from those of erupted komatiites, as these initial melts would contain high concentrations of the incompatible trace elements.

Recent work on melt generation and extraction has shed much light on basalt genesis (Ahern and Turcotte, 1979; McKenzie, 1984; Thompson, 1987; McKenzie and Bickle, 1988). Basalts are generated by decompression melting in upwelling portions of the mantle. The melt escapes when melt fractions are small (perhaps only 2%), but melting continues as the residue continues to ascend. Although these melts are only low degree melts, the residue become more refractory as it continues to ascend, and thus melts from the top of the melting zone will be strongly depleted. All these low degree melts mix to a greater or lesser extent, and so it is possible to produce a melt which is equivalent to >50% melting of the mantle without the amount of melt actually in the melting column ever exceeding a few percent. Thus we have a mechanism for generating the high degree melting which the chemistry of komatiites would seem to require.

Production of a komatiite in this way is illustrated in Figure 1.1. Consider a komatiite lava with *c.*25% MgO (common in the late Archaean). From the curves in McKenzie and Bickle (1988), the amount of melting required to produce such a magma can be calculated as roughly 39%. The top of a melting column which yields a 25% MgO komatiite should therefore lie somewhere along the 39% melt fraction of the source. The P-T ascent paths shown in Figure 1.1 are chosen arbitrarily, but it is clear that to produce a komatiite with 25% MgO requires a mantle potential temperature (T_p) of at least 1770°C. Such a temperature would only be found in unusually hot parts of the mantle, such as in hot rising jets or plumes, and melting would commence at depths of 250km or greater.

This model does not explain all aspects of komatiite genesis. It is still difficult to account for the class of Al-depleted komatiites such as those from Barberton, and the problem of erupting dense komatiite magmas through less dense continental crust remains. The solution to this problem may be related to the surprising observation that we only see volumetrically small flows of komatiite lavas, given that they must be generated in enormous volumes. Possible origins of the Al-depleted komatiites are discussed further in Chapter 7.

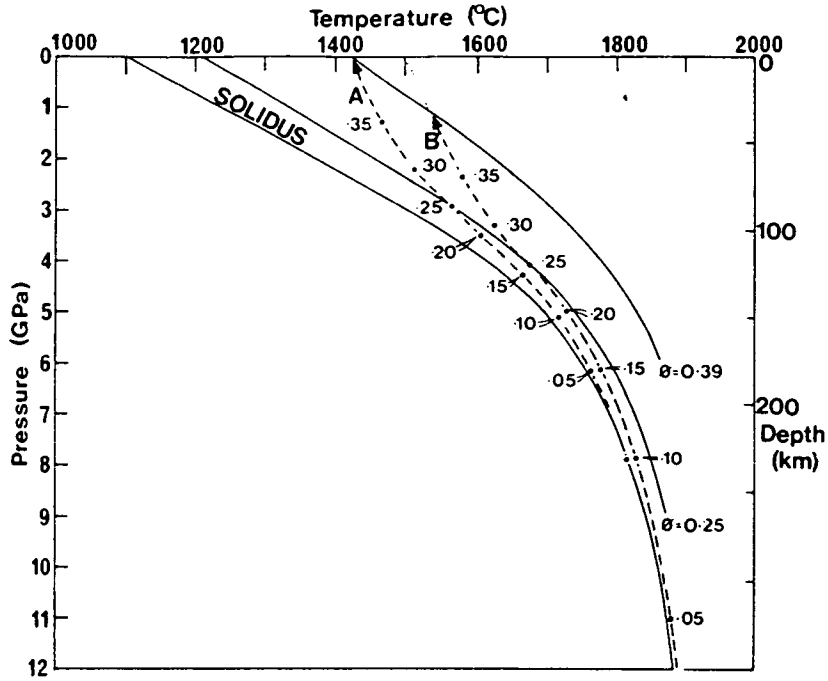

Figure 1.1 Pressure–temperature diagram illustrating the generation of komatiite melts by decompression. Solidus and melt fraction curves constructed using expressions 18 to 22 of McKenzie and Bickle (1988). The illustrated melting paths were constructed assuming that for ascending mantle under the appropriate P–T conditions, the melt fraction (ϕ) increases by approximately 0.1 as T falls by 100°C (McKenzie, 1984). Path A indicates the unlikely and limiting situation where melting continues to the surface. Path B represents melts arriving at the surface at 1500°C. In both cases, melt segregation occurs at $\phi = 0.39$, at which point the melt will have a typical komatiitic composition (MgO = 25%).

1.3.2 High-magnesium basalts

Models for the generation of high-magnesium basalts fall into two camps: those which involve a genetic link with komatiites, and those which don't. The major element compositions of most high-magnesium basalts are consistent with their being the products of fractionation of komatiitic liquids. But the abundances of incompatible trace elementsin high-magnesium basalts are much higher than would be expected if this were the case. Characteristics such as the LREE enrichment found in most high-magnesium basalts indicate that they cannot be derived from (LREE depleted) komatiites.

A mechanism commonly invoked to reconcile these characteristics is crustal contamination. Given the high temperatures of komatiites liquids, this is a possibility (Huppert and Sparks, 1985). Such contamination would explain many of the

geochemical characteristics of these lavas, and there is some clear evidence of contamination in the discovery of 3.4Ga zircons in a 2.7Ga high-magnesium basalt from Kambalda. The only solid conclusion to be drawn from the evidence of contamination is that high-magnesium basalts, like komatiites, were erupted through felsic continental crust. It could also explain discrepancies between the chemical evolution of the komatiites and the high-magnesium basalts, but it is not clear proof of a genetic link.

1.3.3 Tholeiitic basalts

Compared to modern tholeiites with similar MgO contents, Archaean tholeiites are enriched in Fe, Cr, Co and Ni. Understanding of these differences, and of the generation of modern tholeiites is the key to understanding these Archaean tholeiites. The higher Ni and Fe than modern equivalents is explained as simply a function of the higher degree and deeper onset of melting (Arndt, 1989). It is also possible that some of the tholeiites seen associated with komatiites could also be derived from these ultramafic lavas, by a process of fractionation and crustal assimilation.

1.4 Summary: petrogenetic ideas

Komatiites occur in spatial association with tholeiitic and high magnesium basalts in Archaean greenstone belts. Komatiites require very high eruption temperatures (>1700°), which implies the initiation of mantle melting at much greater depths and temperatures than required for the generation of modern basalts. Tholeiitic basalts are plausibly produced by lower degree or shallower mantle melting, or from komatiite magma by low pressure fractionation and crustal contamination. The enrichment of incompatible trace elements noted in high-magnesium basalts associated with komatiites would seem to require some degree of crustal contamination - to which they would have been very susceptible as a result of their high temperature and turbulent ascent and eruption.

2

REGIONAL GEOLOGY

2.1 Introduction

2.1.1 Synopsis

There has been a great deal of work on the rocks of the Belingwe greenstone belt, which has been summarised by Scholey (1992) and more fully in Bickle & Nisbet (1993), a compilation of several detailed studies on particular aspects of the geology of the belt. This chapter simply offers a brief overview of the stratigraphy and structural relationships of the area to put the subsequent chapters in a geological framework. For a more comprehensive description of the Belingwe greenstone belt, the reader is referred to Bickle & Nisbet (1993) and references therein.

2.1.2 Previous work on the Belingwe greenstone belt

The earliest depictions of the Belingwe greenstone belt appear in regional mapping by Fletcher and Espin (1897) and Menell (1910). The komatiites were first described as "limburgites" (and thought to be intrusive) by Keep (1929), in a study of the Shabani asbestos ore body and adjacent areas. The first map of the entire belt resulted from compilations of Geological Survey mapping (Worst, 1956) and aerial photograph interpretation (Tyndale-Biscoe, 1958). The unconformable nature of the base of the greenstone sediments on the surrounding gneisses was first recognised by Macgregor (1951), and later confirmed by the work of Laubscher (1963), Oldham (1968, 1970) and Morris (1969). The basal unconformity at the National Monument locality (see Figure 3.1) was first described in a field guide by Morrison and Wilson (1971), and its presence was inferred in the western limb of the belt, dividing the greenstones into two distinct successions, which have become known as the Lower and Upper Greenstones (e.g. Wilson *et al.*, 1978; Wilson 1979, 1981) or as the Lower and Upper Bulawayan Groups (e.g. Stagman, 1978). This study is only concerned with rocks in the Upper Bulawayan (the Upper Greenstones)

The recognition that komatiites might provide useful clues to the composition and temperature of the Archaean mantle, advances in radiometric dating techniques which

enabled a relative chronology to be established and indicated the great age of these rocks, and the revolutionary plate tectonic concept made it possible to begin to understand Archaean crustal evolution. The fundamental problem of whether greenstone belts represented ancient ophiolites (tectonically emplaced) or whether they were erupted *in situ* onto pre-existing continental crust still remained, however, and Wilson's (1973) recognition of the basal unconformity in Belingwe offered a potential solution to this problem. This led to the collaborative work between the University of Zimbabwe, the Geological Survey of Zimbabwe and Oxford University which became the **Archaean Crustal Study Project**, and which expanded, took in other institutions, and resulted in a very large number of publications on the Belingwe belt (see Bickle & Nisbet, 1993, pp. 233-244 for a complete list).

Three significant features of the Belingwe succession (the basal unconformity, stromatolites and the komatiites) were described by Bickle *et al.* (1975), and Survey mapping of the belt produced excellent 1:100,000 maps of the entire belt, two doctoral theses (Martin, 1983; Orpen 1978), and several special publications of the Geological Survey (e.g. Martin 1978, 1980). Regional structural relationships were considered by Coward *et al.* (1976), and a chronological framework has been established based on Rb-Sr, Sm-Nd and Pb-Pb whole-rock dating of tonalitic gneisses and intrusives (Hickman, 1974, 1978; Hawkesworth *et al.*, 1975, 1979; Moorbath *et al.*, 1977) and volcanic rocks (Hawkesworth *et al.*, 1975; Jahn and Condie, 1976; Hamilton *et al.*, 1977; Chauvel *et al.*, 1983, 1993).

The investigation into the possible ophiolite origin for the Belingwe belt, and attempts to try and understand the mantle source and petrogenesis of komatiites led to a great deal of interest in the ultramafic volcanic rocks of the Reliance Formation (Bickle *et al.*, 1975, 1976, 1977; Nisbet *et al.* 1977, 1982). Recent work has concentrated on exceptionally well preserved komatiites from one location (the SASKMAR drill site and surrounding area, see Figure 3.1), (e.g. Nisbet *et al.* 1987; Renner 1989; Bickle *et al.*, 1993; Renner *et al.*, 1994; McDonough & Ireland, 1993). All of these studies have focused almost exclusively, however, on the Reliance Formation, and the much more volumetrically significant Zeederbergs Formation has received little attention.

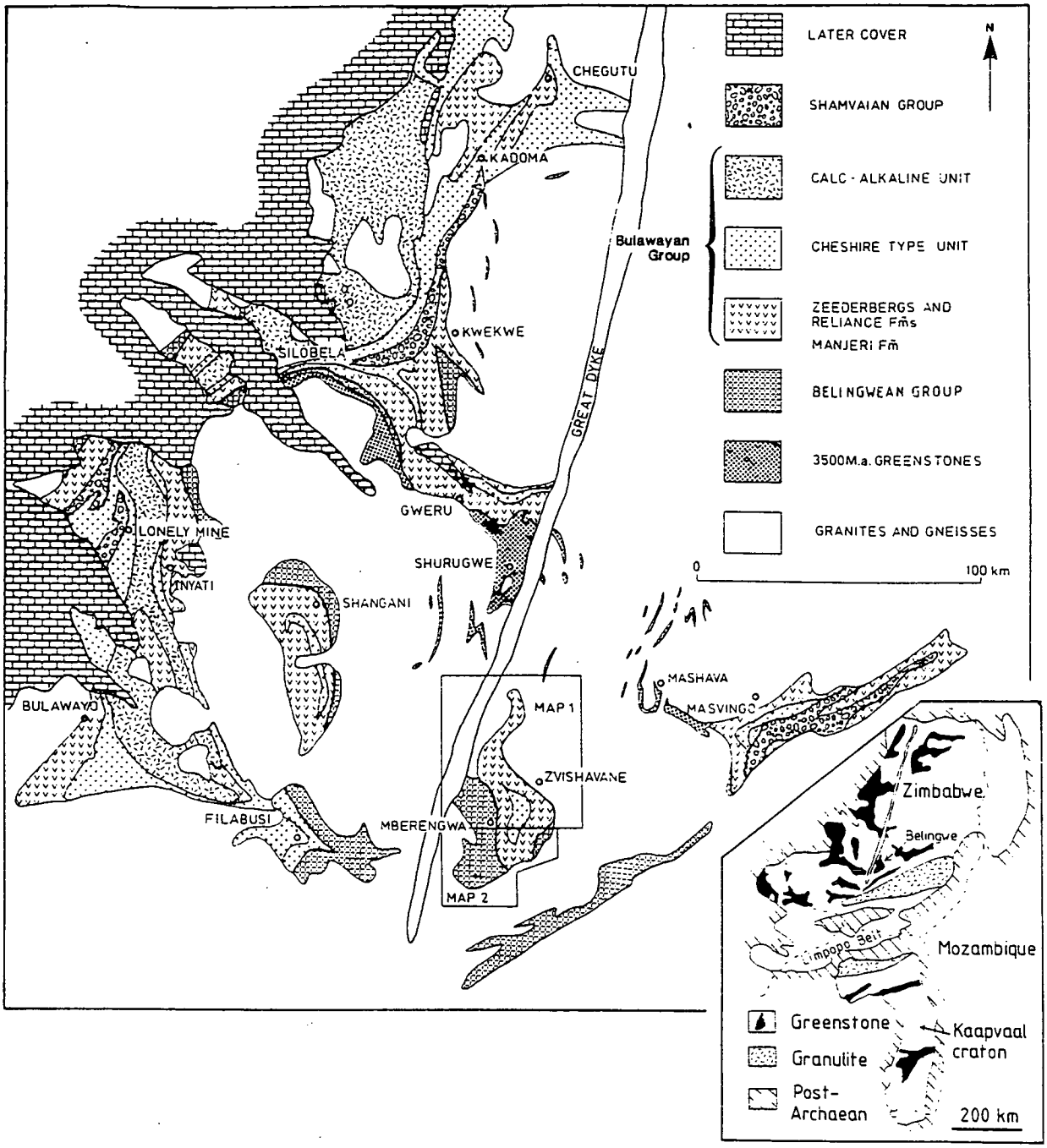

Figure 2.1 Geological map of the central part of the Zimbabwe Archaean Craton. Maps 1 and 2 on diagram refer to Geological Survey maps. Map 1 is Zimbabwe Geological Survey Map, Belingwe-Shabani, 1:100 000, Martin (1978). Map 2 is Zimbabwe Geological Survey Map, Belingwe Peak, 1:100 000, Orpen *et al.* (1986). From Bickle *et al.*, 1993.

2.2 The Zimbabwe craton

2.2.1 Overview

The Zimbabwe craton is a low-grade Archaean granite-greenstone terrain which forms the central part of Zimbabwe and extends into Botswana in the south-west and Mozambique in the north-east (Figure 2.1). To the north, east and west the craton is overlain by younger strata or abuts younger orogenic provinces. To the south-east and south-west the craton borders the Limpopo mobile belt, a high-grade terrain of gneissic rocks in the age range 3600-2600Ma, the contact being a thrust plane in some areas, and a zone of increasing strain towards the Limpopo belt in others.

In simple terms, the history of the craton can be thought of in terms of two accretionary "super-events" (Wilson and Nutt, 1990; Wilson, 1990), each involving rifting, sedimentation, volcanism, plutonism and tectonism. The first of these, at about 3600 - 3400 Ma, accounts for most of the material which is considered as 'basement' in this study, and the second produced the Lower and Upper Bulawayan greenstones, which form the Belingwe belt. The second "super-event" culminated in cratonisation, and the craton has undergone little deformation since that time.

The Belingwe greenstone belt lies within the *Tokwe segment* of the craton (e.g. Wilson and Nutt, 1990; Wilson, 1990), which preserves a near-complete record of Archaean crustal development in the region (see Table 3.1). The descriptions below apply specifically to the Tokwe segment, and may be slightly different in other parts of the craton. The stratigraphy in the Belingwe region is shown in Table 3.2.

2.2.2 The 'basement'

'Basement' in the context of the Belingwe greenstone belt refers to those rocks underlying the greenstones of the belt, and is largely composed of material from the first "super-event" (see above). These are dominated by 3.6 - 3.5 Ga tonalitic intrusives and remobilised gneisses. Tightly infolded into these are heavily deformed remnants of mafic and ultramafic orthogneisses (derived from lavas and dykes) and rare pelitic paragneisses, which represent the remaining fragments of the ca. 3.5Ga greenstones (the Sebakwian Group) formed in the first "super-event".

Table 2.1 Sequence of tectonic, depositional and intrusive events in the Tokwe Segment of the Zimbabwe Craton. (From Bickle *et al.* 1993). Sources and details of ages tabulated in Martin *et al.* (1993), Table 2.3

Time Ma	Deformational and metamorphic events	Intrusive events	Depositional events
	Dextral faulting and folding related to Mtshingwe Fault		
2460 ± 16		Great Dyke and East Dyke	
2470	Uplift and cooling from regional greenschist facies metamorphism		
2590	Folding and main cleavage formation in greenstones		
2570 ± 25		Chilimanzi Suite adamellite plutons	
	North-south synclinal folding of the Ngezi Group		
2692 ± 9		Mafic-ultramafic intrusion ?Mashaba-Chibi dyke suite	Deposition of Ngezi Group
	SW to NE synclinal folding of Mtshingwe Group		
2833 ± 43		Chingezi Tonalite in west	
		Mashaba Tonalite in east	Deposition of Mtshingwe Group
2900	Deformation and metamorphism Chingezi Gneiss terrain	Intrusion of precursors to Chingezi Gneisses	
	Amphibolite facies metamorphism		
3500 ± 800		Ngezi Tonalite Plug	
	Shabani Gneiss Complex Isoclinal folding of Shabani Gneiss Complex		
ca. 3500		Homogenous Shabani plutons, aplites and pegmatites	
	Intense flattening of Shabani Gneiss		
		Precursors to Shabani migmatitic gneiss	Deposition of greenstone precursors to schist inclusions in Shabani Gneiss (the Sebakwian Group)

2.2.3 The Bulawayan greenstones

The 'post-basement' greenstones in the craton (formed in the second "super-event") are dominated by the Bulawayan group, with the few deposits of the slightly younger Shamvian group confined to the north-west of the province and absent from the Tokwe segment. The Bulawayan group can be divided into two distinct successions, which have become known as the Lower and Upper Bulawayan (or Lower and Upper Greenstones), and correspond in the Belingwe belt to the Mtshingwe and Ngezi Groups respectively.

The Lower Bulawayan Group is most extensively preserved in the southern and central parts of the craton, largely as folded and partially eroded remnants beneath younger Upper Bulawayan greenstones. The age of these greenstones is less well constrained than the Upper Bulawayan, but they are thought to be in the range 2900 - 2800 Ma.

Much of the Upper Bulawayan group is preserved in what appear to be synclinal belts with relatively little internal strain (except in localised shear zones) and with metamorphic recrystallisation only to greenschist facies. They are thought to represent an eroded supracrustal cover which originally extended throughout the Zimbabwe craton (e.g. Wilson *et al.*, 1978, 1990), and the apparently continuous sequence of thin sediments, ultramafic to mafic volcanics and upper, pelite-dominated sediments which forms the Ngezi Group in Belingwe has been adopted as the 'type' succession. The volcanic rocks have been dated at 2.7 Ga (see §6.4), and the basal stromatolitic limestone at ca. 2.8 Ga (Moorbath *et al.*, 1987).

The basal sediments, which transgress older rocks in the craton, and the overlying ultramafic (Reliance Formation) and mafic (Zeederbergs Formation) volcanics are tentatively correlated throughout the craton, over a strike length of 700 km, and 200km laterally (e.g. Wilson *et al.*, 1978, 1990; Wilson 1979; Taylor *et al.*, 1991), especially the thick Zeederbergs Formation, which is seen in nearly all Upper Bulawayan successions. The uppermost pelite- and basalt-dominated unit (of which only the lower sediments, the Cheshire Formation, are seen in Belingwe) does not correlate as well, and in the west of the craton seems to correspond to bimodal and calc-alkaline volcanic units. Deposition of the comparable lower parts of the successions in the eastern and western (roughly linear) greenstone belt successions within a major continental rift, and the subsequent development of a magmatic/volcanic arc in the west has been speculated (e.g. Wilson, 1981; Nisbet *et al.*, 1981; Wilson and Nutt, 1990).

2.2.4 Plutonism

Within the Tokwe segment, the basement to the Upper Bulawayan greenstones is intruded by the dominantly peridotitic Mashaba and Shabani complexes and other smaller bodies, which have been considered to represent the remains of the magma chambers that fed the Upper Bulawayan volcanics (e.g. Nisbet, 1982). The east-west trending mafic dykes of the Mashaba-Chibi swarm are possibly a remnant of the feeder system for these volcanics.

Extensive granitoid plutonism is also associated with the period of Bulawayan greenstone formation, deformation and metamorphism towards the end of the second "super-event", and can be divided into two distinct suites (e.g. Wilson, 1979, 1981; Nisbet, 1987; Foster, 1989; Wilson and Nutt, 1990). The older (ca. 2.7 - 2.6 Ga), mainly tonalitic Sesombi suite is mainly found intruded into the Upper Bulawayan greenstones in the western part of the craton (it is not found in the Tokwe segment), and possibly represents a mantle- or deep crustally derived late plutonic equivalent (Scholey, 1992) of the calc-alkaline upper part of this succession (see §2.2.3). The younger (ca. 2.6 Ga) potassic granites of the Chilimanzi Suite are most extensive in the southern and eastern parts of the craton. They are essentially post-tectonic granites, associated with the last stages of cratonisation, and plutons from this suite are intruded at each end of the synclinal Belingwe belt, resulting in increased metamorphic grades and fold culminations.

2.2.5 Post-cratonisation

There has been little internal deformation of the Zimbabwe craton since it became stabilised as a continental block around the end of the Archaean (defined by the intrusion of the Great Dyke at ca. 2.5 Ga, e.g. Nisbet, 1987). The Great Dyke lies to the west of the Belingwe belt, and its satellite, the East Dyke, just cuts the eastern margin of the belt. Deformation has been limited to fracturing associated with this and other events. Belingwe is also cut by the large NW-SE trending Mtshingwe and Jenya faults, which may be associated with this deformation, or may represent re-activation of pre-existing lines of weakness (E. Nisbet, pers. comm., 1994)

Table 2.2 Major Geological units: Belingwe area. (from Martin *et al.*, 1993)

Intrusive Units	**Supracrustal** *Groups*	**units** *Formations*	**Lithology**
Great Dyke 2460 ± 60 Ma			
Chillimanzi Suite - Chibi Batholith 2570 ± 25 Ma			
		Cheshire	Conglomerate, limestone, shale
	Ngezi Group	Zeederbergs	Basalt
	2692 ± 9 Ma	Reliance	Komatiite, komatiitic basalt, basalt
		Manjeri	Clastic sediments
	Unconformity ~~~~~~~~	~~~~~~~~~~~~~~~~~~~~	~~~~~~~~~~~~~~~~~~~~
Mashaba Tonalite 2870 ± 160 Ma Chingezi Tonalite 2833 ± 43 Ma			
		Koodoovale	Conglomerate, felsic agglomerate
		Bend	Komatiite, komatiitic basalt, ironstone
	Mtshingwe Group	Brooklands *	Conglomerate, siltstone, quartzite, ironstone, komatiite, komatiitic basalt, basalt
		Hokonui	Intermediate to felsic volcanics, mostly pyroclastic, mafic volcanics
	Possible Unconformity	~~~~~~~~~~~~~~~~~~~~	~~~~~~~~~~~~~~~~~~~~
		Bvute **	Amphibolite
Chingezi Gneiss 2810 ± 70 Ma			Banded grey gneisses
Shabani Gneiss Complex ca. 3500 Ma			Banded grey gneisses 'Schist inclusions'

*Correlation of Brooklands Formation in east with other Mtshingwe Group formations in west is not known.
**Stratigraphic and structural relationships of Hokonui and Bvute Formations and Chingezi Gneiss are uncertain.

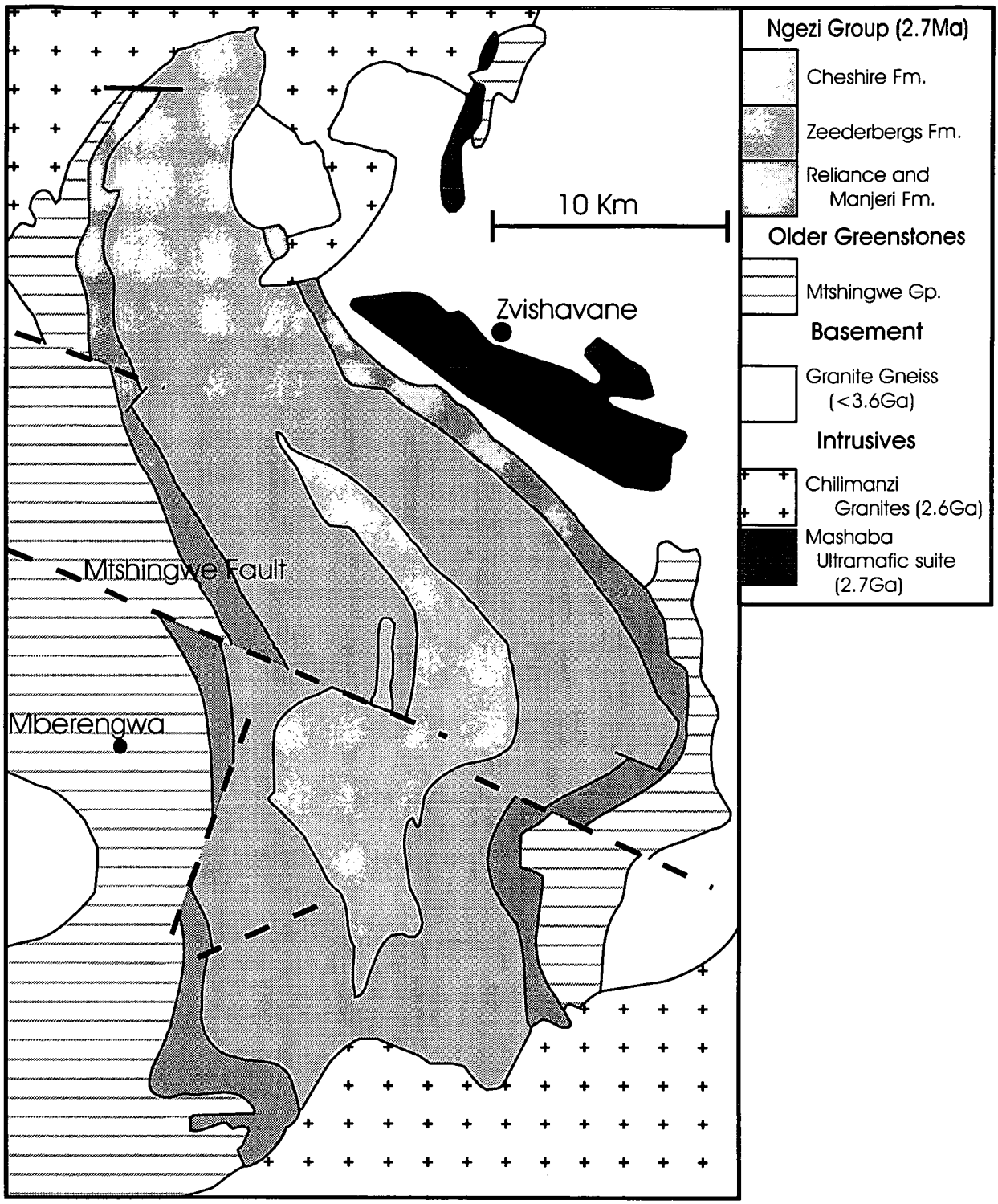

Figure 2.2

A simplified map of the Belingwe greenstone belt.

2.3 The Mtshingwe Group (The Lower Bulawayan in Belingwe)

2.3.1 Overview

The Mtshingwe group is seen in two distinct areas, on the east and west sides respectively of the synclinal Ngezi Group. It comprises four formations: The Hokonui, Bend and Koodoovale Formations in the west, and the Brooklands Formation in the east. Orpen (1978) recognises a fifth major unit in the west, the Bvute Formation, consisting of isoclinally folded and foliated amphibolite between the Chingezi Gneiss and the overlying Mtshingwe Group. However, the structural relationships between this formation and the Hokonui Formation are not well understood, and the exact significance of the Bvute Formation is not known. The whole group has been subjected to major deformational and erosional events before the deposition of the overlying Ngezi Group.

The age of the Mtshingwe Group greenstones is bracketed by the intrusive (and possibly cogenetic) Chingezi Tonalite (ca. 2833 ± 43 Ma) and the unconformably overlying Ngezi Group greenstones (2692 ± 9 Ma, see §6.4). The Brooklands Formation (correlated with the Hokonui and Bend Formations) is tentatively correlated with the Buchwa quartzite in the Mweza greenstone belt, which yields a youngest detrital zircon U-Pb age of 3210 ± 20 Ma (Dodson *et al.*, 1988).

2.3.2 The Hokonui Formation

The Hokonui Formation is a calc-alkaline sequence of andesitic, dacitic and rhyolitic lavas, with pyroclastic and resedimented volcanic material of a similar composition, and minor amounts of intrusive dolerite and fine-grained greenstone. The stratigraphic thickness of the unit is uncertain, as the outcrop width may include the Bvute Formation, and some of it may represent structural repetition, but it is thought to total perhaps 2-3 km (Scholey, 1992). Volcaniclastic deposits form the bulk of the formation, ranging from coarse volcanic agglomerates (including one recognised vent agglomerate) to fine tuffs, displaying shallow marine sedimentary structures but clearly erupted subaerially (Martin *et al.*, 1993). The Formation represents the remains of a large calc-alkaline volcanic pile, perhaps a single major volcanic complex.

2.3.3 The Bend Formation

The Bend Formation is dominantly komatiitic, and consists of repeated cycles of komatiites, komatiitic basalts and basalts, interbedded with ironstone and chert. It overlies the Hokonui Formation in the north and the Bvute Formation in the south (apparently conformably, although the contact is now the Mberengwa Fault, and so the exact nature of the contact cannot be determined (Martin *et al.*, 1993). Its present day thickness ranges from 6km to 2km, but these thicknesses have been greatly affected by deformation and erosion. The volcanic rocks are clearly extrusive (spinifex textures in the komatiite flows), and mainly clearly submarine (pillows in the less magnesian lavas). The ironstone horizons (at least ten in the whole formation) are mostly thin (2-30m), but the uppermost horizon is 100m thick.

2.3.4 The Koodoovale Formation

This Formation consists mainly of conglomerates and assorted finer-grained sedimentary rocks, with a locally developed unit of felsic agglomerate. It overlies the Bend Formation unconformably (an erosive contact with a few major channels), but there is no evidence for angular unconformity or any major time gap (Martin *et al.*, 1993). It ranges from 1km to 2km thick, but, like the Bend Formation, these thicknesses have been affected by deformation. Clasts in the conglomerate include typical fragments from the underlying units (the Chingezi Gneiss and the Hokonui and Bend Formations).

2.3.5 The Brooklands Formation

The Brooklands Formation forms the supracrustal rocks overlain unconformably by the Manjeri Formation (the base of the Ngezi Group) in the southeast portion of the greenstone belt. The sequence consists of a conformable set of sedimentary and volcanic rocks, thought to have been laid down on the older gneissic basement, and has been divided into four members:

1. **Ndakosi Member** Mainly sediments (phyllites, siltstones and conglomerates) together with some mafic and ultramafic rocks (possibly intrusive).
2. **Roselyn Member** Komatiites and komatiitic basalts, with some massive serpentinite bodies.
3. **Mnene River Member** A laterally continuous conglomerate overlain by varied fine grained and silicified sedimentary rocks.

4. **Pemba Member** Basalt and komatiitic basalts with minor fine grained sediment, chert and ironstone.

The correlation of the Brooklands Formation with the Mtshingwe group on the western side of the belt is not straightforward, and is based mainly upon structural relations. If the belt were unfolded, the Brooklands Formation would lie 30km or more from the western part of the group and, given the large lateral facies variation *within* the Brooklands Formation, equating it with the western suite is not unreasonable (Martin *et al.*, 1993).

2.4 The Ngezi Group (The Upper Bulawayan in Belingwe)

2.4.1 Overview

The 2.7Ga Ngezi Group is thought to represent a well preserved and detailed record of the development of a greenstone succession on continental crust, despite doubts that have been recently cast on its contiguous and supracrustal nature (see §3.2.2). It consists of four formations, the Manjeri, Reliance, Zeederbergs and Cheshire Formations. The group has been folded into a large synclinal structure, but there is little internal deformation, and the quality of preservation is excellent throughout the whole succession. The Reliance and Zeederbergs Formations are known collectively as the Ngezi Group volcanics.

2.4.2 The Manjeri Formation

The Manjeri Formation represents the base of the Upper Bulawayan greenstones in Belingwe, and is a sedimentary succession laid down on a varied terrain of tonalite, gneiss and eroded older greenstones relics. The Formation is typically 50-100m thick. The significant feature of the formation is the clear basal unconformity, clearly seen at three localities, on top of the gneissic basement or the older greenstones. At the National Monument locality (see Figure 3.1), basal conglomerates pass upward into varied intertidal sandstones and siltstone and associated chert and banded ironstone. Above this are slightly deeper water sediments, including graded arkosic sandstone and greywacke, and the formation is capped by a thin bed of sulphide-facies ironstone (characteristically gossenous in outcrop). This sulphide-facies ironstone is often sheared, but the persistence of this thin horizon around most of the outcrop of the

Ngezi Group is a strong argument against the idea that there is any major structural break at this level (Martin *et al.* 1993). Near Zvishavane, the sequence shows banded ironstone passing up into arkosic sandstone and conglomerate, and is capped by the sulphide-facies ironstone. On the western side of the belt, in the Mtshingwe River, basal conglomerates pass into shallow water sandstone, siltstone and then to laminated quartzite. A further notable feature of the Manjeri Formation is the presence of stromatolites (Bickle *et al.*, 1975; Martin *et al.*, 1980), which probably formed in intertidal conditions.

Three important conclusions have been drawn from the study of the Manjeri Formation (e.g. Bickle *et al.*, 1975; Nisbet *et al.*, 1977; Martin, 1978; Scholey, 1992), which provides valuable evidence for the pre-volcanic environment:

- The Manjeri sediments rest unconformably on pre-existing continental crust and older greenstones.
- The condensed facies sequence within the formation records limited clastic input to a rapidly subsiding, asymmetric basin of unknown dimensions (but $>10^2$ km).
- Sulphide-facies ironstones at the top of the Manjeri succession represent deep submarine (>1000m) exhalative deposits heralding the onset of volcanism.

All of these lend support to the important conclusion that the Ngezi Group volcanics (which overlie the Manjeri Formation, apparently conformably) were erupted through pre-existing continental crust into a rifted basin. A cartoon of a possible depostional model for the Manjeri Formation is shown in Figure 2.3 (from Nisbet *et al.*, 1993).

2.4.3 The Reliance Formation

The Reliance Formation rests apparently conformably on the Manjeri Formation or directly on the gneissic basement, though there is some dispute about the nature of this contact (see §3.2.2). A detailed description of the stratigraphy, petrography and geochemistry of the Reliance Formation is presented in later chapters. In summary, it is a ca. 1km thick sequence of ultramafic and mafic extrusive lavas, with komatiites in the central part.

2.4.4 The Zeederbergs Formation

The Reliance Formation passes upwards into the Zeederbergs Formation, a pile of mafic lava flows and minor volcaniclastic sediment some 3km thick. Detailed descriptions of the stratigraphy, petrography, alteration style and geochemistry of the Zeederbergs Formation form the bulk of this study.

2.4.5 The Cheshire Formation

The uppermost formation in the Ngezi Group, the Cheshire Formation records a return to sedimentary conditions. It rests generally conformably on the Zeederbergs Formation, although it does contain some clastic material derived in part from that formation. It is probably >2km in thickness, but this is difficult to determine exactly, as the top of the formation is not seen. Typically, a basal conglomerate (containing well rounded clasts of Zeederbergs Formation material) or limestone is overlain by argillite & siltstone (which form much of the formation) and sandstone. Sedimentary structures in the siltstone indicate shallow marine deposition, and near the top of the sequence, thin banded ironstones are common. To the west of the syncline axis is a very important limestone member containing thick algal laminated limestone. In several localities stromatolites are seen, associated with intercalations of sandstone and siltstone which show common sedimentary structures indicating shallow marine conditions (ripples, cross-bedding and polygonal mudcracks) (Martin *et al.*, 1993).

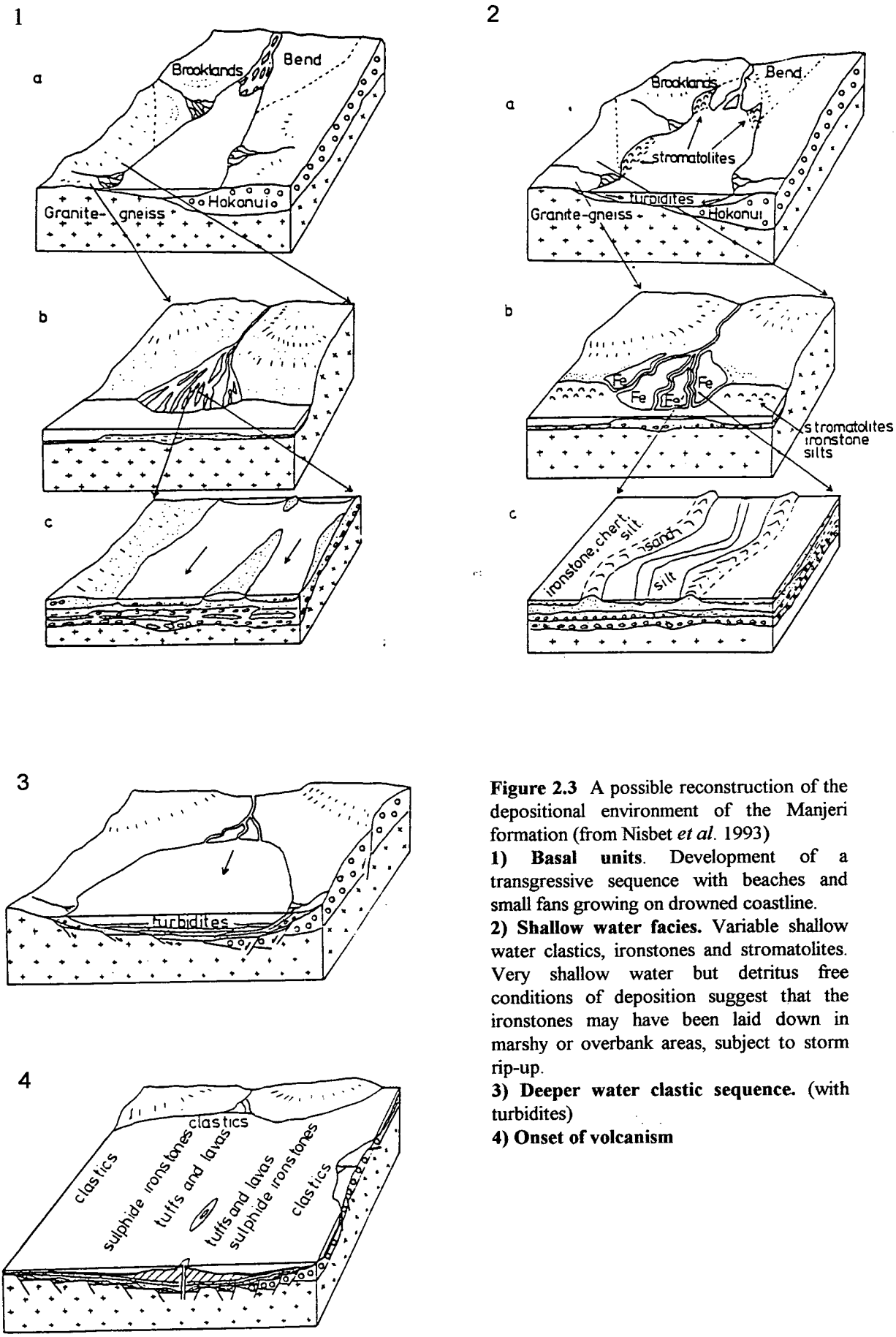

Figure 2.3 A possible reconstruction of the depositional environment of the Manjeri formation (from Nisbet *et al.* 1993)

1) Basal units. Development of a transgressive sequence with beaches and small fans growing on drowned coastline.

2) Shallow water facies. Variable shallow water clastics, ironstones and stromatolites. Very shallow water but detritus free conditions of deposition suggest that the ironstones may have been laid down in marshy or overbank areas, subject to storm rip-up.

3) Deeper water clastic sequence. (with turbidites)

4) Onset of volcanism

2.5 The Ngezi Group: Tectonic and depositional setting

The tectonic and depositional setting of the Ngezi Group is not clear, but Nisbet *et al.* (1993) provide some interesting speculative ideas on the problem. They assume that the interpretation of the entire group as supracrustal is valid, and consider the possible origins of the sequence seen. A brief summary of their ideas is presented here.

The most significant question is whether the greenstone belt represents an isolated basin, or preserves part of a more widespread cratonic covering sequence. Correlation of the Belingwe stratigraphy across much of the craton (Wilson *et al.*, 1978; Wilson 1979) suggests the latter, but there is still the distinct possibility of significant thickness variation (Nisbet *et al.*, 1981). The exposed section of the Manjeri Formation is perhaps too limited to provide direct evidence of a localised basin, though its absence from the northern part of the belt could be interpreted as representing the rapid attainment of deeper water conditions in the more central parts of the belt, with little sedimentation on the periphery before the onset of volcanism (though the evidence for this is weak). The Cheshire Formation is a little more informative, as it contains virtually only volcanic derived clasts, with no granite, implying that the granitoid crust was not exposed at the time of deposition, and supporting a craton-wide cover model.

It is important to consider the large degree of subsidence needed to accommodate the complete Ngezi succession, which is in the order of 5-10km thick. Clear shallow water sediments at the base and top of the group attest to this subsidence, and the clearly sub-marine eruptive volcanics, with only minor resedimented volcaniclastic material intercalated suggests very rapid subsidence during the volcanic phase. Extension of the lithosphere, and subsequent adiabatic decompression of the underlying mantle would provide a reasonable explanation for both the subsidence (and basin formation) and the volcanic activity (McKenzie and Bickle, 1988; McKenzie, 1978).

Extensional models have been suggested as widely applicable to Archaean greenstone belts (McKenzie *et al.* 1980; Bickle and Eriksson, 1982), though there is the problem that syn-rift (associated with initial rifting) and post-rift (associated with slower thermal subsidence) should be clearly distinguishable, as they are in modern sedimentary basins. In Belingwe, the 'syn-rift', or 'proto-basinal' phase of sedimentation before the onset of volcanism can only be represented by the Manjeri

Formation, which is too thin (according to reasonable models of rifting (Jackson and McKenzie, 1983)) and shows no apparent rift faults. In fact, no apparent rifts are seen anywhere in the Ngezi Group stratigraphy. One possible solution is that the Belingwe greenstone belt was located marginal to a more heavily rifted area of crust, and the subsidence could be attributed to non-uniform stretching of crust, or possibly the elastic flexural response to loading of the lithosphere (Figure 2.4, from Nisbet *et al.* 1993). In this scenario, volcanic sequence would represent lavas generated some distance from the belt, but which blanketed a large area to a fairly uniform thickness in a style characteristic of high-temperature low-viscosity lavas (e.g. the ca. $10^6 km^2$ extent of the Deccan Trap flood basalts (Cox, 1989)).

Another possibility which could account for very localised and extreme subsidence is that the belt was formed in some kind of strike-slip pull-apart basin (E. Nisbet, pers. comm. 1994). It could be that the Great Dyke was emplaced along some pre-existing fault line, potentially a strike slip system, and that the Mberengwa Fault is actually the reactivation of subsidiary en-echelon fault on which a pull-apart basin developed. Pull-apart basins are known to have high rates of subsidence with very limited areal extents (N. McMahon, pers. comm. 1994), and although this idea is highly speculative, it has some appealing qualities.

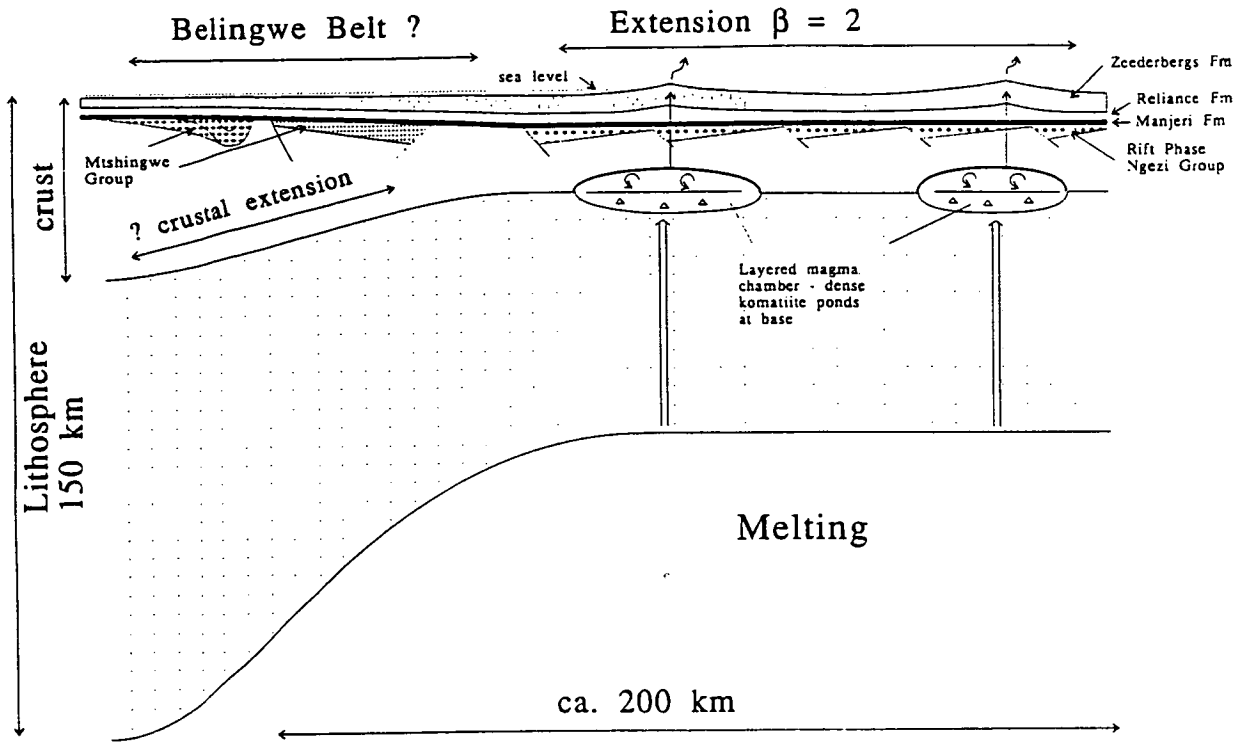

Figure 2.4 Possible model for development of the Reliance and Zeederbergs Formations. Note vertical exaggeration of Manjeri and Reliance Formations. Belingwe greenstone belt situated adjacent to actively extending upper crust. Precise correlation of Manjeri Formation and volcanics with rift-fill facies is unknown. After initial Manjeri-subsidence, melts from the asthenosphere are able to rise directly to the surface. Later, crustal magma chambers develop and only light fractionated basaltic liquid can ascend. Residue of magma chamber remains as crustal ultramafic complex. (From Nisbet *et al.*, 1993).

2.6 Deformation and alteration of the Ngezi Group

2.6.1 Deformation

The major structural elements of the Belingwe greenstone belt (Coward *et al.*, 1976; Martin, 1978, 1983; Orpen, 1978) and the nearby greenstone belts have been attributed to deformation associated with late Archaean, thin-skinned, east-west crustal shortening (e.g. Coward *et al.*, 1976; Wilson, 1990). The Ngezi Group forms a tight syncline structure, with a generally north-south trending axis, previously activated during the folding of the Mtshingwe Group. The rocks of the Ngezi Group are all quite steeply dipping, and young towards the core of the syncline, with localised shear zones (most notably in the banded ironstones of the Manjeri Formation) accommodating the flexural slip associated with this folding. The major structural features of the area are shown in Figure 2.5.

The syncline axis plunges away from the northern and southern ends of the belt towards the centre, possibly a result of uplift associated with the post-tectonic intrusion of the Chilimanzi Suite granites at these extremities. The belt is cut by the sub-vertical Mtshingwe Fault, which was perhaps originally associated with the emplacement of the Limpopo belt (Wilson *et al.*, 1987), and has seen some subsequent reactivation (Wilson *et al.*, 1987). The displacement associated with this fault is thought to have been accommodated in the Belingwe belt at shallow levels in a zone of en-echelon faults and sub-parallel shearing (Scholey, 1992, from Martin's (1980) map). Exactly where this fault passes through the rocks of the Zeederbergs Formation in the vicinity of the Ngezi River section (see Chapter 3) is not at all clear, as there is little evidence of any shearing or fault displacement to be seen, and the section is apparently complete (see §3.5.7)

2.6.2 Alteration and metamorphism

Metamorphic grades in the Ngezi group are low, usually only reaching low-greenschist (e.g. Martin *et al.*, 1978, 1983; Nisbet *et al.*, 1977, 1987). The alteration of the Ngezi Group volcanics is examined in detail in Chapters 4 and 5, so little will be said here. The sedimentary rocks show minor recrystallisation (to Quartz-Chlorite-Mica assemblages), but all textures are very well preserved, as are most original igneous textures. There is a detectable increase in metamorphic grade towards the northern and southern ends of the belt, thought to be associated with the intrusion of the Chilimanzi Suite granites.

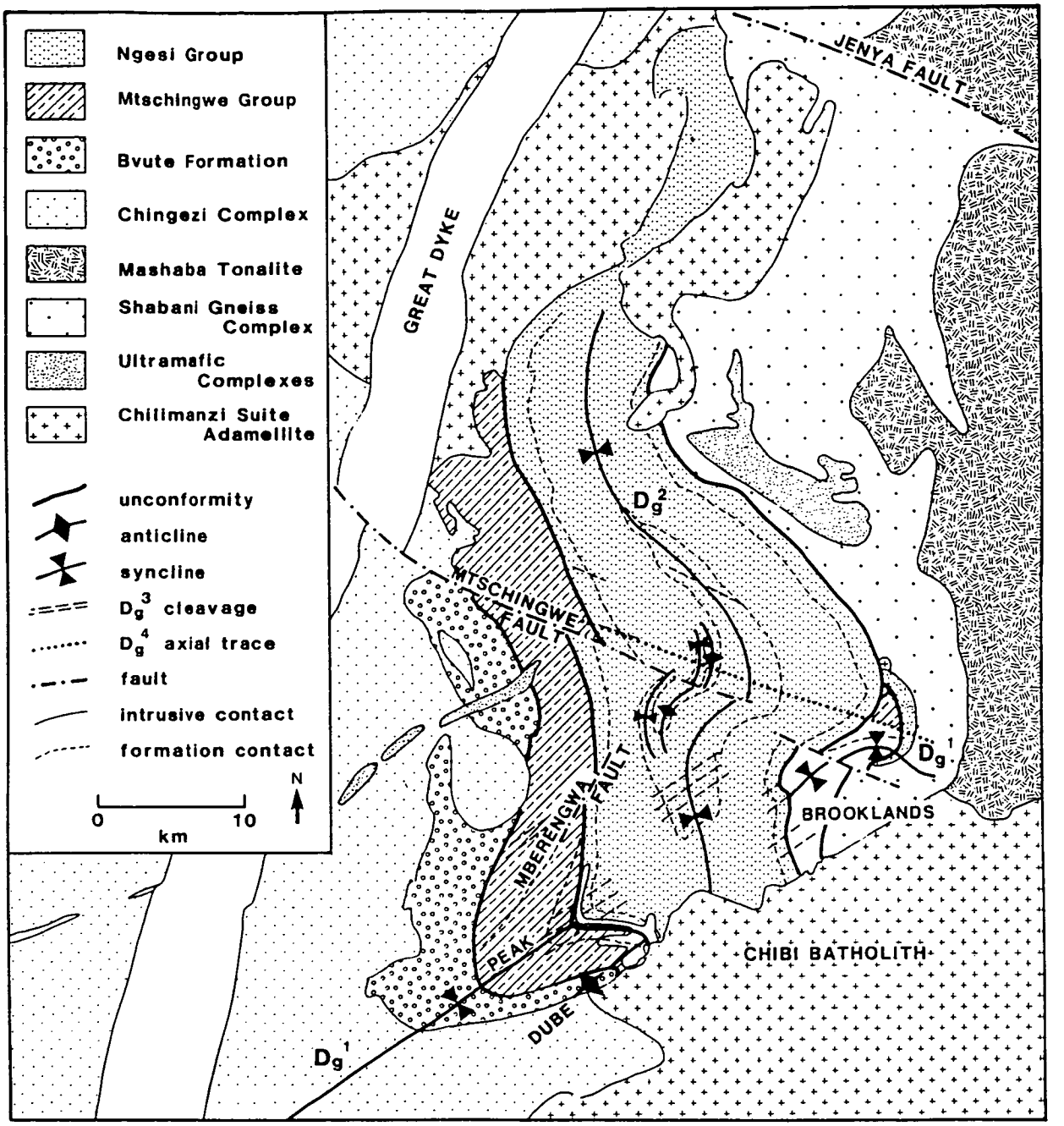

Figure 2.5 Outline structural map of the Belingwe belt (from Bickle *et al.* 1993)

Bickle *et al.* (1993) conclude that the Ngezi Group underwent up to four distinct metamorphic events:

1. Localised but intense early (syn-volcanic) hydrothermal alteration.

2. A pre-Chilimanzi Suite upper-greenschist to amphibolite event in the very north of the belt (the Snake's Head).

3. A localised amphibolite facies thermal aureole adjacent to the Chillimanzi Suite granites in the north and south of the belt.

4. A regional greenschist (to sub-greenschist in parts of the Cheshire Formation) event over the whole belt.

3

STRATIGRAPHY AND FIELD RELATIONS

3.1 Introduction

This chapter is broadly split into two parts, a detailed physical description of the Ngezi Group volcanics in the field, followed by an examination of the chemical stratigraphic variation in the rocks of the Zeederbergs Formation.

The stratigraphy and field relations of the Reliance Formation are summarised in §3.2. Special attention is paid to the nature of the basal contact of the formation, as it has been the subject of much recent debate (see §3.2.2), and is crucial to the question of whether the volcanic sequence was erupted *in situ* or tectonically emplaced, as is the question of correlation of the Reliance Formation stratigraphy around the belt. The bulk of new descriptive work on the Zeederbergs Formation relates to the type section in the Ngezi River (see §3.3). A complete and detailed log and description of this section are presented here for the first time. The other sections through the formation sampled in this study are only described in more general terms, to demonstrate they are of a very similar nature to the type section.

The detailed work on the chemical stratigraphy of the Zeederbergs Formation (see §3.5) led to the discovery of a horizon of a new type of basalt not previously recognised in Belingwe. In addition, correlation of the chemical stratigraphy between the three sections sampled in detail has led to a reassessment of the total thickness of the formation (see §3.5.7)

3.2 The Reliance Formation

3.2.1 General overview

The Reliance Formation contains some of the most well preserved Archaean komatiites in the world, and its stratigraphy and field relationships are well documented (Bickle *et al.*, 1975; Nisbet *et al.*, 1977, 1987; Martin, 1978, 1983; Orpen, 1978; Bickle and Nisbet, 1993, Scholey, 1992). All that is given here is a brief

summary of current knowledge, mostly taken from Bickle & Nisbet (1993) and Scholey (1992). The reader is referred to these for a more complete description. The formation is composed mainly of komatiite and komatiitic basalt. It contains some volcaniclastic material (<10%), but there is very little intercalated terrigenous sediment. It is approximately 1km thick, and several different cooling unit morphologies can be identified in the field (Table 3.1).

Table 3.1 Reliance Formation physical volcanology: classification and description of cooling unit morphology (from Scholey, 1992).

Type	Thickness	Characteristics
Thick flows	>10m; maximum known is 45m	Extreme textural layering in thick, high-magnesium basalt flows (repeated in some compound units) otherwise massive; margins often rubbly
Thin flows	<10m	Usually massive; weak textural differentiation may occur in thin komatiite flows; margins generally rubbly
Lobes	Lateral extent <10m, usually <5m thick	Usually massive; weak textural differentiation may occur
Pillows	0.1-1.0m	Individual pillows recognised from curvilinear contacts or glassy rims; commonly concentrically zoned; form both discrete piles up to several tens (hundreds?) of metres thick and upper part of some layered flows
Hyaloclastite	Fills interstices between pillows	
Tuffs	Extremely variable	Form piles up to several tens (hundreds ?) of metres thick; individual sets within these may not be distinguishable
Sills	Known examples *ca.* 2, 25, 120 m	Usually differentiated; may be indistinguishable from flows if not markedly transgressive
Dykes	Largest known is *ca.* 10m wide	Generally recognisable from discordant contacts with sub-perpendicular columnar jointing

Several different sections through the Reliance Formation, both exposed and drilled, have been studied (See Figure 3.1 for section locations). The near complete exposure through the formation in Mvobo Spruit was established as the type section by Martin (1978), and is described in great detail in Nisbet *et al.* (1977) and Scholey (1992). In addition to this section, the Reliance Formation on the east side of the belt has been examined in the stream section at the National Monument locality (Martin, 1978; Scholey, 1992) a drill core from Union Carbide drill hole DDH 493/2 (Scholey, 1992), and in the stream section and drill core from the SASKMAR drill site (Nisbet *et al.*, 1987; Renner, 1989; Renner *et al., 1994)*. The principal sections documented on the western side of the belt are the N.A. Mine area (Scholey, 1992), and Hall's section (Hall, 1983; Scholey, 1992).

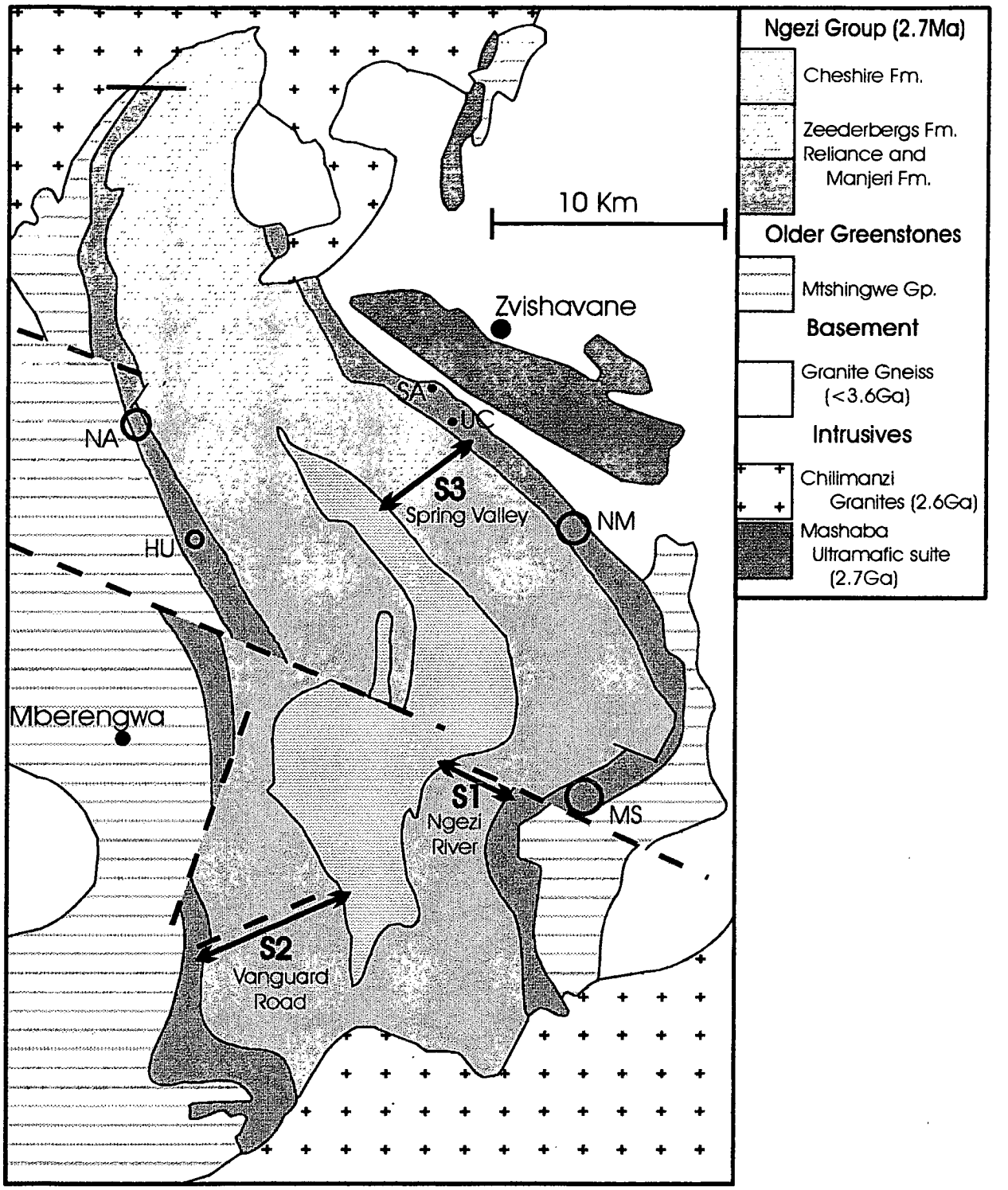

Figure 3.1.

A simplified map of the Belingwe greenstone belt showing localities referred to in text.
Significant localities of the Reliance Formation : MS, Mvobo Spruit (type section); NM, National Monument locality; SA, SASKMAR drill site; UC, Union Carbide drill site 493/2; NA, N.A. Mine area; HU, Hall's unit.
Traverses through the Zeederbergs Formation used in this study : S1, Section 1, Ngezi River (type section); S2, Section 2, Vanguard Road; S3, Section 3, Spring Valley.

3.2.2 Basal contact of the Reliance Formation

Some controversy surrounds the nature of the basal contact of the Reliance Formation on the underlying sediments of the Manjeri Formation. Whether this contact is stratigraphic or tectonic is central to the debate over whether the Ngezi group represents an emplaced allochthon or was erupted *in situ* on continental crust (see Chapter 2). The basal contact in Mvobo Spruit is seen as a 15m exposure gap separating thick tholeiitic basalt flows from slump-folded ferruginous pelites and banded ironstones of the Manjeri Formation (Scholey, 1992), and whilst it is apparently conformable, its exact nature is uncertain. The contact is also hidden by exposure gaps in the sections on the western side of the belt.

Most argument about the nature of the contact has focused on the section at the National Monument locality. Scholey (1992) describes this contact as 'a soil filled crack *ca.* 3 cm in width, considered here to represent a detachment surface', and describes a shear fabric in the basal 8-10m of the volcanic succession, which is interpreted as 'resulting initially from slump or tectonic emplacement of the volcanics'. Kusky and Kidd (1992) and Kusky *et al.* (1994) interpret the uppermost Manjeri Formation as a 'deepening-upward sequence', representing tectonic loading associated with the emplacement of their postulated allochthon. They stress the presence of shear zones in the ironstone bands below the contact, and of a foliation fabric in the lowermost Reliance Formation, and interpret them as being associated with a major detachment zone. Blenkinsop *et al.* (1993) interpret the Manjeri Formation in the area as consisting of 'at least three deepening-upward, parasequence- or sequence-scale cycles (*sensu* Van Wagoner *et al.*, 1988)', and contest that 'collectively, the three cycles show a net deepening upsection, consistent with a relative sea-level rise'. They point out the presence of completely unstrained material a few metres above and below the contact, and interpret the shear zones as resulting simply from flexural slip on the least competent units in the succession, associated with the synclinal folding of the belt.

Nisbet *et al.*(1993), state that the contact is best seen in the core from the Union Carbide drill site (DDH 493/2), which shows 'thin beds of quartz grit intermingled with tuffs of the basal Reliance Formation, implying that some clastic sediment was deposited after the onset of volcanic activity.' Shear fabrics near the contact are absent from the sections throughout the formation on the western side of the belt (Scholey, 1992), which is surprising if the contact does indeed represent a major detachment surface. The basal contact is interpreted here as conformable, with the shearing being the result of flexural slip.

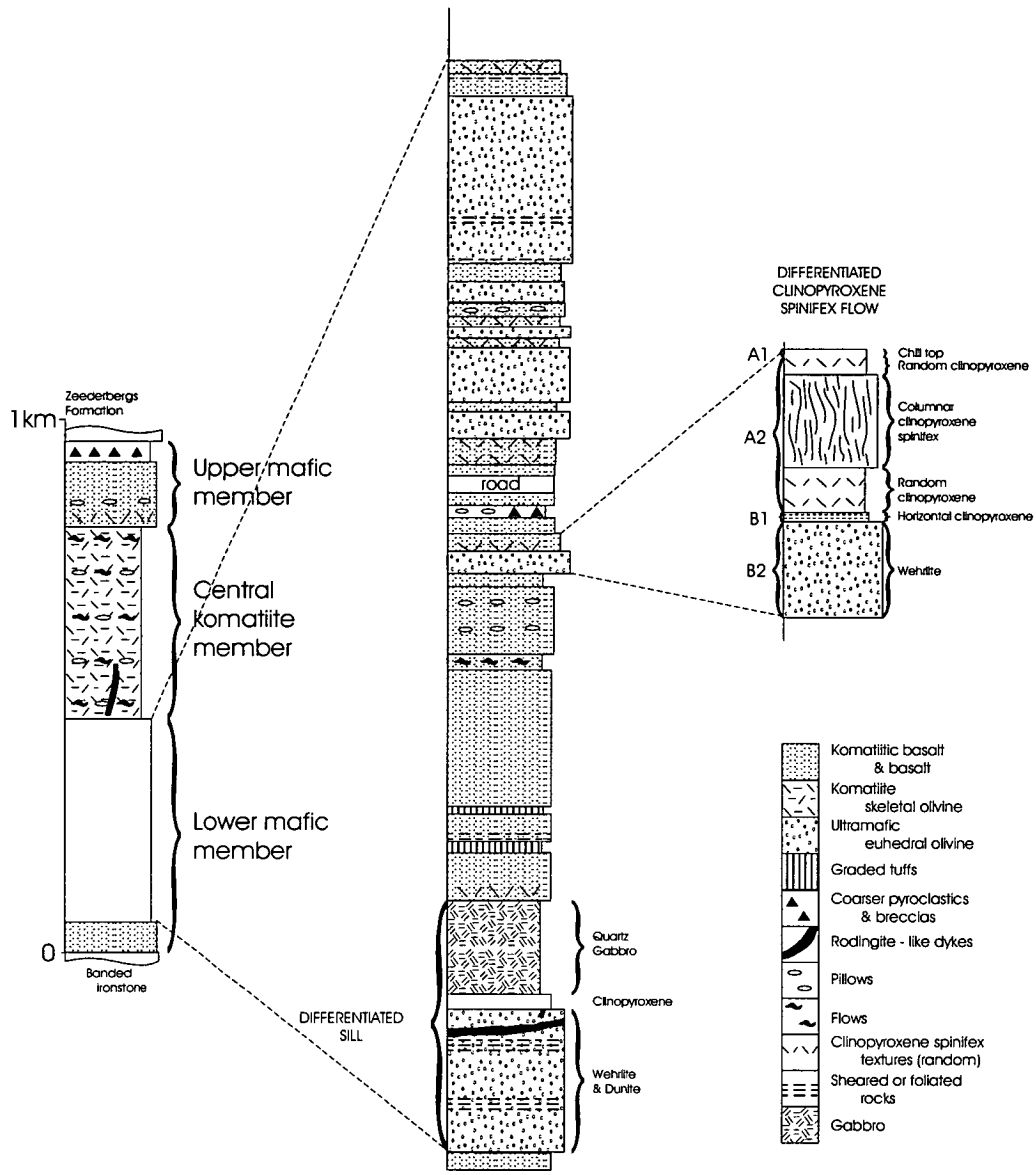

Figure 3.2.
Stratigraphic log of the type section of the Reliance Formation, Mvobo Spruit (from Nisbet et al. 1993).

3.2.3 Stratigraphy of the Reliance Formation

The Reliance Formation was originally divided into four units (Nisbet *et al.*, 1977), but in more recent work (Nisbet *et al.*, 1993), the lower two of these have been combined as a single member. Scholey (1992) re-examined all the sections around the belt, and proposed a return to the original four units. But for simplicity the three divisions of Nisbet *et al.* (1993) have been used here. The type section can be divided into a lower mafic member (400m thick, basalt and komatiitic basalt), a central komatiite member (400m thick, dominantly komatiite) and an upper mafic member (approximately 200m thick, mafic lavas and some tuffs). A log of the type section is given in Figure 3.2.

The lower part of the lower mafic member comprises basalt and komatiitic basalt flows, mostly massive, but with some pillowed tops. Overlying these is a thick (90-120m) differentiated igneous body (the Ngolubi Sill), showing cumulate dunite and wehrlite at the base, grading up into quartz gabbro at the top. Above this sill are approximately 200m of basalt and komatiitic basalt flows and some graded tuffs, the lower half being mainly pillows, lobes and thin flows. The upper half is dominated by thick, layered flows, commonly with basal cumulates, and 'string-beef' clinopyroxene seen in the upper parts of flows. Elsewhere in the belt, the lower mafic member shows well developed columnar jointing, and pillowed, spinifex or massive textured basalt and komatiitic basalt flows up to 500m thick. About 150m above the base of the formation, a tuff layer 1-2m thick is often seen (traceable for several kilometres on the eastern side of the belt). This layer is rich in accretionary lapilli (fine grained, ellipsoidal and spherical, often graded, 0.5-1cm in diameter). The presence of these lapilli, together with the fiamme textures seen, are thought to represent subaerial eruption, in phreatoplinian events (Nisbet *et al.*, 1993).

The central komatiite member is dominantly ultramafic, made up of many thin (mostly <4m) simple and pillowed flows. The individual flows can be clearly seen near the SASKMAR locality (Nisbet *et al.*, 1987), and usually show a rubbly base, a more massive centre, and a rubbly top passing into pillows. Pillows tend to be small (20-50cm), and often show a creamy weathering colour (due to serpentinisation) in the field. Olivine spinifex textures are very well preserved in some samples (especially from the SASKMAR drill core (Nisbet *et al.*, 1987; Renner, 1989; Bickle *et al.*, 1993; Renner *et al.*, 1994)), but are generally rare in outcrop. Scholey (1992) reports 'abrupt lateral variations in both the morphology and thickness of individual units' making any attempted correlation of units along strike a 'futile exercise'.

The upper mafic member contains a variety of komatiitic basalts, basalts and tuffs, but is generally very poorly exposed. A distinctive volcaniclastic horizon present around much of the belt is used to define the contact with the Zeederbergs Formation. This contact is rather arbitrary, but does correspond to a general break in slope and change in topography seen throughout the belt. It is considered unlikely that there was any noticeable hiatus in volcanic activity, just a change in volcanic products.

3.2.4 Correlation of the Reliance succession around the belt.

Scholey (1992) suggests that the lower part of the Reliance Formation (the lower part of the lower mafic member) is absent from the National Monument section and the Union Carbide drill hole DDH 493/2, and postulates their removal during emplacement of the Ngezi Group volcanics as an allochthonous block. Much of the evidence for this seems to rely on the lateral continuity of quite specific field relations (eg. 'a rutile bearing tholeiitic sill intruded into hyaloclastic tuffs'), and on the assumption that the flows evenly covered a uniformly flat surface. He does concede that the omission of these parts of the section 'may plausibly be attributed to topographic influences', but does not pursue this idea.

Removal of section during thrust emplacement requires the interpretation of the basal contact to the Reliance Formation as tectonic. As this contact is interpreted in this work as being conformable (see §3.2.2), this mechanism is not a realistic option. It is acknowledged that there are significant differences between the sections through the Reliance Formation, but whether the flows were laterally continuous enough, and the inter-flow variability large enough, to say for certain that part of the section is missing is questionable. Given the uncertainty in how much, if any, of the formation is missing from certain sections, and the perfectly reasonable explanation of this as being due to surface topography, it is not considered here to represent a strong argument for an allochthonous origin of the Ngezi Group. The interpretation of the whole succession as conformable is still considered the most reasonable option.

3.3 The Zeederbergs Formation type section, Ngezi River

3.3.1 Location of section and contribution of this study

The type section through the Zeederbergs Formation is along the Ngezi river on the east of the belt (see Figure 3.1). In comparison to the work on the rocks of the Reliance Formation, the Zeederbergs Formation, even in its type section, has received little attention, and has often been described as a pile of 'monotonous mafic volcanics'. Over two field seasons, the type section was mapped on 1:6250 aerial photographs, the log of the volcanic succession (Figure 3.3) was compiled, and the section was sampled on a flow by flow basis.

The river bed through the section ranges from 20 to 80m wide, on average being about 30m or so. There was little water in the river during the field seasons, just a series of large pools, leaving many superb water washed outcrops exposed. The rocks are mainly very fine grained, and so all morphological division was based upon structures best seen in such outcrops. Away from the river bed, the rocks all had the typical brown tropical weathering crust, and little detailed work was possible. The strike of the section is generally between 065° and 080°, but rotates around to about 030° in the lower few hundred metres. Where dips were measurable, they were all sub-vertical to vertical, and all the rocks that showed facing directions younged into the core of the syncline.

3.3.2 Overview of section and description of contacts

The formation as seen in the section is just over 2.8km thick, and is dominated by fine grained mafic lava flows, the majority of which show clear pillow structures. Where pillow structures are absent, the rocks have a massive habit, and it is generally impossible to say whether they are massive flows or sills. Volcaniclastic horizons are reasonably common, and range from fine grained ash flows to (minor) quite coarse volcaniclastic breccias. Hyaloclastite material is also seen, both as inter-pillow fill, and in separate distinct horizons. Intrusive material (excepting the possibility of some of the massive units being sills) is rare, and is seen as discordant bodies of similar material to the rest of the formation (interpreted as feeder dykes), and concordant bodies of clearly different material (later ultramafic sills). One large 'feeder vent' structure is seen at just over 1.1km above the base of the formation, in a particularly well exposed part of the section.

Figure 3.3.

Log of the volcanic succession in the Ngezi River type section through the Zeederberg s Formation

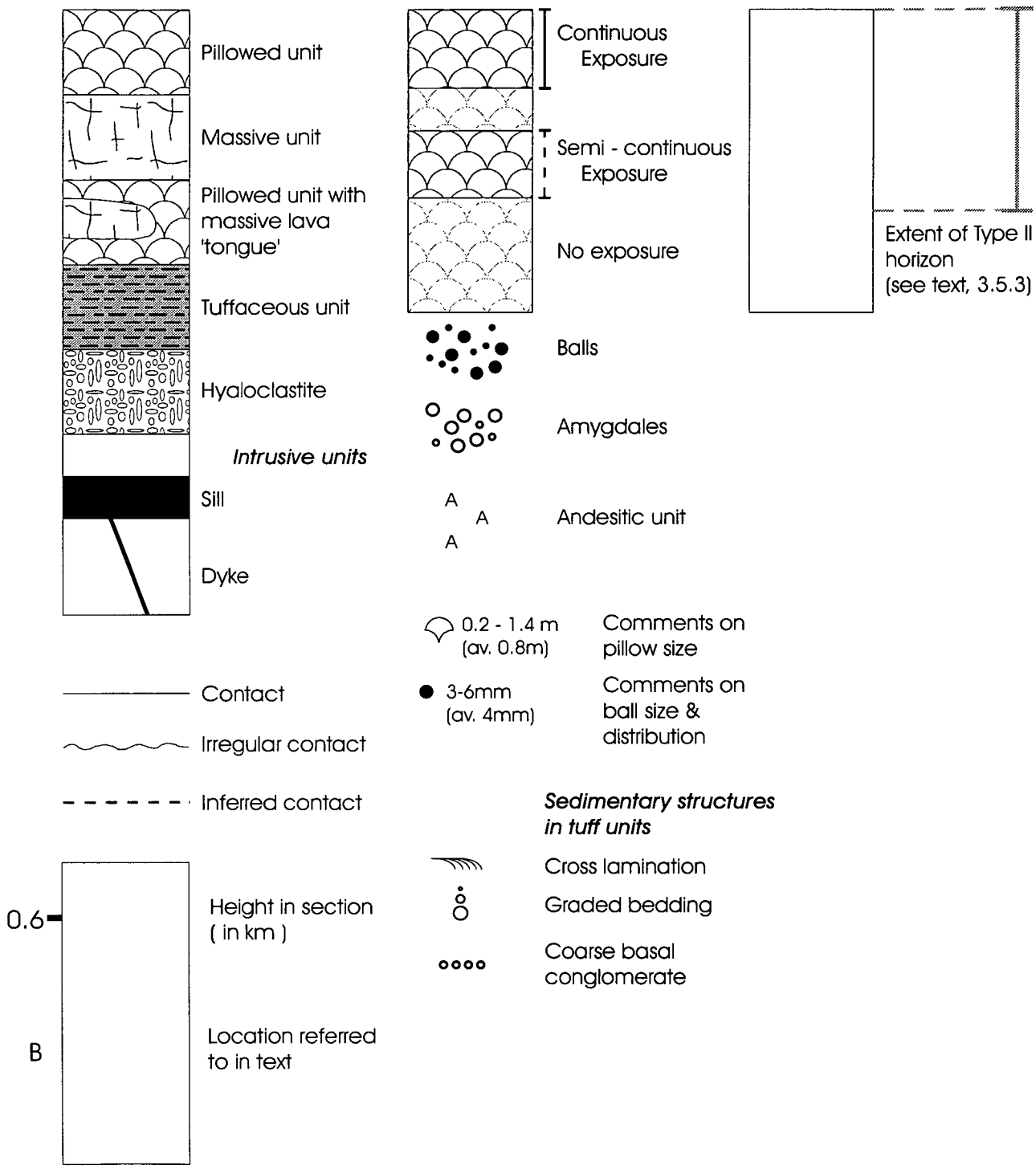

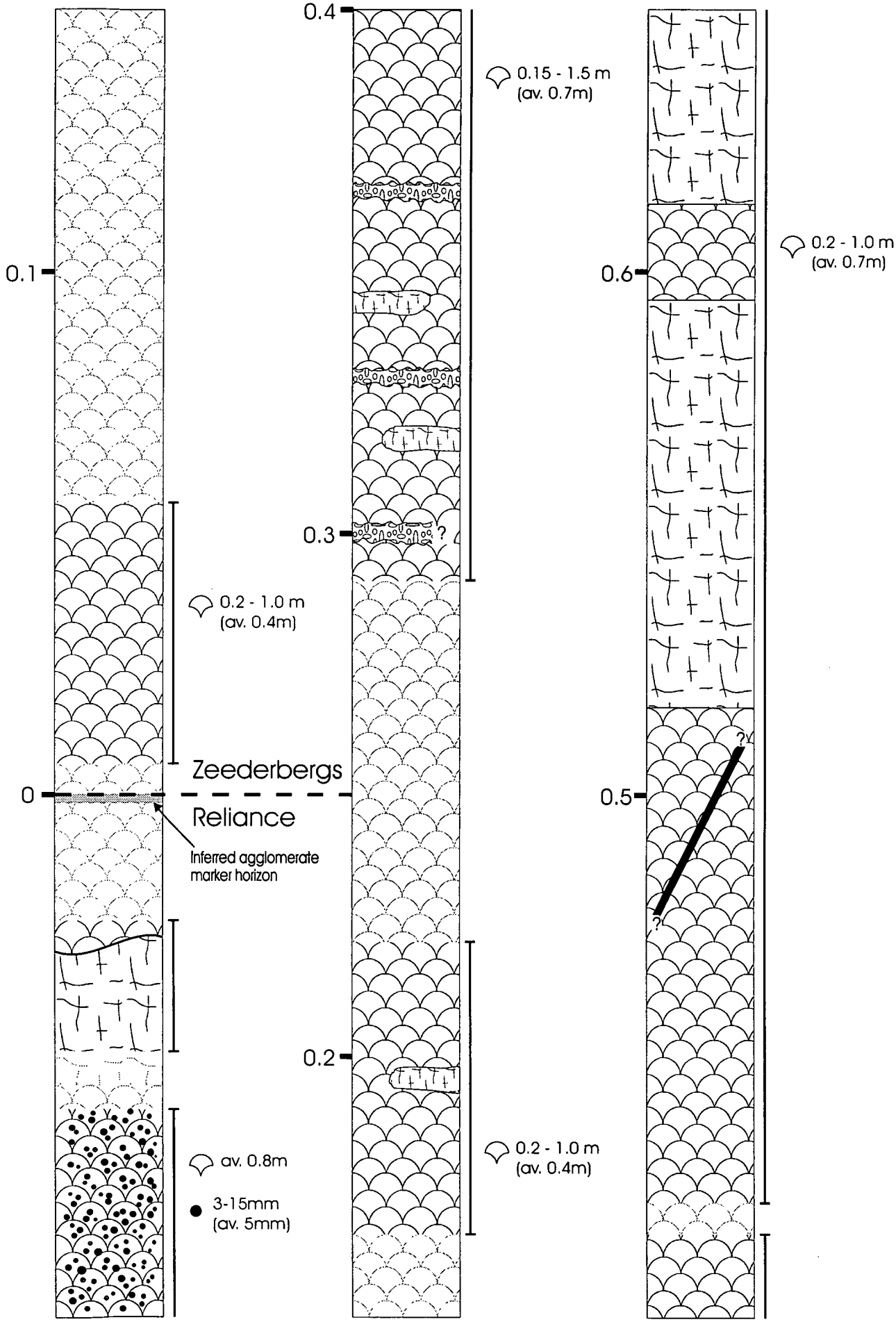
0.4
0.15 - 1.5 m
(av. 0.7m)
0.1
0.6
0.2 - 1.0 m
(av. 0.7m)
0.3
?
0.2 - 1.0 m
(av. 0.4m)
Zeederbergs
0
Reliance
0.5
?
?
Inferred agglomerate
marker horizon
0.2
av. 0.8m
3-15mm
(av. 5mm)
0.2 - 1.0 m
(av. 0.4m)

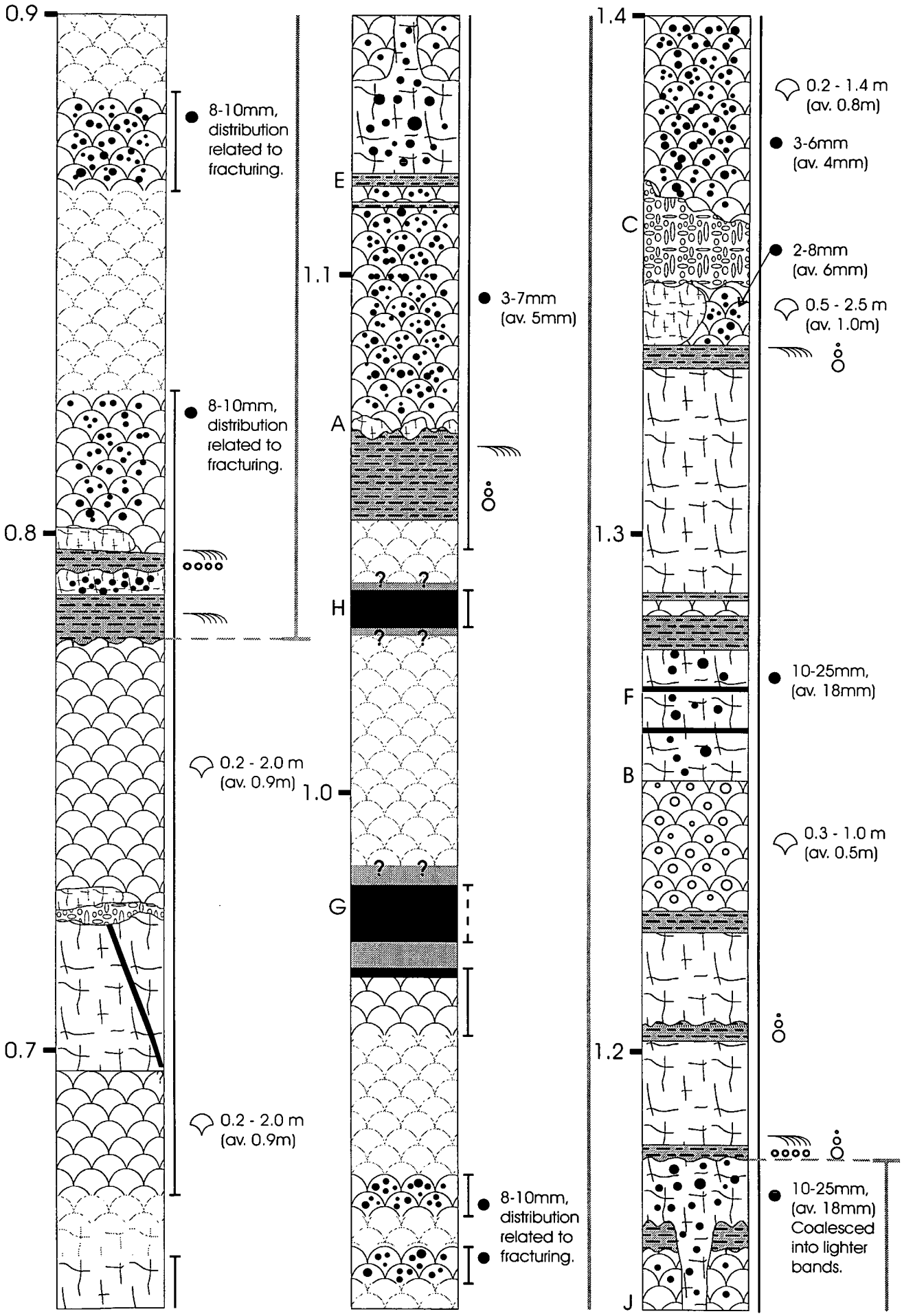
0.9
8-10mm, distribution related to fracturing.
8-10mm, distribution related to fracturing.
0.8
0.2 - 2.0 m (av. 0.9m)
0.7
0.2 - 2.0 m (av. 0.9m)
E
1.1
3-7mm (av. 5mm)
A
H
1.0
G
8-10mm, distribution related to fracturing.
1.4
0.2 - 1.4 m (av. 0.8m)
3-6mm (av. 4mm)
C
2-8mm (av. 6mm)
0.5 - 2.5 m (av. 1.0m)
1.3
10-25mm, (av. 18mm)
F
B
0.3 - 1.0 m (av. 0.5m)
1.2
10-25mm, (av. 18mm) Coalesced into lighter bands.
J

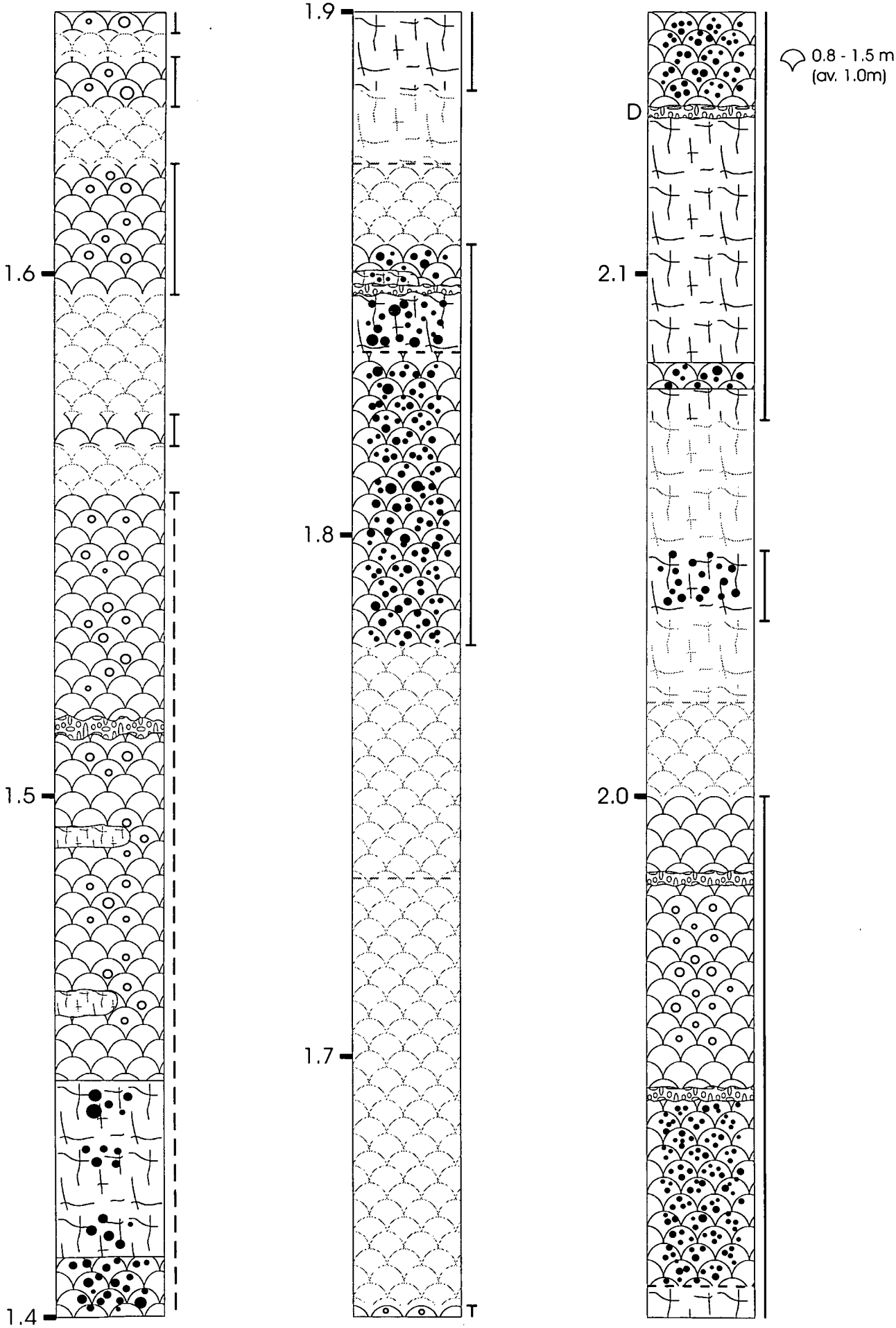
1.6
1.5
1.4
1.9
1.8
1.7
T
D
2.1
2.0
0.8 - 1.5 m
(av. 1.0m)

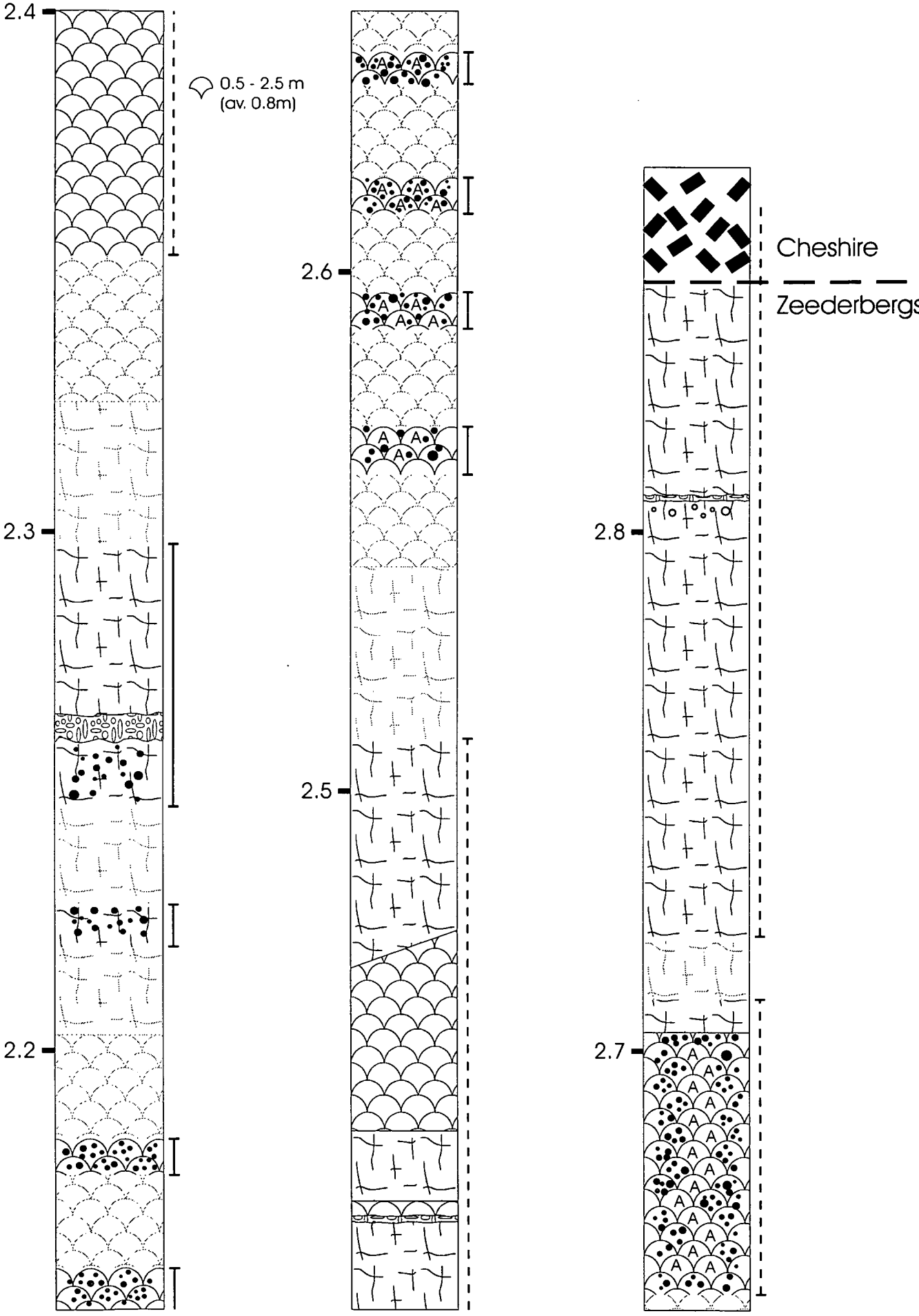
2.4
0.5 - 2.5 m
(av. 0.8m)
2.3
2.2
2.6
2.5
2.8
2.7
Cheshire
Zeederbergs

The Zeederbergs Formation has been described as 'sheared throughout' (Scholey, 1992), but there is very little evidence for this in the well preserved features seen in the type section. There is quite a high degree of fracturing and quartz veining throughout the succession, and the degree of alteration is variable but usually high (see Chapter 4), but there is little or no structural deformation in most of the section. 'Spheroids' are commonly seen in flow units, but are looked at in detail in Chapter 4, and will be only briefly mentioned here.

The lower contact of the Zeederbergs Formation is, as mentioned above (see §3.2.3), somewhat arbitrary, and is generally defined as a clear break in slope seen around the belt. The volcanic agglomerate marker horizon used to define the contact in the type section of the Reliance Formation is not exposed in the vicinity of the Ngezi River, but the break in slope and change in topography is quite clear (especially when seen on aerial photographs over several kilometres along strike), and the contact is assigned to an exposure gap in the river bed corresponding to this feature. The upper contact is clearly seen as abrupt transition from a massive volcanic unit into a coarse conglomerate unit (dominated by clasts from the underlying volcanics) at the base of the Cheshire Formation.

3.3.3 Flow unit morphology : Pillowed and massive units

The lava flows are mostly fine grained and medium to dark grey-green in colour. In the absence of any useful mineralogical differences the only distinction that can really be made in the field is between pillowed and massive textures in outcrop. It is quite probable that some of the massive units in the section are shallow sills, intruded contemporaneously with the rest of the section, but in the absence of any definite evidence (eg. the presence or absence of rubbly flow tops) it is impossible to be certain of the nature of any particular unit. There are no obvious geochemically discordant units (see §3.5), so this uncertainty does not seem to pose a significant problem in the interpretation of the section.

Plate 3.1

a) 'Pavement' of pillow lavas, Ngezi River section

A large, flat, outcrop displaying excellent pillow forms. Note the variation in pillow size and shape, the thinness of the inter-pillow material, and the remarkable lack of deformation. Morag Hunter kindly provides scale.

b) Conglomerate filled lava tube, Ngezi River section

A large pillow (>1.5m diameter) with a large internal lava drainage tube which has been subsequently filled with a coarse conglomerate (probably shortly after eruption). Lens cap = 60mm diam.

Plate 3.2
Amygdales in pillow lava, Ngezi River section

Writing on outcrop indicates top (T) and bottom (B) of pillow, together with younging direction arrow (-<). Note the calcite-filled 'pipe' amygdales around the edge of the central pillow, with no clear preference for top or bottom. Lens cap = 60mm diam.

The pillowed units show extremely well preserved textures, and there are several large expanses of pillowed 'pavement' (see Plate 3.1a). Pillow size ranges from about 20cm to 2.5m, and is usually in the range 0.4 - 1.2 m. In places the pillows have a clear cylindrical habit (a 'bolster' pillow shape), and all the units clearly young into the core of the syncline. Lava tubes in the centre of pillows, now collapsed and infilled by quartz mineralization (and, in one case, a coarse pebbly conglomerate (see Plate 3.1b) are quite common, and amygdales (in both ball and pipe morphologies) are seen in several units, often distributed around the edges of pillows, but not usually showing any clear preference for top or bottom (see Plate 3.2). The pillow skin is sometimes quite glassy, often a dark green colour, and usually heavily fractured (interpreted as associated with cooling).

Massive units are simply defined as those units which clearly cooled from a basaltic liquid, but which show no clear pillow structures (so obvious is their nature when present). In the absence of such structures the rocks are usually fairly featureless, and the outcrop texture is dominated by the pattern of fracturing and quartz veining. Some units are quite coarse (1-2mm average grain size), and a fining upwards pattern can be seen in some of the thicker units, interpreted as being a result of crystal settling during cooling (though whether in a sill or a thick flow is unclear, as mentioned above). A moderately coarse acicular texture, with needles up to 3mm in length, is sometimes discernible in the field, and is discussed in Chapter 4. 'Tongues' of massive material (a few metres thick) are often seen in the middle of a pillowed unit, and in places the break-up into pillows can be clearly distinguished.

In places it is possible to see basal structures to the flows. A lava channel cutting down through the underlying tuff is clearly visible at location A (Figure 3.3), where large blocks (<50cm) of tuff can be seen in the lower few metres of the pillowed flow, and pieces of pillow breaking off into the massive flow above are present at location B (Figure 3.3). 'Spheroids' are common in both pillowed and massive units, and are described in detail in Chapter 4. The distinctive andesitic horizon near the top of the section (see §3.5) has quite a different appearance. The pillows are generally about 0.8 - 1.2m in diameter, but the main difference is in the inter-pillow material, which is extremely thick (often 30 to 40cm or more), and resembles hyaloclastite material seen elsewhere in the section (see Plate 3.3b). 'Spheroids' are also noticeably different and more abundant in this horizon.

Plate 3.3

a) Hyaloclastite, Ngezi River section

Smooth, well rounded lobes of lava in a coarse clastic matrix. Note the distinctive pistachio green colour of the matrix, du to the presence of epidote and chlorite. Lens cap = 60mm diam.

b) Angular hyaloclastite, Ngezi River section. (Location C, Figure 3.3)

Angular blocks of solidified lava (thought to be broken off fragments of the unit below) in a fine grained matrix. Note the apparent softening and deformation of some of the blocks. Lens cap = 60mm diam.

3.3.4 Hyaloclastites

Hyaloclastites are reasonably common throughout the section, usually occurring as thin (mostly between 0.5m and 10m thick) horizons within or between pillowed and massive flow units. The most commonly seen type of hyaloclastite is made up of smooth, usually well rounded 'lobes' of lava (approximately 10cm - 60cm diameter) in a quite coarse clastic matrix (see Plate 3.3a). The lava 'lobes' are very similar to the material seen in the flow units (fine grained and medium to dark grey-green), and the matrix is a distinctive pistachio green colour (due to the presence of chlorite and epidote). These horizons usually have quite irregular top and bottom contacts, and are sometimes clearly associated with the top of massive 'tongues', or thicker massive flows, where they break up into pillows.

The thick hyaloclastite horizon at location C (Figure 3.3) is quite different to others seen in the section. Here the unit is dominated by angular blocks (5cm - 30cm +) in a fine grained matrix. The blocks are lava flow material, and are thought to be broken off fragments of the unit below. This interpretation is supported by the presence of very large (several metres across) broken off blocks of lava in the 5m of the horizon. Some of the blocks seem to have been softened and deformed slightly by their re-incorporation in a flowing lava (see Plate 3.3b). The whole unit is interpreted as a large lava and debris flow (G. Fitton, pers. comm., 1993). The hyaloclastite at location D is also slightly different to the norm, being a collection of small (<5cm) very angular fragments of lava in a fine black matrix, and closely resembles a modern flow top breccia (Cas and Wright, 1988).

3.3.5 Tuffaceous units

Tuffaceous horizons are quite common in the more well exposed parts of the section (between 0.7km and 1.4km), and it is thought that their absence from the rest of the section is more a function of exposure bias (the tuffs erode away more easily then the other units) than of physical absence. They usually occur in composite horizons of a few metres, and are mostly fine grained and a similar colour to the lava flows. Away from freshly water-washed surfaces the tuff layers appear strongly foliated and sheared parallel to bedding, and have been often interpreted in the past as shear zones (Nisbet *et al.*, 1993). On freshly eroded surfaces, none of the tuff horizons shows any shearing or deformation whatsoever, and clear sedimentary structures are extremely well preserved (see below). This raises doubts as to whether the units interpreted as shear zones, preferentially accommodating flexural slip associated with the folding of

the syncline, are in fact shear zones, or whether they just weather to give that appearance.

Clear sedimentary structures are seen in nearly all the tuff units. Bedding and lamination on a sub-mm to several cm scale is ubiquitous, and cross lamination is often seen (see Plate 3.4a). Some tuff units have clear basal conglomerates, mostly composed of angular fragments of the unit below (see Plate 3.5b). Graded sequences (from coarse sand size to fine ash) are common, as are sedimentary loading and water escape structures (see Plate 3.4b). At location E (Figure 3.3), a clear channel structure is seen (see Plate 3.5a). It is approximately 20cm deep, with nearly vertical sides, and lies in the middle of a composite tuff horizon about metre thick. It is filled with a coarse conglomerate, dominated by large (2-5cm) extremely angular clasts.

3.3.6 Intrusives

Excepting the possibility that some of the massive units are actually contemporaneous intrusive sills (see §3.3.3), intrusive bodies are rare in the Zeederbergs Formation in the Ngezi River and elsewhere. Two narrow (<2m) dykes are seen, composed of exactly the same material as the surrounding country rock, and are interpreted as minor feeder dykes to overlying flows. Four ultramafic sills are the only chemically distinctive units in the section. Two of them (location F) are only about 30cm thick, but the other two are several metres thick (locations G & H), and the samples taken seem to have originally been dominated by cumulus olivine (now very heavily altered to carbonate). The exact field relations of the bodies at G&H are hard to determine, as they are only present on one bank of the river, and appear to have been faulted into a zone of exposure on the opposite bank, but a pair of intrusive sills seems the most reasonable interpretation.

3.3.7 'Feeder vent' structure

At location J there are some interesting field relations which suggest the existence of a large feeder vent from one massive unit through to a higher level one. The bulk of the actual feeder vent is now the path of the river, and so is unexposed, but its margins, and the disruption caused to the adjacent units, can be clearly seen. These field relations are illustrated in Figure 3.4.

Plate 3.4

a) Cross laminated tuff, Ngezi River section

Cross lamination in a very fine-grained tuff unit. Note the coarser unit at the base of the picture. Lens cap = 60mm diam.

b) Water escape structure in tuff, Ngezi River section

Brecciation of overlying fine-grained unit due to de-watering of the coarser unit below. Note the fragments of the fine-grained unit (to the right of the arrow) in a matrix of the coarser material from beneath. Lens cap = 60mm diam.

Plate 3.5

a) Channel structure in tuff unit, Ngezi River section (location E, Figure 3.3)

A channel filled with coarse, angular volcaniclastic debris in a finer grained tuff unit. The lens cap is on the right hand edge of the channel, to the left of it is the coarse material, to the right of it if the fine-grained tuff. Note the extreme angularity of the material in the channel, and the steepness of the channel margin. Lens cap = 60mm diam.

b) Basal conglomerate in tuffaceous horizon, Ngezi River section

A basal conglomerate to a tuffaceous horizon, made up of angular clast of the unit below. Lens cap=60mm diam.

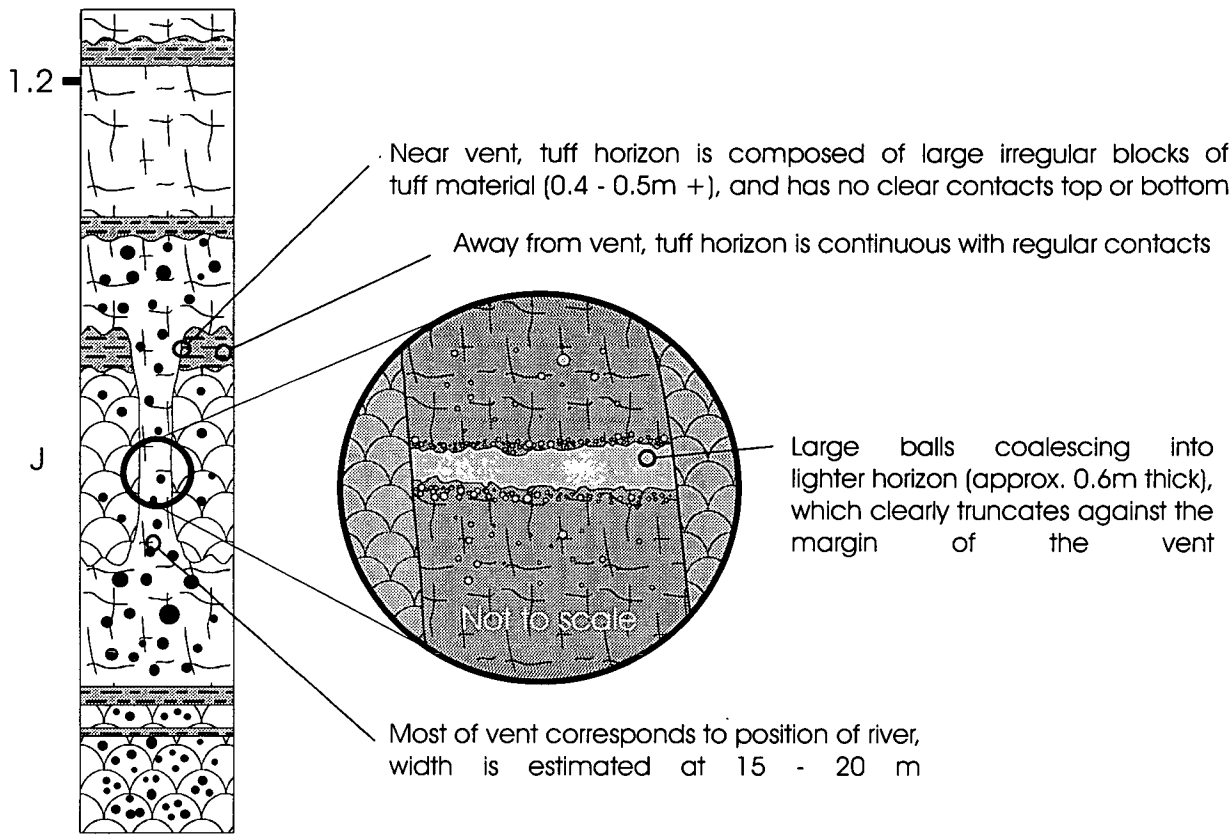

Figure 3.4.
Detail of field relations near the 'feeder vent' structure at location J

3.4 The Zeederbergs Formation elsewhere in the Belingwe greenstone belt

3.4.1 General Exposure

The general degree and quality of exposure of the Zeederbergs Formation around the rest of the belt is not high enough to allow mapping at the same level as in the Ngezi River. As mentioned above, most of the distinctions between units in the type section were based upon textures seen in reasonably large, water-washed outcrops, and are much less obvious elsewhere. Away from the river, the rocks all have a brown weathering crust up to a centimetre thick, and surface detail is often obscured. It is possible to recognise pillow structures, and sometimes tuffaceous units, but the apparent absence of such textures may well be a function of the exposure rather than whether they are actually there. The best exposures are still found along stream beds and road cuttings, and these determined the location of the other traverses. Three other sections were examined, and two were sampled in detail.

3.4.2 Main Road section

The main road between Zvishavane and Filabusi (to the west) cuts through the northern end of the syncline, and provides two sections through the Zeederbergs Formation (on the east and west side of the syncline) separated by a thin section through the overlying Cheshire Formation in the core of the syncline. There are approximately 20 roadside cuttings along the 8km stretch of road, and often reasonably large outcrops have been generated. These sections were examined briefly by Scholey (1992), but the quality and intermittent nature of the outcrop make them unsuitable for use in this study.

3.4.3 Vanguard Road section

In the south-west of the belt, an unsurfaced road provides a convenient site for a traverse through the Zeederbergs Formation on the western side of the syncline. The name is derived from the proximity of the section to the Vanguard asbestos mine to the west. The section is approximately 5km from base to top, but as very few clear dip angles could be measured, the exact thickness of the formation can not be calculated. The base of the section is marked by a $\approx$200m thick dolerite sill. The degree of exposure within 100m or so of the road allows a small enough sample spacing (<200m) for the section to be used in this study, and 37 samples were collected.

Pillow structures were occasionally clearly seen, as were tuffaceous horizons (including one quite felsic one near the top of the section, see §3.5). Some flow units contained spheroids or amygdales, and were all generally very similar to those seen in the Ngezi River.

3.4.4 Spring Valley section

The Spring Valley section followed, for most of its length, two small stream beds, flowing east and west from the centre of the ridge formed by the Zeederbergs Formation. The name is derived from the Spring Valley farm just to the north-east. The section is approximately 4.5km from base to top, but, again, no dips were measurable, and so no accurate thickness can be calculated. The base of the section is seen as a clear transition from ultramafic pillows (MgO > 21wt%) of the Reliance Formation to tholeiitic basalts of the Zeederbergs Formation, and is actually a few hundred metres above its position on the Geological Survey map of the region (the Belingwe - Shabani sheet). However, correlation of geochemical marker horizons between the three sections works best if the base of the section is defined by its position on the map. The mapping of this region was based on widely spaced traverses, with the Zeederbergs - Reliance contact mapped on a regional scale from air photos (as a clear break in slope), and variation from this placement is interpreted as surface relief on the top of the Reliance Formation. It is thought that the Zeederbergs formation blanketed this surface, progressively infilling any relief, and so it is possible that the lower parts of the formation are absent from those areas which corresponded to positive relief on the top of the Reliance Formation.

3.5 Chemical stratigraphy

3.5.1 Overview

The Ngezi River section has a considerably higher sample density (mostly on an individual flow unit basis) than the other two sections, and most of the chemical stratigraphy is based upon features seen in this section and then subsequently recognised elsewhere. The obvious existence of two distinct lava types was first recognised as a result of examination of the chemical stratigraphy, and the detailed study of their differences and similarities form a major part of this thesis. This detailed work is reported in Chapter 6, however, and the purpose of this section is simply to establish the existence of these two types, and to establish the lateral continuity of their respective horizons. Similarly, detailed studies on the more evolved rocks are also discussed in Chapter 6, and will only be briefly mentioned here. Five parameters are used to define the chemical stratigraphy of the formation (Figures 3.5 to 3.9). An exhaustive chemical description is not considered necessary here.

3.5.2 The use of 'Level', or relative stratigraphic height

To enable direct comparison of the chemical variation with height within the formation in the three different sections, some way of correcting for the different inclination (and hence the different apparent thickness) of these sections was needed. As no clear dip measurements were possible in the Vanguard Road and the Spring Valley sections, a direct correction was not possible, so the idea of using relative height within the section, or 'Level', was conceived. Quite simply, the level of a sample in a section is the horizontal distance of that sample from the base of the section (measured perpendicular to the strike of the contact) normalised to the horizontal width of the formation in that section. This effectively gives each sample a dimensionless position in the formation with a value between 0 and 100.

It is acknowledged that there are certain assumptions made when using this technique, such as constant dip and strike within a section, which may not be perfectly justifiable, but the match of the three chemical profiles from the different sections suggests that it provides a valid comparison. Figures 3.5 to 3.9 all use level as a measure of stratigraphic height, and all consist of three separate plots (corresponding to the three different sections) and a combined plot, with all three sections overlain on the same axes.

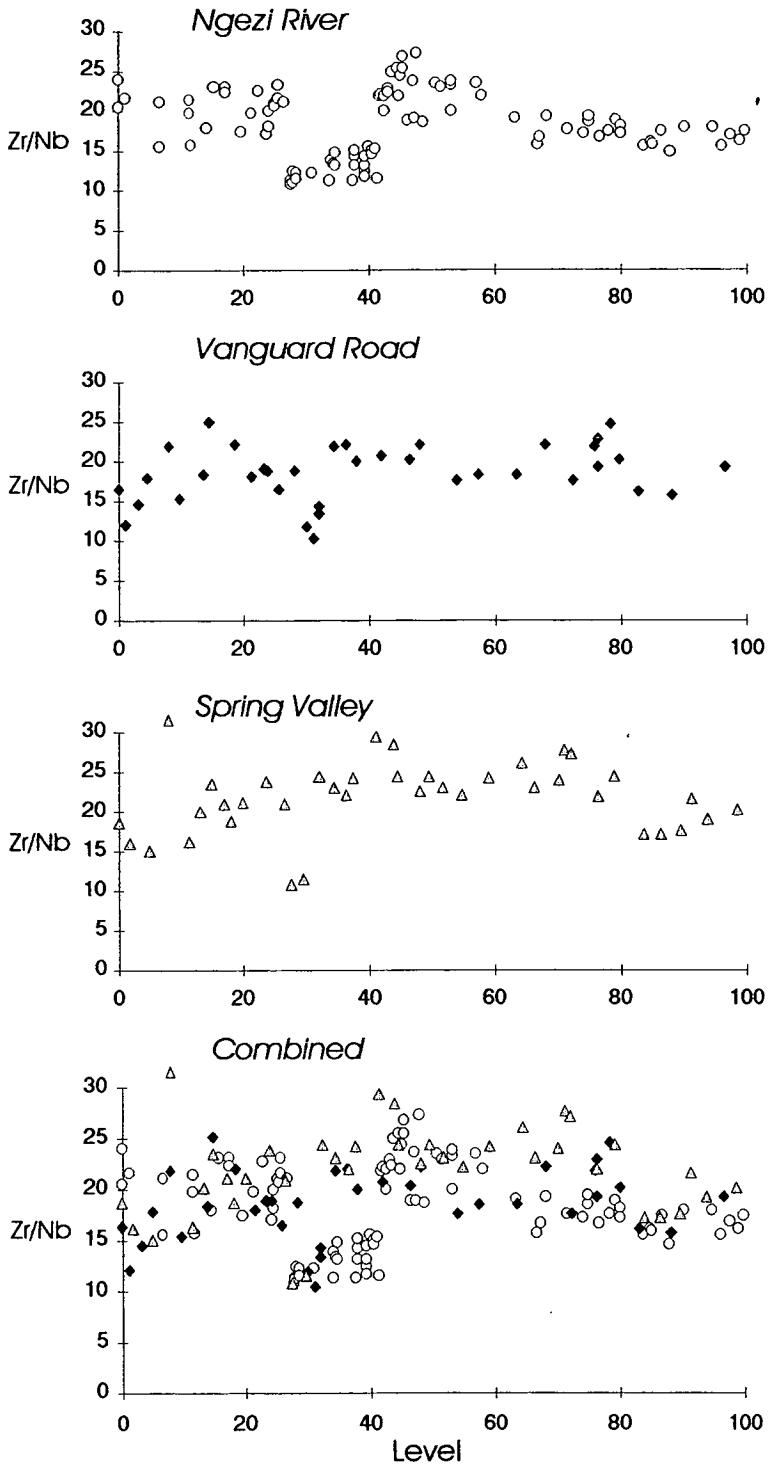

Figure 3.5. Variation of Zr/Nb ratio with level in section for the three sections used in this study. Markers on the *Combined* plot correspond to the markers used on the individual plots. All samples are included. See text for explanation of 'Level'.

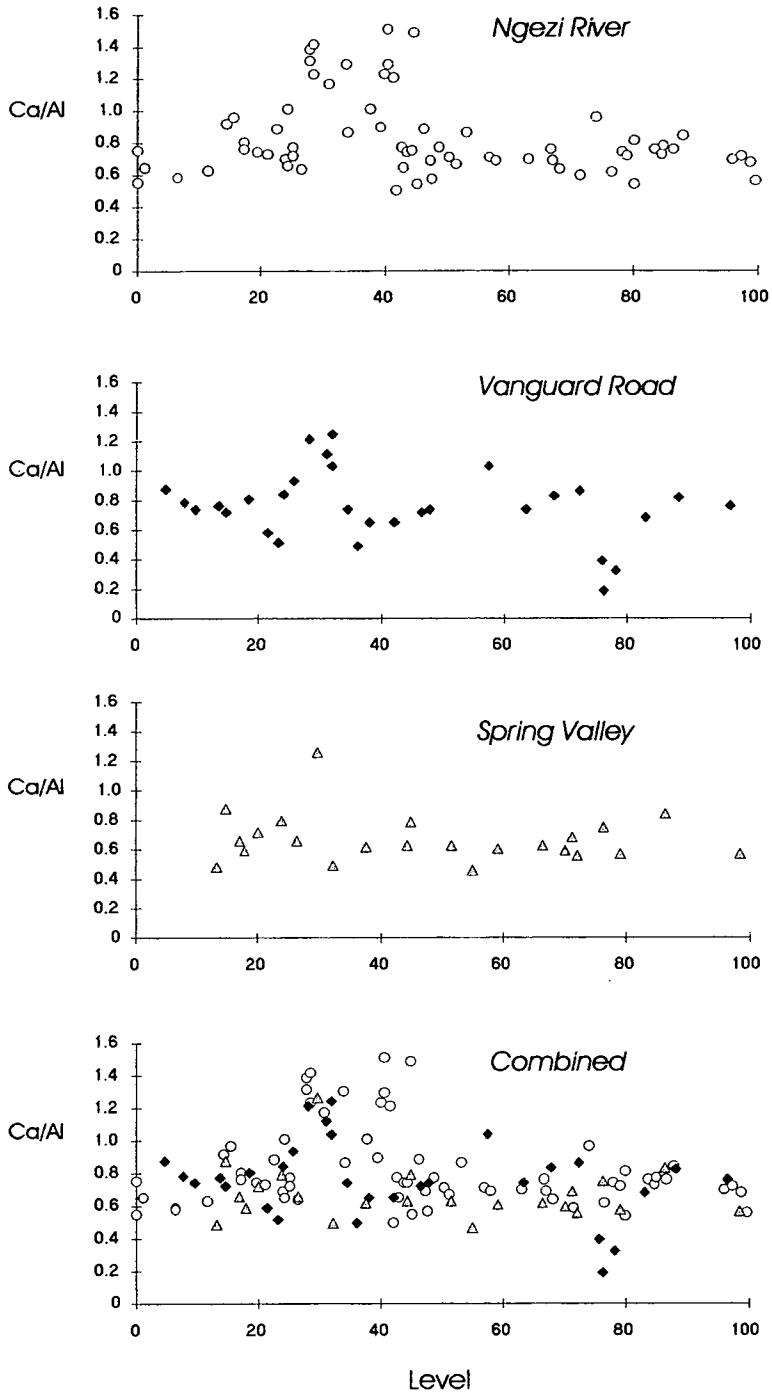

Figure 3.6. Variation of CaO/Al_2O_3 ratio with level in section for the three sections used in this study. Markers on the *Combined* plot correspond to the markers used on the individual plots. Samples have been screened to remove tuffs and heavily altered lavas (see Chapter 5). See text for explanation of 'Level'.

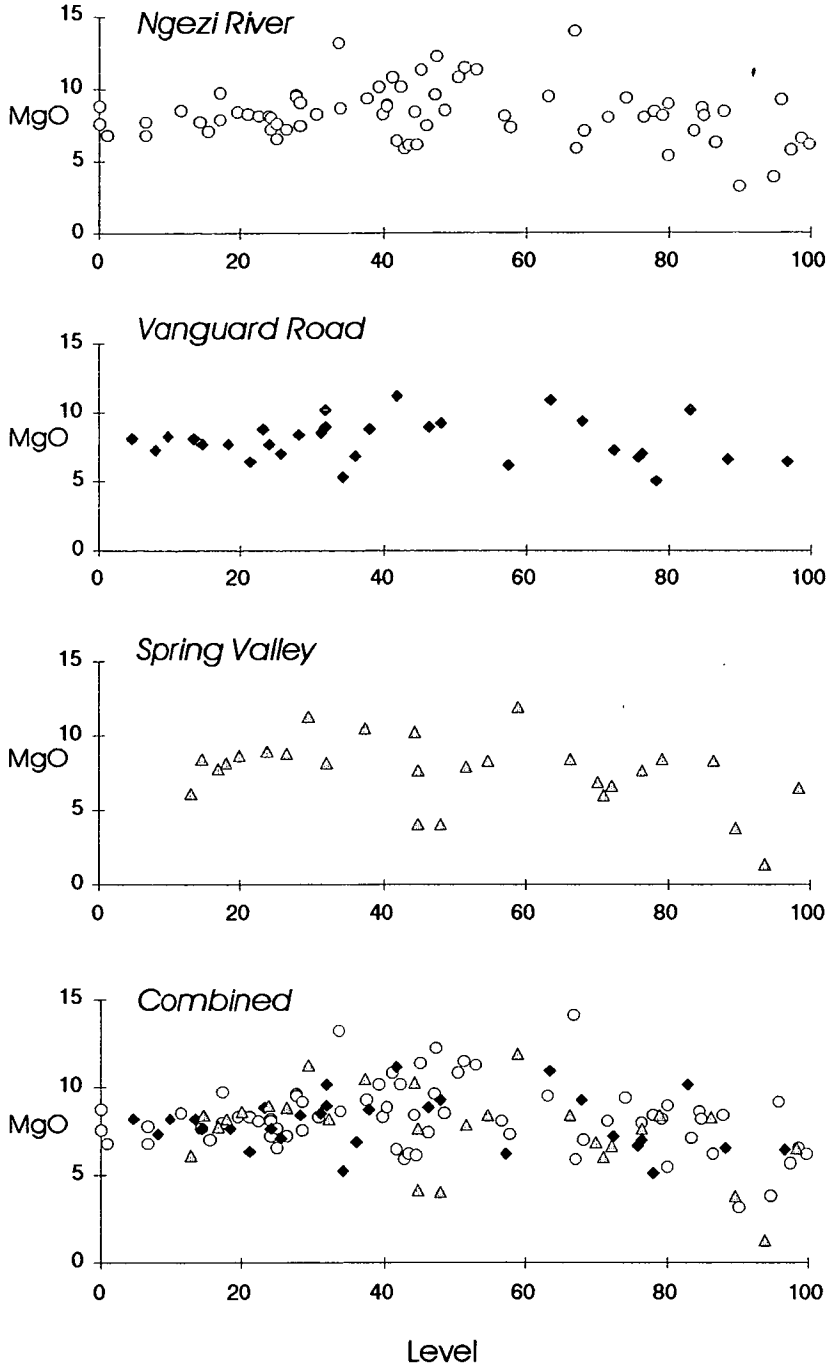

Figure 3.7. Variation of MgO with level in section for the three sections used in this study. Markers on the *Combined* plot correspond to the markers used on the individual plots. Samples have been screened to remove tuffs and heavily altered lavas (see Chapter 5). See text for explanation of 'Level'.

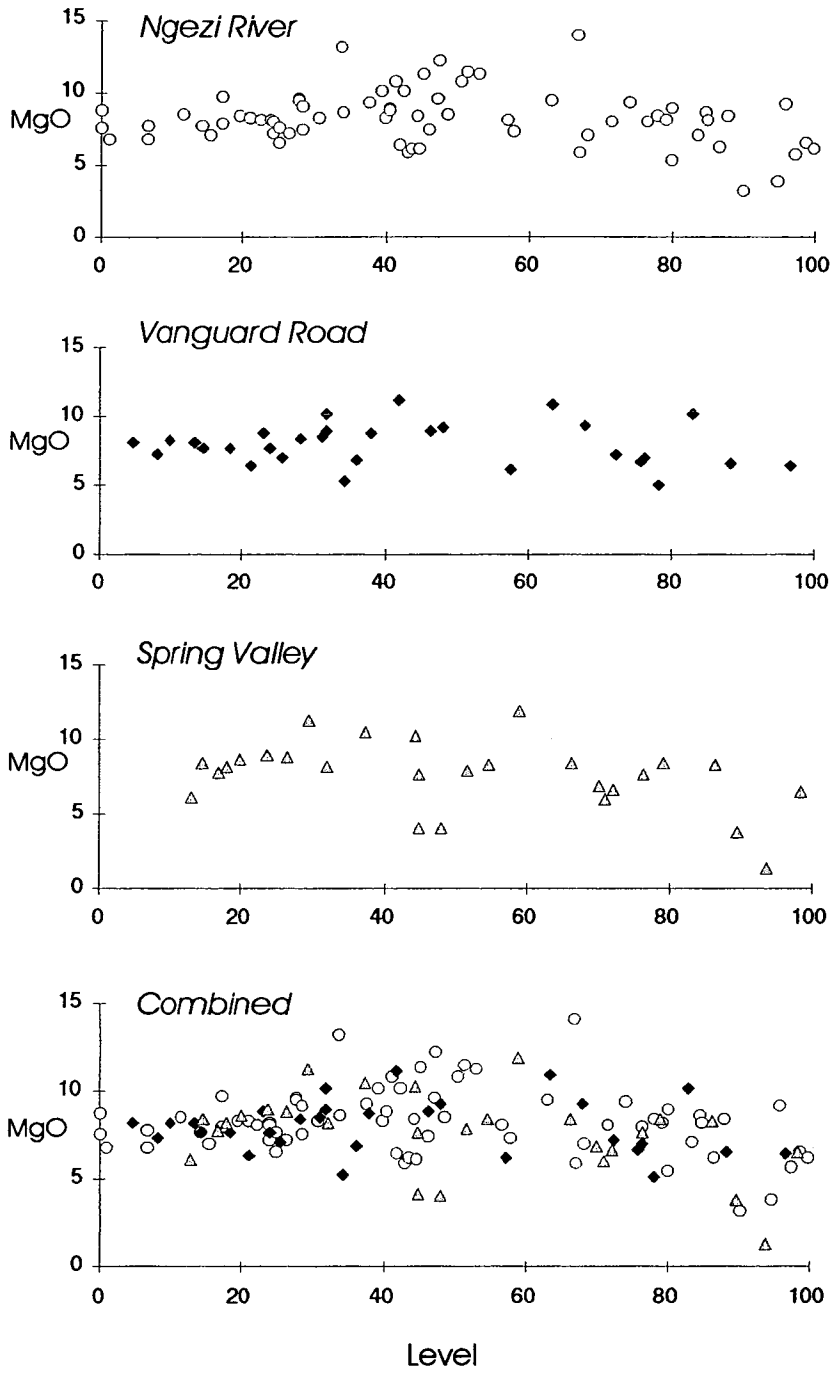

Figure 3.7. Variation of MgO with level in section for the three sections used in this study. Markers on the *Combined* plot correspond to the markers used on the individual plots. Samples have been screened to remove tuffs and heavily altered lavas (see Chapter 5). See text for explanation of 'Level'.

3.5.3 Variation in Zr/Nb

Zr/Nb is a useful indicator of primary trace element characteristics, as both Zr and Nb are relatively immobile (see Chapter 5) and both can be accurately measured by XRF (see Appendix 2). The variation in Zr/Nb within the Zeederbergs Formation is shown in Figure 3.5. In the Ngezi River section, the existence of a horizon of lower Zr/Nb ratios than the rest of the section between levels 25 and 40 is quite clear, and has been marked on the log of this section (Figure 3.3). The transitions from high to low Zr/Nb at the top and bottom of this horizon are very sudden, and correspond to a single tuff unit (and therefore possibly a brief hiatus in volcanic activity) in each case. Similar (but clearly thinner) horizons of lower Zr/Nb are seen in the Vanguard Road and Spring Valley sections at approximately the same level. This would suggest that this horizon is not a localised or alteration phenomenon, but forms a layer within the lava pile which is laterally continuous over at least 15 - 20 km.

3.5.4 Variation in CaO/Al_2O_3

The variation of CaO/Al_2O_3 within the Zeederbergs Formation is shown in Figure 3.6. The significance of this ratio is in its possible implications for parental magmas, and is discussed more fully in Chapters 6 & 7, it is sufficient here to point out the obviously similar (if inverted) pattern to the one seen in Zr/Nb. The samples which show low Zr/Nb generally show higher CaO/Al_2O_3 than those from the rest of the section. It is important to note that not all samples are shown in Figure 3.6, as CaO and Al_2O_3 concentrations are liable to alteration, and those samples with potentially altered values have been removed through the screening methods detailed in Chapter 5. The major influence on this ratio is actually the Al_2O_3 content of the lavas, which is significantly lower in those lavas with low Zr/Nb (see Chapter 6).

3.5.5 Variation in MgO

The variation of MgO within the Zeederbergs Formation is shown in Figure 3.7. The important feature to note is that the horizon of low Zr/Nb lavas does not show up in this variation, and is therefore not a simple function of magma evolution from the same parent. There is generally very little discernible correlation in the MgO stratigraphy between sections, with the only clear similarity being the horizon of more evolved lavas (lower MgO contents) at a level of 90 -95 in the Ngezi River and Spring Valley sections.

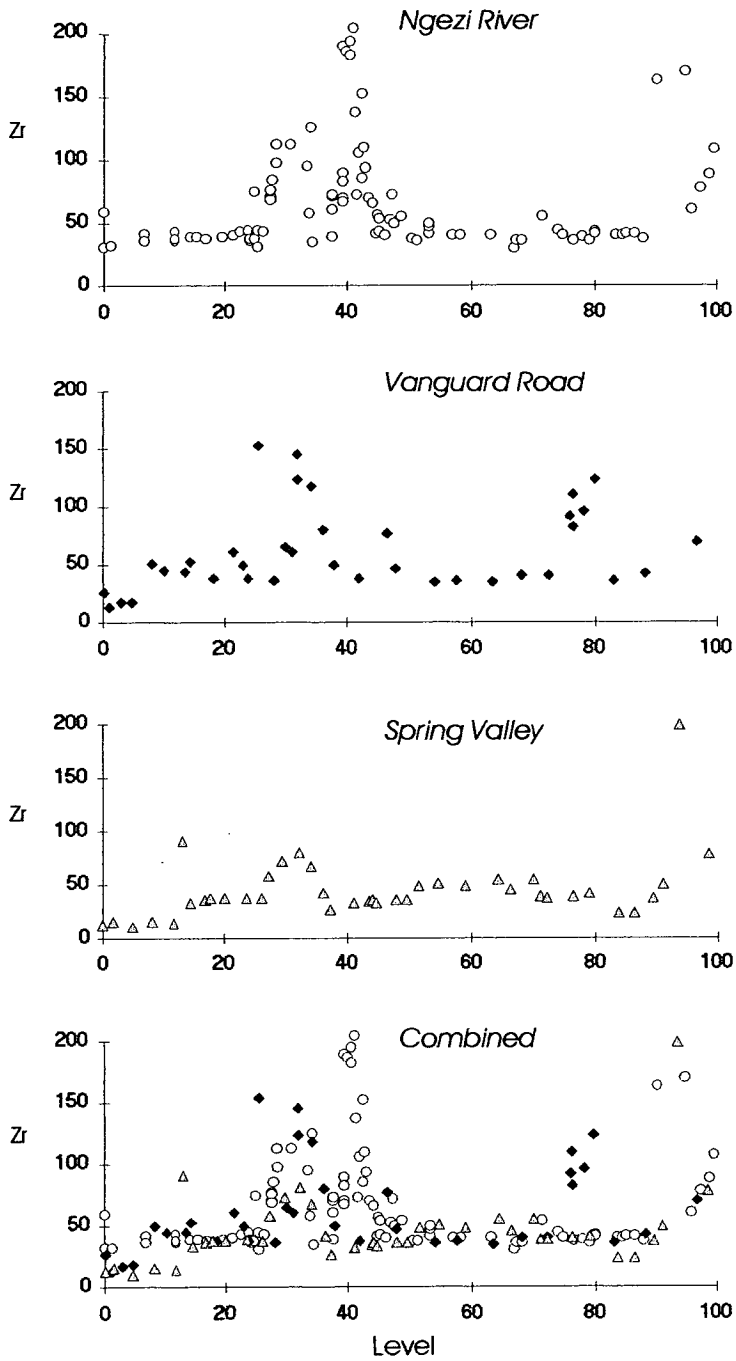

Figure 3.8. Variation of Zr with level in section for the three sections used in this study. Markers on the *Combined* plot correspond to the markers used on the individual plots. All samples are included. See text for explanation of 'Level'.

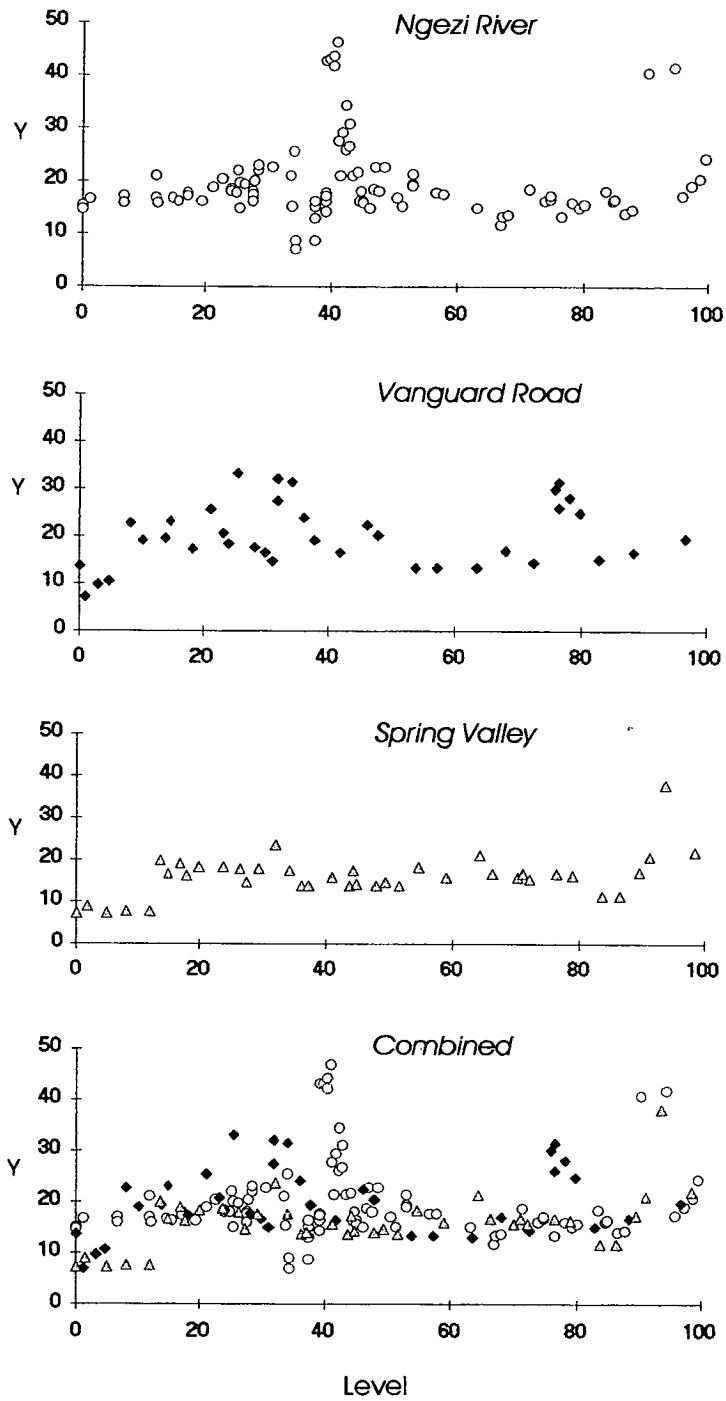

Figure 3.9. Variation of Y with level in section for the three sections used in this study. Markers on the *Combined* plot correspond to the markers used on the individual plots. All samples are included. See text for explanation of 'Level'.

3.5.6 Variation in Zr and Y

Zr and Y are chosen as representative of incompatible trace element behaviour because they are relatively immobile (see Chapter 5), and both are present in easily measurable concentrations. The stratigraphic variation for both elements (shown in Figures 3.8 and 3.9) is quite similar, though is perhaps a little more pronounced for Zr than for Y. Higher concentrations are seen in all sections at the level of the low MgO content lavas, which would be expected for an incompatible element in a fractionating magma system. More surprising, however, is that there is also a very significant increase in concentrations in those sample with a lower Zr/Nb.

3.5.7 Summary, the classification of Type I and Type II lavas, and the thickness of the Zeederbergs Formation

The most significant feature of the chemical stratigraphy is the existence of a distinct horizon of lavas with lower Zr/Nb and higher CaO/Al_2O_3 and incompatible trace element concentrations than the rest of the formation. 'Normal' lavas, from the rest of the succession, are classified as type I , and lavas from the low Zr/Nb horizon are classified as type II. There is no apparent systematic difference between the two types in MgO contents. The horizon of type II lavas is seen to be laterally continuous over at least 15 - 20km (the distance between the sections) The existence of a thin horizon of more evolved rocks near the top of the formation is also suggested by the low MgO and high incompatible trace element concentrations.

The fact that these horizons exist in all three sections, at approximately the same relative stratigraphic position, suggests that all three sections are complete. The only section with common, reliably measurable dip indicators is the Ngezi River, where the entire sequence appears to be approximately vertical. The horizontal width (and, correspondingly, the vertical thickness) of the formation in this section is just under 3km (see Figure 3.3), which would seem to suggest that this is in fact the true thickness of the formation in the greenstone belt. The other sections (and, indeed, the majority of exposure of the formation around the belt) show a greater thickness simply because of a lower inclination. In the past, the thickness of the Zeederbergs formation has been quoted as 5-6km, an estimate based on the average width of the formation around the belt, and assuming the Ngezi River section to represent an incomplete succession (with shear zones to account for the missing section). The detailed geochemical work presented in this chapter suggests that this is not the case, and the detailed field observations suggest

that the 'shear zones' apparently seen in this section are in fact fairly undeformed tuff horizons, which simply give that appearance in weathered outcrop (see §3.3.5).

3.6 Conclusions

- The basal contact of the Reliance Formation is conformable on the sediments of the underlying Manjeri Formation, and there is no conclusive evidence for any removal of section from the Reliance Formation in any part of the belt. Consequently, the interpretation of the Ngezi Group volcanics as a tectonically emplaced allochthon would seem to be invalid.

- The Zeederbergs Formation is predominantly composed of pillow lavas, with some massive flow units, and minor tuff and hyaloclastite horizons. The vast majority of the lavas were clearly erupted under water, and all the tuffs show shallow marine sedimentary structures.

- Correlation of distinct geochemical marker horizons around the belt, and accurate logging of the Ngezi River type section suggest that the true thickness of the Zeederbergs Formation is only ≈3km, rather than the 5-6km usually quoted. No evidence was found for removal of section in the Ngezi River type section.

- This good correlation of geochemical marker horizons around the belt also suggests that there has been no tectonic removal of section from the Zeederbergs Formation, which supports the interpretation of the volcanic sequence as erupted *in situ*, rather than tectonically emplaced.

- There is an apparently continuous horizon of clearly geochemically distinct lavas present in the Zeederbergs Formation, about a third of the way up the section, present around the belt. These lavas have lower Zr/Nb ratios and higher CaO/Al_2O_3 ratios and Zr & Y abundances than the majority of the Zeederbergs Formation lavas. They have been called Type II lavas, and the rest of the Zeederbergs lavas are known as Type I lavas.

- There is a thin horizon of more evolved material (andesitic) near the top of all three sections through the Zeederbergs Formation.

4

PETROGRAPHY

4.1 Introduction

Before examining their geochemistry, it is important to establish a petrographic framework for the lavas of the Ngezi Group. This is actually less important for study of the Zeederbergs Formation lavas than it is for those of the Reliance Formation, as there is much less variation within the formation. It is, however, still necessary to consider it, and to see if there are any physical differences between the Type I and Type II lavas.

The petrography of the Reliance Formation lavas has received a great deal of attention, and classification of these lavas is based upon their petrography. This classification scheme is summarised and a brief description of the mineralogy of the formation is given. A general petrographic description of the Zeederbergs Formation lavas is adequate for most of the formation. A description of the mineralogy of the common phases is given, and the less typical rocks in the formation are described separately.

The final section considers a specific feature of the Ngezi Group lavas common to many Archaean lavas, described variously as 'ocelli' or 'varioles' and referred to here as 'spheroids'. A summary of previous ideas on the origins of these features is given and their occurrence in the Zeederbergs Formation is considered in terms of their origins and petrogenetic implications.

4.2 The Reliance Formation

4.2.1 General Overview

The rocks of the Reliance Formation generally show good preservation of mineralogy for a greenstone belt volcanic suite. In some samples, the preservation is remarkable, and samples containing fresh olivine and even fresh volcanic glass have been found in the SASKMAR drillhole (e.g. Nisbet *et al.*, 1987). Usually, however, the primary

assemblages have been at least partially replaced by metamorphic assemblages associated with conditions up to mid-greenschist facies, but the original textures are frequently very well preserved. Scholey (1992) gives an exhaustive account of the petrography of the Reliance Formation, and the reader is referred to this for a more complete description, this section being essentially a summary of that work.

There are a large number of terms used to describe and classify Archaean ultramafic and mafic volcanic rocks, with various petrographic, geochemical and genetic connotations. The classification scheme considered (Scholey, 1992) to be most appropriate to the Reliance Formation is one based upon descriptive mineralogical and textural criteria (after MacKenzie *et al.*, 1984). Geochemically based schemes (e.g. Arndt and Brooks, 1980; Arndt and Nisbet, 1982a), usually variants on the theme of basalt, komatiitic (or high-magnesium) basalt, and komatiite, are sometimes a little arbitrary when applied to individual suites, and are difficult to apply reliably in the field. The classification scheme (Table 4.1) of Scholey (1992) divides the rocks of the formation into four varieties:

- mafic and related types
- high-magnesium basalts
- komatiites
- peridotitic cumulates

Primary phases and textures are referred to as if the rock were unaltered, regardless of its current mineralogy of the rock (a convention suggested by Thompson (1983)).

4.2.2 Mineralogy

Olivine has commonly been heavily altered by hydrothermal activity, metamorphism and pervasive tropical weathering, but unaltered olivines have been recovered from two locations, and olivine morphologies are often still clearly recognisable in altered samples. Granular, poly- or euhedral, hopper, bladed, plate- and chain-like habits are all seen[1], and the compositions of olivine spinifex grains are commonly thought to reflect the primary liquid composition (e.g. Bickle, 1982), though it has been suggested that they represent a 'type of crescumulate fabric' (Scholey, 1992). Unaltered olivines from the SASKMAR drillsite (Nisbet *et al.*, 1987; Renner, 1989;

[1]Terminology from Scholey (1992), modified after that of Donaldson (1982), related to effects of cooling rate and degree of super-cooling.

Bickle *et al.*, 1993; Renner *et al., 1994)* show compositions from $Fo_{92.0-88.7}$ (cores) to Fo_{84} (rims) in spinifex-textured samples, and $Fo_{93.6-91.2}$ in cumulus olivines. Granular crystals from the basal cumulate in Hall's Unit (a compound cooling unit described in great detail by Scholey (1992)) show compositions of $Fo_{83.4-79.4}$.

Table 4.1. Rock types in the Reliance Formation: classification and characteristics (from Scholey, 1992)

Rock type/texture	(Micro)phenocrysts: phase: abundance; size (mm); habit	Matrix phases and textures
MAFIC AND RELATED TYPES:		
Tholeiite (extrusive) **Dolerite** (intrusive)	pl: <40%; <1, some <2; laths cp: <30%; <2, some <6; prism., poik. (both sometimes glomerophric) rt: <5%; <1; anh.-subh., mostly skel.	pl-cp-gl-qz; inequigranular, usually sub-ophitic to intersertal in basalt, (sub)ophitic in dolerite
Pyroxene-phyric variolitic-textured basalt	cp: <30%; <3; prism.-clmr. op? (→ct): rare; <2; euh. prisms ol: rare; <0.5; euh.	pl-cp-gl-qz-(rt); commonly variolitic - spherulitic, otherwise inequigranular
Tuffs	pl-cp-mt: usually <5%, rarely <25%; <0.5, some <4.0; fragments	near-holohyaline with cryptocrystalline fragments
HIGH-MAGNESIUM BASALTS:		
Pyroxene microspinifex and hyaline textures	cp: <50%; <10, diam <0.1; acic.	semi-radiating to parallel sheaves, plumose and dendritic crystallites and felty intergrowths of cp in gl
Random pyroxene-phyric and spinifex textures **'String-beef' pyroxene spinifex textures**	cp: <50%; diam 0.5-1.0; clmr./blocky, usually skel., zoned (sub-calcic, pigeonite core to augitic rim); randomly-oriented to fanned (laterally-linked) in random types, sub-parallel in optically-continuous domains in 'string beef'	gl-cp-(pl); hyaline or microspinifex-textured matrix
Olivine spinifex textures	ol: <25%; 0.5-2.0 x 2-10 x <25; parallel to semi-radiating plates or chains, sub-perpendicular to flow margin	cp-gl; microspinifex-textured
Porphyritic types	ol: <30%; diam <2.0, rarely >0.5; euh., hopper and bladed	cp-gl; microspinifex-textured
KOMATIITES (porphyritic):	ol: 30-40%; diam. <2.0, rarely >0.5; euh., hopper and bladed	cp-gl; microspinifex-textured
PERIDOTITIC CUMULATES: (terminology from Pyke *et al.*, 1973)		
B_2 zone (ortho- and adcumulates)	ol: 40-90%; <1, some <10; gran., euh. cp-(op): <5%; diam. <0.5; clmr., acic.	cp-gl; microspinifex textured
B_1 zone (horizontally-aligned)	cp: <50%; diam. <1; clmr., acic. ol: <25%?; diam. <1; hopper, plate	cp-gl; microspinifex textured
Transitional B - A zone	ol: <50%; usually <1; gran. - euh. - hopper, bladed	cp-gl; microspinifex textured

Abbreviations: ol: olivine, cp: clinopyroxene, op: orthopyroxene, pl: plagioclase, qz: quartz, rt: rutile, mt: magnetite, gl: glass; euh., subh. and anh.: eu-, sub- and anhedral; gran.: granular, prism.: prismatic, clmr.: columnar, acic.: acicular, skel.: skeletal,

Pyroxenes are generally better preserved, with the bulk of compositions ranging from salite through augite to ferroaugite. Clinopyroxene spinifex textures are characteristically made up of 'blocky, hollow or skeletal columns with a sub-calcic or pigeonite core and augitic rim' (Scholey, 1992). These sometimes occur in optically-continuous parallel growth sheaves ('string-beef' texture), and chain, dendritic and

feathery morphologies are also seen. There are some (rare) phenocrysts pseudomorphed by chlorite and clinozoisite which may have been orthopyroxenes (Scholey 1992), but orthopyroxene is generally absent from the rocks of the formation.

Fine laths and rare microphenocrysts of plagioclase are found in some mafic rocks in the formation, but its crystallisation is generally suppressed, and any normative feldspar forms a component of the glassy matrix. Chromite was often the first crystallising phase in many of the ultramafic rocks, with clusters of chromite grains (often with overgrowth rims of magnetite) quite common, and magnetite, pyrite and rutile are all often found in the mafic rocks of the formation. Mafic and ultramafic volcanic rocks often have a devitrified glassy matrix composed largely of pyroxene and plagioclase, and commonly altered to a fine-grained aggregate dominated by chlorite, amphibole and serpentine.

Alteration assemblages are generally hydrated. Olivine is usually replaced by serpentine and chlorite (and sometimes tremolite). Clinopyroxenes may be wholly or partially altered to amphibole, mostly actinolite (pigeonite rims in spinifex crystals are altered to chlorite). Plagioclase is commonly replaced by albite (with clinozoisite inclusions), and quartz is often present, occasionally as a primary phase (in less mafic rocks) but is generally interpreted as a replacement product after devitrified glass (with chlorite and clinozoisite).

4.2.3 Textural features

The textural basis of Scholey's classification is described in detail in Table 4.1, but a few additional comments are considered necessary. 'Mafic and related type' rocks are often aphanitic, and 'pyroxene-phyric variolitic textured basalt' is only distinguishable in the field if heavily porphyritic, whilst tuffs are usually identifiable by the presence of cross-lamination, or other sedimentary structures. Most olivine spinifex textured rocks in the Reliance Formation have MgO contents of 15-18%, making them 'high-magnesium' basalts rather than true komatiites, according to the definition of Arndt & Nisbet (1982a). Porphyritic komatiites which do not show spinifex textures are still clearly volcanic, as demonstrated by their pillowed, lobed and thin flow morphologies, and do therefore still satisfy Arndt & Nisbet's (1982a) definition of a komatiite as an 'ultramafic (MgO > 18%), volcanic rock. The habit of the olivine in these rocks is very much controlled by their relative position in the individual flow unit.

4.3 Mineralogy of the Zeederbergs Formation basalts

4.3.1 General Description

The basalts of the Zeederbergs Formation are generally fine grained, hyalocrystalline, and moderately to sparsely porphyritic. The dominant phenocryst phase is clinopyroxene (often altered), though occasional laths of plagioclase are found, especially in the few slightly coarser grained rocks (usually forming a subophitic intergrowth with clinopyroxene). No fresh olivines are seen in the formation, and possible relict grains are very rare. Sphene is quite common, and rutile and chromite are also found. Groundmass textures range from devitrified & altered holohyaline to holocrystalline, and comprise largely clinopyroxene (often as variolitic sprays), plagioclase (often as fine microlitic needles), and quartz (potentially an alteration phenomenon). The degree of alteration is extremely variable, but some degree of recrystallisation is ubiquitous. Pyroxenes are altered to tremolite-actinolite (or occasionally to clinozoisite and quartz), plagioclase is usually albitised, and the groundmass is altered to aggregates of albite, quartz, amphibole, chlorite, and often epidote and clinozoisite. Locally some rocks may be heavily calcitised, and veining (usually quartz, but occasionally calcite) is common.

In the classification scheme of Scholey (1992), described above, most of the rocks of the Zeederbergs Formation would be classed as 'mafic and related types', with possibly some 'high-magnesium basalts'. This distinction is based upon the presence or absence of plagioclase, and the compositional fields of the two types overlap considerably. The highest MgO content seen in the Zeederbergs lavas is about 14%, and there is little or no relation between presence or absence of plagioclase and composition (in the range 7 - 15% MgO). In addition, no subdivision was possible in the field as nearly all the rocks are aphanitic. It was therefore decided not to attempt any sub-division of the mafic lavas of the Zeederbergs Formation, beyond the chemical distinction between Type I and Type II lavas.

Plate 4.1

Clinopyroxene Morphology

a) Clinopyroxene glomerocrysts

Large clinopyroxene phenocrysts clustered in a glomerophyric texture in a fine-grained groundmass of clinopyroxene, plagioclase and devitrified glass.
XPL. Field of view = 4mm. Sample CBZ 173

b) Variolitic spray of clinopyroxene

Variolitic groundmass texture of clinopyroxene with some plagioclase.
XPL. Field of view = 4mm. Sample CBZ 037

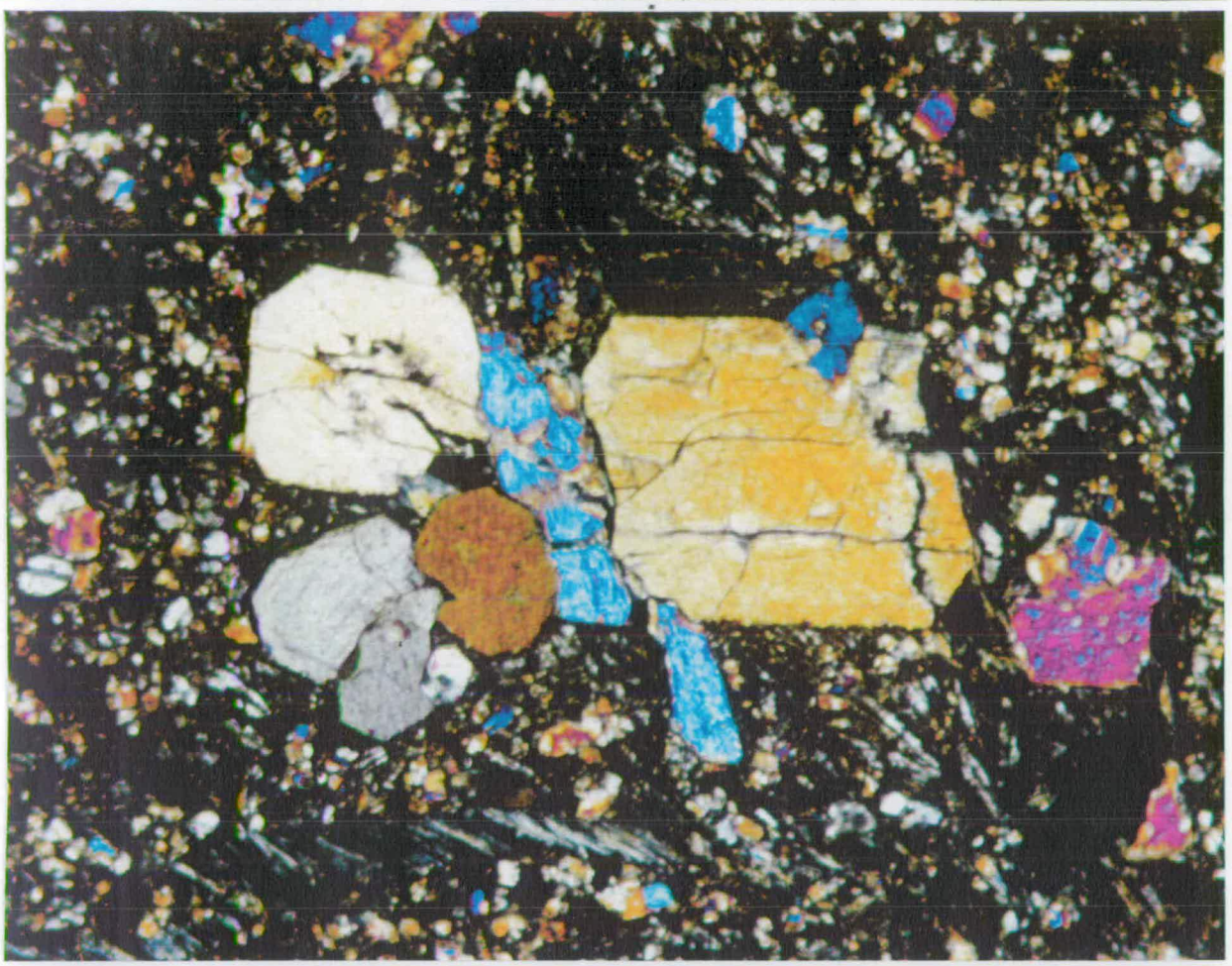

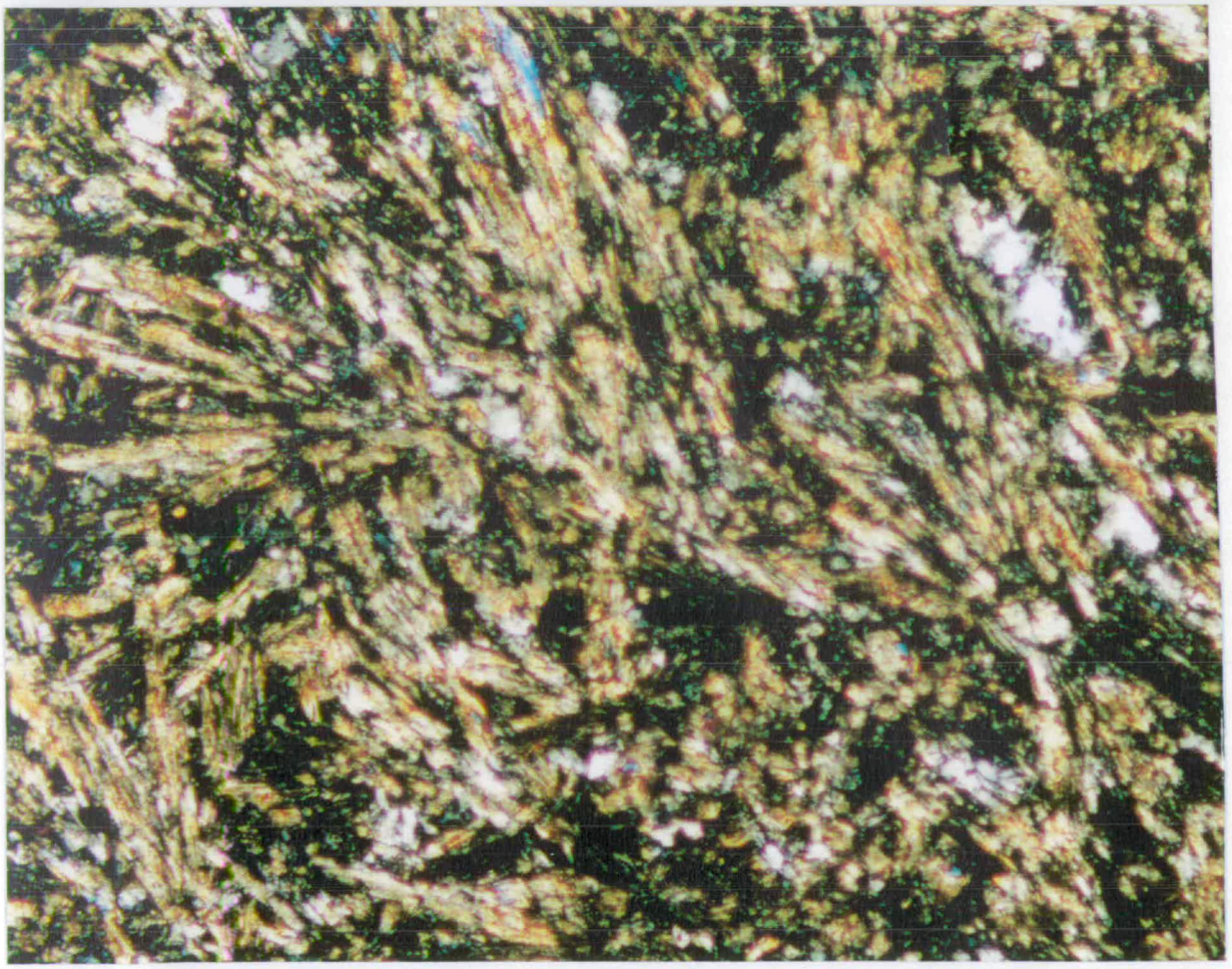

Plate 4.2

Plagioclase morphology

a) Subophitic intergrowth of plagioclase and clinopyroxene

A moderately coarse groundmass texture showing a subophitic intergrowth of plagioclase and clinopyroxene. Much of the clinopyroxene has been altered to amphibole. Note the presence of epidote (high birefringence, right of centre) and clinozoisite (anomalous blue colour, left of centre).
XPL. Field of view = 4mm. Sample CBZ 187

b) Microlitic plagioclase

Microlitic needles of plagioclase in a devitrified glass groundmass.
PPL. Field of view = 4mm. Sample CBZ 162

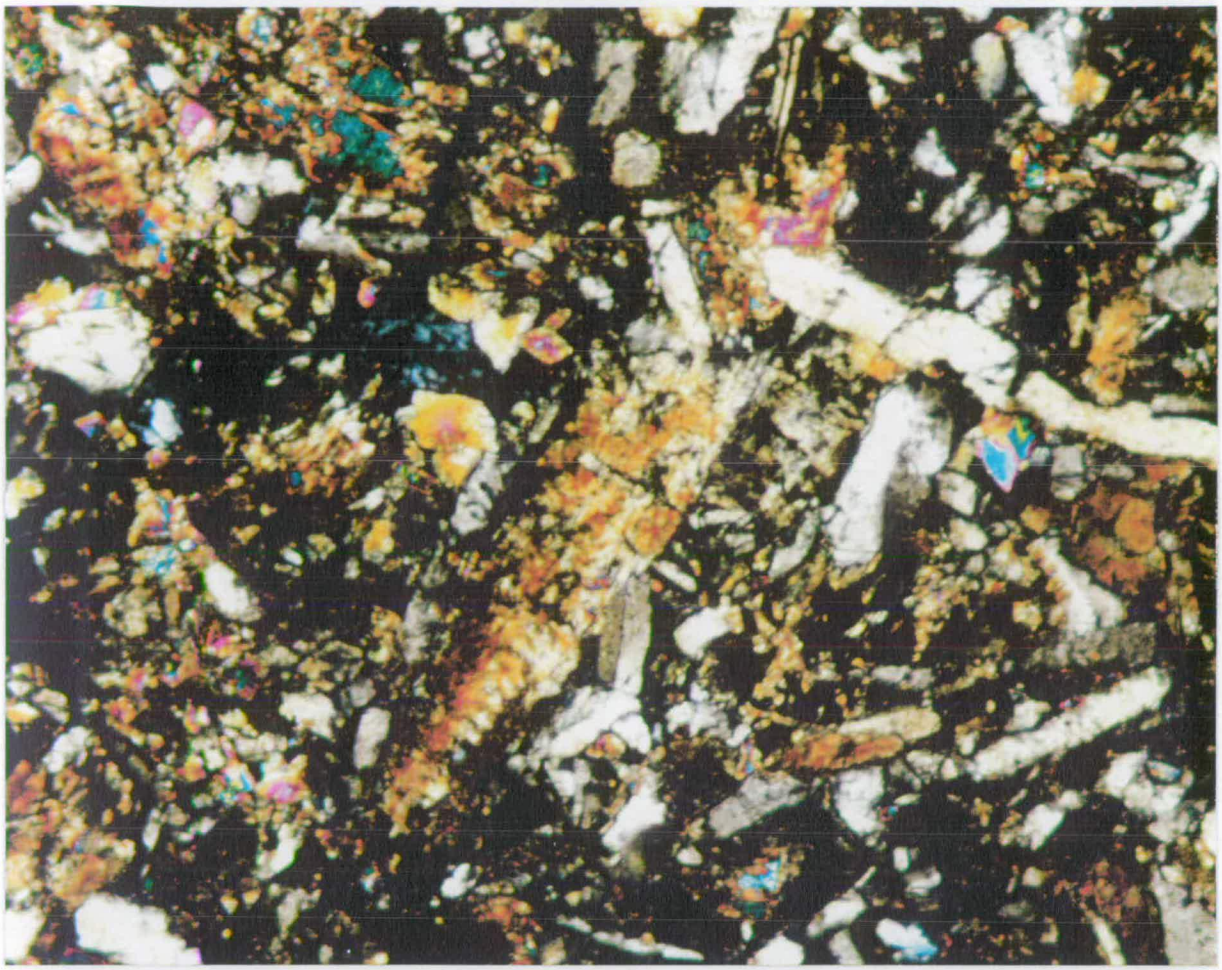

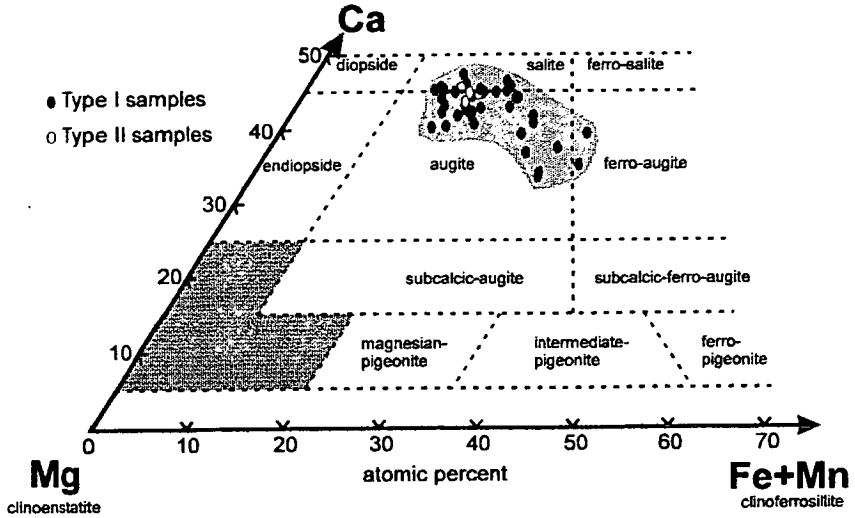

Figure 4.1 Pyroxene compositions from the Zeederbergs Formation. Data from 58 analyses presented in Appendix A5, projected in the En-Fs-Wo ternary (after Poldevaart and Hess, 1951; Deer, Howie and Zussman, 1966).

4.3.2 Pyroxenes

Clinopyroxene is the only common phenocryst phase in the rocks of the formation, and usually occurs as small (mostly <0.5mm), equant, reasonably euhedral grains. Larger grains are seen, but mostly in more generally coarse-grained rocks (possibly contemporary intrusive dolerite, see §3.3.3). Where the rocks are noticeably porphyritic, the percentage of phenocrysts rarely exceeds 30%, and is generally less than 20%, and the pyroxenes may sometimes be clustered in a glomerophyric texture. All the pyroxenes analysed were either augite or ferroaugite (Figure 4.1), with no systematic difference between those from Type I and Type II lavas, and no evidence of any orthopyroxene. Some grains show a small degree of compositional variation, usually with a slightly more iron-rich rim. The clinopyroxenes are commonly still very fresh, but may be altered to amphibole (tremolite - actinolite) or composite assemblages including (variably) chlorite, epidote, clinozoisite and quartz. Groundmass clinopyroxene occurs as fine crystal aggregates or in variolitic sprays (often with plagioclase). Typical clinopyroxene morphologies are shown in Plate 4.1

4.3.3 Plagioclase

Plagioclase phenocrysts are relatively rare, but small laths are sometimes found, mostly in slightly coarser grained or more evolved rocks, commonly forming a subophitic intergrowth with clinopyroxene. The majority of plagioclase has been altered to albite (<10% An), but the few fresh grains analysed were bytownite (70-

80% An) in composition. None of the Type II lavas seemed to contain any plagioclase, but since it is not ubiquitous in the Type I lavas little significance can be attached to this observation. Very fine microlitic needles of plagioclase (mostly <0.5mm long) are commonly found in the groundmass, especially if glassy, and the plagioclase sometimes forms variolitic sprays with clinopyroxene. Typical plagioclase morphologies are shown in Plate 4.2

4.3.4 Accessory phases

Small grains of sphene are commonly found in many lavas, small grains of rutile are also often present, and occasional grains of chromite and magnetite are found. It is possible that some of the quartz grains are primary, especially in the more evolved rocks, but the majority are thought to be formed by post-eruptive processes.

4.3.5 Glass and cryptocrystalline matrix

The basalts usually have a very fine-grained (often cryptocrystalline) or glassy matrix. Where crystalline, it is composed of an equigranular aggregate of clinopyroxene and plagioclase (sometimes in a variolitic texture), quite often with quartz. This is often altered to low greenschist assemblages including chlorite, amphibole (actinolite), albite, epidote and clinozoisite. Where the matrix was originally glassy, it has devitrified to a partially opaque dirty brown material, which often contains tiny plagioclase microlites. Semi-quantitative EDS analysis suggests that this material is now largely albite, quartz and pyroxene, with tiny grains of epidote.

4.3.6 Alteration phases

The alteration phases in the Zeederbergs Formation are very similar to those in the Reliance Formation, being generally hydrated, low-greenschist facies mineral assemblages. Clinopyroxenes alter to amphiboles (mostly actinolite) or aggregates of chlorite epidote-group minerals and quartz. Plagioclase is mostly altered to albite, and the groundmass material alters to an assemblage of chlorite, amphibole and epidote group minerals. Quartz is common, and is generally thought to be secondary, probably a product of post eruptive silica mobility, not necessarily associated with the greenschist event. There is no petrographic evidence for large scale chemical mobility, but it is important to note that many of the subsequent conclusions of this thesis are conditional upon this lack of mobility. Typical alteration phase assemblages and morphologies are shown in Plate 4.3

Plate 4.3

Secondary Phases

a) Chlorite and epidote

Large area of chlorite (pale green in PPL, anomalous deep blue in XPL) with several crystals of epidote (euhedral, high relief, very high birefringence) around the edge.
PPL on left, XPL on right. Field of view = 4mm. Sample CBZ 187

b) Clinozoisite

Two patches of clinozoisite (anomalous blue birefringence colours) immediately left and right of centre.
XPL. Field of view = 4mm. Sample CBZ 035B

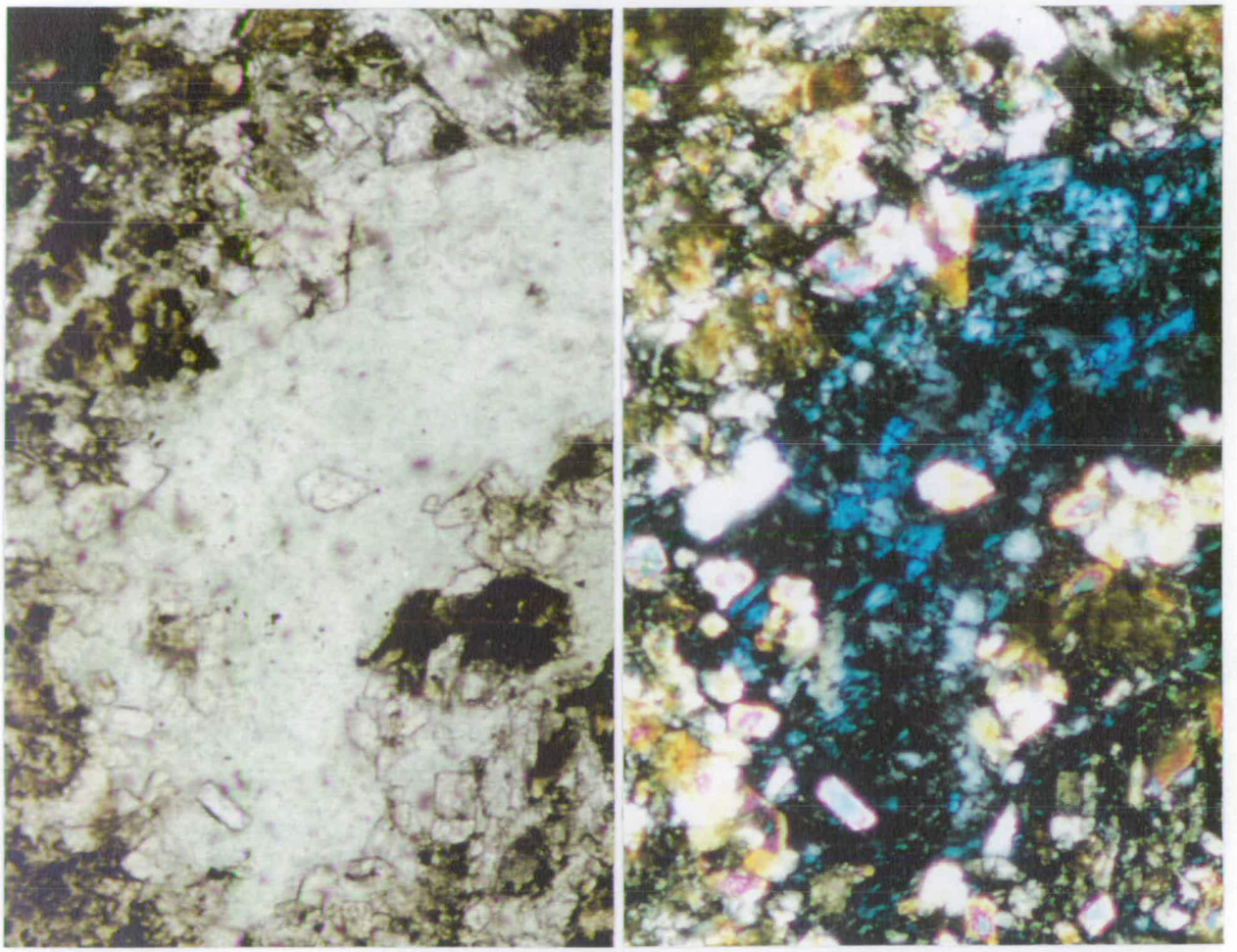

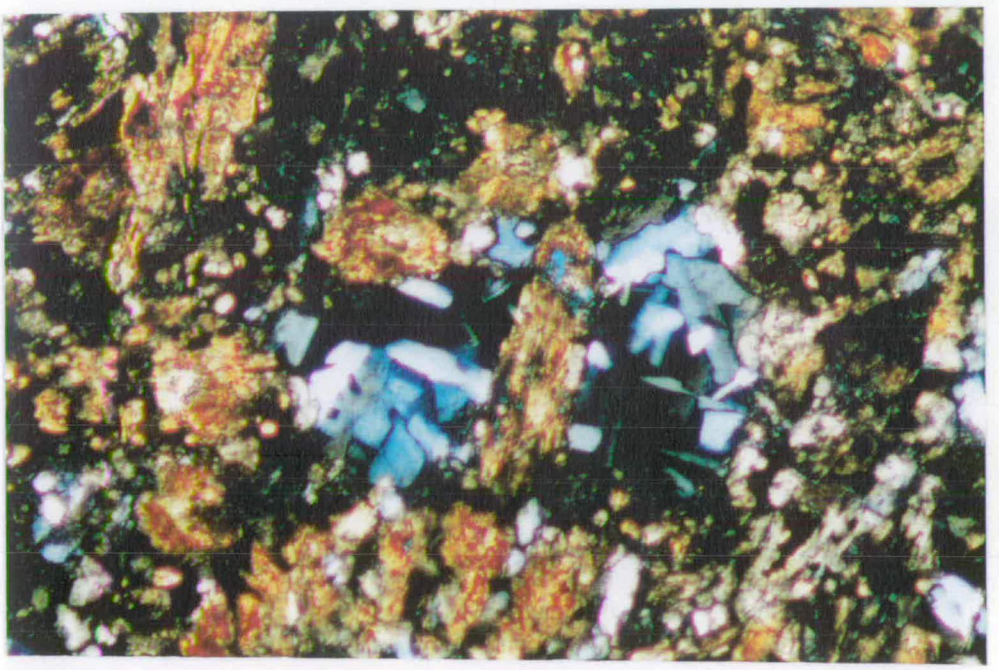

4.4 Other rocks in the Zeederbergs Formation

4.4.3 More evolved rocks

The andesitic horizon near the top of the formation has quite a different appearance to most of the rocks of the formation. In the pillowed unit in the Ngezi River (location C in Figure 3.3., see §3.3.3), the most obvious features are the very high percentage of 'spheroids' (>70% in most of the outcrops), and the great thickness of the inter-pillow hyaloclastite material (see description in §4.4.3), often 30-40cm or more, which in thin section resembles the matrix material in many of the hyaloclastites (see §4.4.3). The actual pillows are mainly glassy (now recrystallised, see §4.3.5) in texture, with very few phenocrysts.

4.4.2 Tuffs

A description of the outcrop-scale sedimentary structures found in most tuffs is given in §3.3.5. In thin section, they are fine to medium grained; cryptocrystalline when fine, and clearly composed of rounded, glassy fragments and rare angular lapilli (mostly clinopyroxene) when medium-grained. They display the usual recrystallisation to albite-quartz-chlorite-amphibole-clinozoisite assemblages. There is no evidence of any shear fabric in any of the thin sections examined. Typical tuff textures are shown in Plate 4.4.

4.4.3 Hyaloclastites

An outcrop scale description of the hyaloclastite units is given in §3.3.4. In thin section the hyaloclastites range from textures very similar to the fine grained basalts to textures similar to the tuff units. Lithic fragments (lava 'lobes', or angular blocks, sometimes tuff) appear exactly the same as their type rocks do *in situ*. The matrix material is variable, and ranges from cryptocrystalline aggregates (similar to those in fine-grained basalts), through fine-grained tuffaceous fabrics, to coarse clastic textures similar to those seen in the coarser tuff units. These coarser clastic textures often contain large, slightly deformed glassy globules. As usual, re-crystallisation to a low greenschist assemblage is the norm. A typical hyaloclastite texture is shown in Plate 4.5b.

Plate 4.4

Tuffs

a) Coarse tuff

A typical coarse tuff composed of larger lithic fragments and some single crystals (mostly clinopyroxene). Note lack of any indication of shearing or deformation.
XPL. Field of view = 15mm. Sample CBZ 215

b) Fine tuff

A typical fine tuff. Individual grains indistinguishable. Note lack of any shearing or evidence of deformation.
XPL. Field of view = 15mm. Sample CBZ 168

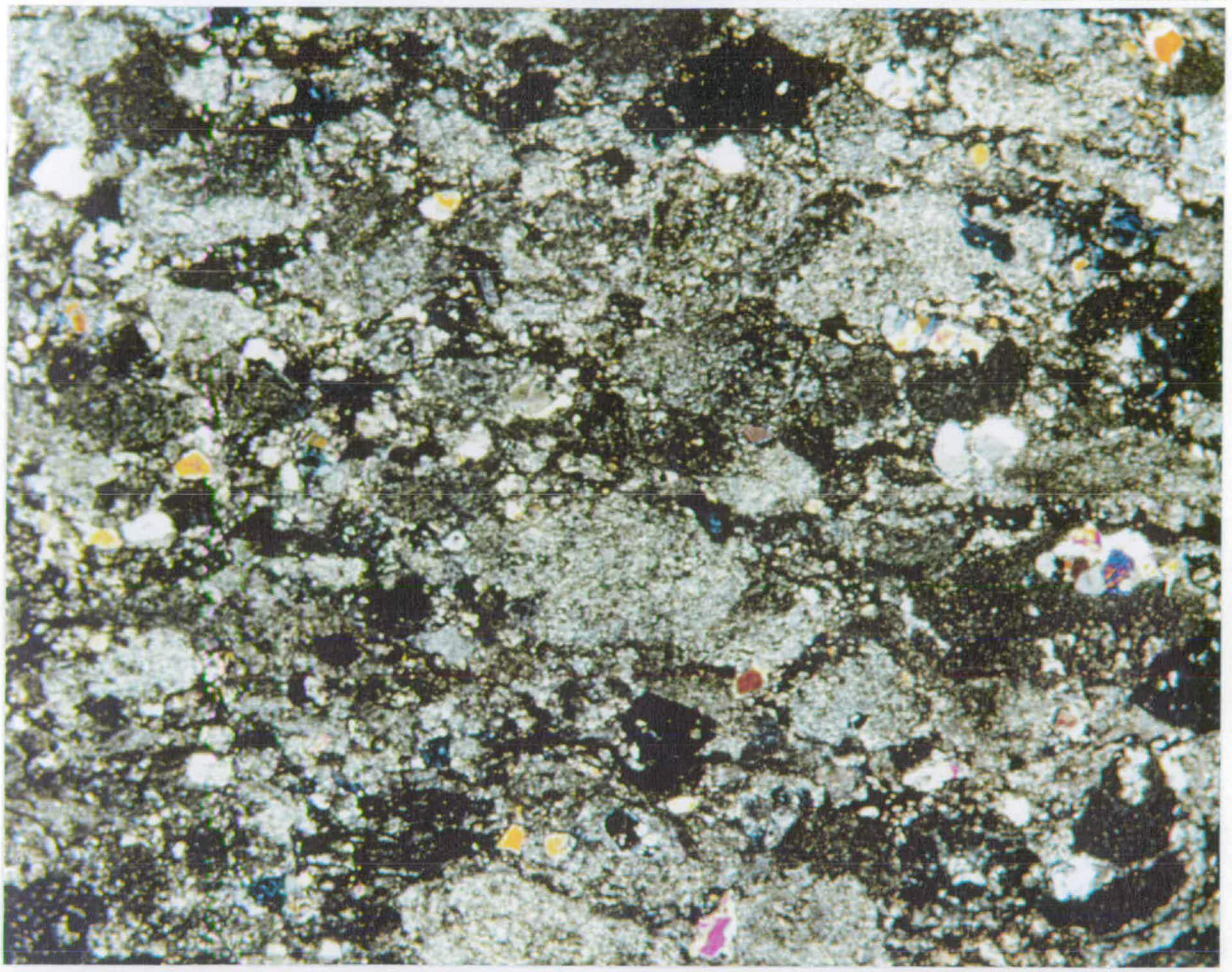

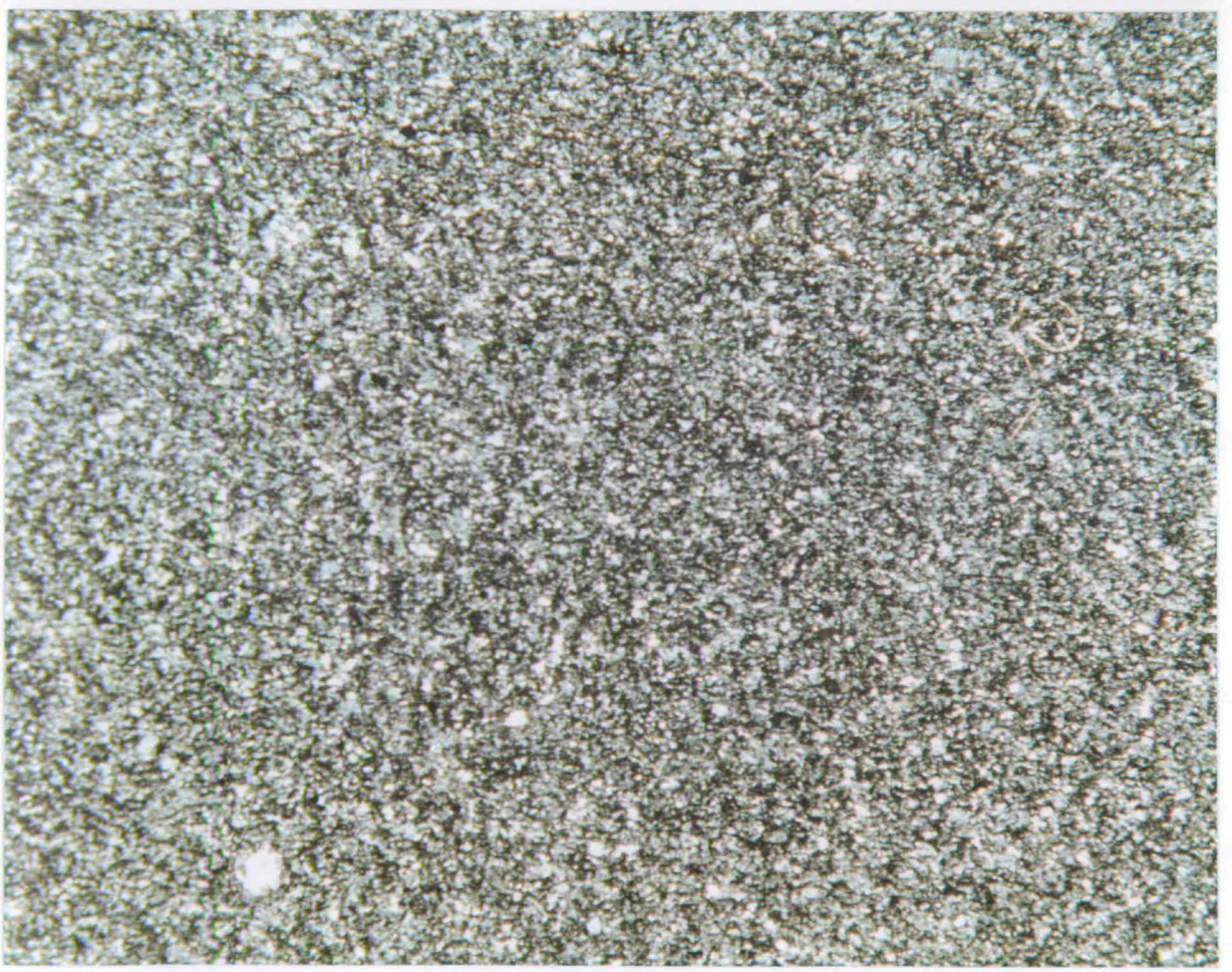

Plate 4.5

Other Textures

a) Cumulate texture

Coarse cumulate texture. Originally olivine, but now mostly altered to calcite. Note the presence of ilmenite (black specks).
PPL. Field of view = 4mm. Sample CBZ 177

b) Hyaloclastite

Typical hyaloclastite texture. Larger, amorphous, heavily fractured & altered lumps in a more 'flowing' matrix (now mostly chlorite).
PPL. Field of View = 15mm. Sample CBZ 160

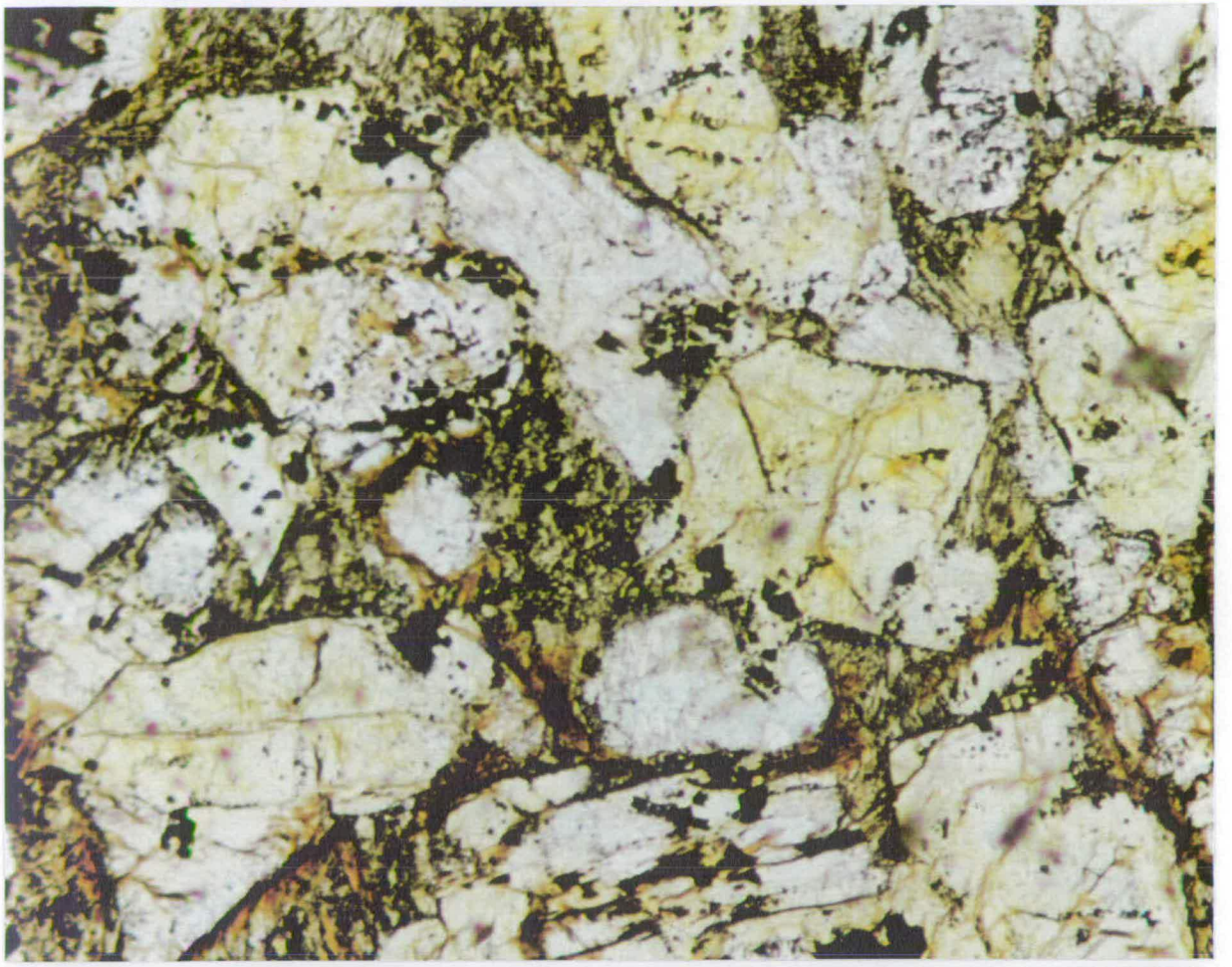

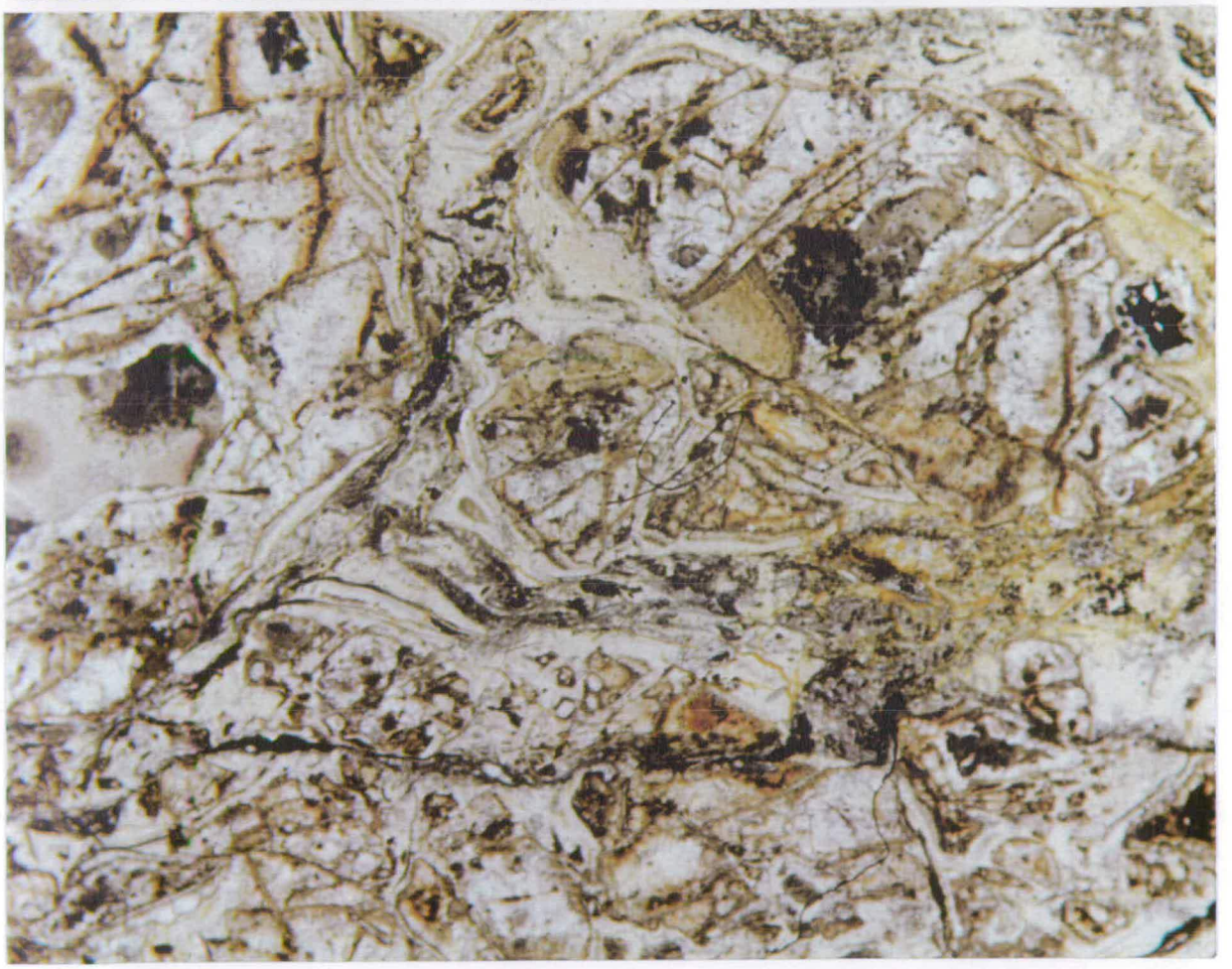

4.4.4 Intrusives

Intrusive bodies are rare in the formation, and often those that are seen are identical to the rest of the sequence, and therefore interpreted as feeder bodies to overlying flows. Two clearly distinct types of intrusive rocks are, however, clearly seen in the Ngezi River section at locations F, G and H (Figure 3.3). The thin sills at location F consist of clinopyroxene and pseudomorphs after olivine phenocrysts in a microcrystalline matrix, mainly clinopyroxene. The bodies at G and H are a little more unusual, and display what appears to be quite a coarse olivine cumulus texture, but are now nearly totally altered to carbonate (shown in Plate 4.5a).

4.5 'Spheroids'

4.5.1 Introduction

A common feature of the Zeederbergs Formation basalts are lighter coloured spheroidal structures, between about 3 and 8 mm in diameter, and often coalesced into larger areas of lighter material. Similar structures are quite common and well documented in Archaean basalts and komatiitic basalts, and have been given several different names. Unfortunately, the names used all have genetic implications for these features, when their exact origins are still not clear. Consequently, the non-genetic term 'spheroids' is used here to avoid any contradictions in terminology.

This study focuses on the origins of the spheroids in the Zeederbergs Formation lavas, and whether they have any bearing on the petrogenetic history of these lavas. The conclusions of this work may not be generally applicable to similar structures seen elsewhere, though the careful approach to classification of these structures would possibly be valuable in other areas.

4.5.2 Nomenclature

Three names have been used to describe similar lighter spherical features in Archaean basalts, and each has distinct implications for the origin of the structures:

- ***Ocellus (pl. ocelli).*** This term was applied, without genetic implication to a radial or tangential arrangement of prismatic or platy crystals around a larger, euhedral crystal of some other mineral (e.g. MacKenzie *et al.*, 1982). The first suggestion that the term should be applied to spheroidal structures thought to represent globules of immiscible liquid in Archaean lavas was by Hughes (1977), though in fact he disagreed with this explanation for their origin.
- ***Varioles.*** This seems to have been the first name used to describe pale coloured spheroidal structures in Archaean lavas. Gélinas *et al.* (1976) used the term to describe structures in tholeiites from the Abitibi region which they attributed to liquid immiscibility as a result of unmixing during cooling. Hughes (1977) disagreed with this conclusion, but pointed out that if this were their true origin, then the term 'ocelli' was better. Strictly, a variole (or variolite) is a spherical structure composed of a variolitic 'spray' texture (see §4.3.2) radiating from a point, and few of the spheroidal structures documented have such a texture.
- ***Spherulites.*** These are described as spheroidal aggregates of acicular crystals radiating from a nucleus (e.g. MacKenzie *et al.*, 1982), and are considered by

Scholey (1992) to be distinct from 'ocelli' in the Reliance Formation since they occur in some chilled margins.

4.5.3 Previous work

Study of similar features in Archaean basalts elsewhere has led to the suggestion of several possible origins:

1. Spherulitic crystallisation directly from a liquid (Phillips, 1973; Philpotts, 1976, 1977; Fowler *et al.*, 1987)
2. Silicate liquid immiscibility (Ferguson and Currie, 1972; Gélinas *et al.*, 1976, 1977; Cawthorn, 1977; Cawthorn and Fraser, 1979; Coltorti *et al.*, 1987; Frost and Groves, 1988; Scholey, 1992), either as a result of incomplete mixing with assimilated material (e.g. Frost and Groves, 1988; Scholey, 1992), or due to 'liquid-splitting' during cooling around a miscibility gap (e.g. Gélinas *et al.*, 1976)
3. Segregation of a residual liquid (e.g. Anderson *et al.*, 1984)
4. Spherulitic crystallisation during devitrification, metasomatic alteration or metamorphism of glassy volcanic rock (e.g. Hughes, 1977; Claoué-Long, 1986)

The most significant aspect of the above list is that models 1-3 all require the spheroids to have existed as globules of liquid within another liquid, and only model 4 allows a post solidification origin. The most important question to be considered of any occurrence of the features is exactly this; did they ever exist as globules of liquid within another liquid ?

The occurrence of spheroidal features in the Ngezi Group volcanics has been noted by Hall (1983), in the western Reliance Formation, and Nisbet *et al.* (1993) in the Zeederbergs Formation. Scholey examined several occurrences of what he termed 'ocelli' in the Reliance Formation as possible examples of immiscible liquids or 'xenomelts' generated by crustal contamination of komatiite lavas.

Plate 4.6

Spheroids in polished section

a) Spheroids in basalt

Light grey spheroids in a dark grey matrix. Note that the light grey of the spheroids is the same as the colouring of the fractures on the right of the picture, suggesting that this colouring is due to post-eruptive silicification.
Sample CBZ 207

b) Spheroids in basalt

Light grey spheroids in a dark grey matrix. Note that the light grey of the spheroids is the same as the colouring of less regular shaped areas in the middle of the sample, suggesting that this colouring is due to post-eruptive silicification.
Sample CBZ 181

c) Spheroids in basalt

Light grey spheroids in a dark grey matrix. The brown area to the left of the photo is a weathered surface. Note the highly cuspate nature of the spheroid contacts, and that it is still possible to distinguish individual spheroids within larger coalesced areas.
Sample CBZ 190

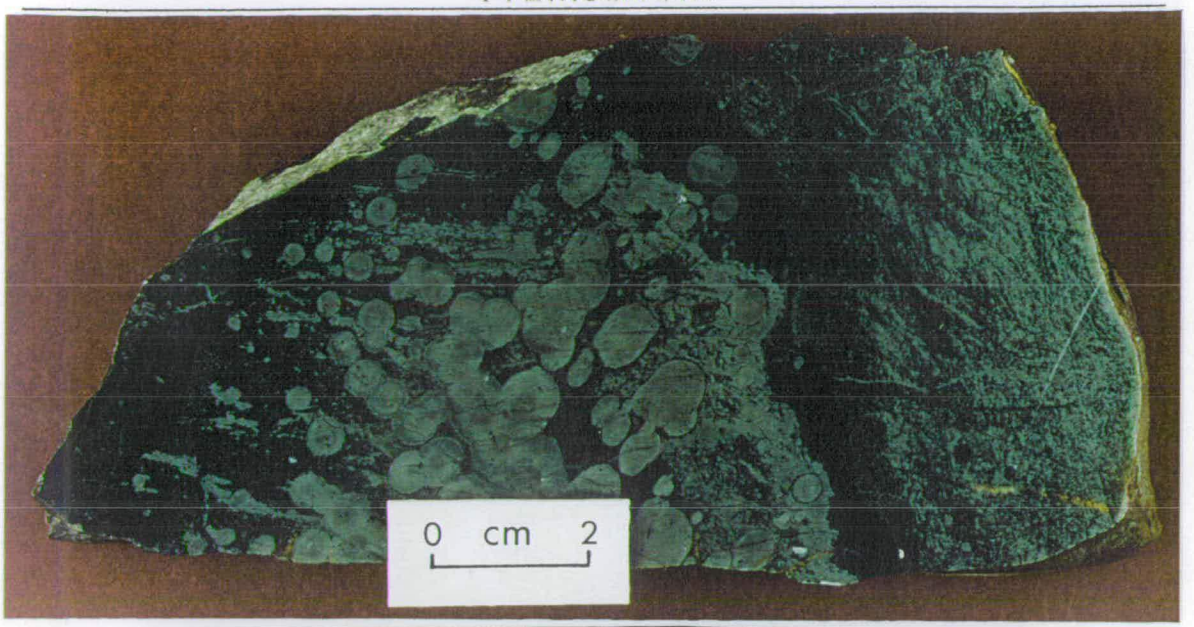
0 cm 2

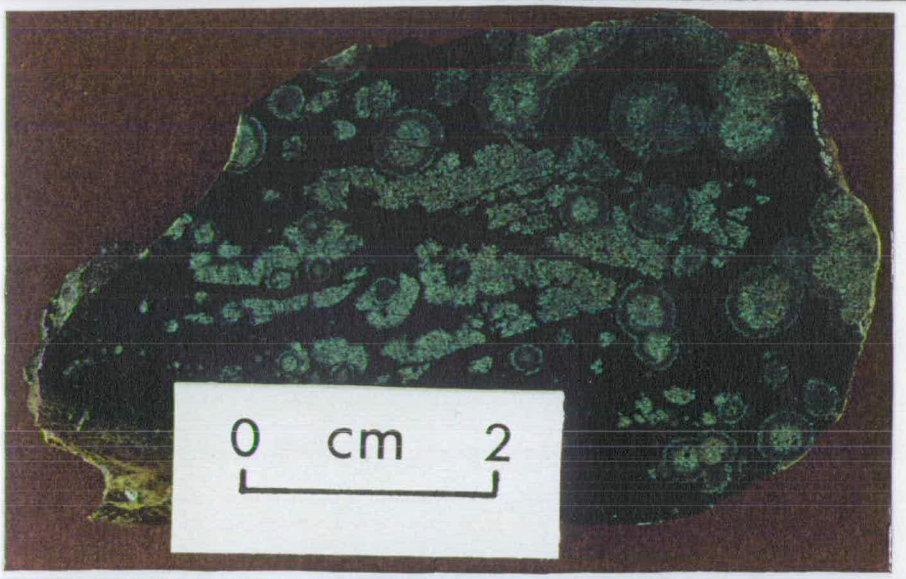
0 cm 2

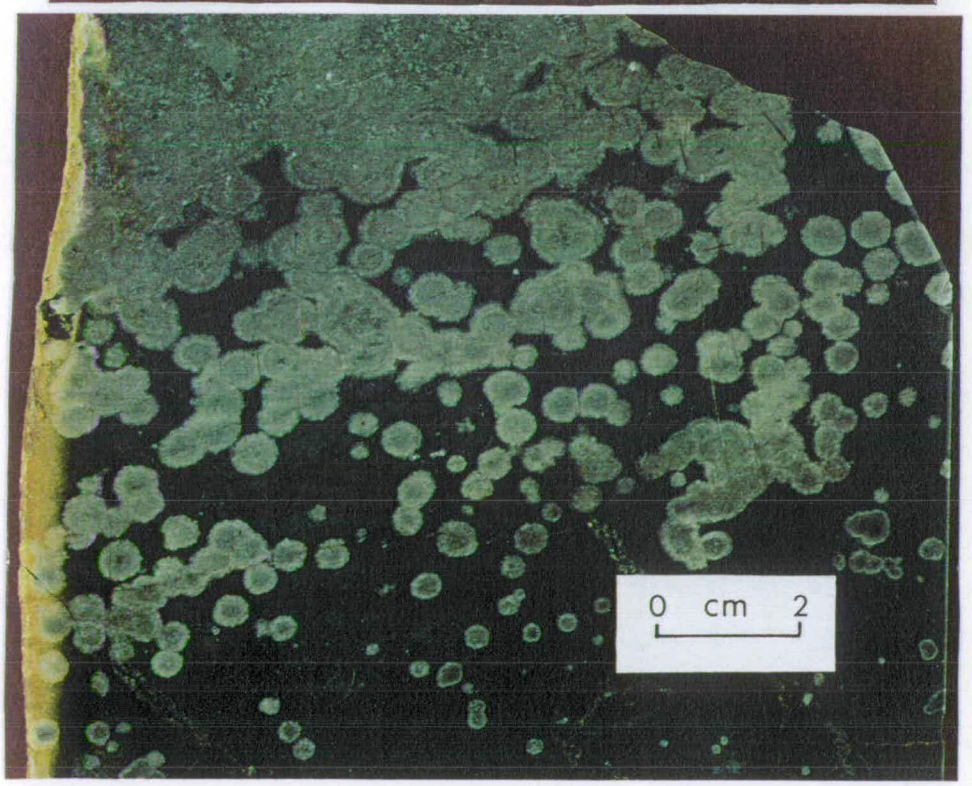
0 cm 2

Plate 4.7

a) Spheroids in basalt outcrop, Ngezi River section

Very light grey spheroids in a medium grey rock. Note the arrangement of the spheroids in linear groups, corresponding to fractures in the rock.
Lens cap is 60mm in diameter

b) Devitrification in rhyolite glass, polished section.

Light grey devitrification features in a dark, glassy rhyolite. The devitrified area are very porous compared to the glass, and do not polish well. Many can be seen as cavities within the rock. Rhyolite sample from Kenya, collected by B.G.J.Upton.

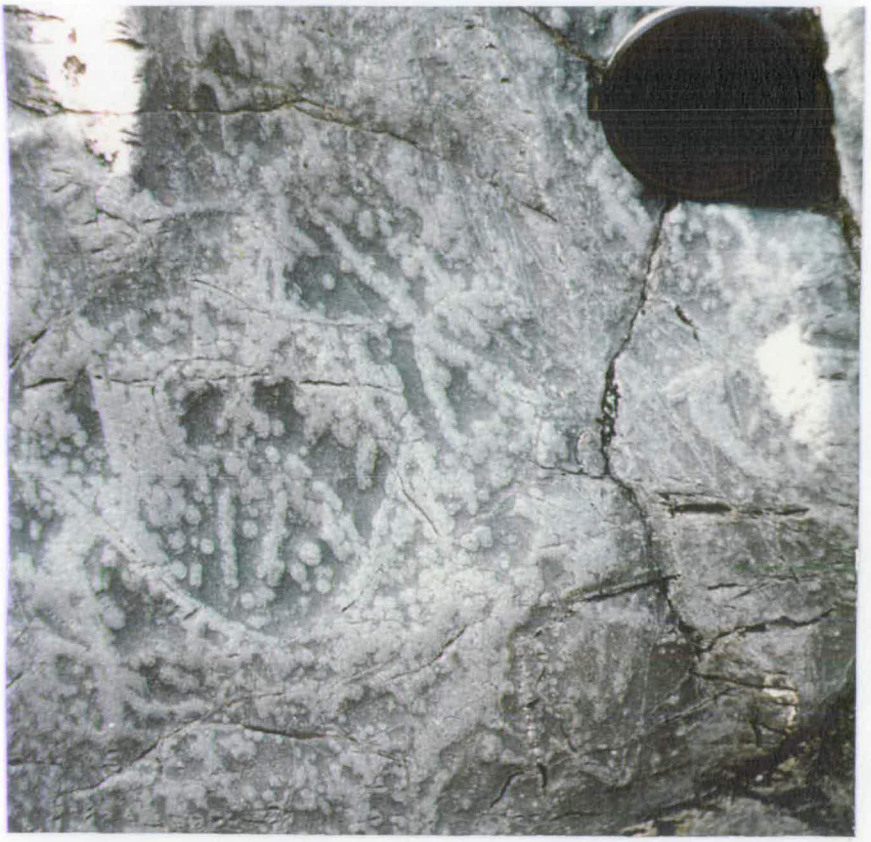

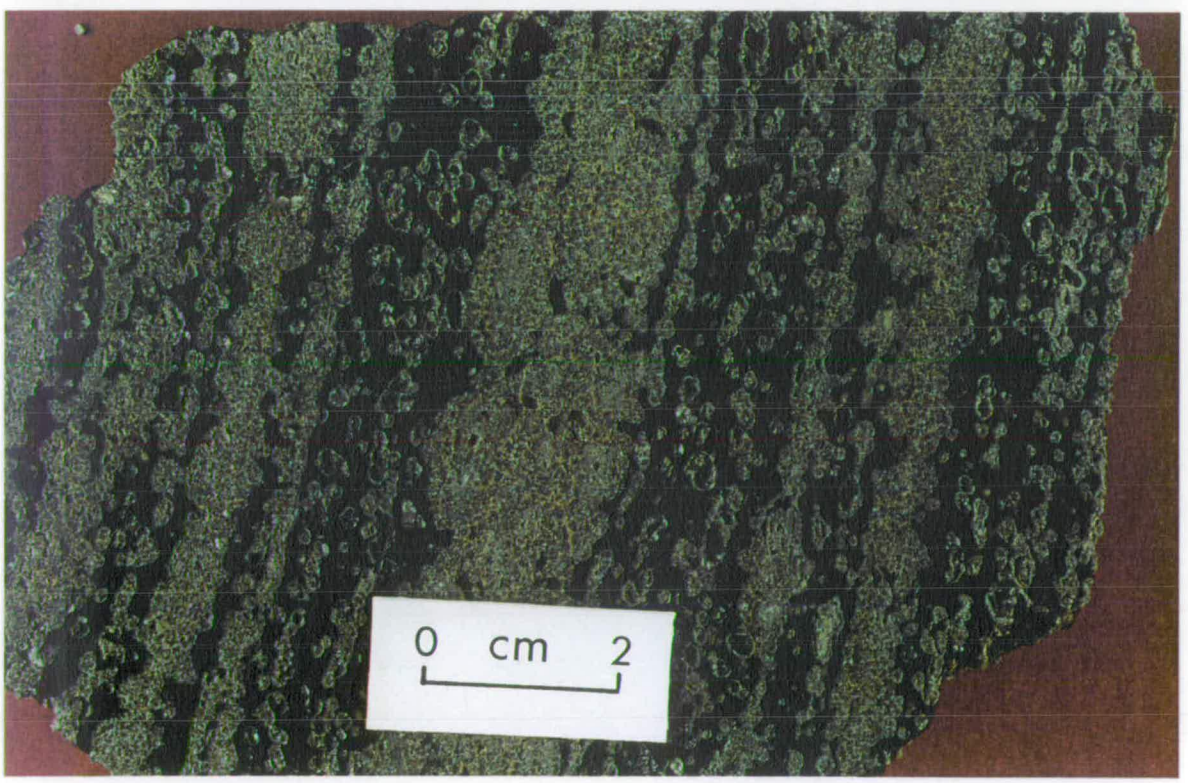
0 cm 2

Plate 4.8

Spheroids in outcrop

a) Spheroids in pillow lava, Ngezi River section

A large coalesced area of spheroid material within a large pillow (from the same outcrop as CBZ 190, see Plate 4.6). The irregular shape would appear to have been determined by flow processes, but it is thought that these acted on particles which subsequently became nuclei for devitrication.
Lens cap is 60mm in diameter.

b) Spheroids in andesite, Ngezi River section

Bands of spheroid material within a large pillow structure (from the andesitic horizon near the top of the formation). The irregular shapes would appear to have been determined by flow processes, but it is thought that these acted on particles which subsequently became nuclei for devitrication.
Hammer Shaft is 30cm long.

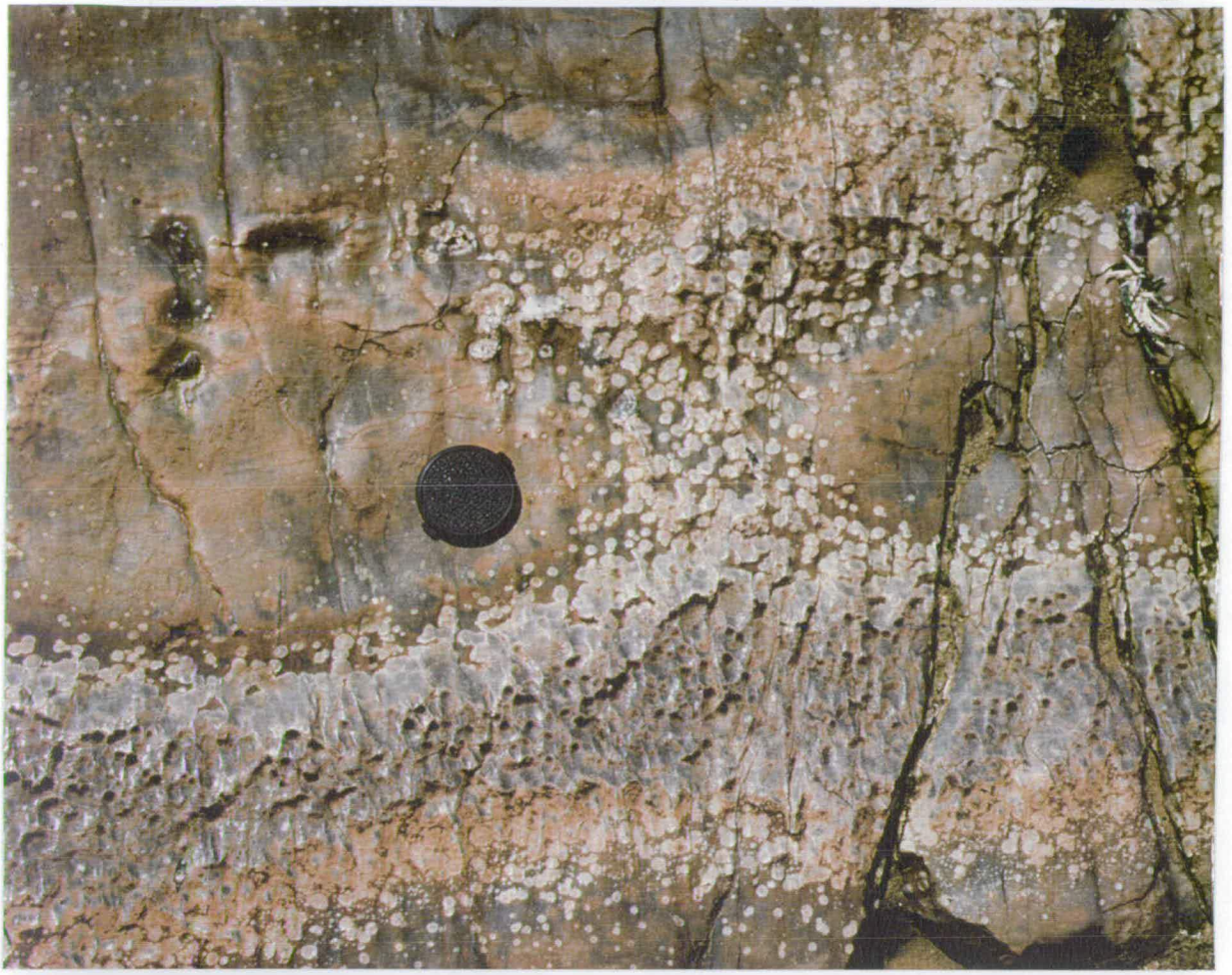

Table 4.2. A comparison of ocelli seen in the Reliance Formation (Scholey, 1992) with 'spheroids' seen in the Zeederbergs Formation. Examples of spheroids in the Zeederbergs Formation can be seen in Plates 4.6, 4.7 and 4.8.

Scholey's (1992) 'Ocelli' **Reliance Formation**	*This study, 'Spheroids'* **Zeederbergs Formation**
	Field Relationships
Occur as horizons (<1m thick) at varying levels within thicker piles of non-ocellar, but otherwise similar pillows.	Occur throughout individual pillowed units, often up to 100-200m thick.
Host rocks restricted to fine-grained, hypocrystalline **high-magnesium** basalts (mostly MgO>12%)	Host rocks mainly fine-grained and hypocrystalline, but spheroids are seen in rocks across the whole compositional range of the Zeederbergs Formation. The most notable occurrence in the Ngezi River section is in the thick, evolved, andesitic horizon near the top of the succession (see Fig. 3.3).
Most ocellar pillowed units have an obvious spatial relationship with tuff horizons, occurring just above them.	No obvious spatial relationship with tuffs.
Size ranges from 0.5 - 5 mm diameter, often coalesced into larger bodies.	Size ranges from 3 - 12 mm (in places up to 25 mm), often coalesced into larger bodies, but the outlines of individual spheroids can often still be clearly seen in these 'coalesced' bodies.
'Ocelli' often segregated towards the core and margin of pillows (forming concentric zones), and also seen in more irregular, flow-related shapes.	Spheroids found segregated into irregular, flow-related shapes, occasionally in concentric zones, and quite often in linear forms related to fracturing within the rock.
	Microtextures
Sharp, approximately spherical outlines which show irregularities at grain scale.	Sharp spherical outlines at hand-specimen scale, but contacts are much less distinct in thin-section, very irregular at grain scale.
Clinopyroxene in both ocelli and host altered & replaced; by amphibole (ocelli and host) and chlorite (host only).	Clinopyroxene in both spheroid and host sometimes altered to amphibole ± chlorite. Groundmass of spheroid and host alter slightly differently; both appear dominated by chlorite, in the host it is a clear green colour, but a brown colour in the spheroid. Occurrence of quartz is more common in the spheroids than in the host.
Ocelli **internally differentiated**, sub-divided into 3 concentric zones; rim zone, inner zone and core.	**Little internal structure**. Some spheroids show thin rim zones in polished slab sections. The only difference in thin section is the different shade of the groundmass, in X-polars the spheroids are virtually impossible to distinguish.
Boundaries between adjacent/adjoining ocelli are **non-cuspate**.	Boundaries between adjacent/adjoining spheroids are clearly **highly cuspate** and irregular.
	Geochemistry
Ocellar zones are andesitic (e.g. 62% SiO_2, 5.7% MgO) in high-magnesium erupted liquids (e.g. 54% SiO_2, 12.3% MgO). Segregated ocellar zone in Steve's Flow enriched in Al_2O_3 and SiO_2, depleted in MgO, P_2O_5, TiO_2 and other incompatible trace elements.	No geochemical work was carried out on the spheroids in the Zeederbergs Formation, as their origin is not crucial to the main question of this thesis. It is worth noting, however, that the occurrence of spheroids is exactly the same in both Type I and Type II lavas.

4.5.4 Origin of the 'spheroids' in the Zeederbergs lavas

The only serious study of these textures in the Ngezi Group volcanics was that of Scholey (1992), who examined 'ocelli' in the high-magnesium lavas of the Reliance Formation and interpreted them as globules of assimilated crustal melts which had not been thoroughly mixed in to the lava. Table 4.2 contains a summary of all his evidence, together with the equivalent observations from the occurrences of 'spheroids' in the Zeederbergs Formation. Clearly there are very significant differences between the 'ocelli' in Scholey's (1992) study and the spheroids in the Zeederbergs Formation. His interpretation of the origin of the ocelli is not questioned here, though it is worth noting that his description of the boundaries of adjacent ocelli as non-cuspate does not agree with his photographs of these features, where these boundaries appear highly cuspate!

As mentioned above, a crucial question to be considered when looking at these features is whether or not they ever existed as globules of one liquid within another. Scholey (1992) compiled a list of textural and geochemical criteria for liquid immiscibility, which is reproduced in Table 4.3, and compared to the characteristics of the spheroids in the Zeederbergs Formation. The spheroids appear to fulfil none of the criteria satisfactorily, and it would appear very unlikely that they ever existed as globules of an immiscible liquid.

Accepting a post-solidification origin for the spheroids constrains them to model 4 in §4.5.3, and comparison to devitrification textures in other volcanic rocks (see Plate 4.7b) suggests that this is a reasonable interpretation. This model explains many of the characteristics of these spheroids in the Zeederbergs lavas:

- Spherulitic devitrification could well be nucleated about pre-existing particles in the melt, which would have been distributed by flow movement. This would explain the apparent flow related shapes formed by the spheroids in some lavas. (see Plate 4.8)
- In examples where the distribution is more linear and related to fractures, the fractures are highlighted by material similar to that forming the spheroids. Nucleation of the devitrification could have taken place along such fractures, and the differing geochemical character could have been inherited during subsequent alteration. (see Plate 4.7a)

Table 4.3. Comparison of liquid immiscibility criteria (Scholey, 1992) with equivalent characteristics of spheroids in the Zeederbergs lavas. Examples of spheroids in the Zeederbergs Formation can be seen in Plates 4.6, 4.7 and 4.8.

Textural and geochemical criteria for liquid immiscibility	*Characteristics of spheroids in the Zeederbergs Formation*
(i) In non-tectonised examples, glassy (liquid) phases of contrasting silica under- and over-saturated composition should occur, the latter as spherical globules within the former due to the different surface tensions.	Spherical features of one composition do occur within a host liquid of another, and the paler colouring would suggest that the former were more felsic than the latter. However, both host and spheroids contain crystals of quartz, possibly a post-eruptive addition.
(ii) All stages of unmixing should occur, from homogeneous liquid through the appearance and coalescence of ocelli to the separation of distinct layers. *(in the case of liquid unmixing)*	The smallest spheroids seen in the Zeederbergs lavas are several mm in diameter, and most are 5mm+. Larger areas of apparently 'coalesced' material are common, but within these areas the spherical outlines of the individual spheroids can often still be seen.
(iii) As coalesced droplets become rounded almost instantaneously, contacts between ocelli should not be cuspate.	The contacts between adjoining spheroids are highly cuspate, and large irregular shapes made up of several spheroids are common, with the outline of the individual spheroids still clearly visible.
(iv) The ocellus-host interface should be sharp (<10μm). The extremely steep chemical gradients across the interface indicate limited diffusion across the chilled rim of the cooler liquid.	The contacts of the spheroids appear reasonably sharp in hand-specimen, but are much less so in thin section; considerably coarser than 10μm.
(v) Identical equilibrium phenocrysts should occur in both liquid phases and may penetrate the interface. This does not apply to disequilibrium "quench" crystals.	Identical phenocrysts do occur in both spheroids and host. The groundmass textures also appear very similar, and only the alteration phases seem to differ.
(vi) Liquid immiscibility rather than *in situ* segregation of residual liquid would be favoured if the bulk composition of an ocellar rock fell within a silicate immiscibility field, with a miscibility gap between ocellus and matrix phase compositions. Conversely, bulk compositions of non-ocellar rocks should plot outside immiscibility fields. However, this is not always the case, implying some control from additional factors.	None of the Zeederbergs lavas fall within any silicate immiscibility field, which is generally constrained to fairly unusual bulk compositions.

Immiscibility criteria after Bowen (1928), Philpotts (1976, 1977), Gélinas *et al.* (1976), Cawthorn and Fraser (1979), Frost and Groves (1988).

- If the larger 'coalesced' areas were formed by many spherulitic devitrification sites growing into one another, one would expect these areas to retain some internal structure related to the individual spheroid shapes, as is clearly seen. Also, the boundaries between touching spheroids would be extremely cuspate, again, as seen. (see Plate 4.6)

- Subsequent alteration, especially hydrothermal alteration shortly after eruption, could very well act differently on areas of differing crystallinity. The devitrified areas would be more coarsely crystalline and more porous to fluid flow than would the glass of the host (see example of devitrification in rhyolite, Plate 4.7b), and so chemical mobility might be more extreme. There is strong evidence that silica has been extremely mobile shortly after eruption (see §5.4.7), and this could possibly explain the apparently more felsic nature of the spheroids.

4.5.5 Conclusions

The most likely origin for the 'spheroid' structures in the Zeederbergs Formation seems to be spherulitic devitrification, and so if any name should be applied to them, 'spherulite' would seem most appropriate. It is unclear whether Scholey's (1992) interpretation of similar structures in the Reliance Formation as immiscible globules (xenomelts) of assimilated crustal material (ocelli) is correct, whether the structures he observed were different from those considered here, or whether his interpretation is incorrect. It is possible that there is more than one type of 'spheroid' to be found in the lavas of the Ngezi Group, and it is possible that some of them do represent immiscible liquids, but the majority of these structures examined in this study in the Zeederbergs Formation appear to be devitrification features, with any differences in chemistry from their host rock resulting from differing alteration.

4.6 Conclusions

- Both the Reliance and Zeederbergs Formations show some preservation of original texture and mineralogy. In some places the quality of preservation is excellent. On the basis of mineralogical and textural characeristics, the lavas of the Reliance Formation can be subdivided into 4 different varieties.

- The lavas of the Zeederbergs Formation are generally fine grained, hyalocrystalline, and moderately to sparsely porphyritic. The dominant phenocryst phase is clinopyroxene (mostly augite), with, less commonly, a little plagioclase

- A subdivision of the lavas of the Zeederbergs Formation based on petrographical criteria is not practical.

- Most lavas are altered to hydrated low-greenschist mineral assemblages.

- The most likely origin for the 'spheroid' structures in the Zeederbergs Formation is thought to be spherulitic devitrification.

5

ALTERATION

5.1 Introduction

When studying the geochemistry of such ancient lavas, which have been clearly subject to several post-eruption events which may have affected their chemistry, it is essential to consider the extent and nature of any possible alteration before any detailed consideration of their geochemistry is undertaken. The aim of this chapter is to ascertain which geochemical characteristics are reliable indicators of primary processes, and which have been subject to too much post-eruptive mobility to make them of much use in any further petrogenetic investigation.

Previous work on alteration of rocks of a similar composition and/or age to those of the Ngezi Groups suggests that few generalities can be applied, but is of some help in approaching the problem of 'screening' out heavily altered samples, and identifying elements which have been significantly mobile. Assessment of alteration in the rocks of the Reliance Formation suggests that their chemistry is little affected by the recrystallisation to a hydrous metamorphic assemblage, but that some elements have been significantly mobile.

Consideration of alteration in the Zeederbergs Formation falls into three parts. Mobility of the major and trace elements is assessed by comparison with Zr as an immobile comparator, as is possible bulk mobility of the REE while individual REE mobility is examined by considering REE patterns for individual samples. Finally, the problem of bulk silica mobility and silicification is considered.

5.2 Alteration literature

5.2.1 Alteration studies

Many authors have addressed the problem of element mobility during alteration of basaltic and komatiitic suites, and the findings of some of these studies are shown in Tables 5.1 and 5.2. This selection is by no means exhaustive, but it does clearly

Table 5.1. Major element mobility studies

Rock type	Additional information	Si	Ti	Al	Fe	Mn	Mg	Ca	Na	K	P	Reference
Komatiite		X						X	X	X		Arndt (1983)
Basalt	Hydrothermal alteration	X			X	X	X	X	X	X		Mottl (1983)
Basalt	Hydrothermal alteration	X	X	O	X	X	X	X	X	X		MacGeehan & MacLean (1980)
Basalt	Submarine weathering	X			X		X	X	X	X		Pearce (1976)
Basalt	Weathering	X					X	X	X	X		Pearce (1976)
Basalt	Greenschist facies metamorphism				X		X		X	X		Pearce (1976)
Komatiite & basalt	Reliance Formation	X	O	O			O	X	X	X		Scholey (1992)
Basalt	Abitibi greenstone belt	O	O	O	O	O	X	X	X	X		Jolly (1980)
Komatiite & basalt		O	O	O	O		O	O	X	X		Beswick (1982)
Komatiite & basalt	Munro township suite		O					X				Arndt & Nesbitt (1982)
Basalt	Abitibi belt volcanics		O	X				X				Ludden & Gélinas (1982)
Komatiite	Barberton komatiites		O	O	O		O	O	X	X		Smith & Erlank (1982)
Basalt	Abitibi belt volcanics	O	O	O	X		X	X	X	X	O	Gélinas *et al.* (1982)

Key: O, element immobile; X, element mobile. The first six rows of the table are from Rollinson (1993).

Table 5.2. Trace element mobility studies

Rock type	Additional information	Nb	Zr	Y	Sr	Rb	Th	Pb	Zn	Cu	Ni	Cr	V	Ba	Sc	REE	Reference
Komatiite			X	X								X	X			X	Arndt (1983)
Basalt	Hydrothermal alteration		X	X					X	X	X	X	X			X	MacGeehan & MacLean (1980)
Komatiite & basalt	Reliance formation	O	O	O	X	X		X	O	X	O	O		X		O	Scholey (1992)
Komatiite & basalt					X	X											Beswick (1982)
Komatiite & basalt	Munro township suite	O	O	O	X	X			X	X		O	O	X	O		Arndt & Nesbitt (1982)
Basalt	Abitibi belt volcanics		O	O											O	O	Ludden & Gelinas (1982)
Komatiite	Barberton komatiites		O	O	X	X			X	X		O	O	X	O		Smith & Erlank (1982)
Basalt	Abitibi belt volcanics		O	O	X	X								X		O	Ludden & Gélinas (1982)
Basalt	Sea water alteration	O	O	O	O	X			O			O	O				Hart *et al.* (1974)
Basalts	Hydrothermal alteration		O	O	X					X				X			Humphris & Thomson (1978)

Key: O, element immobile; X, element mobile.

highlight some of the problems in trying to identify the reliability of any geochemical data as representative of primary igneous processes. In different conditions (hydrothermal alteration, weathering, metamorphism etc.), and in rocks with different mineralogies, different elements are mobile. Which elements still reflect magma composition is a function of the whole history of the rock sample. It is also worth noting that three studies on the volcanic rocks of the Abitibi greenstone belt in Canada all identify slightly different levels of mobility for the same elements!

The conclusion drawn from all of this variation is that few generalisations about the relative mobility of an element can be applied to any individual case. The reliability of any element as an indicator of primary igneous processes must be established for each individual suite.

5.2.2 Screening, and discrimination of mobile/immobile elements

It is possible to screen samples of igneous rocks to remove those whose chemistry is likely to be unrepresentative of primary igneous processes. Jolly (1980) used a series of geochemical and petrographic criteria to remove heavily altered samples from his dataset, and the application of similar screens to the dataset of this study is discussed in §5.4.1. One important first step in dealing with basaltic suites is to deal with hydration effects. It is accepted that basic magmas have very low H_2O contents (eg. Green *et al.*, 1975) and crystallise to anhydrous primary assemblages, and that any loss on ignition represents an influx of volatiles. To compensate for this, it is customary to recalculate all analyses to a 100% anhydrous basis, and that convention has been followed here.

Most methods of determining element mobility are based on the assumption that igneous processes which may affect the chemistry of the series will alter relative concentrations in a coherent fashion, whilst alteration processes are generally thought to act in a fairly incoherent manner. In terms of variation diagrams, this translates into the following principle; *any two elements which form a reasonably coherent trend on a variation diagram which can be explained in terms of simple igneous processes (different degrees of partial melting, fractionation) are unlikely to have been mobile during subsequent alteration.* It is important to note that the absence of such a coherent trend (a more scattered variation diagram) does not *necessarily* indicate mobility. There are other more complex primary processes (such as variable crustal contamination) which may result in such scatter. However, in the absence of a coherent trend, it is unwise to place too much trust in the behaviour of the element concerned.

The rare earth elements are generally considered to be relatively immobile, but they have been seen to be slightly mobile in certain circumstances (eg. Hellman *et al.*, 1979). The most obvious indicator of mobility of any particular element is the presence of an anomaly in an otherwise smooth REE pattern. A Eu anomaly is often seen and attributed to plagioclase fractionation, but Sun and Nesbitt (1978) have suggested that Eu is also more prone to mobility during alteration than other REE,

and that this may be a contributory factor. Gross REE depletion or enrichment is harder to identify than such selective mobility, but comparison of REE concentrations with other immobile trace elements can be used, as described above, to exclude such mobility.

5.3 Alteration of the Reliance Formation

In his consideration of the geochemistry of the Reliance Formation, Scholey (1992) gave some consideration to the mobility of major and trace elements during alteration, and a brief summary of this work is presented here.

5.3.1 Alteration style and hydration effects

Assuming that the lavas were originally anhydrous (see 5.2.2) the alteration assemblages in the Reliance Formation obviously imply an influx of water. Since the majority of the rocks are recrystallised to a greater or lesser extent, the secondary migration of all major elements on at least a sub-millimetric scale may be inferred. Since there is little evidence for carbonation (and when it does occur its effects are extreme, see 5.4.1), most of the loss on ignition (LOI) is attributed to H_2O^+. The variation of MgO, Al_2O_3, and CaO with LOI is largely controlled by the amount of serpentine, and hence originally the amount of olivine, the major fractionating phase. Bulk rock chemistry appears little affected by the compositions and proportions of other hydrated alteration phases.

5.3.2 Major element mobility

The Al_2O_3/TiO_2 ratio is remarkably constant in the rocks of the Reliance Formation, at a near chondritic value ($\approx$20.4), and is interpreted as representing a primary trend, with both Al_2O_3 and TiO_2 immobile during subsequent alteration. Both elements show tightly constrained trends with MgO, and this too is considered immobile. The trends displayed by CaO, SiO_2, Na_2O and K_2O when plotted against these three elements all show considerable scatter, which is mainly attributed to mobility during alteration. Scholey (1992) also discussed the problem of dilution/concentration effects associated with major element mobility. The addition or removal of a significant amount of one component (for example, SiO_2) will cause the abundances of all other components to be proportionally reduced or increased. His conclusion is that there is no evidence in any of the Reliance Formation samples for any total mass change of

more than ±3%, and that the dilution/concentration effect on trace element abundances is therefore negligible.

5.3.3 Trace element mobility

The low field strength elements (Na, K, Sr, Rb and Ba) show poor trends with a large degree of scatter, and they are thought to have all been significantly mobile. The high field strength and rare earth elements (Ti, Zr, Y, Nb, La, V and P), however, generally show tightly constrained trends and near chondritic ratios (with the exception of P and V, whose ratios are attributed to core partitioning), and their abundances are considered to be a reliable indicator of primary levels. The transition elements Cu and Pb both show a high degree of scatter, and are interpreted as mobile, but Ni, Zn and Cr show reasonably tight, coherent trends, suggesting that they too are a reliable guide to primary concentrations.

5.4 Alteration in the Zeederbergs Formation

5.4.1 Sample screening

An initial examination of the dataset suggested that it could be significantly 'cleaned up' by the systematic application of a few simple geochemical and petrographical screens, to remove samples whose chemistry was not solely a function of primary igneous processes. These were based on the scheme of Jolly (1980), but have been adapted to suit the sample suite in question. The screens applied were :

1. All samples with LOI greater than 5.5% were removed, to eliminate heavily hydrated samples.
2. All tuffs and hyaloclastites were removed. The reworking involved in their generation means that their bulk compositions are not solely controlled by primary igneous processes.
3. All samples which showed a clear cumulate texture were removed.
4. All samples which showed very heavy alteration in thin section, most commonly heavy alteration to calcite, or very heavy quartz veining, were removed.
5. All samples with potentially more evolved compositions (MgO<4%)were plotted as a separate group.

Scholey (1992) considered that the application of the first screen to the rocks of the Reliance Formation unnecessarily discriminated against those samples with originally high olivine contents, but since there is very little olivine in the lavas of the Zeederbergs Formation, this is not thought to be a problem.

5.4.2 Hydration effects

Figure 5.1 shows loss on ignition plotted against MgO, CaO and Al_2O_3. There is no obvious correlation on these plots, and the common hydrated alteration phases appear to have little effect on bulk rock chemistry. The serpentine controlled trend seen in similar plots of the Reliance Formation lavas (reflecting the amount of olivine, see 5.3.1) is not seen in the Zeederbergs Formation, as there is little olivine present in these lavas.

5.4.3 Assessment of mobility

Following the method outlined in 5.2.2, the mobility of individual elements was assessed by comparing them with one standard tracer which was considered to be immobile. Zr was chosen as the comparator, as it is found to be immobile in all the studies of alteration (see Table 5.2), and its concentrations (in the range 20-200ppm) are easily and accurately measured by XRF. When plotting the different elements against Zr, the dataset (after screening) was split into 3 categories : Type I lavas, Type II lavas, and potentially evolved (low-Mg) samples (see screen 5, 5.4.1). Several different features of the data are considered for each element :

- the coherence of the Type I lavas
- the coherence of the Type II lavas
- the separation between the Type I and Type II lavas
- the position and/or distribution of the low-Mg samples

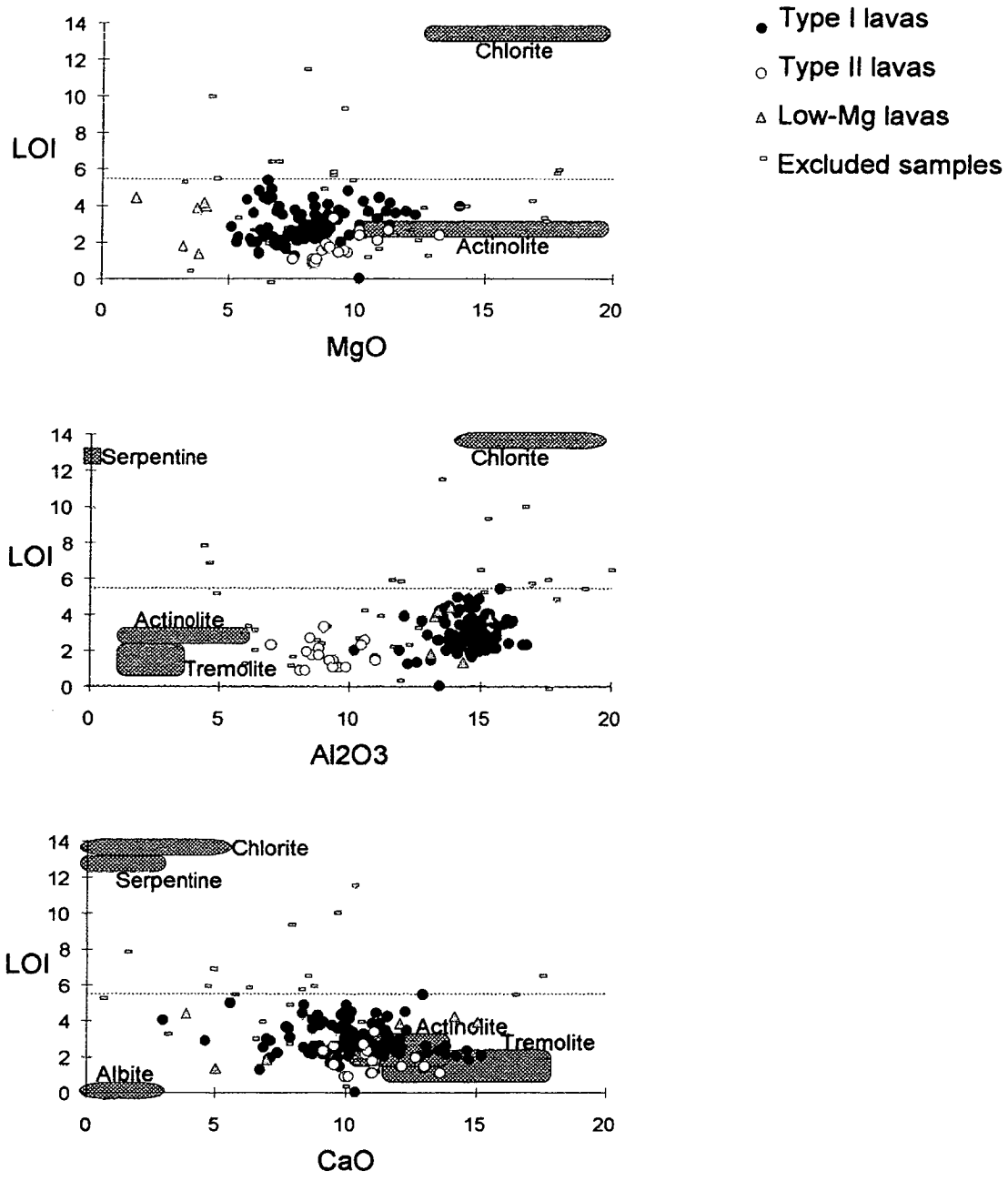

Figure 5.1 Hydration effects. Loss on ignition against MgO, Al_2O_3 and CaO. The dashed horizontal line at 5.5% LOI represents the exclusion limit used in this study. The compositions of the principal secondary phases are shown. (Diagram after Scholey, 1992)

If the Type I lavas show a trend that is reasonably coherent, and which can be explained in terms of simple partial melting or fractional crystallisation trends, then the element in question is considered to be a reasonably reliable indicator of primary abundances. The Type II lavas often show a less coherent trend for the same element than the Type I lavas. Since these lavas are effectively the same in terms of bulk chemistry and mineralogy, demonstration of element immobility in Type I lavas is taken as indication of immobility in Type II lavas, and some other explanation of the

more scattered pattern is to be sought (see Chapter 6). If there is a lack of any clear coherent trend in either dataset, but there is still a reasonably clear separation between the Type I and Type II lavas, then the inference is that limited element mobility has affected the rock, but to a lesser degree than the primary differences between the two types. Those differences are therefore real (primary), even if little detailed information can be derived from the element about the behaviour of either individual suite.

5.4.4 Major element mobility

Figures 5.2 and 5.3 show all the major elements compared to Zr. The following is a brief assessment of the distributions seen, and their implications for element mobility.

- **MgO** There is some scatter on the diagram, but a still recognisable dog-leg trend in the Type I lavas attributable to olivine and olivine + clinopyroxene controlled trends. Three of the low-Mg samples plot at the extreme of the ol+cpx trend, while three plot at the base of a short trend to low Mg and Zr, attributed to dilution by silica addition (see §5.4.7). The Type II lavas show a less coherent and more constant MgO trend.

- **TiO_2** A reasonably good positive correlation for both Types I and II, clustered along two Ti/Zr trends.

- **SiO_2** A large degree of scatter suggests considerable silica mobility. There is a clustering around a steep trend towards 100% SiO_2 at 0ppm Zr, which would correspond to bulk silica addition. This problem of silicification is discussed in §5.4.7.

- **FeO** There is some degree of scatter in the FeO pattern, but a plausible combination of different degrees of partial melting and fractional crystallisation can explain the variation. The Type II lavas show systematically higher FeO contents than those of Type I. (FeO is total Fe calculated as FeO)

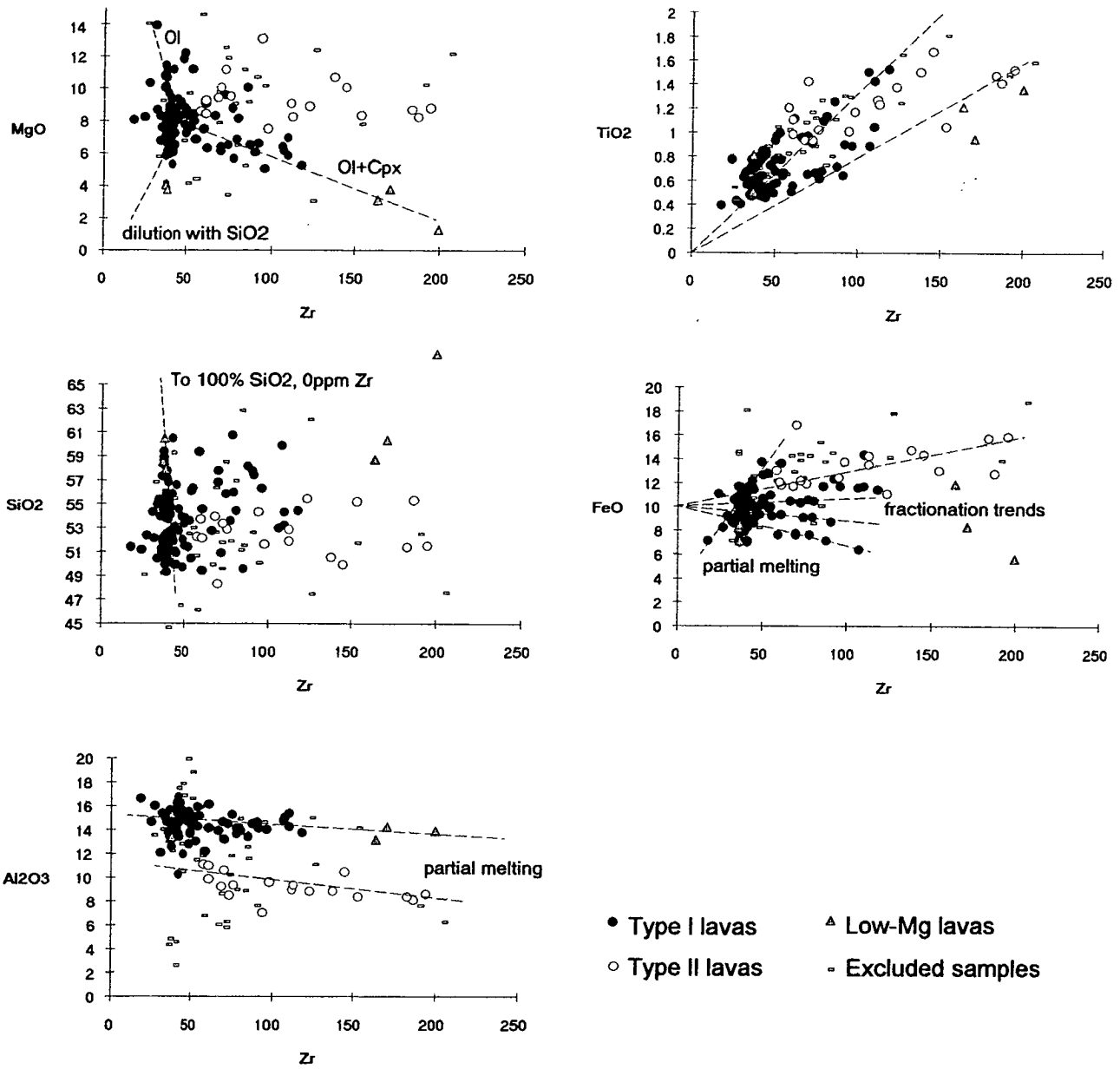

Figure 5.2 Assessment of major element mobility by examination of behaviour with respect to an immobile comparator (Zr). Dashed lines represent plausible explanations for the trends seen, they are not necessarily definitive.

- **Al_2O_3** Aluminium contents are relatively constant across the range of Zr concentrations, suggesting differing degrees of partial melting and fractional crystallisation with Al buffered by the retention of an aluminous phase in the residue. Slight scatter around this line would be caused by fractionational crystallisation. Type II lavas form a clearly distinct field, at significantly lower Al_2O_3 contents.

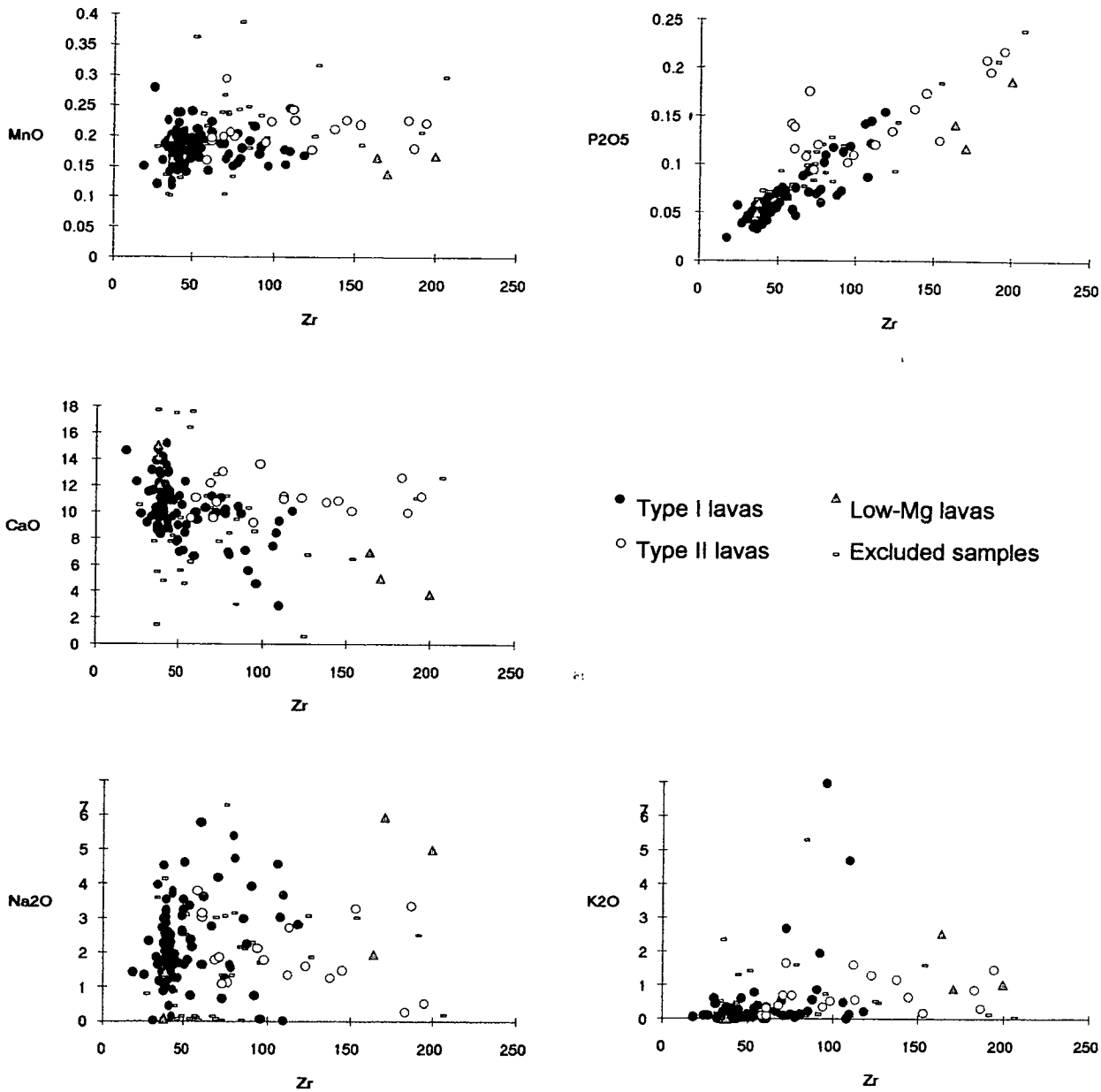

Figure 5.3 Assessment of major element mobility by examination of behaviour with respect to an immobile comparator (Zr).

- **CaO** There is a large degree of scatter, suggesting some CaO mobility. This hypothesis is supported by the heavy alteration to calcite in some samples. The scatter does not appear totally random, however, and is interpreted as loud 'noise' on a pre-existing pattern.

- **MnO** Most MnO contents sit between 0.15 and 0.25%, suggesting buffering of MnO during melting & fractionation, with little subsequent mobility.

- **P_2O_5** A strong positive correlation and a tightly defined trend indicate that phosphorus has been little affected by alteration.

- **Na_2O** and **K_2O** Fairly random distributions suggest a high degree of mobility during alteration.

So, overall, TiO_2, Al_2O_3, MnO and P_2O_5 are interpreted as being immobile, MgO, FeO as slightly mobile, CaO as significantly mobile, and SiO_2, Na_2O and K_2O as very mobile.

5.4.5 Trace element mobility

Figures 5.4, 5.5 and 5.6 illustrate the distribution of trace element concentrations with respect to Zr, loosely grouped into high field strength (HFS) elements (Figure 5.4), low field strength (LFS) elements (Figure 5.5) and transition elements (Figure 5.6).

The **HFS** elements (Figure 5.4) seem to behave quite coherently, suggesting little, if any, mobility during alteration. **Nb, Y, Ce** and **Nd**, all display tightly constrained strong positive correlations, and **V**, while a more complex trend, is still quite tightly constrained. La is not considered here, as analysis by XRF at the low concentrations present is unreliable, but is considered in §5.4.6 along with the other REE. The vaguely discernible trend of **Th** is poor, though the scatter is probably largely due to low precision on XRF measurements of Th, and does suggest genuinely higher Th contents in the Type II lavas. The **LFS** elements all seem to be considerably more mobile during alteration. **Sr, Pb, Ba** and **Rb** all display a fairly random scatter. The **transition** elements are quite variable in their behaviour. **Zn** shows a random distribution; **Cu** and **Sc** show no clear trends, but do display a systematic difference between Type I and Type II lavas; **Ni** and **Cr** both show reasonably coherent 'dog-leg' trends in the Type I lavas which can be attributed to progressive fractional crystallisation, although Type II abundances of these elements are very scattered.

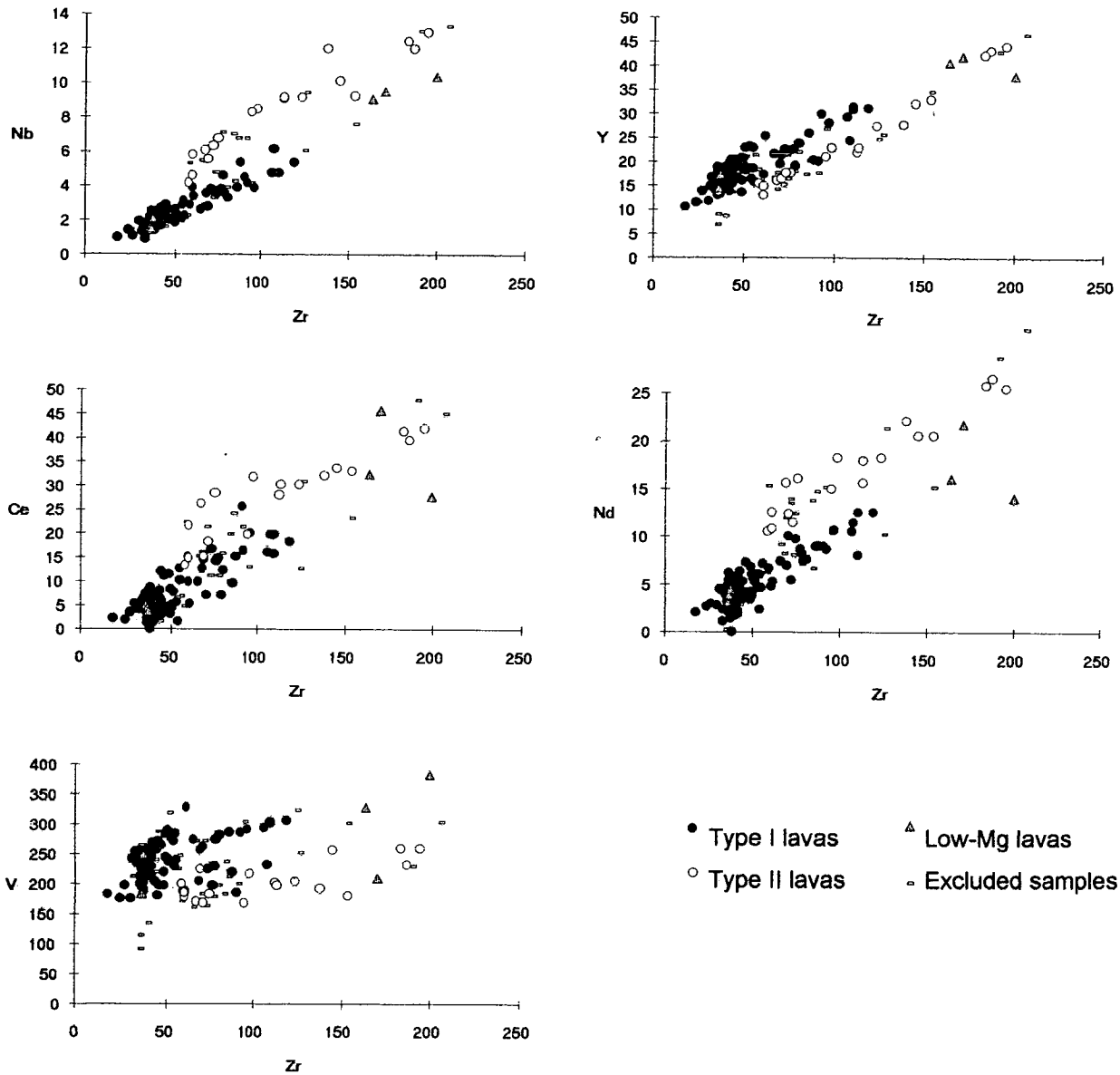

Figure 5.4 Assessment of trace element (HFSE and REE) mobility during alteration by examination of behaviour with respect to an immobile comparator (Zr)

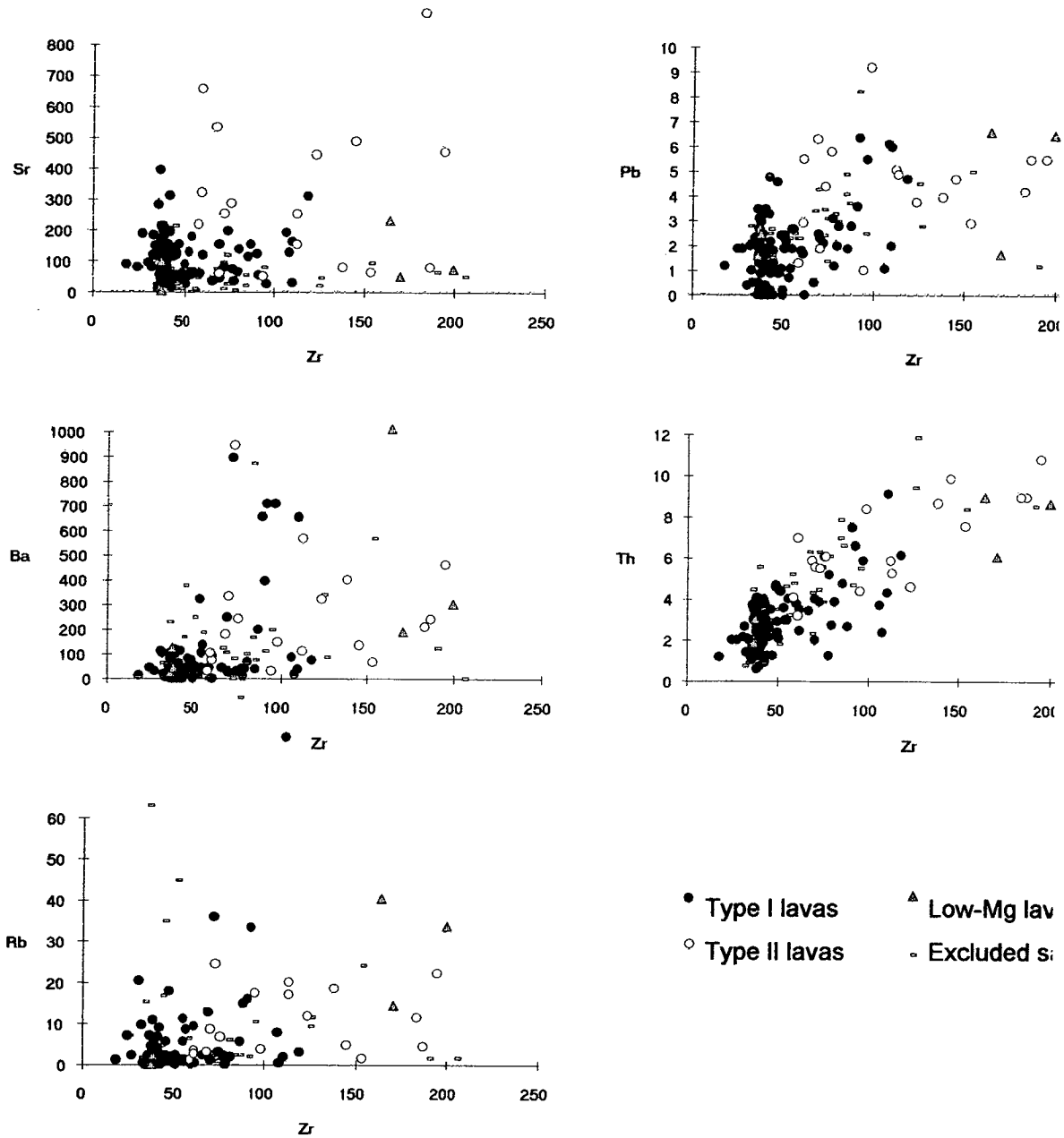

Figure 5.5 Assessment of trace element (Th and the LFSE) mobility during alteration by examination of behaviour with respect to an immobile comparator (Zr)

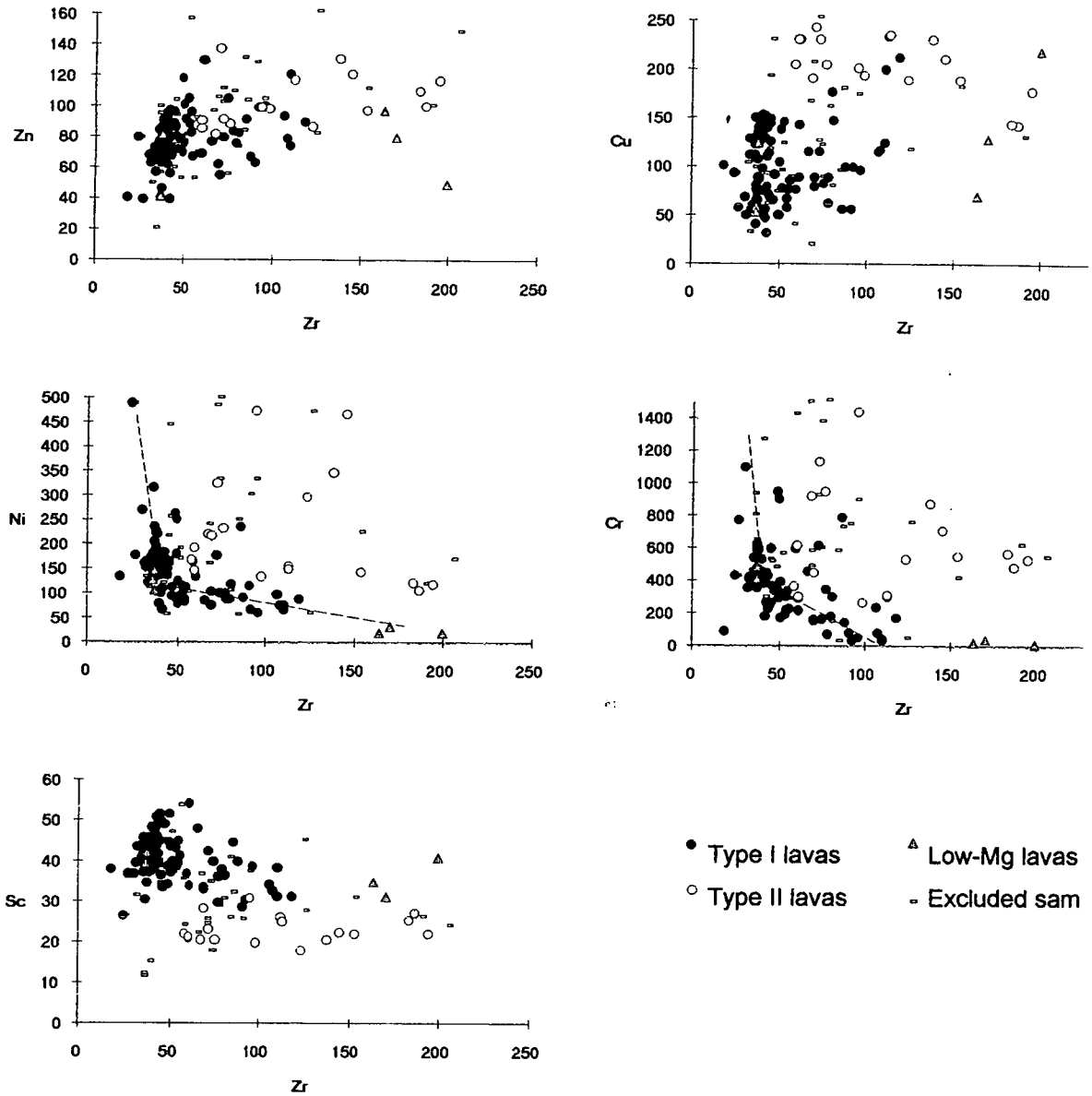

Figure 5.6 Assessment of trace element mobility during alteration (the transition elements) by examination of behaviour with respect to an immobile comparator (Zr)

In conclusion, concentrations of the HFS elements (Nb, Y, Ce, Nd, V, and, of course, Zr) appear to be reliable indicators of primary abundances. Ni and Cr seem to have been fairly immobile, and the behaviour of Th, Sc and Cu is thought to represent primary differences between the two lava types, but Zn and the LFSE (Sr, Pb, Ba, and Rb) would seem to be unsuitable for any serious consideration.

5.4.6 Rare earth element mobility

Hellman *et al.* (1979) suggested that there are several types of REE mobility :

1. Gross REE & selective LREE enrichment
2. Gross REE depletion
3. Selective REE mobility

and, consequently, more than one type of examination of REE data is appropriate to assess mobility during alteration. Mobility of types 1 and 2 can be asessed in a similar way to that used for other chemical data, by comparison with Zr as an immobile, incompatible tracer. Mobility of type 3 is best assessed by examining the individual REE patterns. All natural processes occuring during melting and subsequent melt evolution produce smooth REE traces (with the exception of Eu, which may be fractionated with respect to the other REE by processes involving plagioclase), whereas mobility during alteration can affect each element differently, and produce noticeable anomalies in the chondrite-normalised pattern (Sun & Nesbitt, 1978, Hellman *et al.*, 1979).

Figure 5.7 shows the behaviour of a representative selection of REE with respect to Zr. Most samples lie on fairly well defined, coherent trends, with only a few outliers. Sample CBZ134 lies noticeably below the main trend on plots of La and Ce, perhaps suggesting bulk LREE depletion in this sample. Sample CBZ204 also lies away from the main trend, but since this is one of the low-Mg, potentially evolved samples, there are perhaps pertrogenetic explanations for this. Again, though, the possibility of bulk LREE depletion is worth bearing in mind. The plot of Eu against Zr shows significantly more scatter than the other REE, and this is reflected in the frequent presence of Eu anomalies in the REE patterns. This is attributable to partial melting or fractionation processes involving plagioclase, or possibly to preferential mobility during alteration as a result of the wide range of oxidation states exhibited by Eu (Sun & Nesbitt, 1978).

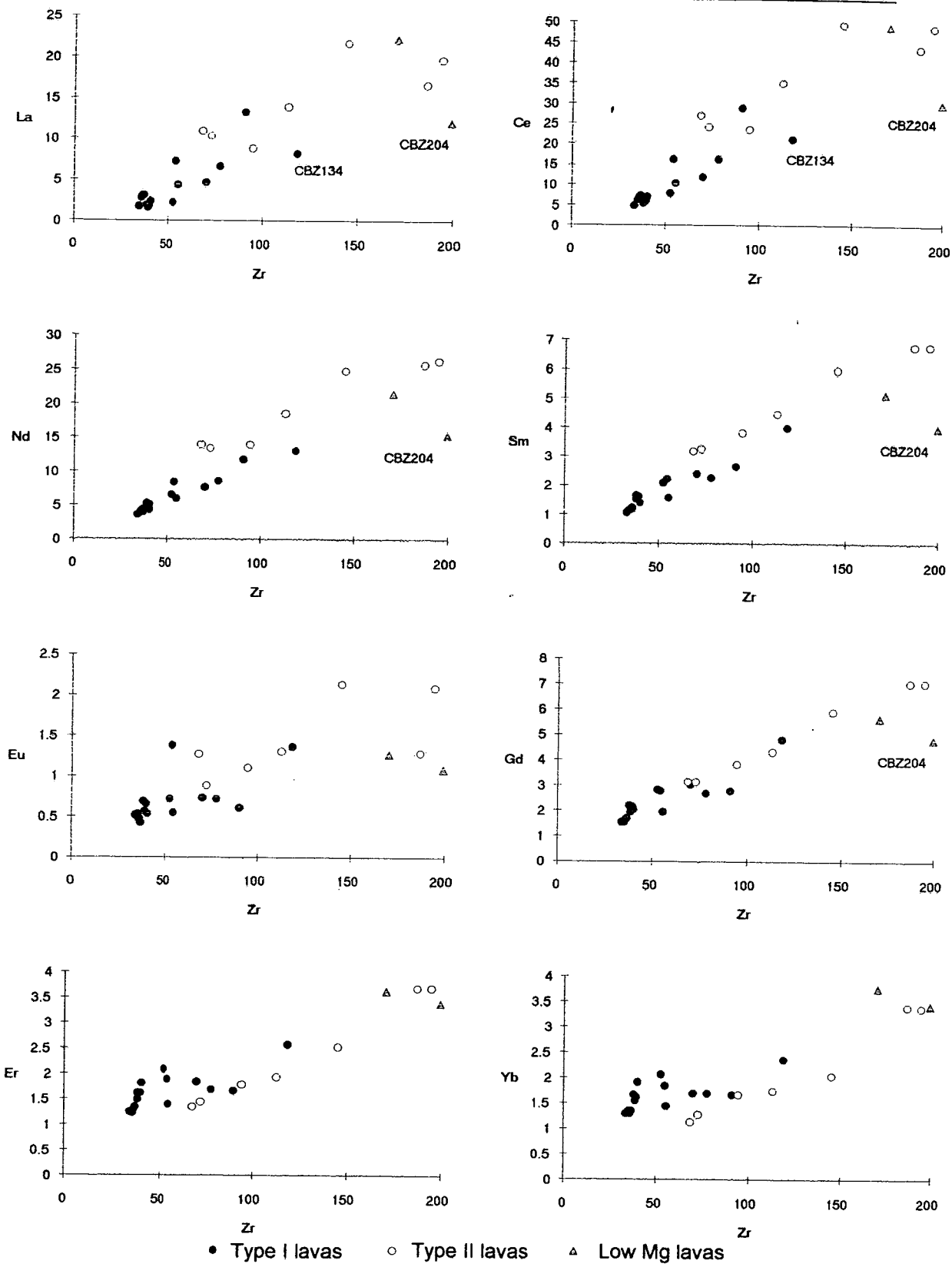

Figure 5.7. Assessment of bulk REE mobility during alteration by examination of behaviour with respect to an immobile comparator (Zr)

As a test of the accuracy of the ICP-AES REE data, the results for Sm and Nd are compared with those obtained by isotope dilution work (conducted in conjunction with the Nd isotope analyses) in Figure 5.8. It is clear that the ICP-AES results compare very well with the ID results, with a little scatter at low concentrations (<5ppm Nd, <2ppm Sm), but nothing more than might be expected from the ICP-AES technique. Sample CBZ042, however, lies clearly off the array for both elements, indicating a significant discrepancy between the two results.

It is not possible to say at this stage which result is in error, but this discrepancy is worth bearing in mind during subsequent discussion of the REE and Nd isotope data.

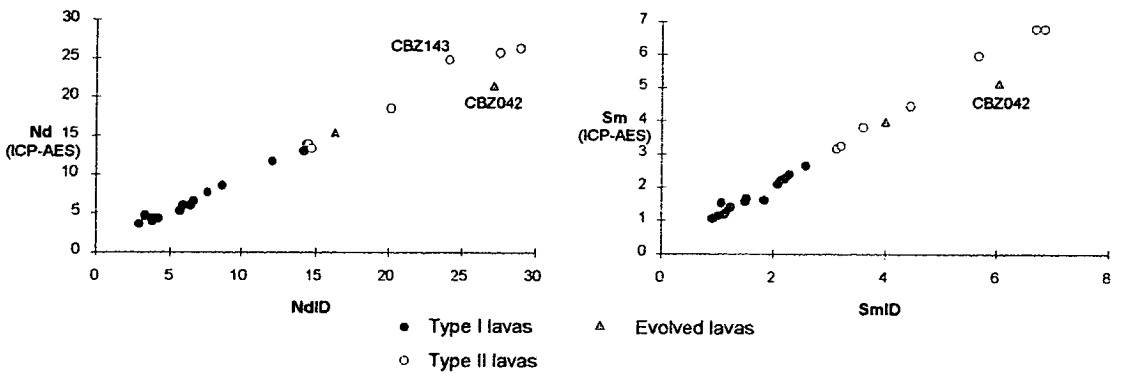

Figure 5.8. Comparison of Nd and Sm concentrations obtained by ICP-AES (used to obtain the full REE spectrum) and ID (used for Sm and Nd only, in conjunction with Nd isotope analysis)

Individual REE patterns (chondrite-normalised) are shown in Figure 5.9. There are very obvious Eu anomalies present in many of the patterns, the origins of which are discussed above. Small Pr anomalies are also common, especially in those samples with less than 10x Chondritic Abundance, probably because this is below the reasonable working detection limit for this element (N.Walsh, pers. comm.). The presence of these, adequately explainable, anomalies may mask other irregularities in the REE patterns, so it is a useful step to correct for them (temporarily). These corrected patterns (with Eu and Pr plotted as Eu* and Pr*, see figure caption for explanation) are shown in Figure 5.10. The smoothness of the patterns strongly suggests that there has been little, if any, selective REE mobility during alteration, and that the patterns are genuine, resulting from petrogenetic and fractionation processes. The pattern for CBZ166 is slightly 'stepped', and the possibility of minor mobility of Gd and perhaps Sm cannot be ruled out. Indeed, there is a very slight negative Sm anomaly detectable in several samples.

In summary, the REE data would appear to be a reliable indicator of primary igneous processes, with post-eruptive alteration apparently having little effect on either bulk REE abundances or on the shape of individual REE patterns.

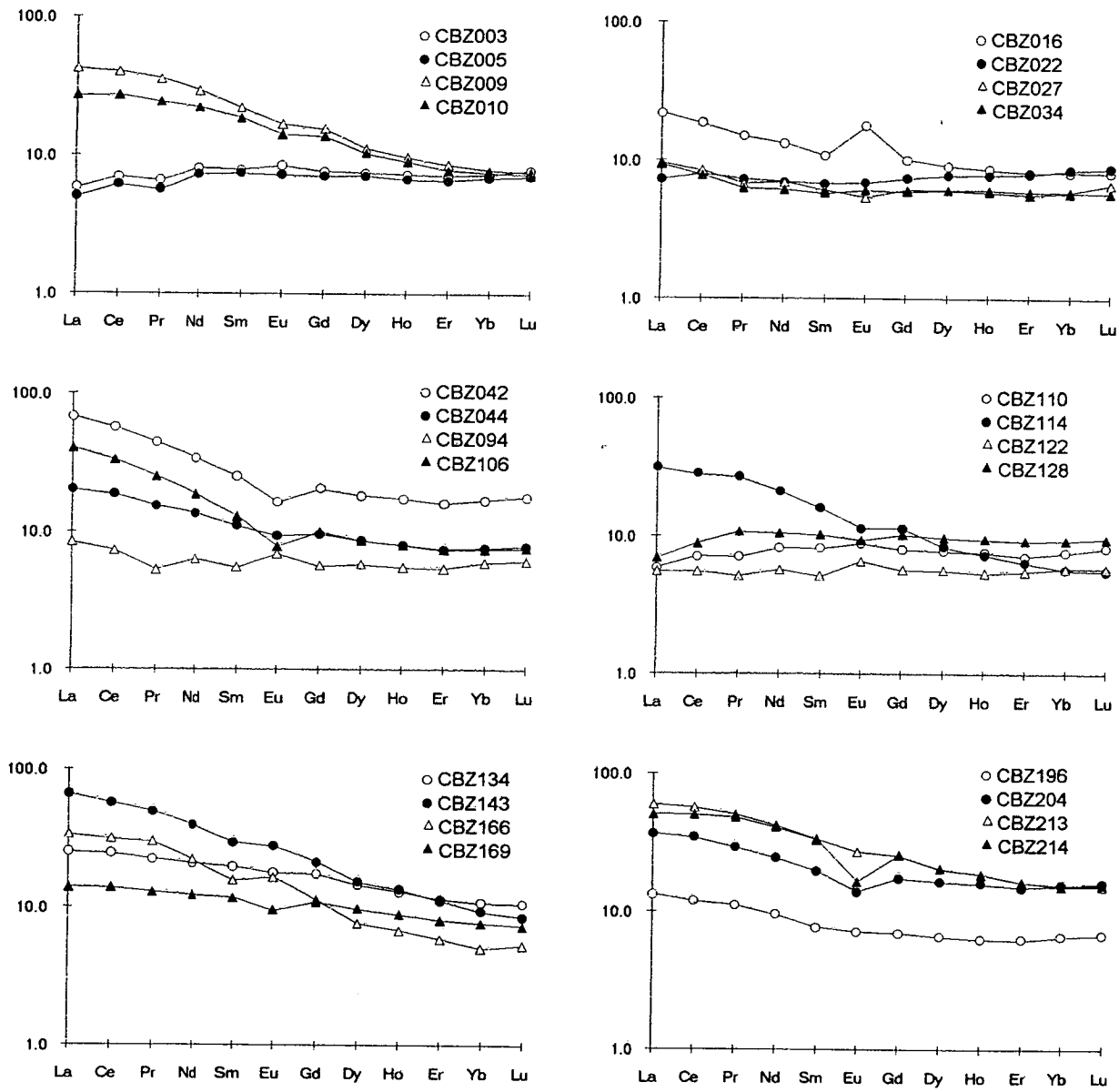

Figure 5.9. REE patterns (normalised to chondritic abundances from Nakamura, 1974). The grouping of the samples is in purely numerical order, and is of no significance. Nor is there any differentiation between Type I and Type II lavas, as it is not relevent at this stage.

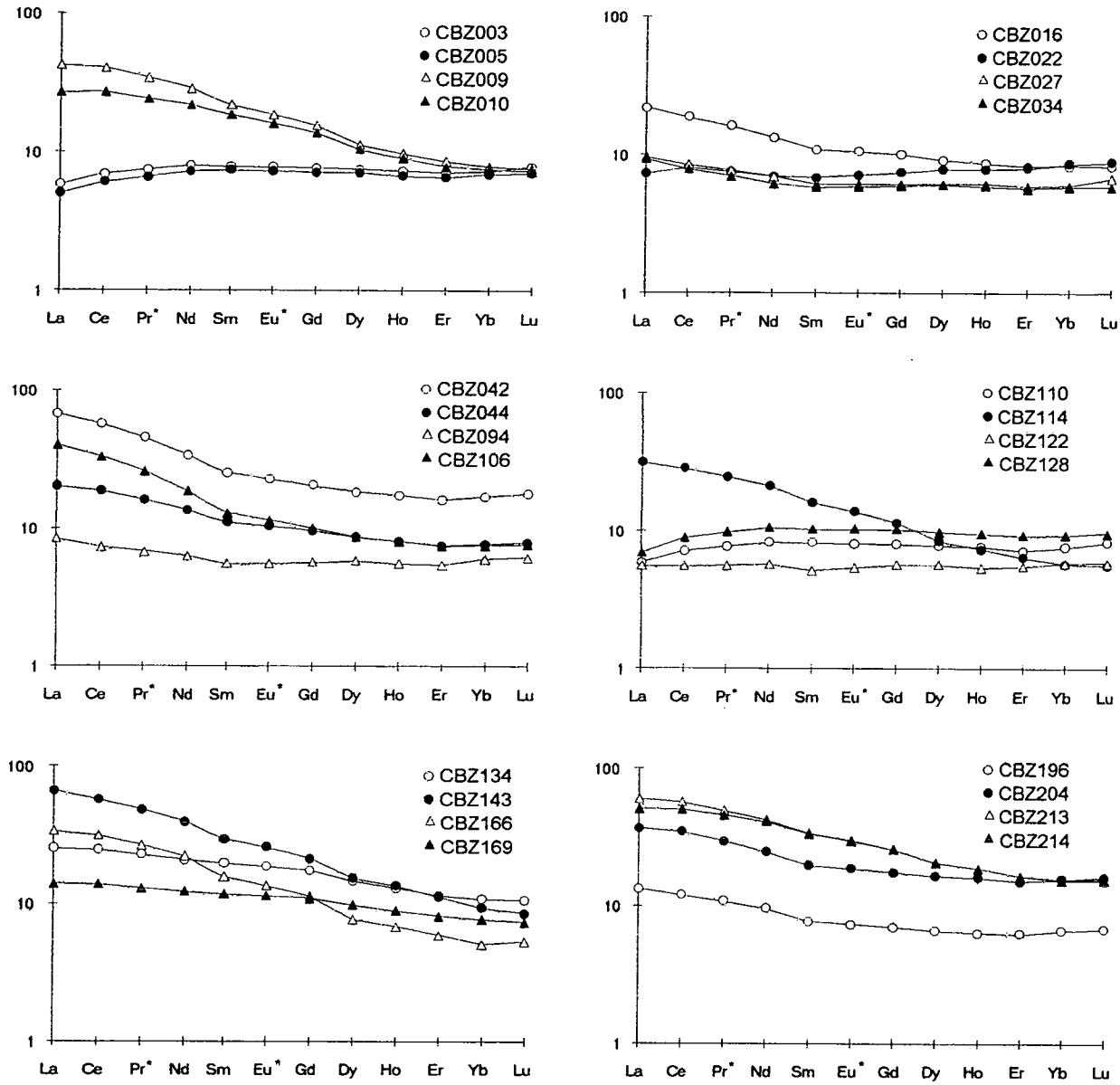

Figure 5.10. REE patterns (normalised to chondritic abundances from Nakamura, 1974), corrected for Eu and Pr anomalies. Eu*=([Gd]+[Sm])/2, Pr*=([Nd]+[Ce])/2.The grouping of the samples is in purely numerical order, and is of no significance. Nor is there any differentiation between Type I and Type II lavas, as it is not relevent at this stage.

5.4.7 Silicification, and bulk SiO_2 mobility

Silicification (bulk SiO_2 addition) has been noted previously as a post-eruptive process in volcanic rocks, and bulk SiO_2 mobility in Archaean greenstone belts in general and the Belingwe belt in particular (M.Bickle, pers. comm.) has been postulated as a significant alteration process. Given the wide range of SiO_2 concentrations seen in the Zeederbergs Formation (49-61%), the possibility of SiO_2 mobility was considered worthy of investigation.

SiO_2 is the major component in nearly all igneous rocks, and identifying its mobility is not as straightforward as for less abundant elements, as addition or subtraction of any appreciable amount of SiO_2 will result in dilution or concentration of the other major elements (the constant sum problem; Rollinson, 1993). However, the same approach may be adopted initially as has been used to assess mobility of other elements, by comparison with Zr. Comparison with modelled data shows that silicification is a possible explanation for the distribution of the SiO_2 data, and further modelling shows how compensating for the effects of this mobility affects the major element data. This technique is only examined briefly here, as it is not clear how it could be applied to the data from the Type II lavas, and since the main purpose of this study is comparison of the two lava types, this makes it of little use here. It is included, though, for the sake of completeness. The line of reasoning used is illustrated in Figures 5.11 and 5.12.

The data from a selection of Reliance Formation lavas (data from Scholey, 1992; and this study) is shown in Figure 5.11a. There is a positive correlation of Zr with SiO_2, consistent with the evolution from low to high SiO_2 contents by fractionational crystallisation of a phase (or phases) with around 40-45% SiO_2, and no significant Zr. The data from the Zeederbergs Formation, however, do not display such a correlation (Figure 5.11b), and although the more evolved lavas are much richer in Zr, the trend of the bulk of the samples seems to be towards slightly lower Zr at higher SiO_2. If the lavas of the Zeederbergs Formation were evolving in a similar way to those of the Reliance Formation, a positive trend similar to that shown as a broken line in Figure 5.11c migh be expected. However, if the lavas had been subjected to a bulk addition of SiO_2 after eruption, they would be displaced along Zr dilution trends towards 100% SiO2, 0 ppm Zr. Modelled trends for starting compositions near to the suggested fractionation trend based upon addition of SiO_2 (in 1% increments) with simple dilution of Zr are shown in Figure 5.11d. There is a very clear similarity between the data spread artificially created in Figure 5.11d, and that of the true data

in Figure 5.11b. Clearly, a large part of the behaviour of SiO_2 *could* be attributed to this process.

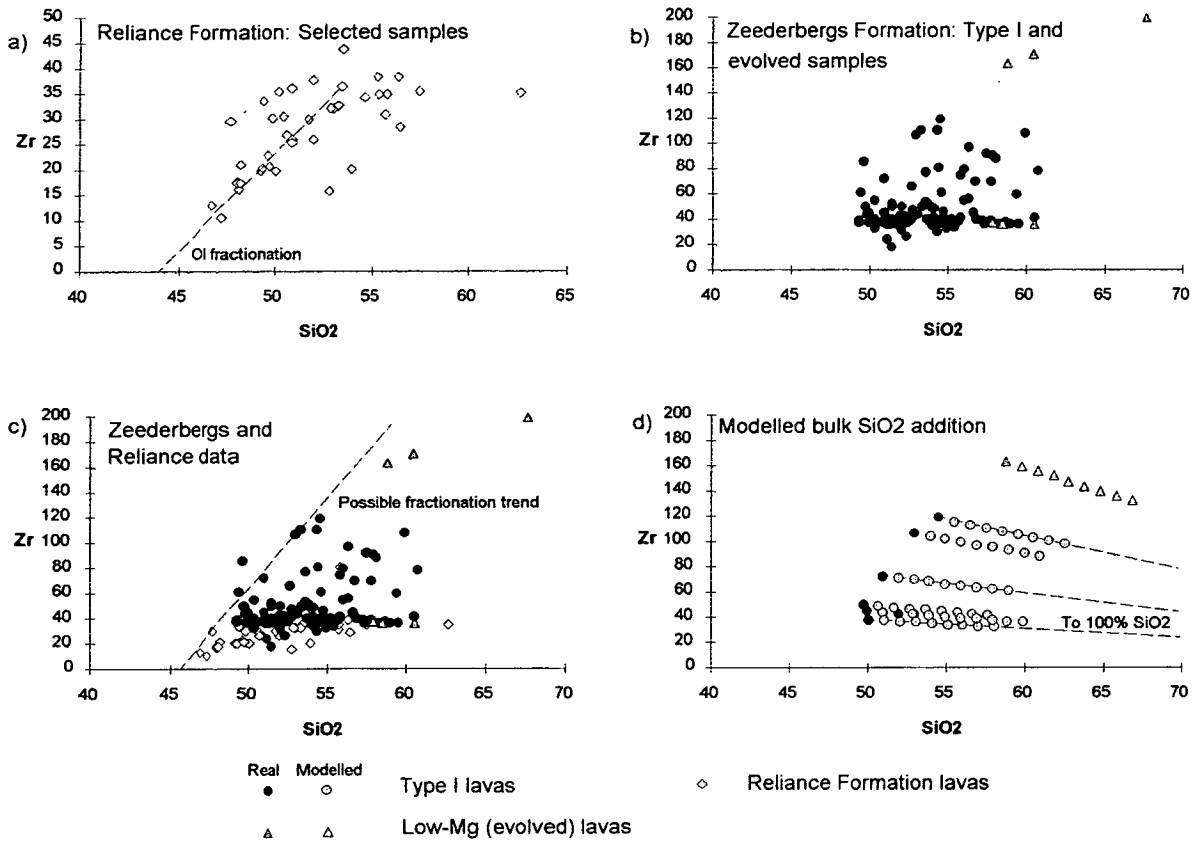

Figure 5.11 Silicification I a) Selected Reliance Formation samples **b)** Type I and low-MgO (potentially evolved) samples **c)** A combined plot of a and b, with a possible fractionation trend **d)** Modelled bulk SiO_2 addition to samples close to the possible fractionation trend in c.

It is possible to correct for potential SiO_2 addition, and to see what effect it would have on the major element chemistry of the lavas. The correction is simple, and simply involves projecting all the data on the Zr-SiO_2 plot back from 100% SiO_2, 0 ppm Zr onto the suggested frationation trend (from Figure5.11c), and then recalculating all the other major- and trace-element data to the projected initial SiO_2 content. This back projection is shown in Figure 5.12a, with all the data projected onto one simple fractionation trend. Figures 5.12b and 5.12c show the *'before and after'* effects of the correction in MgO-SiO_2 space. The correction applied in Zr-SiO_2 space effects a large improvement in the coherence of the major element behaviour, which suggests that the technique has some validity.

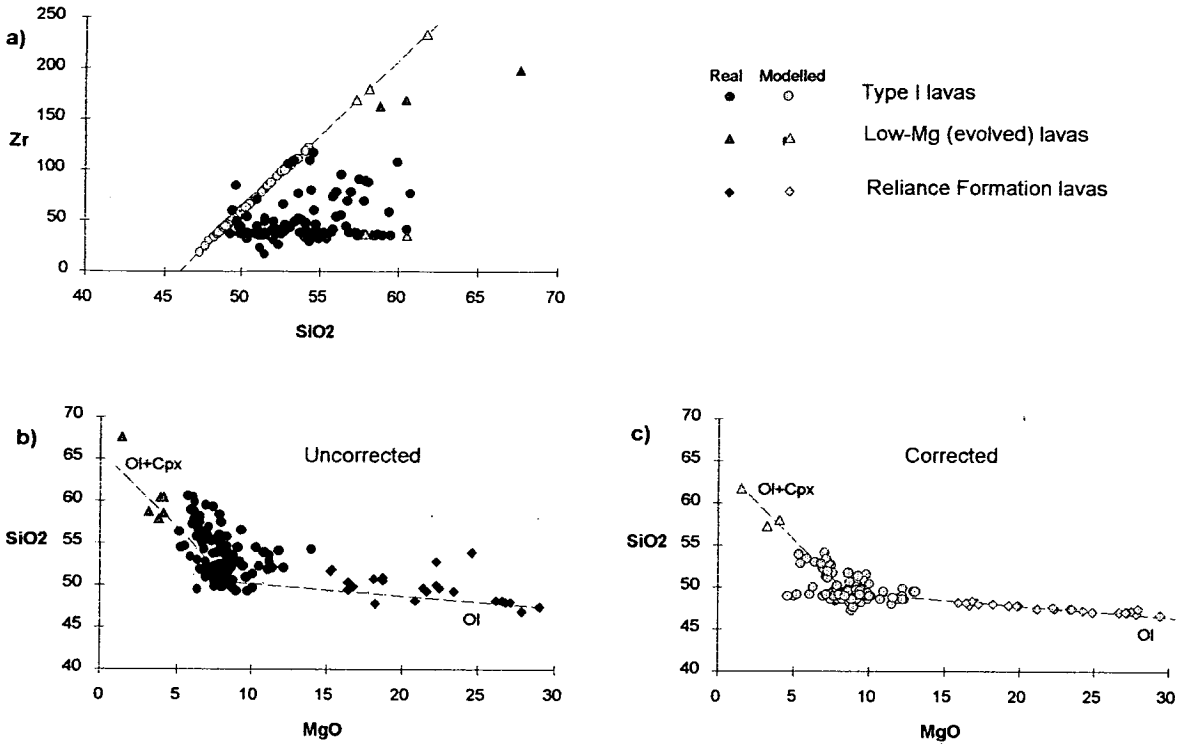

Figure 5.12 Silicification II a) Correction for bulk SiO_2 addition by projection back from 100% SiO_2, 0 ppm Zr onto the possible fractionation trend from 5.11c **b) & c)** The effect of the correction on a SiO_2 - MgO plot.

Clearly there are some large approximations and potential sources of error in this technique. The possible fractionation trend in Zr-SiO_2 space is only an approximate one, and does not allow for more than one fractionating phase (which may affect the slope). However, it would seem that this correction does have some validity. As mentioned earlier, due to the nature of this study, and the difficulties involved in applying a similar correction to the Type II lavas, this technique is not pursued in any further detail here. It is, however, worth bearing in mind that silicification has possibly had some effect on the chemistry of the lavas, though this effect is likely to have been less than 10%, and less than 5% in the majority of cases.

5.5 Conclusions

- All rock suites have different histories, and few generalisations about element mobility can be applied to any specific suite.
- Any two elements which form a reasonably coherent trend on a variation diagram which can be explained in terms of simple igneous processes are unlikely to have been mobile during subsequent alteration. In addition, the best indicator of REE stability during alteration is a smooth REE pattern.
- Work on the Reliance Formation suggests that the bulk chemistry has been little affected by recrystallisation to the current metamorphic assemblage. CaO, SiO_2, Na_2O, K_2O and the LFSE (Sr, Rb and Ba) have all been mobile during alteration, as have Cu and Pb, but the HFSE & REE (Ti, Zr, Y, Nb, La, V and P), Ni, Zn and Cr seem to have been reasonably immobile.
- A series of simple screens can be applied to the samples from the Zeederbergs Formation to remove samples whose composition is not a reliable indicator of primary igneous processes. Bulk chemistry has been little affected by recrystallisation to the current metamorphic assemblage. Element mobility can be assessed by comparison with Zr as an immobile comparator.
- TiO_2, Al_2O_3, MnO and P_2O_5 are interpreted as being immobile, MgO, FeO as slightly mobile, CaO as significantly mobile, and SiO_2, Na_2O and K_2O as very mobile.
- Concentrations of the HFS elements (Nb, Y, Ce, Nd, V, and, of course, Zr) appear to be reliable indicators of primary abundances. Ni and Cr seem to have been fairly immobile, and the behaviour of Th, Sc and Cu is thought to represent primary differences between the two lava types, but Zn and the LFSE (Sr, Pb, Ba, and Rb) would seem to be unsuitable for any serious consideration.
- The REE data would appear to be a reliable indicator of primary igneous processes.
- There is good evidence for silicification and bulk SiO_2 mobility within the Zeederbergs Formation, and it may be possible to correct for this using theoretical fractionation trends with Zr.
- Of the 'Low-Mg' samples set, only three samples appear to be truly evolved, showing very high abundances in all the incompatible elements. The other three samples apparently only show low MgO and high SiO_2 as a result of heavy silicification, and will be excluded from all further investigation.

6

GEOCHEMISTRY

6.1 Introduction

Now that the geochemistry of the lavas has been examined to assess the effects of alteration, it is possible to concentrate on those aspects of the geochemistry which have petrogenetic significance. In this chapter the geochemistry of the Reliance Formation is summarised, and the major element, trace element, REE and isotope geochemistry of the Zeederbergs Formation fully described. The rocks of the Reliance Formation nearly all plot on the world-wide, Al-undepleted komatiitic trend. The suite has been classified into several rock types which make up this komatiitic series, and the geochemistry of these is documented.

The geochemistry of the Zeederbergs Formation is considered with two principal aims in mind; to examine the differences between the Type I and Type II lavas, and to assess which aspect of their behaviour *cannot* be attributed to simple partial melting and fractionation processes. A similar approach is adopted to that used in Chapter 5, systematically examining the behaviour of each component by comparison to one chosen comparator, in this case MgO. Previous isotope work on the Zimbabwe craton and the Belingwe belt is discussed, and a best age estimate for the Ngezi Group is chosen. The Sm-Nd isotope systematics of the Zeederbergs samples are examined in the light of this age, both in terms of apparent isochron dates and initial ε_{Nd} values.

6.2 The Reliance Formation

6.2.1 Principal geochemical characteristics

Scholey (1992) presented his data for the Reliance Formation in terms of the immobile elements Mg, Al, Ti and Fe on a Jensen Cation Diagram (reproduced in Figure 6.1), and demonstrated that the majority of his samples plot on or near the general world-wide komatiitic trend. This diagram also shows the division between komatiites, high-magnesium basalts and tholeiitic basalts (highlighted again in Figure 6.2), and is described by

Table 6.1. Principal geochemical characteristics of the rocks of the Reliance Formation as described by Scholey (1992)

Rock type	Distinguishing features	Major element chemistry	Trace element chemistry
KOMATIITE	Modal olivine >30%	MgO 20.6-29.2% Low concentrations of:- SiO_2 (<50%) Al_2O_3 (3.5-9.5%) Alkalis (<0.4%Na_2O, & <0.45% K_2O) TiO_2 (<0.45%)	Low concentrations of incompatible trace elements:- Y (<11.5ppm) Zr (7.5-25.5ppm) P (50-140ppm) V (125-190ppm) Ratios involving Ti, Zr & Y tightly constrained & near chondritic High concentrations of compatible elements:- Ni 630-1400ppm (behaviour attributable to olivine control) Cr 1900-2850ppm (behaviour requires some Cr-spinel fractionation)
PERIDOTITIC CUMULATES	Cumulate texture	MgO 16-40% Major element abundances similar to komatiites	Incompatible element abundances similar to komatiites Higher concentrations of :- Ni (650-2500ppm) & Cr (1900-3750ppm) due to abundance of olivine & Cr-spinel
HIGH MAGNESIUM BASALTS			
Olivine phyric - aphyric	Petrographically similar to komatiites, but <30% modal olivine	MgO <18.5% Potentially derived from komatiites by fractionation (MgO *possibly* as low as 5.7%)	
Olivine spinifex textured		MgO 12.5-17.4% (thought to reflect unusually low proportion of olivine compared to the olivine phyric-aphyric varieties)) SiO_2 similar to komatiites (45.4-52.3%)	Most incompatible trace element abundances comparable with komatiites
Clinopyroxene spinifex textured (and siliceous high magnesium basalts, SHMB)		MgO 11.4-15.3% (some samples with modal plag. show MgO of 9.6%) Highly siliceous:- SiO_2 >50% (52-57% in plagioclase bearing rocks) Al_2O_3 (9-15%) and TiO_2 (0.44-0.63%) higher than in komatiites	Incompatible element abundances of SHMB higher than in komatiites:- Y 9.5-20ppm Zr 23-45ppm P 100-200ppm V 165-280ppm Ratios involving incompatible major & trace elements differ from chondritic ratios
MAFIC AND RELATED TYPES	Plagioclase bearing	MgO contents lie entirely within range seen in high-magnesium basalts. Tholeiitic basalts 7.6-8.6% Pyroxene-phyric, variolitic textured 8.3-9.5% Dolerites & tuffs 8.0-12.3% Other major element abundances similar to high-magnesium basalts SiO_2 (50-56%) Al_2O_3 (11-15.5%) Alkalis (1-5% Na_2O & <1.25% K_2O) All mafic rocks slightly depleted in TiO_2	Incompatible trace element ratios are generally close to chondritic values (or primitive mantle values, for those involving P) Incompatible trace element abundances generally higher than those in the high magnesium basalts. All mafic rocks slightly depleted in V Flat HREE & depleted LREE patterns similar to modern MORB

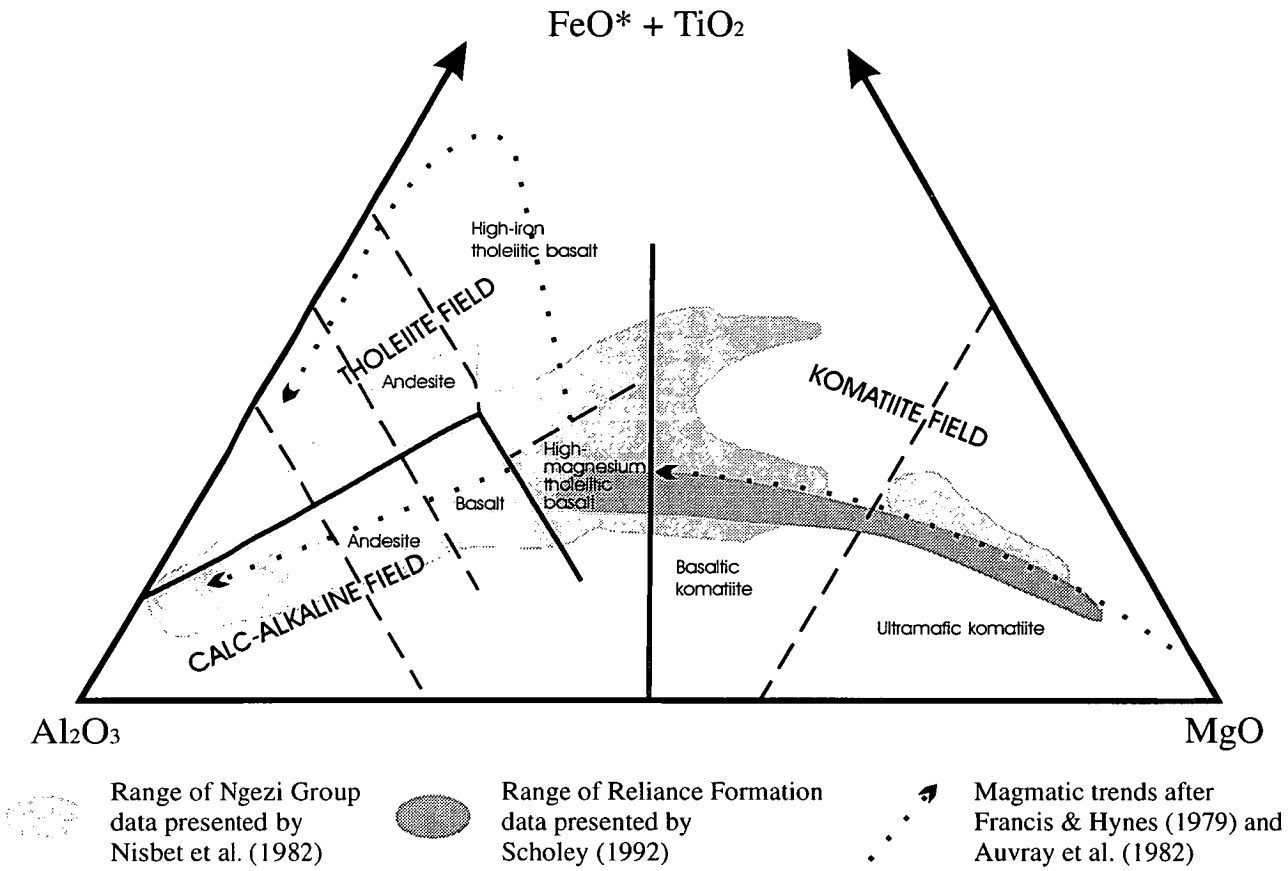

Figure 6.1. Jensen Cation Diagram (after Jensen 1976) showing the Reliance Formation data compiled by Scholey (1992)

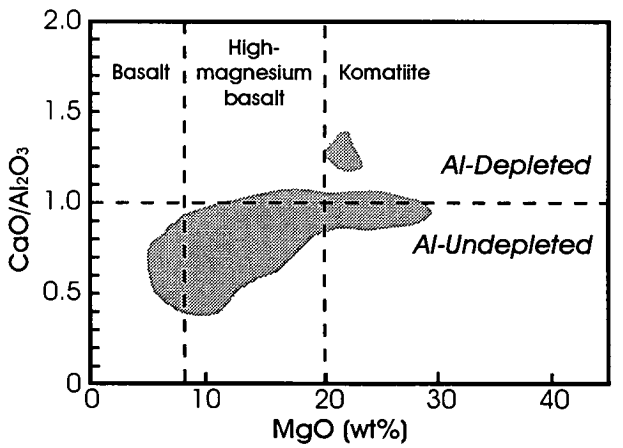

Figure 6.2. Plot of CaO/Al_2O_3 vs. MgO for Scholey's (1992) Reliance Formation data. The accepted divisions into tholeiitc basalts, high-magnesium (komatiitic) basalts and komatiites (eg. Arndt & Nisbet, 1982b) and between Al-undepleted and Al-depleted compositions (Nesbitt et al., 1979) are indicated by the dashed lines. (Diagram from Scholey, 1992)

Scholey (1992) as an evolutionary trend controlled by the extent of fractionation and/or partial melting. He also showed that most unaltered lavas from the Reliance Formation have $CaO/Al_2O_3 < 1$ (Figure 6.2), and can therefore be assigned to the Al- and HREE-undepleted types of Nesbitt *et al.* (1979). The principal characteristics of the Reliance Formation, as described by Scholey (1992), are given in Table 6.1.

There are two areas of uncertainty in Scholey's (1992) interpretation of his data. Firstly, the classification of most of the lavas in the formation as Al-undepleted seems to be broadly valid, but no explanation is given for the group of 6 samples which plot well into the field of Al-depleted lavas. Whether these are genuinely Al-depleted lavas is unclear. Secondly, the division between tholeiitic basalt and high-magnesium basalt seems to be a little contradictory at times. He defines high-magnesium basalts as those which contain no modal plagioclase, which would seem to depend more on the pressure and temperature of fractional crystallisation and partial melting than on the simple extent of these processes. However, whilst acknowledging that the ranges of MgO contents of tholeiitic and high-magnesium basalts overlap to a large degree, he then draws lines defining these separate fields at fixed MgO contents, and attributes MgO content to the degree of fractionation and/or partial melting. These inconsistencies make the distinction between high-magnesium and tholeiitic basalts a very ambiguous and not very useful one, and no attempt is made to sub-divide the lavas of the Zeederbergs Formation sampled in this study in a similar way.

6.2.2 REE geochemistry of the Reliance Formation

Scholey (1992) presents REE data for 25 of his samples, and divides them into two types on the basis of their REE patterns. To avoid confusion, the Type I and II categories defined by him are prefixed by 'R' (Type RI and RII), to distinguish them from the Type I & II basalt classification developed in this study. The division between types RI and RII is based upon whether the samples show LREE depletion (RI) or LREE enrichment (RII). These types are then further sub-divided on the basis of overall REE abundance and/or slope/shape. The classification scheme is summarised in Figure 6.3.

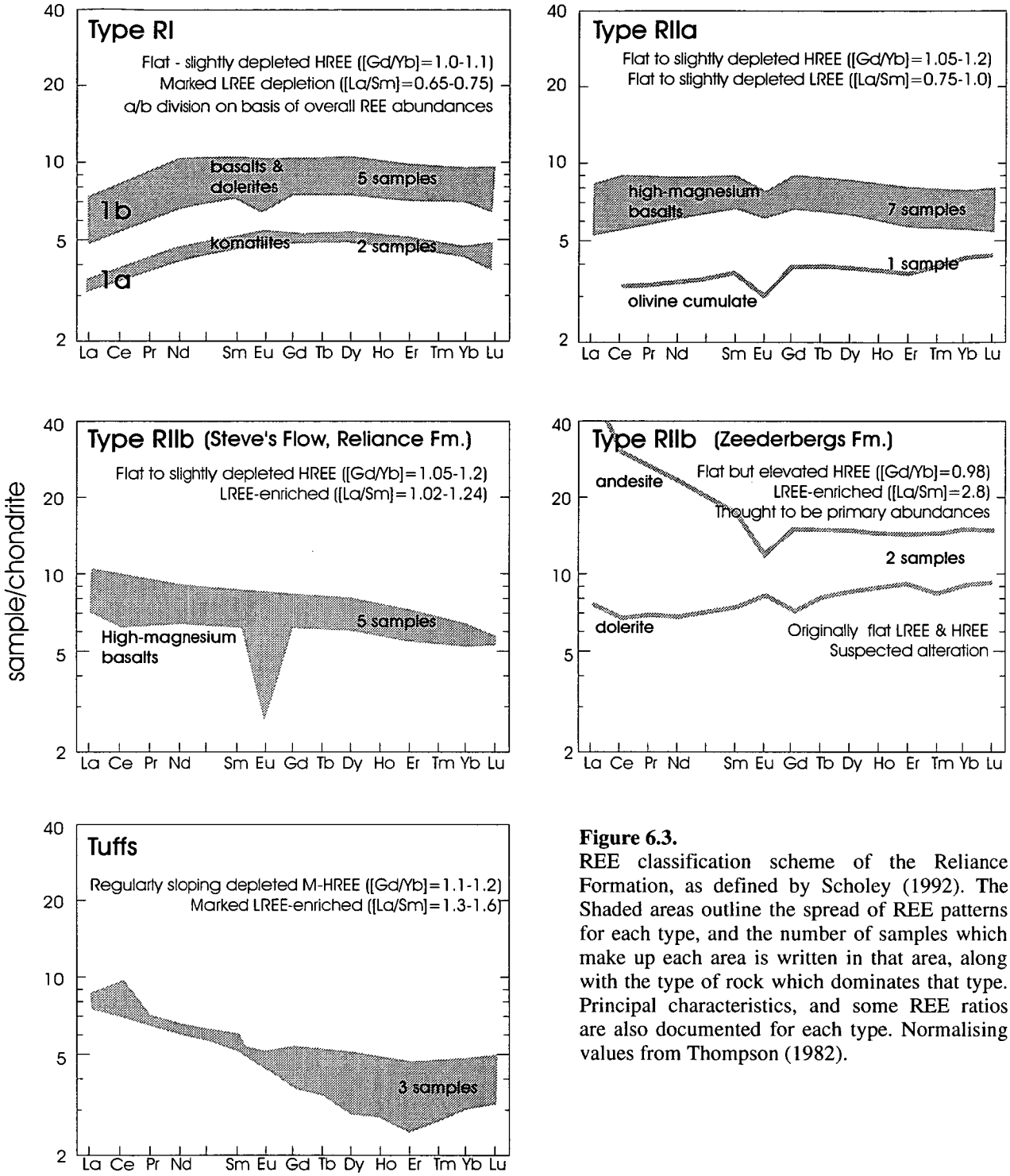

Figure 6.3.
REE classification scheme of the Reliance Formation, as defined by Scholey (1992). The Shaded areas outline the spread of REE patterns for each type, and the number of samples which make up each area is written in that area, along with the type of rock which dominates that type. Principal characteristics, and some REE ratios are also documented for each type. Normalising values from Thompson (1982).

6.2.3 Summary

Scholey (1992) summarises his geochemical classification of the Reliance Formation as follows :

1. **Porphyritic komatiites:** MgO >18%, Al-undepleted, LREE depleted, chondritic trace element ratios.
2. **Peridotitic cumulates:** *ca.* 16-42% MgO, chondritic trace element ratios.
3. **High-magnesium basalts:** *ca.* 8-18% MgO (some aphyric and spinifex textured samples outside this range), enriched in SiO_2 (>50%) and LREE, depleted in Ti relative to Zr & Y.
4. **Mafic and related rock types:** MgO<9.5% in basalts, MgO<12.5% in dolerites & tuffs. Variable LREE, Zr & P enrichment seen in a few Zeederbergs samples, other rocks depleted in LREE, Zr & V.

6.2.4 Other geochemical work on the Reliance Formation

Other geochemical work on the Reliance Formation tends to agree with Scholey's (1992) findings. A good summary of all this work can be found in Bickle *et al.* (1993). The conclusions are broadly similar, both in assessment of elemental mobility during alteration, and in the attribution of most geochemical variation to olivine (perhaps with a little Cr-spinel) fractionation. McDonough & Ireland (1993) reported ion microprobe analyses of glass inclusions in fresh olivines from the SASKMAR drill site (see Figure 3.1), which are probably the most pristine samples to have been analysed. Their conclusion is that the trace element patterns for these glass inclusions strongly suggests an intraplate origin for the lavas. A summary of previous isotope work on the rocks of the Ngezi Group is presented later in this chapter with the isotope data from this study.

6.3 The Zeederbergs Formation: major and trace element chemistry

6.3.1 The aims of this section

It has been shown in Chapter 5, as a stage of assessing elemental mobility, that there is little in the geochemistry of the Zeederbergs Formation, especially the Type I lavas, which cannot be explained by simple processes. The relatively limited range of MgO contents (as compared to studies based on the Reliance Formation), the very limited information available from the petrography of the samples, and the variable degrees of alteration make the sample suite collected in this study unsuitable for any detailed, quantitative study of partial melting or fractional crystallisation processes. The two principal aims of this chapter, then, are :

- To examine the geochemical differences between Type I and Type II lavas.

- To assess which aspects of the geochemistry, particularly of the Type II lavas, cannot be so easily attributed to simple partial melting and fractionation processes.

A similar approach is adopted here, at least initially, as was used in Chapter 5, to examine all the major and trace element behaviour. That is, all elements are plotted against one suitable comparator. The principal requirements for this comparator are that it should be fairly immobile during alteration, that it should show *no* systematic difference between Type I and Type II lavas, and that its abundance can be explained by reasonably simple first order petrogenetic processes which are likely to have affected *both* types. The obvious choice is MgO.

6.3.2 Major element abundances

The behaviour of the major elements with MgO is shown in Figures 6.4 and 6.5, together with vectors for simple processes which can explain much of their distribution. The following is a brief summary of their behaviour.

- **SiO_2** It can be clearly seen that there are no systematic differences between Type I and Type II lavas in terms of SiO_2 content, and this plot also confirms that there is no Type I/II distinction seen in MgO contents

either (other than there being no Type II lavas with MgO<7%). The behaviour of both these elements can be explained in terms of variable degrees of partial melting/fractional crystallisation and some silicification.

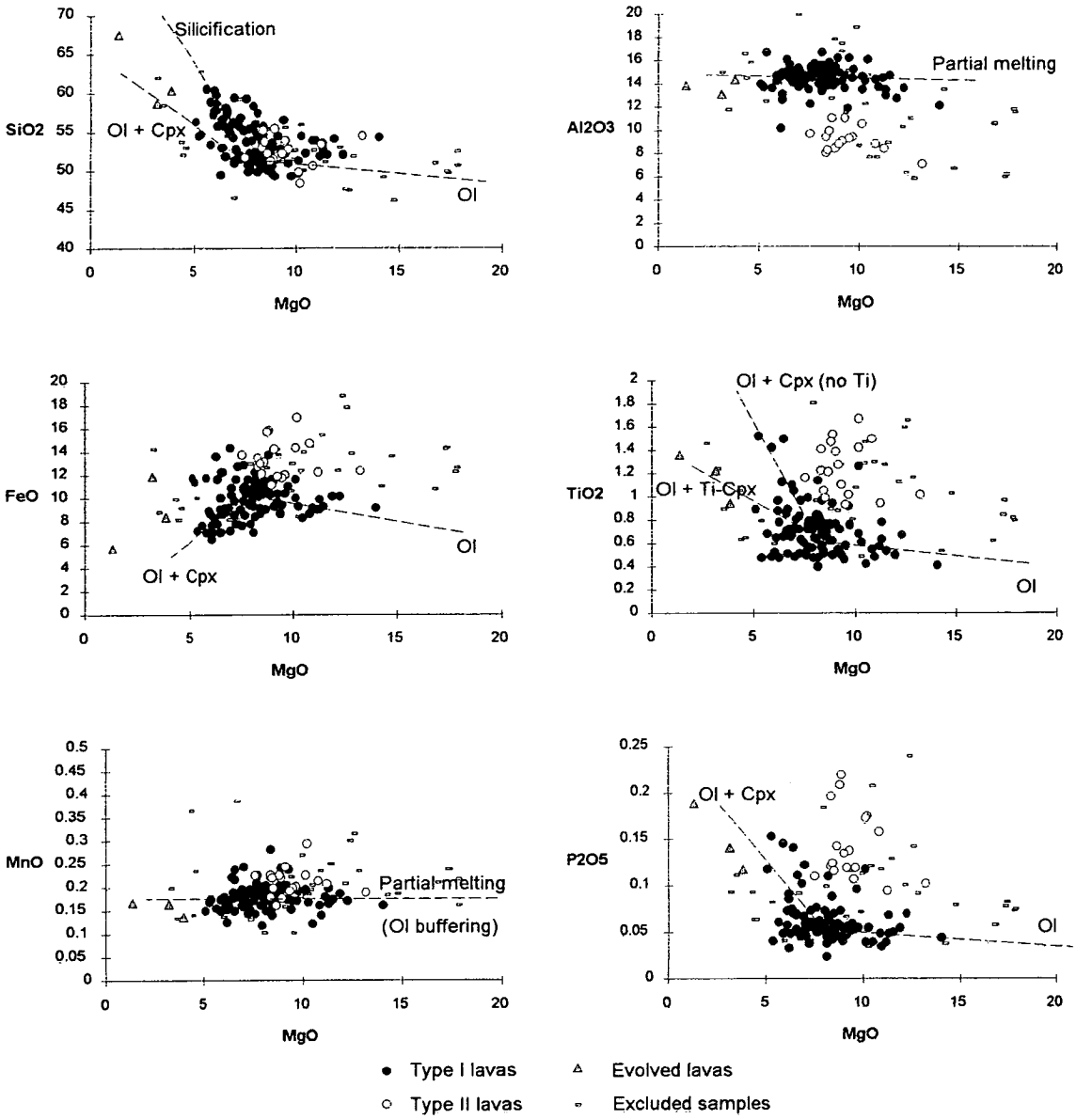

Figure 6.4 Behaviour of less mobile major elements with respect to MgO. Dashed lines represent plausible explanations for the trends seen.

- **Al_2O_3** The separation between Type I and Type II lavas is clearly seen, with the Type II lavas showing significantly lower Al_2O_3 contents for all MgO contents. In fact, these low Al_2O_3 contents are one of the defining and most significant characteristics of the Type II lavas, as no other

tholeiitic basalt analyses have been found anywhere in the world with such low values.

- **FeO** Although the distinction is not as clear as for Al_2O_3, examination of the plot shows that at any given MgO content, Type II lavas have a higher FeO content than Type I.

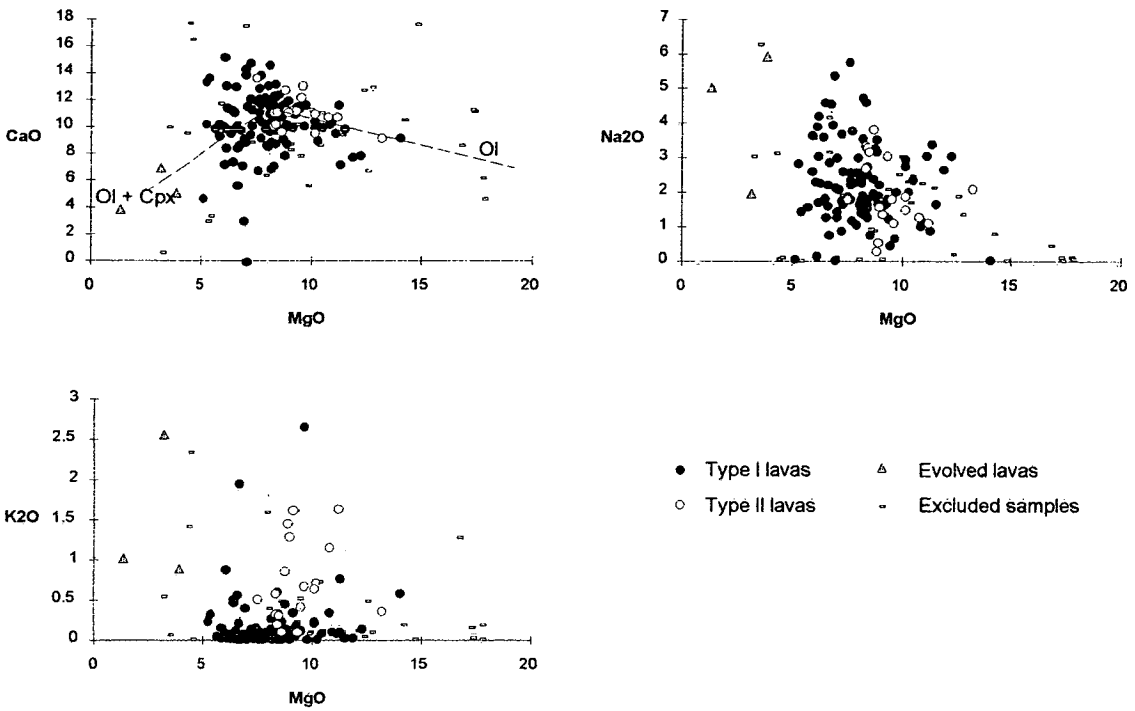

Figure 6.5 Behaviour of more mobile major elements with respect to MgO. Dashed lines represent plausible explanations for the trends seen.

- **TiO_2** Again, a clear distinction is seen between Type I and Type II lavas, with Type II lavas having a consistently higher TiO_2 content for any given MgO content. The distribution of TiO_2 contents within the Type II lavas is not easily attributable to simple melting/crystallisation processes.

- **MnO** No obvious Type I/II distinction. Most MnO contents are clustered around the range 0.15-0.2%, which would correspond to buffering by olivine during melting and fractional crystallisation.

- **P_2O_5** Similar behaviour to TiO_2, with Type II lavas having a significantly higher P_2O_5 content for any given MgO content. Again, the behaviour of

the Type II lavas is not easily attributable to simple melting/crystallisation processes.

- **CaO** There is no obvious distinction between Type I and Type II lavas.
- **Na_2O** Again, no obvious distinction between Type I and Type II lavas.
- **K_2O** Type II lavas would seem to show generally higher K_2O contents, but as K_2O has been shown to be very mobile during alteration, it would be unwise to attach much significance to this observation.

6.3.3 Major element ratios

The only major element ratios which are thought to add anything to the observations from the major element abundances are those involving Al_2O_3, and mg# (wt.% MgO/(MgO+FeO*)), shown in Figure 6.6.

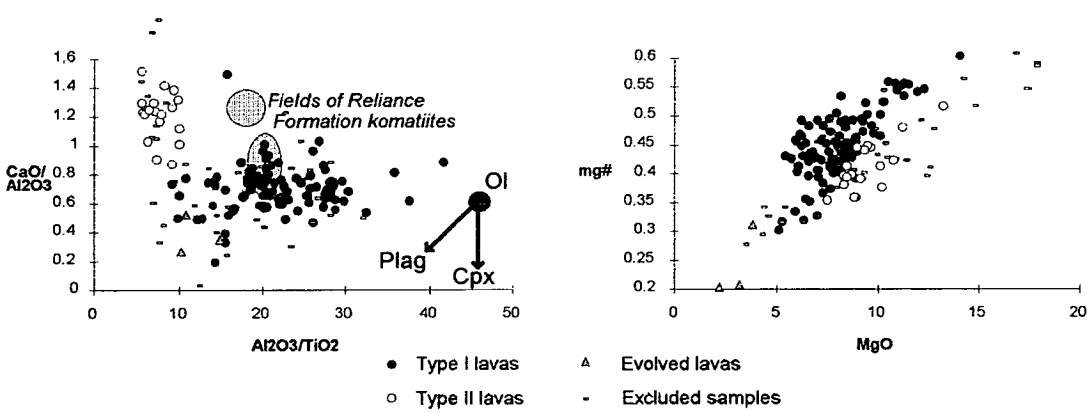

Figure 6.6 Behaviour of selected major element ratios, and systematic differences between Type I and Type II lavas.

The plot of CaO/Al_2O_3 clearly shows the depletion in Al_2O_3 characteristic of the Type II lavas, which show consistently higher CaO/Al_2O_3 (significantly, >1) and lower Al_2O_3/TiO_2 than the Type I lavas. The field of the Reliance Formation komatiites is also shown, together with the fractionation vectors for olivine, clinopyroxene and plagioclase. It is clear that while many of the Type I lavas could be descended from material similar to the Reliance Formation komatiites by simple fractionation of these phases, the Type II lavas, and some of the Type I lavas (those with Al_2O_3/TiO_2 >25) require some additional processes. The field of Reliance Formation material with

CaO/Al_2O_3 >1 corresponds to those samples from Scholey's (1992) study mentioned in section 6.2.1, for which no full explanation is offered, the vast majority of the samples having CaO/Al_2O_3 <1.

The plot of mg# (wt.% MgO/(MgO+FeO)) against MgO essentially re-affirms the lower FeO contents of the Type II lavas, at any given MgO, the Type II lavas have a lower mg#. This plot is included to illustrate the point that at any given MgO content, the Type II material has either: a) undergone a greater degree of fractionation than the Type I material, *or* b) undergone similar amounts of fractionation from a more FeO-rich parent magma.

6.3.4 Trace-element abundances

The behaviour of the trace elements with MgO is shown in Figures 6.7 (HFS elements), 6.8 (LFS elements) and 6.9 (transition elements), together with vectors for simple processes which explain much of their distribution. The following is a brief summary of their behaviour:

HFS elements and selected REE (Figure 6.7)

- **Nb, Zr, Ce, Nd** Consistently higher abundances are seen in Type II lavas. The distribution of Type II abundances is not easily attributable to simple melting/crystallisation processes.

- **Y** There is some overlap, but Y contents in Type II lavas extend to higher values than are seen in Type I lavas at similar MgO contents. Again, distribution of Type II abundances is not easily attributable to simple melting/crystallisation processes.

- **Th** The scatter in the data is large (largely due to analytical uncertainty), but the Type II lavas appear to have consistently higher abundances than Type I lavas.

- **V** There is no apparent difference between Type I and Type II lavas, and no obviously anomalous distribution of abundances.

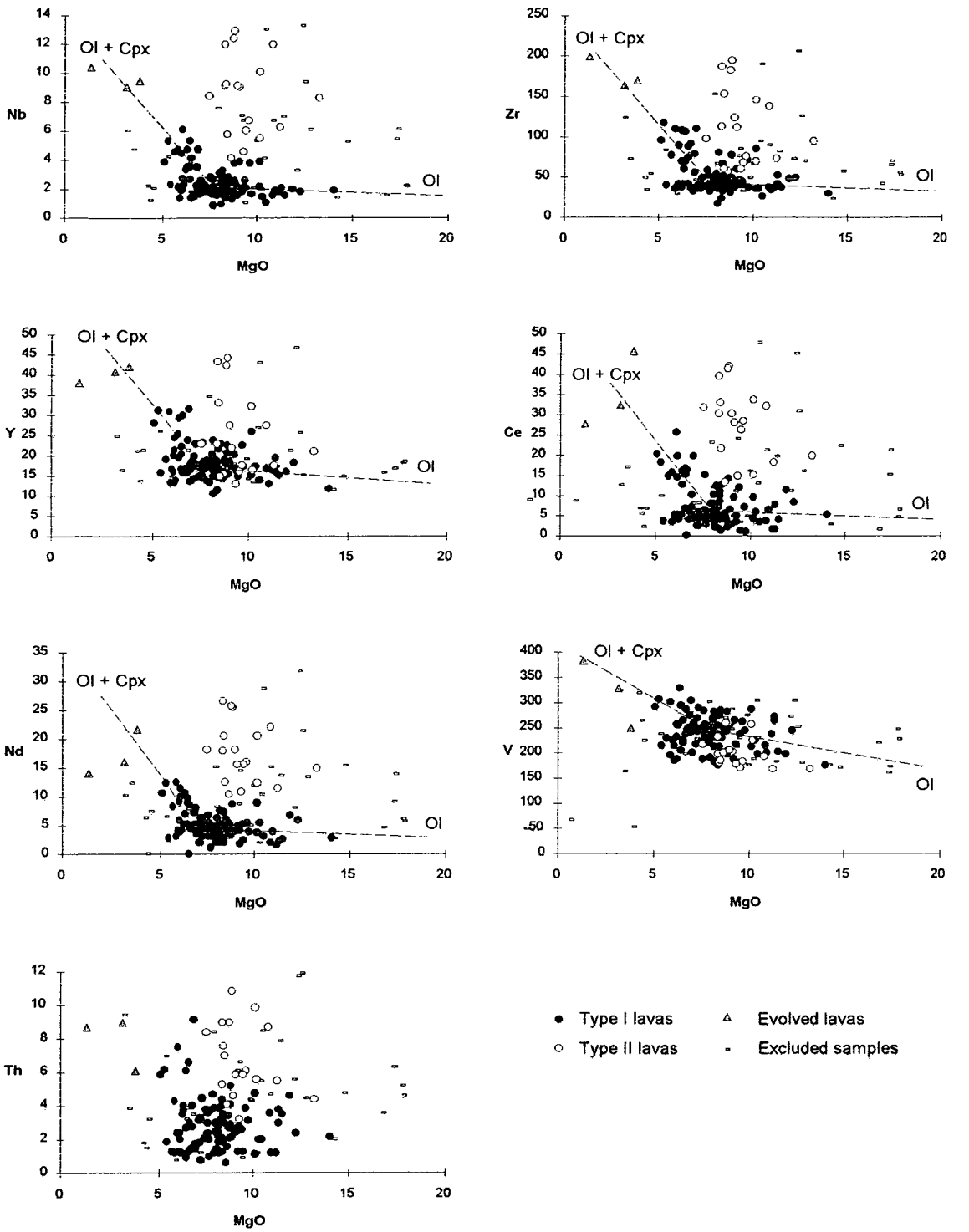

Figure 6.7 Behaviour of HFS elements with MgO, and differences between Type I and Type II lavas. Dashed lines represent plausible explanations for the trends seen.

LFS elements (Figure 6.8)

- **Sr, Pb, Ba** As stated in Chapter 5, it would be unwise to attach too much significance to the abundances of these mobile elements. However, they all seem to show higher abundances at a given MgO in the Type II lavas. Little can be inferred about the operation of petrogenetic processes.

- **Rb** The high degree of mobility makes it difficult to draw any reasonable conclusions from the Rb data.

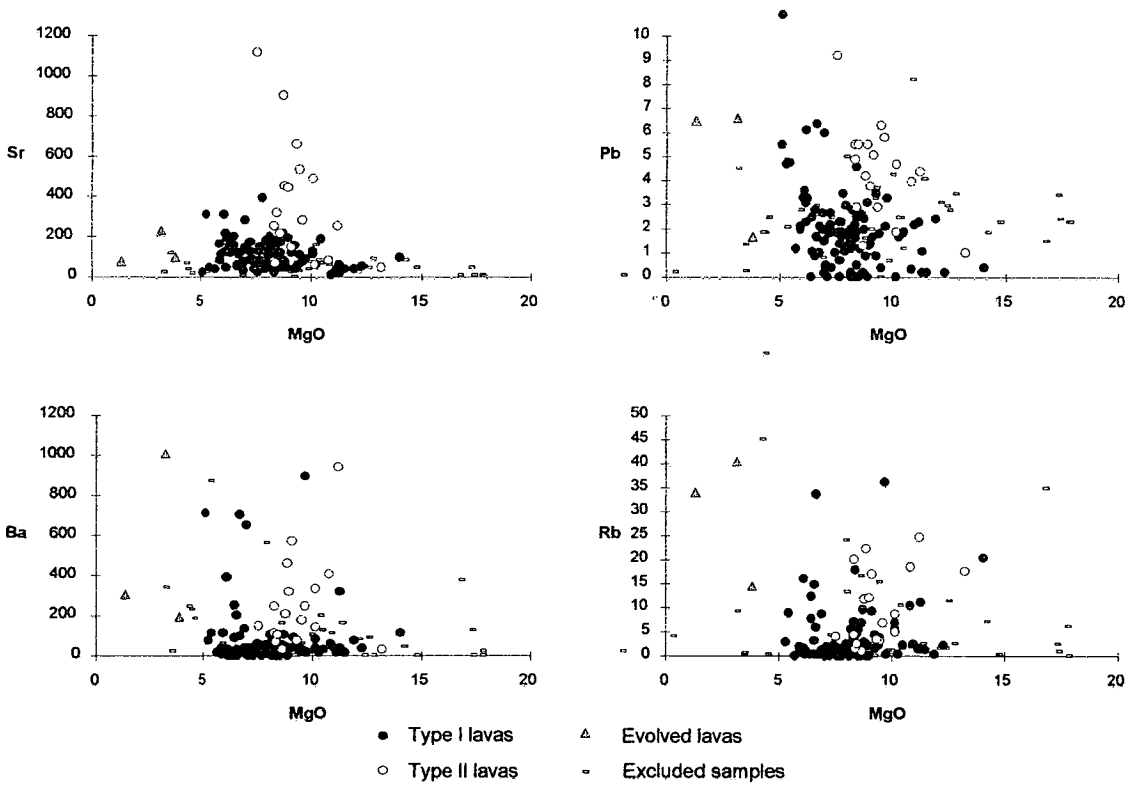

Figure 6.8 Behaviour of LFS elements with MgO, and differences between Type I and Type II lavas.

Transition elements (Figure 6.9)

- **Zn** The high degree of mobility makes it difficult to make any interpretation of the Zn data. The Type II lavas seem to have generally higher concentrations at a given MgO.

- **Cu** The Type II lavas have clearly higher Cu contents than the Type I lavas. The distribution of Cu contents is hard to attribute to simple melting/crystallisation processes.

- **Ni, Cr** Type II lavas show higher abundances at given MgO contents than Type I. Both of these elements are compatible to some degree with the melt residue/crystallising assemblage (especially Cr, as there is evidence of minor Cr-spinel crystallisation (Scholey, 1992; Bickle *et al.* 1993)), so the divergence between the Type I and Type II trends suggests a different primary melt composition.

- **Sc** Type II lavas show clearly lower Sc contents than Type I lavas across the whole range of compositions.

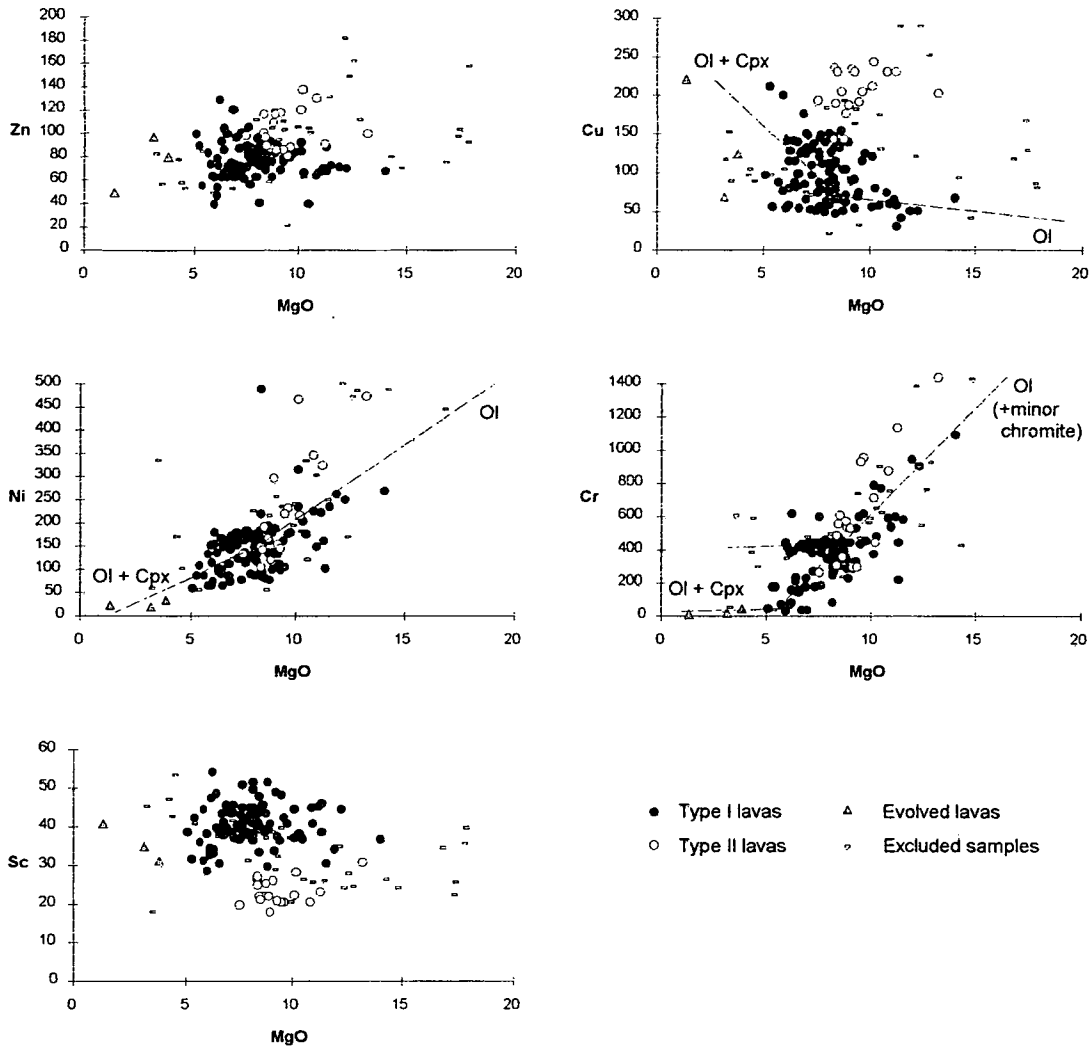

Figure 6.9 Behaviour of transition elements with MgO, and differences between Type I and Type II lavas. Dashed lines represent plausible explanations for the trends seen.

6.3.5 Trace element ratios

The plots of absolute abundances clearly show which elements show systematic differences between Type I and Type II lavas. The majority of the HFS elements show a degree of enrichment in the Type II rocks, but as the discussion of variation of chemistry with stratigraphic height (Section 3.5), and the plots of these elements against Zr (Figure 5.4) clearly show, they are not all enriched to the same degree, and there are systematic differences in the ratios of these elements which accompany their enrichment. These differences are illustrated in Figure 6.10, which shows the behaviour of several HFS element ratios :

- **Zr/Nb** Lower in Type II lavas.
- **Nb/Y** Higher in Type II lavas.
- **Zr/Y** Higher in Type II lavas.
- **Ce/Y** Higher in Type II lavas.
- **Ce/Zr** Slightly higher in Type II lavas, but the two fields overlap heavily.

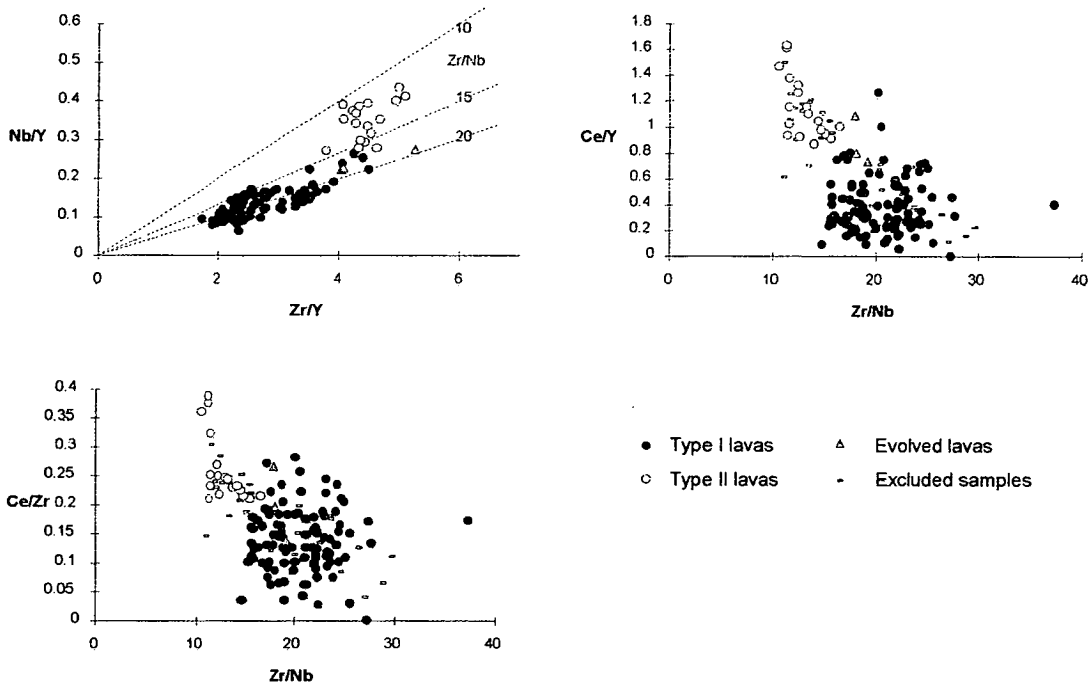

Figure 6.10 Behaviour of selected trace element ratios in order to determine the relative enrichments in Type II lavas

These relationships suggest an order of degree of relative enrichment of the HFS elements in the Type II lavas :

Nb > Ce ≈ Zr > Y

Most enriched Least enriched

These relative enrichments provide valuable clues towards possible explanations for the differences between the two types of lava.

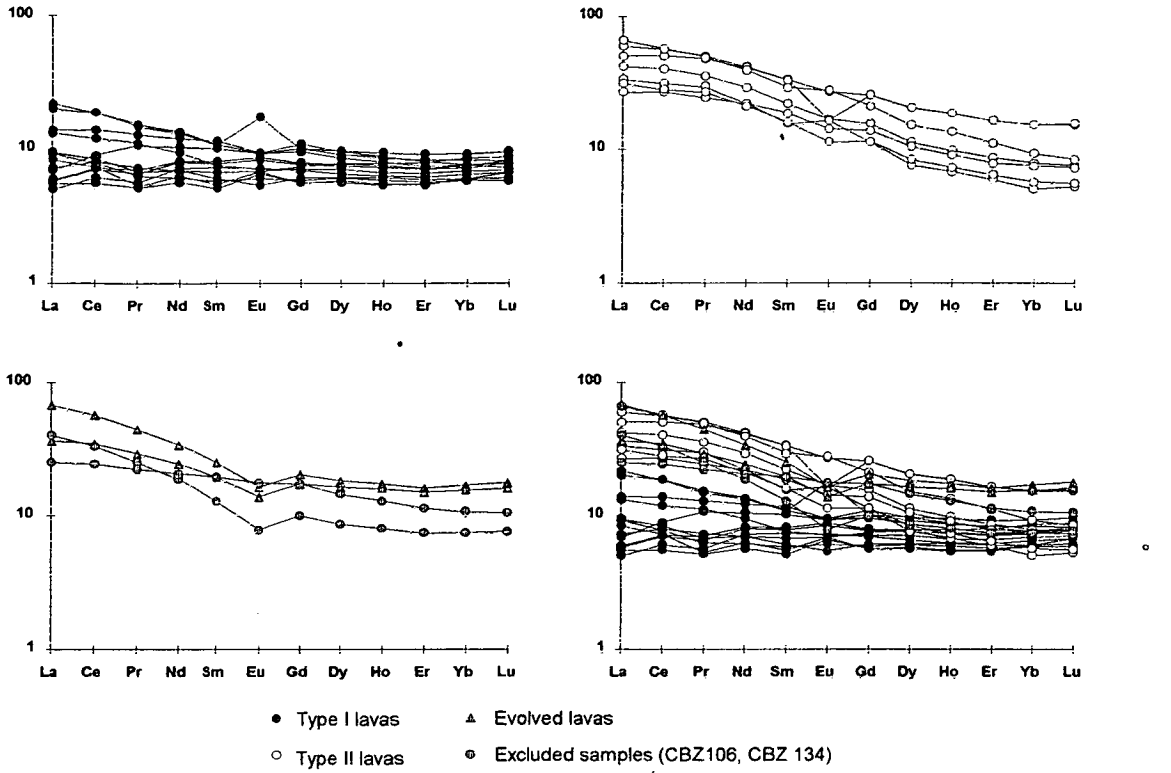

Figure 6.11 REE data normalised to chondrite (Nakamura, 1974).

6.3.6 Rare earth element geochemistry

The REE data for the 24 samples analysed are presented in three formats in Figures 6.11, 6.12 and 6.13. In each case the data for the Type I, Type II and evolved samples are shown separately, and then altogether on a combined plot. A further stage of sample screening was employed with the REE data, which resulted in the exclusion of two Type I samples from the considered dataset. As can be seen, the general Type I REE pattern is fairly flat, but two supposedly Type I samples (CBZ106 and CBZ 134) show distinctly LREE-enriched patterns more akin to the Type II lavas. Both of these samples were shown to plot away from the main Type I group when REE element abundances were plotted against Zr to assess the effects of alteration (Chapter 5), and both show reasonably elevated abundances of other trace elements. Their Zr/Nb ratios are, however, both >20, and their major element chemistry suggests that they are not very evolved rocks. The interpretation here is that they are the possibly the products of Type I/II mixing, or that they have been subject to some degree of alteration to move them away from the main data trend. They will not be considered further in this section (though they are included in Figures 6.11 and 6.12 for comparison.)

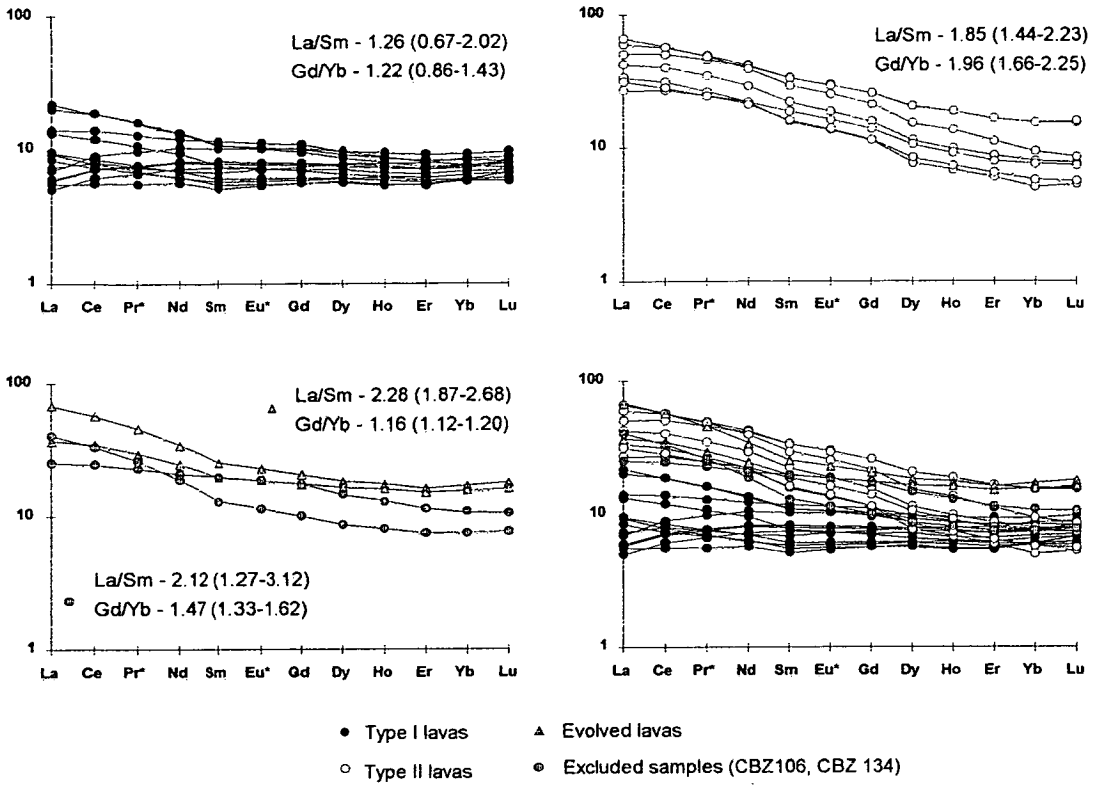

Figure 6.12 REE data normalised to chondrite (Nakamura, 1974), with corrections for Pr and Eu anomalies (Pr* and Eu*). The method for calculating corrected values is given in Figure 5.9. La/Sm and Gd/Yb average ratios and range of values are shown for each category

Figure 6.11 shows the REE data normalised to chondrite, and 6.12 shows the same data corrected for apparent Pr and Eu anomalies (see Chapter 5). La/Sm and Gd/Yb ratios are also shown as a measure of relative LREE and HREE enrichment/depletion. As can be clearly seen, the Type II lavas have significantly higher abundances of the LREE, but HREE abundances are similar for both types. The evolved samples also have abundances of the LREE similar to the Type II lavas, but their HREE abundances are also noticeably higher than both the Type I and Type II lavas. These data are summarised in Figure 6.13, which shows the averages (and $\pm 1\sigma$ limits) for the data.

The La/Sm and Gd/Yb ratios highlight some other interesting features of the data. La/Sm in the Type I lavas shows a large range of values (0.67-2.02) compared to the Type II lavas (1.44-2.23), but a lower average value (1.26 compared to 1.85 for Type II). The evolved samples show a higher average than both types, at 2.28. The contrast in Gd/Yb is even more marked. The Type I and evolved lavas show similar values (1.22 and 1.16), but the Type II lavas show a much higher average value (1.96), with no overlap at all between the range of values for the two lava types. In summary:

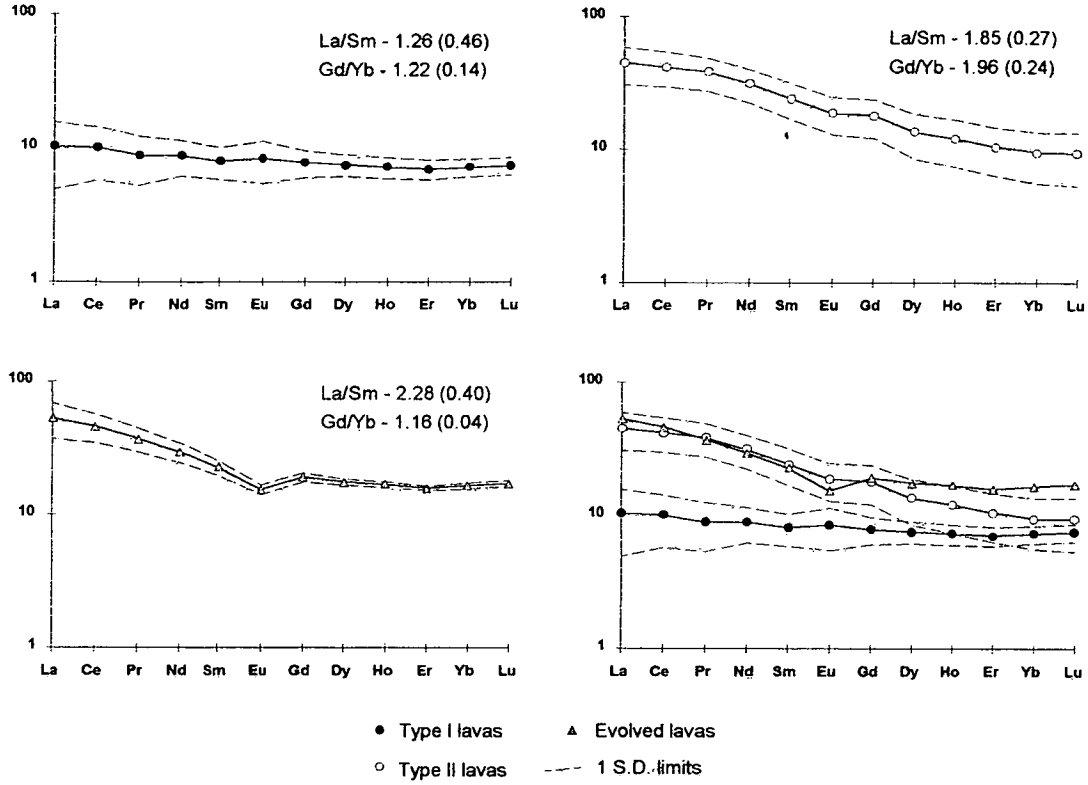

Figure 6.13 Mean REE values for Type I, Type II and evolved samples, normalised to chondrite (Nakamura 1974). The excluded samples on Figures 6.11 and 6.12 have not been included. Dashed lines show ± 1 σ., and are not included for the evolved samples on the combined plot for reasons of clarity. La/Sm and Gd/Yb average ratios and standard deviations are shown for each category.

- **Type I lavas** range from moderately depleted to moderately enriched in the LREE, and have relatively flat to very slightly depleted HREE patterns.

- **Evolved lavas** have highly LREE-enriched, and very slightly HREE-depleted patterns.

- **Type II lavas** are moderately to highly enriched in the LREE, and quite heavily HREE-depleted.

6.4 Isotope geochemistry

6.4.1 Previous isotope work on the rocks of the Belingwe belt

Isotopic studies on the rocks of the Zimbabwean craton have tended to be based on craton-wide sampling. The only study which discusses isotope data exclusively from the rocks of the Belingwe belt is that of Chauvel *et al.* (1993), who also provides a good, brief summary of previous isotope work on the whole craton. Craton-wide geochronological studies have been summarised more fully by Wilson (1979) and Taylor *et al.* (1991), who subdivide the craton into the following sections:

1. A small area of ca. 3.5 Ga felsic gneisses and supracrustal rocks (the Sebakwian Group)
2. More extensive 3.0-2.9 Ga granitoids, gneisses and volcanic rocks (the lower Bulawayan Group, or lower greenstones)
3. Widespread 2.7-2.6 Ga volcanic and sedimentary rocks (the upper Bulawayan Group, or upper greenstones, including the Ngezi Group)
4. ca. 2.6 Ga granitoid plutons which intrude all earlier rocks.

The majority of these ages are from Rb/Sr whole-rock studies (e.g. Hawkesworth *et al.*, 1975; Moorbath *et al.*, 1976, 1977; Jahn & Condie, 1976; Taylor *et al.*, 1991), with some from Sm-Nd whole-rock (Hamilton *et al.*, 1977; Moorbath *et al.*, 1987) and Pb-Pb whole rock (Taylor *et al.*, 1984, 1991; Moorbath *et al.*, 1987) methods. Specific work on the upper greenstones has yielded the following ages:

- 2485 ± 90 Ma. Rb-Sr whole-rock craton-wide isochron, Hawkesworth *et al.* (1975).
- 2700 ± 70 Ma. Rb-Sr whole-rock isochron for the Zeederbergs Formation, Jahn & Condie (1976) (together with data from Hawkesworth *et al.* (1975))
- 2640 ± 140 Ma. Sm-Nd whole-rock isochron from samples from four different (and widely separated) belts (including four from the Reliance Formation). Hamilton *et al.* (1977) quote an initial $\varepsilon_{Nd} \sim 0$. But this isochron has a very large MSWD and may not be reliable.

Chauvel *et al.* (1993) analysed a suite of samples from each of three different sections through the Reliance Formation (localities SA, MS and NM on Figure 3.1) for Sm-Nd and Pb-Pb. Their results are summarised below:

- **Pb-Pb** MS section (komatiitic basalts): Pb-Pb isochron age **2692 ± 9 Ma,** μ_1**=8.4**

  SA section (komatiites): Pb-Pb isochron age **2675 ± 173 Ma,** μ_1**=8.2**

  NM section (basalts): no isochron defined

- **Sm-Nd** Composite isochron (all sections) age **2890 ± 130 Ma** (MSWD=10), initial ε_{Nd}= **+1.8**. This age is significantly older than either of the Pb-Pb ages, and its high MSWD makes it unreliable. It is not possible to construct isochrons for individual sections as the range of $^{147}Sm/^{144}Nd$ is too limited.

So, the Sm-Nd age is significantly older than the Pb-Pb age (+200 Ma). This is a situation which has been found before in Precambrian volcanic rocks (e.g. Newton Township, Ontario, Cattell *et al.* (1984); Usushwana complex, Hegner *et al.* (1984); Kambalda, Western Australia, Chauvel *et al.* (1985); Compston *et al.* (1986)), and in these cases it is thought that the Pb-Pb isochron date is the more reliable (and is often coincident with U-Pb zircon and other reliable ages). Given the extremely good isochron defined by the samples from the MS section (with only a 9 Ma error), this is taken as the most accurate estimate of the age of the volcanic rocks of the Ngezi Group (2962 ± 9 Ma).

The origin of the disagreement between Sm-Nd and Pb-Pb ages will be discussed in the next Chapter, when the petrogenetic history of the lavas of the Zeederbergs Formation is considered. For all age corrections of Sm-Nd data, the Pb-Pb age of 2692 ± 9 Ma is used.

6.4.2 Sm-Nd data from the Zeederbergs Formation

Twenty-four samples were analysed by mass spectrometry to determine their $^{143}Nd/^{144}Nd$ ratio, and the same samples were analysed using isotope dilution mass spectrometry to obtain accurate Sm and Nd concentrations. These samples were the same 24 analysed for REE by ICP-AES, and were chosen to be representative of the range of magma compositions seen within both lava types. All results which had fewer than 90 complete determinations, or $2\sigma > 0.0020$, were rejected. For two samples (CBZ134 and CBZ016) the ID analyses for Sm and Nd, respectively, were unsuccessful, and the concentrations obtained by ICP-AES were substituted. This does not seem to have significantly affected the calculations.

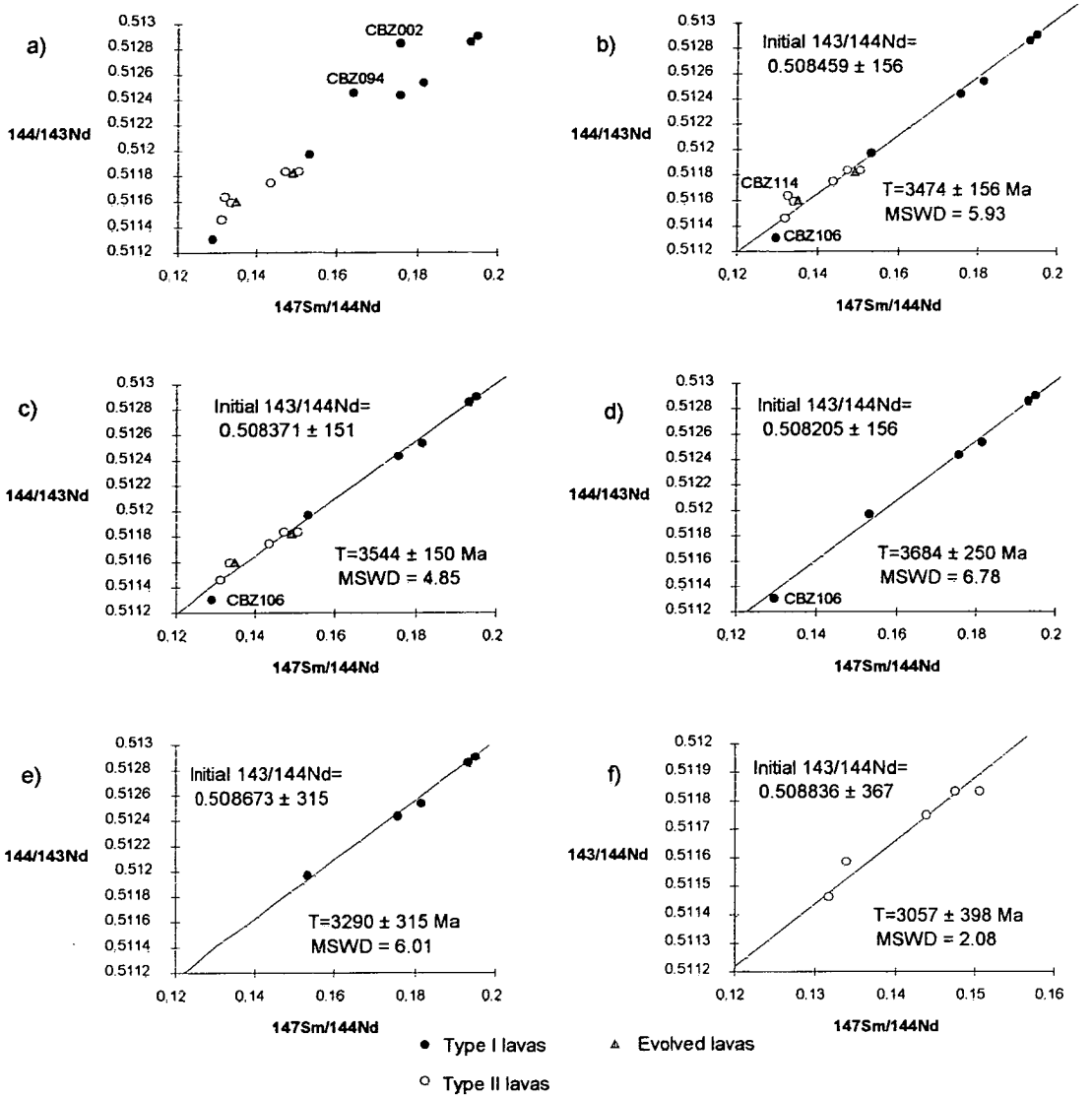

Figure 6.14 a) Measured (present day) $^{144}Nd/^{143}Nd$ vs. $^{147}Sm/^{144}Nd$ for all accepted analyses. **b)** Isochron for all samples used in calculations, **c)** Isochron for all samples with CBZ114 and CBZ106 excluded, **d)** Isochron for all Type I samples considered, **e)** Isochron for Type I samples with CBZ106 excluded, **f)** Isochron for Type II samples (CBZ114 excluded).

The measured $^{143}Nd/^{144}Nd$ ratio is plotted against the $^{147}Sm/^{144}Nd$ ratio in Figure 6.14, which shows a series of isochron plots. The two samples CBZ002 and CBZ094 lie clearly off the main trend, and are excluded from any isochron calculations (possible explanations for this behaviour are discussed in Chapter 7). Figure 6.14 b-f show isochrons and their statistics for five different selections of samples. Figure 6.14 b shows all the data used in the calculations, 6.14 c shows the same data with the removal of CBZ106 (anomalously low Sm/Nd for a Type I lava, noted in Section 6.3.6) and CBZ114 (a Type II lava which also lies off the main trend). Figure 6.14 d

and e show isochrons for only the Type I lavas (with and without CBZ106), and Figure 6.14 f shows the isochron for the Type II lavas (excluding CBZ114).

Clearly, all of the apparent isochron ages are much older than the generally accepted age of 2.7 Ga, and as such display similar behaviour to the Sm-Nd isochrons obtained by Chauvel *et al.* (1993). Few of the isochrons have small enough errors and/or MSWD values to make them worthy of serious consideration, but the best result (Figure 6.14 c) certainly has geological significance, and suggests an apparent Sm-Nd age for the Zeederbergs Formation some 800 Ma older than its actual age. Possible explanations for this behaviour are discussed in Chapter 7.

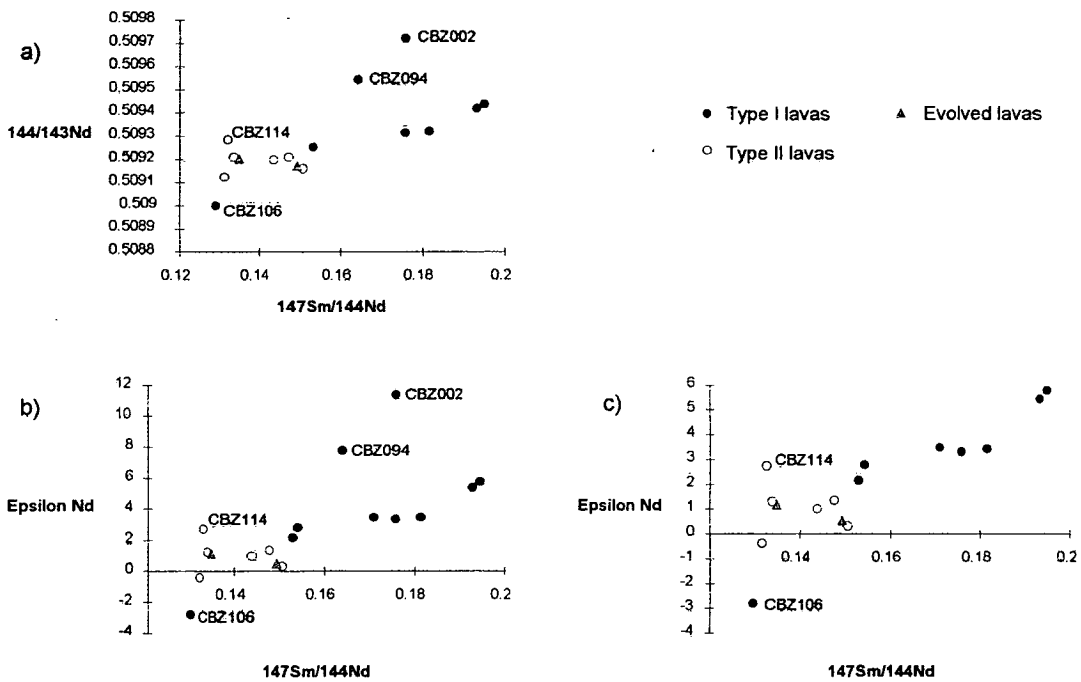

Figure 6.15 a) Initial $^{143}Nd/^{144}Nd$ ratios at 2.7Ga, **b)** The same data expressed as ε_{Nd} values, **c)** as b) but rescaled to exclude CBZ002 and CBZ094, which show anomalously high values.

6.4.3 Initial $^{143}Nd/^{144}Nd$ ratios

Initial $^{143}Nd/^{144}Nd$ ratios (and ε_{Nd} values) were calculated using the best Pb-Pb age for the Ngezi Group, 2692 Ma, and the results are shown in Figure 6.15. This shows a clear departure from the horizontal line that would be expected if all the samples had come from the same mantle source, and had been unaffected by any process which may have altered the $^{143}Nd/^{144}Nd$ ratio (such as assimilation of crust). Figures 6.15 b and c show the same data in ε_{Nd} form, and the average values (and ranges) are shown below:

- Type I samples (all) - **+4.27** (-2.81 - +11.38)
- Type I (excluding CBZ002 and CBZ094) - **+2.94** (-2.81 - +5.78)
- Type I (additionally excluding CBZ106) - **+3.76** (+2.16 - +5.78)
- Evolved samples - **+0.84** (+0.52 - +0.84)
- Type II samples (all) - **+1.05** (-0.39 - +2.74)
- Type II (excluding CBZ114) - **+0.71** (-0.39 - +1.33)

Clearly there was some difference between the Type I and Type II lavas at the time of eruption, and possible origins for this will be examined in Chapter 7. The isotope characteristics of the lava types can be summarised as follows :

- **Type I** - Higher $^{147}Sm/^{144}Nd$ and initial $^{143}Nd/^{144}Nd$ than the Type II lavas (with the exception of CBZ106, which also shows unusual REE compared to the other Type I samples). Most samples lie on the main isochron for the whole suite (with the exception of CBZ002 and CBZ094). Initial ε_{Nd} appears to be around **+2.5** to **+4.0** (depending on which samples are included).

- **Type II** - $^{147}Sm/^{144}Nd$ and initial $^{143}Nd/^{144}Nd$ are lower than Type I lavas. Initial ε_{Nd} = **+1.05** (**+0.71** if CBZ114 is excluded)

- **Evolved** - $^{147}Sm/^{144}Nd$ and initial $^{143}Nd/^{144}Nd$ coincident with the Type II lavas, both significantly lower than the basaltic Type I samples. Initial ε_{Nd} = **+0.84**.

6.5 Conclusions

- The lavas of the Reliance Formation all fall on the world-wide, Al-undepleted, komatiite trend. Olivine and Cr-spinel fractionation can explain most of the behaviour seen within the suite.

- The Type I and Type II lavas are very similar in their major element chemistry, with the notable exception of Al_2O_3 contents, which are considerably lower in the Type II lavas. The Type II lavas also have slightly higher FeO, TiO_2 and P_2O_5 abundances.

- The Type II lavas have higher CaO/Al_2O_3, and lower Al_2O_3/TiO_2 ratios than the Type I lavas, and cannot be descended from these lavas (or any of those in the Reliance Formation) by simple fractional crystallisation.

- The Type II lavas show higher abundances of nearly all incompatible trace elements than Type I lavas. Only Sc is less abundant in the Type II lavas than in the Type I lavas.

- A comparison of trace element ratios of the two lava types leads to a clear order of enrichment in the Type II lavas:

  Nb > Ce ≈ Zr > Y

  Most enriched Least enriched

- The Type I and Type II lavas (and the evolved lavas) show marked differences in their REE chemistry:

  Type I lavas range from moderately depleted to moderately enriched in the LREE, and have relatively flat to very slightly depleted HREE patterns.

  Evolved lavas have highly LREE-enriched, and very slightly HREE-depleted patterns.

  Type II lavas are moderately to highly enriched in the LREE, and quite heavily HREE-depleted.

- Previous Pb-Pb isotope work on the rocks of the Reliance Formation gives the most reliable age for the Ngezi Group volcanics, **2692 ± 9 Ma**.

- Sm-Nd analyses from the Zeederbergs Formation provide some reasonably good isochron ages for the group, a most of which are at *least* 500 Ma *older* than the Pb-Pb date above !

- The initial isotope ratios calculated using the Pb-Pb date significant differences between the lava types: **Type I lavas**- Initial ε_{Nd} = **+2.5** to **+4.0**
  Type II lavas - Initial ε_{Nd} = **+1.05**
  Evolved lavas - Initial ε_{Nd} = **+0.84**

7

INTERPRETATION

7.1 Introduction

All the data collected from the Zeederbergs Formation in this study has now been presented and assessed, along with a comprehensive summary of work on the rest of the Ngezi Group volcanics and the Belingwe greenstone belt. As has been stated, the most significant discovery of this study has been the identification and characterisation of a type of lava not seen before in Belingwe, the Type II lavas in the Zeederbergs Formation. This chapter consists of a series of questions, relating mainly to the differences between the Type I and Type II lavas and their implications for the petrogenesis of the Ngezi Group volcanics.

7.2 Are the differences between the Type I and Type II lavas due to alteration processes ?

7.2.1 Physical evidence

The horizon of Type II material is clearly seen in the three sections through the Zeederbergs Formation examined in this study. It appears to be slightly thicker in the Ngezi River section than in the other two sections, but it does occur at approximately the same level everywhere (see §3.5). The location of the sections mean that this horizon has an areal extent of at least 20km (along strike) by 15km, and that it was clearly present before the main deformation of the belt, as it is present on both sides of the syncline. All of these characteristics make it extremely unlikely that this horizon is a product of alteration.

Additionally, given that the geochemical differences between the two lava types are so pronounced, to attribute them to alteration would imply that the Type II horizon had been subject to some quite extreme alteration processes. If this were the case, one would expect to see some quite clear differences in the physical appearance of the altered lavas compared to the rest of the lava pile. As seen in Chapters 3 and 4, there are no obvious differences between the Type I and Type II lavas in their physical

appearance. Again, this makes the idea that the differences may be due to alteration seem fairly unlikely.

7.2.2 Geochemical evidence

The elements which most clearly define the differences between the two lava types are also those which have been shown to be least affected by alteration. Major element differences between Type I and Type II lavas are limited to a few elements, with lower Al_2O_3 and higher FeO, TiO_2 and P_2O_5 concentrations found in the Type II lavas. As was shown in Chapter 5, TiO_2, Al_2O_3 and P_2O_5 have all been apparently immobile during alteration, and even FeO has only been slightly mobile.

The situation with the trace elements is even more pronounced, with the Type II lavas having abundances of several incompatible elements (eg. Zr, Nb and Y; clearly shown to be immobile during alteration) several times higher than those seen in the Type I lavas. They also show considerably higher abundances of the LREE (again, clearly shown to be immobile). It is very difficult to see how any kind of post-eruptive alteration event could have so enriched such a large volume of rock so uniformly in such immobile and incompatible elements.

Finally, there are the isotopic differences between the Type I and Type II lavas. The Sm-Nd system is virtually completely immune to alteration, and so these differences have to be interpreted as primary.

7.2.3 Conclusion

It is very difficult to conceive how any alteration process could produce the physical and geochemical characteristics of the Type II lavas. Consequently, the differences between the Type I and Type II lavas must be assumed to be primary, representing different petrogenetic histories.

7.3 Could the Type II lavas be descended from the Type I lavas ?

The increased concentrations of incompatibles in the Type II lavas imply that they may be descended from the Type I lavas by some combination of fractional crystallisation and crustal assimilation. The fact that there is no difference between the two lava types in terms of their MgO and SiO_2 contents suggests that this is unlikely, but there are other, more convincing pieces of evidence.

7.3.1 Zr/Nb

The low Zr/Nb of the Type II lavas provides some very useful constraints on their parentage. Zr and Nb have both been shown to be immobile during alteration, and both are analysable reliably at the concentrations present (see Appendix 2), so the measured Zr/Nb represents that of the erupted lavas. This ratio is relatively unaffected by fractional crystallisation of any of the possible crystallising phases (olivine, clinopyroxene, plagioclase, Cr-spinel), and so the only processes which can affect it are partial melting and crustal contamination. During partial melting of the mantle, Nb is more incompatible than Zr, so the initial melt will have a much lower Zr/Nb than the source material. The Zr/Nb of the melt rises rapidly with increasing degree of melting, however, and for more than a few percent of melting, it will be approximately equal to that of the source.

The Zr/Nb systematics of the lavas under consideration are shown in Figure 7.1. The Type I lavas and the Reliance Formation lavas have Zr/Nb between 18 and 22. The potential contaminant used here is average Archaean crust from Taylor & McLennan (1985), considered to represent a reasonable potential contaminant for the erupted lavas (Scholey, 1992). This crustal value of 18 is probably a minimum, as continental crust is always depleted in Nb (Taylor & McLennan, 1985). The primitive mantle value of 15 represents a minimum for the source material, as any depleted mantle will have a value greater than this, the exact value being a function of the degree of depletion. Zr/Nb in the Type II lavas (11-14) is significantly lower than in the Type I lavas and all possible contaminants, suggesting that these Type II lavas *cannot* be descended from any of the Type I lavas or those in the Reliance Formation through crustal contamination..

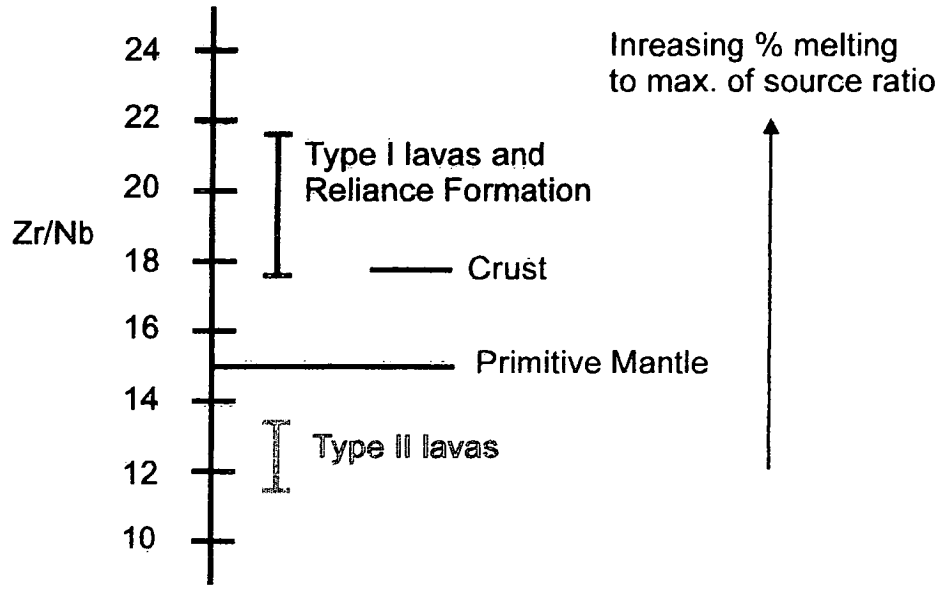

Figure 7.1. Zr/Nb systematics of the Ngezi Group volcanics. Crust from Taylor & McLennan (1985), primitive mantle from Sun & McDonough (1989). Discussion in text.

7.3.2 Al_2O_3 contents

The low Al_2O_3 contents of the Type II lavas also help to constrain the origin of their parental magma. They are significantly lower than in the Type I lavas, and so if a parental relationship is suggested, whatever process has acted on the Type I lavas must have simultaneously enriched the magma in all the incompatible elements and *depleted* it in Al_2O_3. No such process can be identified.

The behaviour of Al_2O_3/TiO_2 and CaO/Al_2O_3 (both measures of Al_2O_3 depletion), as well as that of mg#, also rules out the Type I lavas as possible parents for Type II, as discussed in §6.3.3.

7.3.3 Conclusion

The Type II magmas *cannot* be descended from the Type I magmas by any known petrogenetic process.

7.4 Could both Type I and Type II magmas be descended from the same primary magma ?

If the Type II lavas cannot be descended from the Type I lavas, then is it possible that they are both descended from the same primary magma, and have simply evolved differently ?

7.4.1 Major and trace element chemistry

The behaviour of selected major and trace elements is shown in Figures 7.2 and 7.3. These are essentially reproduced from Figures 6.4 and 6.7, but with the addition of a suite a representative samples from the mafic and ultramafic rocks of the Reliance Formation. Clearly the Type I lavas continue the trends formed by the Reliance Formation suite, and there is no reason to suppose that they are not descended from lavas similar to those parental to the Reliance Formation, or that they are lower degree melts of the same source material. The Type II lavas, however, lie well off these trends, and not on a continuation of a simple fractional crystallisation trend.

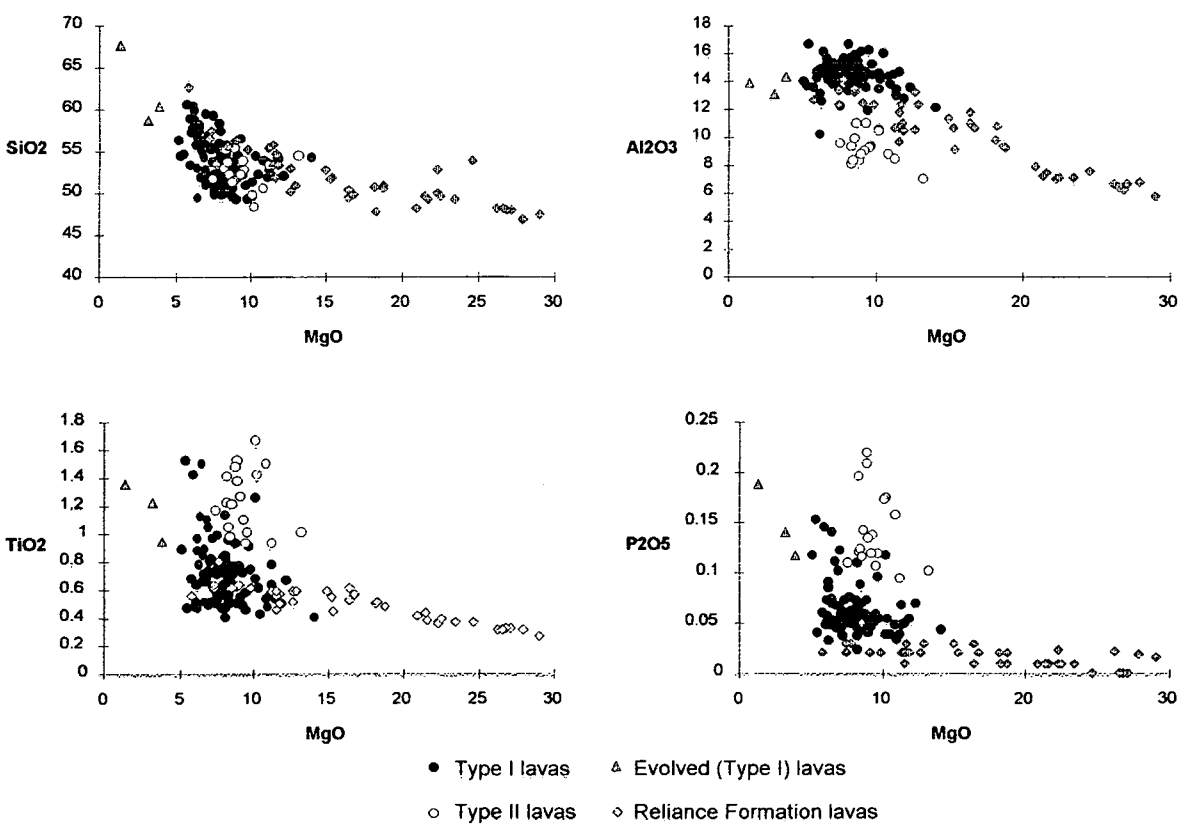

Figure 7.2. Behaviour of selected major elements, and comparison to the Reliance Formation. Reliance Formation data are taken from Scholey (1992). The slight difference in behaviour of P_2O_5 is thought to be due to differing analytical precision between the two datasets.

It is certainly true that some of the deviations from the trend of the Reliance Formation data could be explained by addition of a crustal contaminant. However, as seen in Figure 7.1, the behaviour of Zr/Nb precludes this. The behaviour of Al_2O_3 is also inconsistent with this hypothesis, as shown by CaO/Al_2O_3 and Al_2O_3/TiO_2, see Figure 7.4.

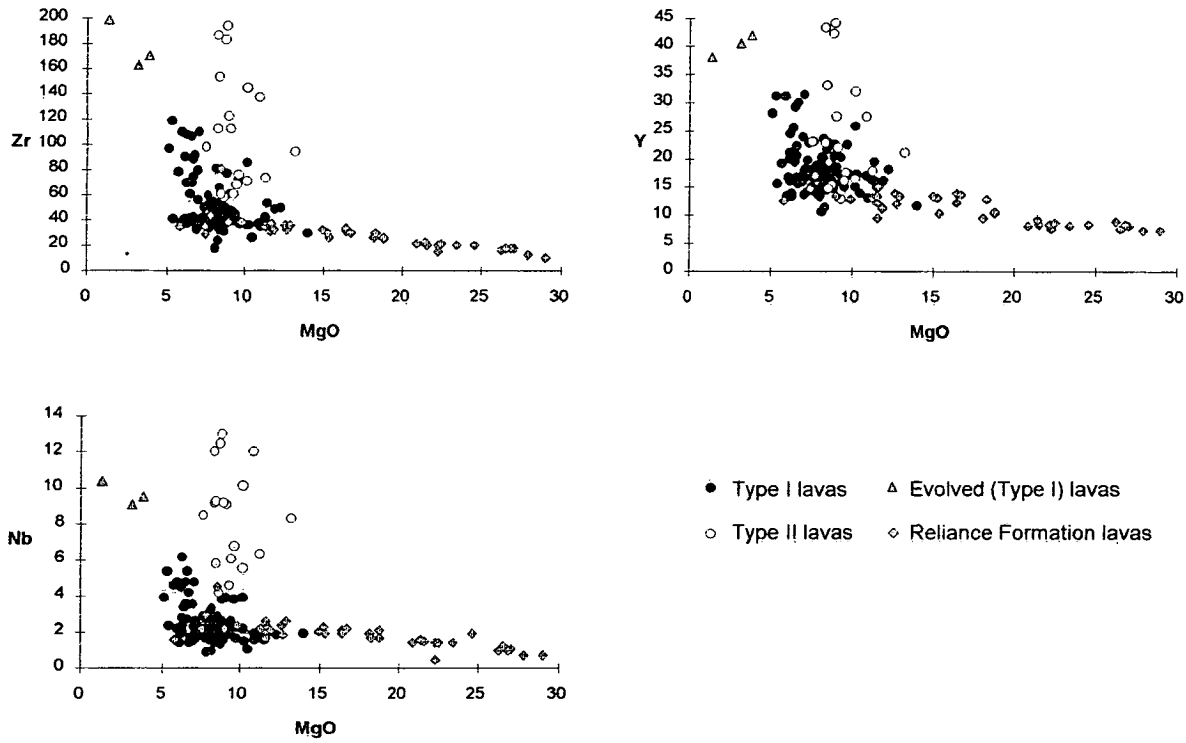

Figure 7.3. Behaviour of selected trace elements, and comparison to the Reliance Formation. Reliance Formation data is taken from Scholey (1992).

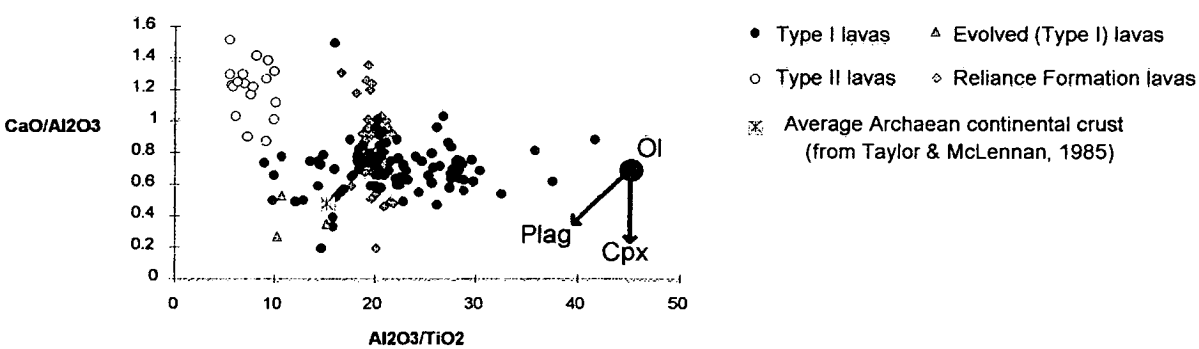

Figure 7.4. Behaviour of CaO/Al_2O_3 and Al_2O_3/TiO_2 ratios, and comparison to the Reliance Formation. Reliance Formation data from Scholey (1992).

Again, the compositions of the Type I lavas are consistent with their evolution from lavas similar to those of the Reliance Formation. The fact that many of the samples plot at higher Al_2O_3/TiO_2 ratios than the Reliance Formation lavas suggests that they are actually derived from lower degree melts than the Reliance Formation. It is quite clear that no combination of fractional crystallisation or assimilation of continental crust could produce the Type II lavas from any rocks in the Reliance Formation.

7.4.2 Isotope geochemistry

The isotope characteristics of the lavas are described in §6.4. The average ε_{Nd} values of the Type II lavas are lower than those of the Type I lavas and the Reliance Formation. The range of values seen in the Reliance Formation and the Type I lavas are consistent with their derivation from the most mafic material in the suite (ε_{Nd} = +3.5, Chauvel *et al.* 1993) by the addition of a small amount (<2%) of crustal contaminant (Bickle *et al.* 1993). The Type II lavas, however, have much lower ε_{Nd} values, similar to those of the evolved lavas. These values would require the addition of significantly more crust if both types were descended from the same parent magma, and yet both the Type I and Type II lavas are fairly similar in their major element chemistry, an observation inconsistent with such a hypothesis.

7.4.3 Conclusion

It would seem to be impossible for the Type I and Type II lavas to be descended from the same parent magma.

7.5 What were the primary magmas ?

It has been shown that the two lava types seen in the Zeederbergs Formation must be descended from different primary magmas, so what were the primary magma compositions, and are they ever seen erupted ?

7.5.1 Primary magma modelling; Incremental olivine addition

A very simple approach to determining primary magma compositions is by incremental addition of equilibrium olivine. The rationale is simple; when the primary magma separates from the mantle it will be in equilibrium with the olivine in the residue. As it fractionates olivine, the equilibrium olivine composition will evolve towards lower Fo contents (as clearly seen in zoned olivine crystals). Assuming that olivine has been the only fractionating phase it is possible to model this process in reverse. The olivine composition in equilibrium with the erupted lava is calculated, and a small amount (0.1%) of this olivine is added to the lava. The new bulk composition is calculated, as is the new equilibrium olivine composition, and the process is repeated until the equilibrium olivine is that of the mantle residue.

The most Fo-rich composition (Fo_{92}) thought to correspond to a primary liquid is found in the cores of spinifex olivines in the komatiite flows of the Reliance Formation (see §4.2.2). This corresponds to a reasonable value for mantle olivine, and so this is the composition used in this study. Figure 7.5 shows the results of olivine addition on the Type I and Type II lavas. Only those lavas with $SiO_2 < 52\%$ were used, to eliminate samples which had undergone significant clinopyroxene fractionation and/or SiO_2 mobility (see §5.4.7). Both lava types were modelled using the same mantle olivine composition (Fo_{92}).

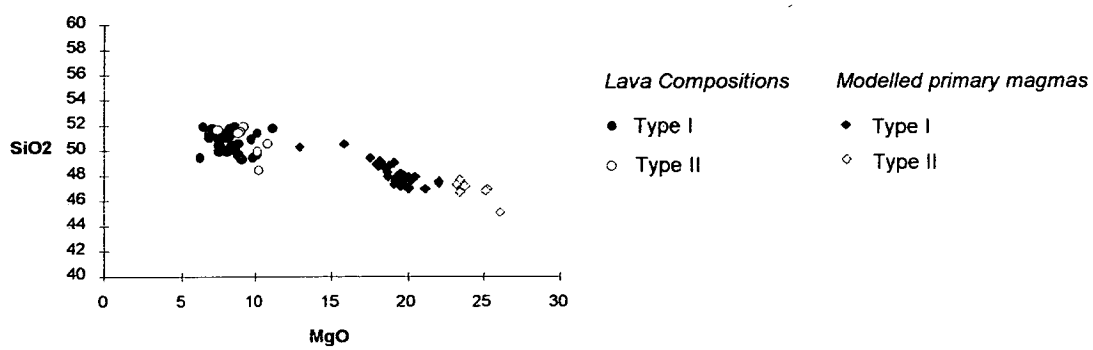

Figure 7.5 Primary magma modelling by incremental addition of equilibrium olivine back to a mantle olivine composition of Fo_{92}. $Fe_2O_3/FeO = 0.15$.

This modelling clearly suggests that the Type II lavas are descended from a more magnesian primary liquid than the Type I lavas (as was also suggested by the mg# values, see §6.3.3). There are a number of limitations to this method which make it unsuitable for calculating true primary magma compositions (crustal assimilation and fractionation of any phase other then olivine are not allowed for; assumptions must be made about initial olivine Fo contents and initial magma Fe_2O_3/FeO values), and so the actual compositions calculated are not very reliable. However, the *relative* results for the two types of lava are immune to these effects, and so this modelling is consistent with the hypothesis that the Type II lavas are descended from a more basic parent than the Type I lavas.

7.5.2 Probable parental magmas for the Type I lavas

It was clearly demonstrated in §7.4 that there was no reason why the Type I lavas could not be descended from the more basic magmas represented by the Reliance Formation. Isotope calculations suggest that addition of small amounts (around 1-2%) of crustal contaminant (with the isotopic composition of the Shabani Gneiss (Luais & Hawkesworth, 1994)) to magmas represented by the more mafic (MgO >16%) lavas of the Reliance Formation can satisfactorily account for the range of isotopic compositions seen in the Type I lavas. There is no evidence to contradict the conclusions of Scholey (1992) and Bickle & Nisbet (1993) that the majority of lavas in the Ngezi Group (the Reliance Formation and the Type I lavas of the Zeederbergs Formation) are descended from primary magmas similar to the Reliance Formation komatiites, by fractional crystallisation of olivine and minor Cr-spinel (and later, clinopyroxene) and assimilation of minor (1-2%) amounts of crust.

7.5.3 Probable parental magmas for the Type II lavas

As has been shown in §7.4, the Type II lavas of the Zeederbergs Formation cannot be descended from any of the lavas in the Reliance Formation, so another parental magma is required. The most unusual feature of the geochemistry of the Type II lavas is their very low Al_2O_3 contents, and this has been the most important factor to consider when looking for a possible parent. A comprehensive search was unable to unearth any other basaltic lavas with such low Al_2O_3 contents. The only basic lavas which do show such low Al_2O_3 contents are olivine melilitites, but these differ in the rest of the major element chemistry, and such rocks invariably show concentrations of incompatible elements many times those seen in the Type II lavas. It would seem

likely that these Type II lavas had evolved from a more mafic composition (as implied by other evidence already mentioned).

So, are there any other basic lavas in existence which could have evolved into lavas similar to the Type II basalts ? The only likely candidates found were the Al-depleted class of komatiites, such as those found in the Barberton greenstone belt, South Africa. These komatiites have long been recognised as being significantly different to the majority of Archaean komatiites worldwide (see Chapter 1), and are characterised by very high MgO contents (MgO>28%) and $CaO/Al_2O_3 > 1$.

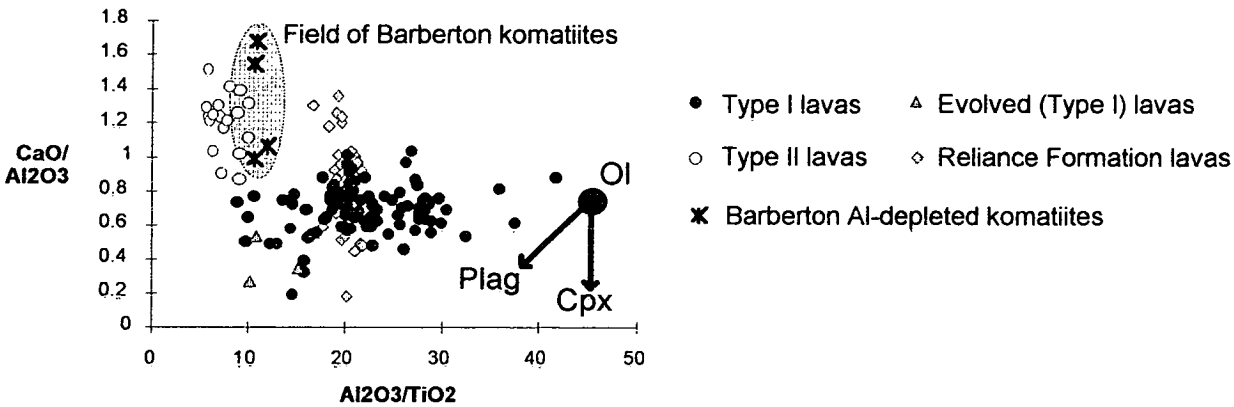

Figure 7.6. Comparison of the Al-depleted komatiites from Barberton with the lavas of the Ngezi Group. Barberton data from Smith and Erlank (1982).

Figure 7.6 shows these Barberton komatiites and the lavas of the Ngezi Group on a plot of CaO/Al_2O_3 vs Al_2O_3/TiO_2. Clearly the Barberton lavas are much closer to the Type II lavas than the rocks of the Reliance Formation, and lavas of this composition could feasibly have evolved into basaltic compositions similar to the Type II lavas. The few samples from the Reliance Formation with $CaO/Al_2O_3 > 1$ (see §6.2.1) have only been reported by Scholey (1992), and whether they represent a different lava type, or alteration, is unclear. They do not seem to show genuine Al_2O_3 depletion, however, and they are not considered to represent possible parental magmas for the Type II lavas. The behaviour of the major elements (Figure 7.7) also suggests that lavas similar to the Barberton Al-depleted komatiites could evolve into the Type II lava compositions seen.

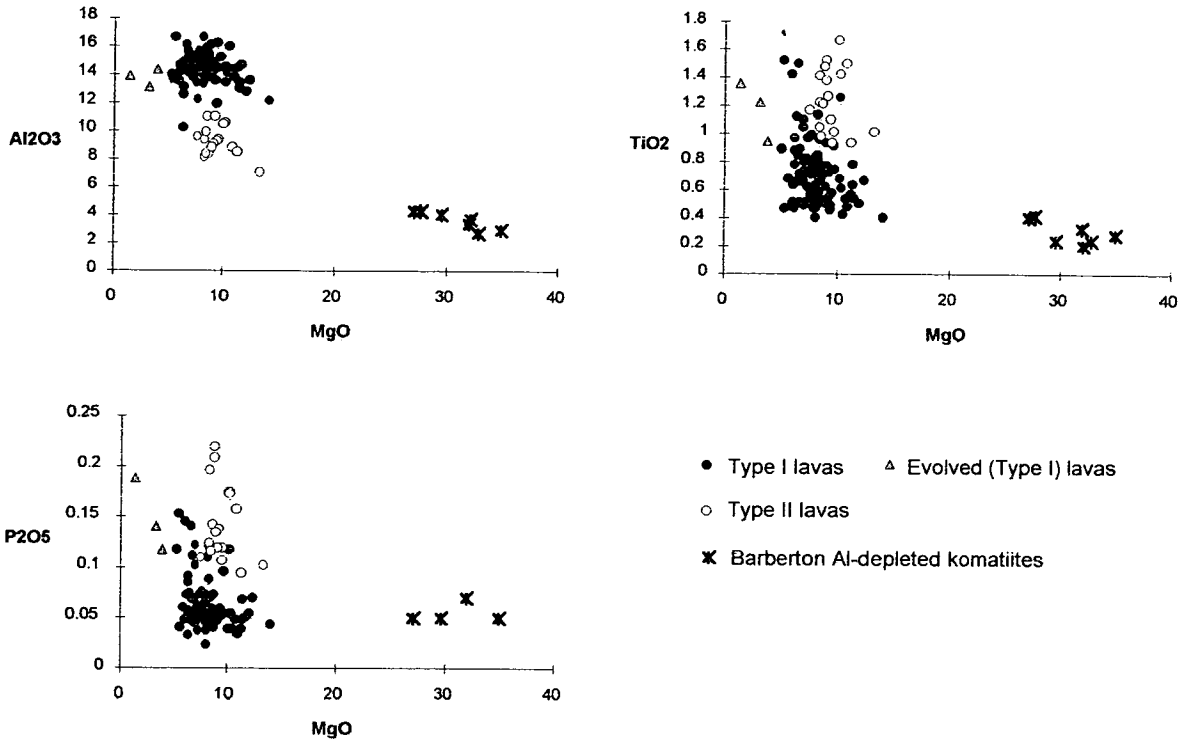

Figure 7.7 Behaviour of selected major elements, and comparison to the Al-depleted komatiites from Barberton. Barberton data from Smith and Erlank (1982).

7.5.4 Conclusions

There is no reason to suppose that the Type I lavas (the majority of the Zeederbergs Formation) could not have evolved from lavas similar to those seen in the Reliance Formation. The only possible parental magma for the Type II lavas which corresponds to any known magma composition would be a very high-magnesium (MgO>28%), Al-depleted komatiitic liquid, similar to those seen in the Barberton greenstone belt.

7.6 Were the different primary magmas from the same source ?

Now that it has been shown that there must have been two quite distinct primary magmas for the Ngezi Group, the obvious question to ask is whether they were generated by melting of the same mantle source, with different melt column geometries, or whether they were produced by melting of different mantle sources. The two end members of probable mantle compositions would be depleted and primitive mantle.

7.6.1 Isotopic evidence

One of the most common ways of distinguishing between mantle sources (particularly in distinguishing primitive and depleted mantle signatures) is to look at the isotopic composition of the lavas produced, as this is unaffected by any melting processes. In this case, can the ε_{Nd} values tell us anything reliable about the mantle source ? Unfortunately, the answer is probably no, as the principal control on the ε_{Nd} values of the Zeederbergs Formation lavas is the amount of crust asimilated during the evolution of these lavas. The initial ε_{Nd} values of the Type I lavas and the Reliance Formation, which have only seen small (<2%) degrees of crustal contamination are between +2.5 and +4.0, implying that the mantle source was depleted. The evolved Type I lavas have a much lower initial ε_{Nd} value (+0.84), which is to be expected if their evolution has involved assimilation of larger amounts (10-15%) of crust. The initial ε_{Nd} of the Type II lavas is around +0.71 - +1.05, which is entirely consistent with the primary magmas having the same initial ε_{Nd} value as those for the Type I lavas (>+4.0), but having assimilated considerably more crust (10-15%) during evolution to their current basaltic composition.

So, in conclusion, the isotopic differences between the two lava types are consistent with the primary magmas having identical initial ε_{Nd} values, but the Type II lavas having assimilated considerably more crust than the Type I lavas during their evolution. Given that there is other evidence of relatively large amounts of crustal assimilation in the Type II lavas (enriched LREE and incompatible trace elements, see §7.7), the initial ε_{Nd} values of the erupted lavas would be quite difficult to explain if the initial ε_{Nd} value of the primary magma for the Type II lavas was much less than that for the Type I primary magma.

7.6.2 Zr/Nb

We have seen that the primary magmas for the Type II lavas were almost certainly more mafic than those for the Type I lavas, and the isotopic evidence strongly suggests that both primary liquids were generated by melting of the same source. The simplest explanation would be that the primary liquids for the Type II lavas were simply higher degree melts. However, the behaviour of Zr/Nb is not consistent with this idea. The Zr/Nb systematics of the Ngezi Group volcanics is shown in Figure 7.1. If the Type II primary magmas were generated by higher degree melting of the same source, they should have identical Zr/Nb to the Type I lavas. Crustal Zr/Nb lies within the range of the Type I values, so the different degree of crustal assimilation would not affect this. As we have seen, the Type II lavas do in fact have much lower Zr/Nb than the rest of the Ngezi Group (11-13), so how is this to be explained ?

One explanation would be that the mantle source for the Type II primary magma was primitive, with a Zr/Nb of about 13-15, and produced a melt with a slightly lower Zr/Nb of 11-13.

7.6.3 Conclusions

The isotope chemistry of the two lava types is consistent with Type I and Type II parental magmas having similar ε_{Nd} values. Their different values on eruption is attributed to differing degrees of crustal assimilation during their evolution. The behaviour of Zr/Nb is not consistent with the Type II primary magma being simply a larger degree melt of the same source as the Type I primary magma. It is much more consistent with the Type II magma being produced by melting of a more primitive mantle source.

The Al_2O_3 contents of the Type II lavas do, however, remain an anomaly. There is no reason why a primitive mantle source should lead to such very low Al_2O_3 contents in the magma. The explanation for this rests with the melting process, and will be discussed in §7.7.

To summarise, the parental liquids to the two lavas types would seem to have been isotopically similar, but chemically distinct. Similar relationships are seen in other large basalt provinces today, such as the Ontong Java plateau, and in Iceland, where they are attributed to different mantle source compositions.

7.7 So how were the different lava types generated ?

7.7.1 Overview

The geochemistry of the Type I lavas is consistent with their derivation from more basic magmas similar to those represented by the Reliance Formation. These are quite typical komatiites, and the current consensus is that they simply represent very large degree melts of the mantle probably associated with a thermal anomaly, or plume. So, the more interesting problem is how were the Type II lavas generated ? The primary magmas for these lavas were apparantly quite unusual, and the only possible analogues found in the geological record are the Al-depleted komatiites such as those found in Barberton. So, how could magmas like this be generated, and how could they evolve into the Type II lava compositions seen ?

7.7.2 Generation of Al-depleted komatiites

The exact origins of Al-depleted komatiites are not well understood, but there are certain aspects of their petrogenesis where there is some consensus. As well as being depleted in Al_2O_3, showing $CaO/Al_2O_3 > 1$ and $Al_2O_3/TiO_2 < 12$, these komatiites also contain low concentrations of the trace elements V, Sc, Ga, Y and the HREE. These characteristics strongly point towards garnet as the mantle phase responsible, but its exact role is unclear. Garnet cannot have been a residual phase at high degrees of melting (>30%) at depths less than 250km, as it would have been already exhausted. Its apparent signature has been attributed to fractionation of majorite garnet from the source, either prior to melting (Herzberg and Ohtani, 1988) or during the melting event that generated the komatiites (e.g. Arndt and Jochum, 1990). More recently, experimental work on high pressure phase relations (e.g. Herzberg, 1992; Ohtani *et al.*, 1995) has suggested another possibility. There is a change in the mantle phase relations at about 10 - 12 GPa (300 - 360 km), below which majorite garnet is the liquidus phase rather than olivine. This means that initial melts below this depth will be ol + cpx melts, komatiitic in composition (e.g. Herzberg, 1992; M. Cheadle, pers. comm.), and the garnet will not contribute at all to the early stages of melting.

This idea raises several problems, some of which may be explained, some of which may not. Experimental results suggest that melts generated at these depths are denser than the residue, and would therefore sink (e.g. Ohtani *et al.*, 1995), though whether these experimental results are applicable to true mantle conditions is questionable (M. Cheadle, pers. comm.). If the onset of melting was at so great a depth, the degree of melting at more shallow levels would be very large, and the more conventional

komatiitic melts produced would contribute the vast majority of the final melt mixture, completely masking the more unusual chemistry of the deeper melts. This problem can be explained if the melt regime has a thick (150km or greater) crustal lid (e.g. Nisbet *et al.*, 1993; M.Cheadle, pers. comm.), and therefore there is no large degree melting at shallower depths. It is also unclear exactly how hot the mantle would have to be to begin melting at such great depths (possibly up to 500km), as the exact position of the solidus at these pressures is not well enough defined. The paradox of komatiite eruption through continental crust (where the liquid is denser than the crust it has risen through) is even harder to explain, as the liquids are denser, and the crust is thicker !

However, it seems clear that garnet does play the major role in the production of these Al-depleted lavas, and the simplest mechanism for this role lies in a deep onset of melting (>350km), in a region where garnet is the liquidus phase, underneath a thick crustal lid (>150km). The most recent modelling of Al-depleted komatiite melt production requires a primitive source (M. Cheadle, pers. comm.). This is entirely consistent with the primitive mantle source for the the Type II lavas suggested by the Zr/Nb ratio. This deep melting also explains the extremely low Al_2O_3 contents of these lavas.

7.7.3 Evolution of the Type II lavas

Working on the assumption that the Type II lavas are descended from Al-depleted komatiite parent magmas similar to those seen in Barberton by a process of fractionation and crustal assimilation, the distinctive features of these lavas may now be attributed to one of two origins :-

- A primary feature attributable to the role of garnet and the primitive nature of the source, or

- A secondary feature due to the large degree of crustal assimilation.

The effects of crustal assimilation will most clearly be seen in those elements which show low concentrations in the magma but large concentrations in the crust, and those elements which are abundant in the magmas but less so in the crust will be least affected.

Major element abundances: The higher FeO content of the Type II lavas (and their lower mg# values) can be attributed to both the greater degree of fractionation and the deeper melting, or probably a combination of the two. The lower Al_2O_3 contents are the strongest indicator of the involvement of garnet in the melting regime.

Major element ratios: The lower Al_2O_3/TiO_2 and higher CaO/Al_2O_3 of the Type II lavas are the defining characteristics of Al-depleted komatiite, and are therefore attributable to the involvement of garnet in the melting regime. The lower mg# are attributable to a combination of deeper melting and a greater degree of fractionation, as mentioned above.

Trace element abundances: The enrichment in the HFS elements is easily attributable to crustal contamination, as continental crust is much richer in these elements. The fact that the enrichment in Y is less uniform and less pronounced, and the lack of any enrichment in V could reflect original depletion in these elements in the primary magma, as they are characteristically depleted in Al-depleted komatiites. The lower Sc contents of the Type II lavas are very indicative of the involvement of garnet, and are thought to be a feature of the primary magma.

Trace element ratios: The only trace element ratio which cannot be attributed to crustal assimilation is Zr/Nb, as explained above (see §7.6.2). This is thought to be a function of a more primary mantle source for the Type II parent magmas.1

REE: The REE chemistry of the Type II lavas is quite consistent with this model. The LREE enrichment ($La/Sm_N = 1.85$)[1] is characteristic of crustal contamination, while the HREE depletion ($Gd/Yb_N = 1.96$) is characteristic of Al-depleted komatiites, and consistent with reduced contribution of garnet to the melt. It is significant that the LREE enrichment is also seen in the evolved Type I lavas which have seen similar degrees of crustal contamination to the Type II lavas, but the HREE depletion is not, the Type I and evolved lavas having very similar values ($Gd/Yb_N = 1.22$ and 1.16, respectively)

Sm-Nd: As discussed above, the initial Nd isotopic compositions of the two lava types are consistent with different degrees of crustal addition to primary magmas with the same isotope ratios. There is no reason why garnet should have any effect on the

[1] All quoted REE ratios are average chondite normalised values, taken from Figure 6.13.

isotopic compositions of the derived melts. As suggested in §7.6.3, it would appear that the two lava types were isotopically similar, even though they were chemically distinct.

7.7.4 Conclusions

The differences between the two types of lavas would seem to be explained by a combination of processes. The Type II lavas are descended from deeper melts of a more primitive source than the Type I parent magmas, and show a clear garnet signature. They have also seen considerably more crustal contamination than the Type I lavas.

7.8 Conclusions

- **Are the differences between the Type I and Type II lavas due to alteration processes ? - No**
  It is very difficult to conceive how any alteration process could produce the physical and geochemical characteristics of the Type II lavas. Consequently, the differences between the Type I and Type II lavas must be assumed to be primary, representing different petrogenetic histories.

- **Could the Type II lavas be descended from the Type I lavas ? - No**
  The Type II magmas *cannot* be descended from the Type I magmas by any known petrogenetic process.

- **Could both Type I and Type II magmas be descended from the same primary magma ? - No**
  It would seem to be impossible for the Type I and Type II lavas to be descended from the same parent magma.

- **What were the primary magmas ?**
  There is no reason to suppose that the Type I lavas (the majority of the Zeederbergs Formation) could not have evolved from lavas similar to those seen in the Reliance Formation. The only possible parental magma for the Type II lavas which corresponds to any known magma composition would be a very high-magnesium (MgO>28%), Al-depleted komatiitic liquid, similar to those seen in the Barberton greenstone belt.

- **Were the different primary magmas from the same source ? No**
  The parental liquids to the two lavas types would seem to have been isotopically similar, but chemically distinct. Similar relationships are seen in other large basalt provinces today, such as the Ontong Java plateau, and in Iceland, where they are attributed to different mantle source compositions.

- **So how were the different lava types generated ?**
  The differences between the two types of lavas would seem to be explained by a combination of processes. The Type II lavas are descended from deeper melts of a more primitive source than the Type I parent magmas, and show a clear garnet signature. They have also seen considerably more crustal contamination than the Type I lavas.

8

CONCLUSIONS

8.1 Summary of conclusions

This final chapter summarises the conclusions from the end of each chapter, and attempts to draw all the ideas together.

In **Chapter 3, Stratigraphy and Field Relations**, the type section of the Zeederbergs Formation in the Ngezi River was examined in detail, and the chemical stratigraphy of the formation as seen in three sections was compared. It was concluded that :-

- The basal contact of the Reliance Formation is conformable on the sediments of the underlying Manjeri Formation, and there is no conclusive evidence for any removal of section from the Reliance Formation in any part of the belt. Consequently, the interpretation of the Ngezi Group volcanics as a tectonically emplaced allochthon would seem to be invalid.

- The Zeederbergs Formation is predominantly composed of pillow lavas, with some massive flow units, and minor tuff and hyaloclastite horizons. The vast majority of the lavas were clearly erupted under water, and all the tuffs show shallow marine sedimentary structures.

- Correlation of distinct geochemical marker horizons around the belt, and accurate logging of the Ngezi River type section suggest that the true thickness of the Zeederbergs Formation is only ~3km, rather than the 5-6km usually quoted. No evidence was found for removal of section in the Ngezi River type section.

- This good correlation of geochemical marker horizons around the belt also suggests that there has been no tectonic removal of section from the Zeederbergs Formation, which supports the interpretation of the volcanic sequence as erupted *in situ*, rather than tectonically emplaced.

- There is an apparently continuous horizon of clearly geochemically distinct lavas present in the Zeederbergs Formation, about a third of the way up the section, present around the belt. These lavas have lower Zr/Nb ratios and higher CaO/Al_2O_3 ratios and Zr and Y abundances than the majority of the Zeederbergs Formation lavas. They are referred to as Type II lavas, and the remainder as Type I lavas.

- There is a thin horizon of more evolved material (andesitic) near the top of all three sections through the Zeederbergs Formation.

In **Chapter 4, Petrography**, the mineralogy of the Zeedebergs Formation lavas was described in detail. In addition, the origin of the 'spheroid' features common in the formation was examined. It was concluded that :-

- Both the Reliance and Zeederbergs Formations show some preservation of original texture and mineralogy. In some places the quality of preservation is excellent. On the basis of mineralogical and textural characeristics, the lavas of the Reliance Formation can be subdivided into 4 different varieties.

- The lavas of the Zeederbergs Formation are generally fine grained, hyalocrystalline, and moderately to sparsely porphyritic. The dominant phenocryst phase is clinopyroxene (mostly augite), with, less commonly, a little plagioclase.

- A subdivision of the lavas of the Zeederbergs Formation based on petrographic criteria is not practical.

- Most lavas are altered to hydrated low-greenschist mineral assemblages.

- The most likely origin for the 'spheroid' structures in the Zeederbergs Formation is thought to be spherulitic devitrification.

In **Chapter 5, Alteration**, the mobility of elements during post-eruptive alteration processes was examined. It was concluded that :-

- All rock suites have different histories, and few generalisations about element mobility can be applied to any specific suite.

- Any two elements which form a reasonably coherent trend on a variation diagram which can be explained in terms of simple igneous processes are unlikely to have been mobile during subsequent alteration. In addition, the best indicator of REE stability during alteration is a smooth REE pattern.

- Work on the Reliance Formation suggests that the bulk chemistry has been little affected by recrystallisation to the current metamorphic assemblage. CaO, SiO_2, Na_2O, K_2O and the LFSE (Sr, Rb and Ba) have all been mobile during alteration, as have Cu and Pb, but the HFSE & REE (Ti, Zr, Y, Nb, La, V and P), Ni, Zn and Cr seem to have been reasonably immobile.

- A series of simple screens can be applied to the samples from the Zeederbergs Formation to remove samples whose composition is not a reliable indicator of primary igneous processes. Bulk chemistry has been little affected by recrystallisation to the current metamorphic assemblage. Element mobility can be assessed by comparison with Zr as an immobile comparator.

- TiO_2, Al_2O_3, MnO and P_2O_5 are interpreted as being immobile, MgO, FeO as slightly mobile, CaO as significantly mobile, and SiO_2, Na_2O and K_2O as very mobile.

- Concentrations of the HFS elements (Nb, Y, Ce, Nd, V, and, of course, Zr) appear to be reliable indicators of primary abundances. Ni and Cr seem to have been fairly immobile, and the behaviour of Th, Sc and Cu is thought to represent primary differences between the two lava types, but Zn and the LFSE (Sr, Pb, Ba, and Rb) would seem to be unsuitable for any serious consideration.

- The REE data would appear to be a reliable indicator of primary igneous processes.

- There is good evidence for silicification and bulk SiO_2 mobility within the Zeederbergs Formation, and it may be possible to correct for this using theoretical fractionation trends with Zr.

- Of the 'Low-Mg' samples set, only three samples appear to be truly evolved, showing very high abundances of all the incompatible elements. The other three samples only have low MgO and high SiO_2 as a result of heavy silicification, and were excluded.

In **Chapter 6, Geochemistry**, with the degree of elemental mobility known, the detailed geochemistry of the Zeederbergs lavas was examined. It was concluded that :-

- The lavas of the Reliance Formation all fall on the world-wide, Al-undepleted, komatiite trend. Olivine and Cr-spinel fractionation can explain most of the behaviour seen within the suite.

- The Type I and Type II lavas are very similar in their major element chemistry, with the notable exception of Al2O3 contents, which are considerably lower in the Type II lavas. The Type II lavas also have slightly higher FeO, TiO_2 and P_2O_5 abundances.

- The Type II lavas have higher CaO/Al_2O_3, and lower Al_2O_3/TiO_2 ratios than the Type I lavas, and cannot be descended from these lavas (or any of those in the Reliance Formation) by simple fractional crystallisation.

- The Type II lavas show higher abundances of nearly all incompatible trace elements than Type I lavas. Only Sc is less abundant in the Type II lavas than in the Type I lavas.

- A comparison of trace element ratios of the two lava types leads to a clear order of enrichment in the Type II lavas:

$$\mathbf{Nb > Ce \approx Zr > Y}$$

Most enriched Least enriched

- The Type I and Type II lavas (and the evolved lavas) show marked differences in their REE chemistry:

  Type I lavas range from moderately depleted to moderately enriched in the LREE, and have relatively flat to very slightly depleted HREE patterns.

  Evolved lavas have highly LREE-enriched, and very slightly HREE-depleted patterns.

  Type II lavas are moderately to highly enriched in the LREE, and quite heavily HREE-depleted.

- Previous Pb-Pb isotope work on the rocks of the Reliance Formation gives the most reliable age for the Ngezi Group volcanics, **2692 ± 9 Ma**.

- Sm-Nd analyses from the Zeederbergs Formation provide some reasonably good isochron ages for the group, most of which are at *least* 500 Ma *older* than the Pb-Pb date above!

- The initial isotope ratios calculated using the Pb-Pb age show significant differences between the lava types:

  Type I lavas- Initial ε_{Nd} = **+2.5** to **+4.0**

  Type II lavas - Initial ε_{Nd} = **+1.05**

  Evolved lavas - Initial ε_{Nd} = **+0.84**

In **Chapter 7, Interpretation**, several questions were asked about the origin of the Zeederbergs Formation lavas:-

- **Are the differences between the Type I and Type II lavas due to alteration processes ? - No**

  It is very difficult to conceive how any alteration process could produce the physical and geochemical characteristics of the Type II lavas. Consequently, the differences between the Type I and Type II lavas must be assumed to be primary, representing different petrogenetic histories.

- **Could the Type II lavas be descended from the Type I lavas ? - No**

  The Type II magmas *cannot* be descended from the Type I magmas by any known petrogenetic process.

- **Could both Type I and Type II magmas be descended from the same primary magma ? - No**
  It would seem to be impossible for the Type I and Type II lavas to be descended from the same parent magma.

- **What were the primary magmas ?**
  There is no reason to suppose that the Type I lavas (the majority of the Zeederbergs Formation) could not have evolved from lavas similar to those seen in the Reliance Formation. The only possible parental magma for the Type II lavas which corresponds to any known magma composition would be a very high-magnesium (MgO>28%), Al-depleted komatiitic liquid, similar to those seen in the Barberton greenstone belt.

- **Were the different primary magmas from the same source ? No**
  The parental liquids to the two lavas types would seem to have been isotopically similar, but chemically distinct. Similar relationships are seen in other large basalt provinces today, such as the Ontong Java plateau, and in Iceland, where they are attributed to different mantle source compositions.

- **So how were the different lava types generated ?**
  The differences between the two types of lavas would seem to be explained by a combination of processes. The Type II lavas are descended from deeper melts of a more primitive source than the Type I parent magmas, and show a clear garnet signature. They have also seen considerably more crustal contamination than the Type I lavas.

8.2 Concluding remarks

The discovery of the Type II lavas in the Zeederbergs Formation raises interesting questions about the origins of the Ngezi Group volcanics, and Archaean volcanism generally. If they are indeed descended from primary magmas similar to the Al-depleted komatiites seen in Barberton, then ideas of how lavas of this composition relate to mantle temperatures, or how those temperatures have changed through time, might need to be re-examined.

Exactly how the parental magmas for the two lava types were generated is also of interest. Were they produced in the same area, sampling different mantle compositions, or do they represent input of lavas from different, possibly widely separated, volcanic centres ?

These questions are beyond the scope of this thesis, but may form the basis for further work in the region.

REFERENCES

Agee, C.B., and Walker, D., 1988. Static compression and olivine flotation in ultrabasic silicate liquid. *Journal of Geophysical Research*, **93 B**, 3437-3449.

Ahern, J.L., and Turcotte, D.L., 1979. Magma migration beneath an ocean ridge. *Earth and Planetary Science Letters*, **45**, 115-122.

Anderson, A.T. Jr., Swihart, G.H., Artioli, G., and Geiger, C.A., 1984. Segregation vesicles, gas filter-pressing, and igneous differentiation. *Journal of Geology*, **92**, 55-72.

Arndt, N.T., 1977. Ultrabasic magmas and high degree melting of the mantle. *Contributions to Mineralogy and Petrology*, **64**, 205-221.

Arndt, N.T., 1983. Element mobility during komatiite alteration. *Eos*, **64**, 331.

Arndt, N.T., and Jenner, G.A., 1986. Crustally contaminated komatiites and basalts from Kambalda, Western Australia. *Chemical Geology*, **56**, 229-255.

Arndt, N.T., and Brooks, C., 1980. Penrose Conference Report: Komatiites. *Geology*. **8**, 155-156.

Arndt, N.T., and Nisbet, E.G., 1982a. *Komatiites*. London: George Allen & Unwin, 562pp

Arndt, N.T., and Nisbet, E.G., 1982b. What is a komatiite?, *in* Arndt, N.T., and Nisbet, E.G. (eds.), *Komatiites*. London: George Allen & Unwin, 19-27.

Arndt, N.T., and Nesbitt, R.W., 1982. Geochemistry of Munro Township basalts, *in* Arndt, N.T., and Nisbet, E.G. (eds.), *Komatiites*. London: George Allen & Unwin, 309-329.

Arndt, N.T., and Jochum, K.P., 1990. Komatiites: Unreliable witnesses of the Archaean mantle, *in* Glover, J.E., and Ho, S.E. (compilers), Abstract, *Third International Archaean Symposium*. Perth: Geoconferences (WA) Inc., pp. 147-148.

Arndt,N.T., and Lesher, C.M., 1992. Fractionation of rare earth elements by olivine and the origin of Kambalda komatiites, Western Australia. *Geochimica et Cosmochimica acta*, **56**, 4191-4204.

Arndt, N.T., Naldrett, A.J., and Pyke, D.R., 1977. Komatiitic and iron-rich tholeiitic lavas of Munro Township, northeast Ontario. *Journal of Petrology*, **18**, 319-369.

Arth, J.G., Arndt,N.T., and Naldrett, A.J., 1977. Genesis of Archaean komatiites from Munro Township, Ontario: Trace element evidence. *Geology*, **5**, 590-594.

Barley, M.E., 1986. Incompatible element enrichment in Archaean basalts: a consequence of contamination by older sialic crust rather than mantle heterogeneity, *Geology*, **14**, 947-950.

Beswick, A.E., 1982. Some geochemical aspects of alteration and genetic relations in komatiitic suites, *in* Arndt, N.T., and Nisbet, E.G. (eds.), *Komatiites*. London: George Allen & Unwin, 283-308.

Bickle, M.J., 1982. The magnesium contents of komatiitic liquids, *in* Arndt, N.T., and Nisbet, E.G. (eds.), *Komatiites*. London: George Allen & Unwin, 479-494.

Bickle, M.J., 1990. Mantle evolution, *in* Hall, R.P., and Hughes, D.J. (eds.), *Early Precambrian basic magmatism*. Glasgow and London: Blackie, pp. 111-135.

Bickle, M.J., and Eriksson, K.A., 1982. Evolution and subsidence of Early Precambrian sedimentary basins. *Philosophical Transactions of the Royal Society of London*, **A 305**, 225-247.

Bickle, M.J., and Nisbet, E.G., 1986. Greenstone belt tectonics - Thermal constraints, *in* De Wit, M.J., and Ashwal, L. (eds.), *The tectonic evolution of greenstone belts*. Lunar and Planetary Institute, Houston Workshop, 57-64.

Bickle, M.J., and Nisbet, E.G., (eds). 1993. *The geology of the Belingwe Greenstone Belt, Zimbabwe*. Rotterdam: A.A.Balkema.

Bickle, M.J., Martin, A., Nisbet, E.G., 1975. Basaltic and peridotitic komatiites and stromatolites above a basal unconformity in the Belingwe greenstone belt, Rhodesia. *Earth and Planetary Science Letters*, **27**, 155-162.

Bickle, M.J., Hawkesworth, C.J., Martin, A., Nisbet, E.G., O'Nions, R.K., 1976. Mantle composition derived from the chemistry of ultramafic lavas. *Nature*, **263**, 577-580.

Bickle, M.J., Ford, C.E., and Nisbet, E.G., 1977. The petrogenesis of peridotitic komatiites: evidence from high pressure melting experiments. *Earth and Planetary Science Letters*, **37**, 97-106.

Bickle, M.J., Orpen, J.L., Nisbet, E.G., Martin, A., 1993. Structure and metamorphism of the Belingwe Greenstone Belt and adjacent granite-gneiss terrain: The tectonic evolution of an Archaean craton, *in* Bickle, M.J., and Nisbet, E.G., (eds). 1993. *The geology of the Belingwe Greenstone Belt, Zimbabwe*. Rotterdam: A.A.Balkema.

Bickle, M.J., Nisbet, E.G., Martin, A., Orpen, J.L., 1993. Introduction: The Zimbabwe Craton and controversies over Archaean granite-greenstone terrains, *in* Bickle, M.J., and Nisbet, E.G., (eds). 1993. *The geology of the Belingwe Greenstone Belt, Zimbabwe*. Rotterdam: A.A.Balkema.

Bickle, M.J., Arndt, N.T., Nisbet, E.G., Orpen, J.L., Martin, A., Keays, R.R., and Renner, R., 1993. Geochemistry of the igneous rocks of the Belingwe greenstone belt: Alteration, contamination and petrogenesis, *in* Bickle, M.J., and Nisbet, E.G., (eds). 1993. *The geology of the Belingwe Greenstone Belt, Zimbabwe*. Rotterdam: A.A.Balkema.

Blenkinsop, T.G., Fedo, C.M., Bickle, M.J., Eriksson, K.A., Martin, A., Nisbet, E.G., Wilson, J.F., 1993. Ensialic origin for the Ngezi Group, Belingwe greenstone belt, Zimbabwe. *Geology*, **21**, 1135-1138.

Bowen, N.L., 1928. *The evolution of igneous rocks*. Princeton, N.J.: Princeton University Press, 332 pp.

Brooks, C., and Hart, S.R., 1974. On the significance of komatiite. *Geology*, **2**, 107-110.

Campbell, I.H., and Arndt,N.T., 1982. Pyroxene accumulation in spinifex-textured rocks. *Geology Magazine*, **6**, 605-610.

Campbell, I.H., Griffiths, R.W., and Hill, R.I., 1989. Melting in Archaean mantle plumes: heads it's basalts, tails it's komatiites. *Nature*, **339**, 697-699.

Cameron, W.E., Nisbet, E.G., and Dietrich, V.J., 1979. Boninites, komatiites and ophiolitic basalts. *Nature*, **280**, 550-553.

Cas, R.A.F., and Wright, J.V., 1988. *Volcanic Successions: modern and ancient*. London: Unwin Hyman Ltd, 528 pp.

Cattell, A.C., 1987. Enriched komatiitic basalts from Newton Township, Ontario: their genesis by crustal contamination of depleted komatiitic magma. *Geol. Mag.*, **124**, 303-309.

Cattell, A.C., and Arndt, N.T., 1987. Low- and high-alumina komatiites from a Late Archaean sequence, Newton Township, Ontario. *Contributions to Mineralogy and Petrology, **97**,* 218-227.

Cattell, A.C., and Taylor, R.N., 1990. Archaean basic magmas, *in* Hall, R.P., and Hughes, D.J. (eds.), *Early Precambrian basic magmatism.* Glasgow and London: Blackie, pp. 11-39.

Cattell, A.C., Krogh, T.E., and Arndt, N.T., 1984. Conflicting Sm-Nd whole rock and U-Pb zircon ages for Archaean lavas Newton Township, Abitibi Belt, Ontario. *Earth and Planetary Science Letters*, **70**, 280-290.

Cawthorn, R.G., 1975. Degrees of melting in mantle diapirs and the origin of ultrabasic liquids. *Earth and Planetary Science Letters*, **27**, 113-120.

Cawthorn, R.G., 1977. Archaean variolites - quenched immiscible liquids: Discussion. *Canadian Journal of Earth Sciences*, **14**, 2178-2179.

Cawthorn, R.G., and Fraser, D.G., 1979. Element partitioning in immiscible volcanic liquids: a statiscal model. *Chemical Geology*, **27**, 99-113.

Chauvel, C., Dupré, B., Arndt, N.T., 1993. Pb and Nd isotopic correlation in Belingwe komatiites and basalts, *in* Bickle, M.J., and Nisbet, E.G., (eds). 1993. *The geology of the Belingwe Greenstone Belt, Zimbabwe.* Rotterdam: A.A.Balkema.

Chauvel, C., Dupré, B., and Jenner, G.A., 1985. The Sm-Nd age of Kambalda volcanics is 500 Ma too old!. *Earth and Planetary Science Letters*, **74**, 315-324

Chauvel, C., Dupré, B., Todt, W., and Jenner, G.A., 1983. Pb and Nd isotopic correlation in Archaean and Proterozoic greenstone belts. *EOS*, **64**, 330.

Cloué-Long , J.C., 1986. *Archaean komatiitic and tholeiitic volcanics at Kambalda, Western Australia.* Unpublished Ph.D. thesis, University of Southampton.

Coltorti, M., Girardi, V.A.V., and Schorscher, J.H.D., 1987. Liquid immiscibility in the Archaean greenstone belt of Piumhi, Minas Gerais, Brazil. *Lithos*, **20**, 77-91.

Cox, K.G., 1989. Hot plumes from the mantle. *Nature*, **340**, 541-542.

Crawford, A.J., Falloon, T.J., and Green, D.H., 1989. Classification, petrogenesis and tectonic settings of boninites, *in* Crawford, A.J. (ed.), *Boninites.* London: Unwin Hyman, 1-49.

Compston, W., Williams, I.S., Campbell, I.H., and Gresham, J.J., 1986. Zircon xenocrysts from the Kambalda volcanics: age constraints and direct evidence for older continental crust below the Kambalda - Norseman greenstones. *Earth and Planetary Science Letters*, **76**, 299-311.

Condie, K.C., 1990. Geochemical characteristics of Precambrian basaltis greenstones, *in* Hall, R.P., and Hughes, D.J. (eds.), *Early Precambrian basic magmatism.* Glasgow and London: Blackie, pp. 40-45.

Condie, K.C., and Crow,C., 1990. Early Precambrian within plate basalts from the Kaapval craton in Southern Africa: a case for crustally contaminated komatiites. *Journal of Geology*, **98**, 100-107.

Cooper, M.R., 1990. Tectonic cycles in southern Africa. *Earth-Science Reviews*, **28**, 321-364.

Coward, M.P., James, P.R., Wright, L., 1976. Northern margin of the Limpopo mobile belt, southern Africa. *Bulletin of the Geological Society of America*, **87**, 601-611.

Deer, W.A., Howie, R.A., and Zussman, J., 1966. *An introduction to the rock-forming minerals*. London. Longman.

Dodson, M.H., Compston, W., Williams, I.S., and Wilson, J.F., 1988. A search for ancient detrital zircons in Zimbabwean sediments. *Journal of the Geological Society of London*, **145**, 977-983.

Ferguson, J., and Currie, K.L., 1972. Silicate immiscibility in the ancient basalts of the Barberton Mountain Land, Transvaal. *Nature and Physical Science*, **235**, 86-89.

Fletcher, R.A., and Espin, W.M., 1897. *Geological sketch map of Matabeleland.* Scale 1 inch = 20 miles. Edward Stamford, London.

Foster, R.P., 1989. Archaean gold mineralisation in Zimbabwe: implications for metallogenesis and exploration, *in* Keays, R.R., Ramsay, W.R.H., and Groves, D.I. (eds), The geology of gold deposits: the perspective in 1989. *Economic Geology Monograph* **6**, 54-70.

Fowler, A.D., Jensen, L.S., and Peloquin, S.A., 1987. Varioles in Archaean basalts: products of spherulitic crystallisation. *Canadian Mineralogist*, **25**, 275-289.

Frost, K.M., and Groves, D.I., 1988. Ocellar units at Kambalda: evidence for sediment assmilation by komatiite lavas, *in* Proceedings of 5th Magmatic Sulphides Field Conference, Harare, Zimbabwe. *Institute of mining and Metallurgy, London*, 207-214.

Gansser, A., Dietrich, V.J., and Cameron, W.E., 1979. Paleogene komatiites from Gorgona Island. *Nature*, **278**, 545-546.

Gélinas, L., Brooks, C, and Trzcienski, W.E. Jr., 1976. Archaean variolites - quenched immiscible liquids. *Canadian Journal of Earth Sciences*, **13**, 210-230.

Gélinas, L., Mellinger, M., and Trudel, P., 1982. Archaean mafic metavolcanics from the Rouyn-Noranda district, Abitibi greenstone belt, Quebec. 1. Mobility of the major elements. *Canadian Journal of Earth Sciences*, **19**, 2258-2275.

Gélinas, L., Trzcienski, W.E. Jr., and Brooks, C., 1977. Archaean variolites - quenched immiscible liquids: Discussion. *Canadian Journal of Earth Sciences*, **14**, 2945-2958.

Green, D.H., Nicholls, I.A., Viljoen, M.J., and Viljoen, R.P., 1975. Experimental demonstration of the existence of peridotitic liquids in earliest Archaean magmatism. *Geology*, **3**, 11-15.

Govindaraju, K., 1994. 1994 compilation of working values and sample description for 383 geostandards, *Geostandards Newsletter* **18**, 1–158.

Gruau, G., Jahn, B.M., Glikson, A.Y., Davy, R., Hickman, A.H., and Chauvel, C., 1987. Age of the Archaean Talga-Talga Subgroup, Pilbara Block, Western Australia, and early evolution of the mantle: new Sm-Nd isotopic evidence. *Earth and Planetary Science Letters*. **85**, 105-116.

Hall, R.C.B., 1983. *The geology of the country around the Belvedere Mine, Belingwe greenstone belt*. Unpublished B.Sc. (Hons) thesis, University of Zimbabwe.

Hamilton, P.J., O'Nions, R.K., Evensen, N.M., 1977. Sm-Nd dating of Archaean basic and ultrabasic volcanics. *Earth and Planetary Science Letters*, **36**, 263-268.

Hart, S.R., Erlank, A.J., and Kable, E.J.D., 1974. Sea floor basalt alteration: some chemical and Sr isotope effects. *Contributions to Mineralogy and Petrology*, **44**, 219-230.

Hawkesworth, C.J., Moorbath, S., O'Nions, R.K., and Wilson, J.F., 1975. Age relationship between greenstone belts and granites in the Rhodesian Archaean craton. *Earth and Planetary Science Letters*, **25**, 251-262.

Hawkesworth, C.J., and O'Nions, R.K., 1977. The petrogenesis of some Archaean volcanic rocks from Southern Africa. *Journal of Petrology*, **18**, 487-520.

Hawkesworth, C.J., Bickle, M.J., Gledhill, A.R., Wilson, J.F., Orpen, J.L., 1979. A 2.9b.y event in the Rhodesian Archaean. *Earth and Planetary Science Letters*, **43**, 285-287.

Hegner. E., Kroner, A., and Hoffman, A.W., 1984. Age and isotope geochemistry of the Archaean Pongola and Usushwana suites in Swaziland, southern Africa: A case for crustal contamination of mantle derived magma. *Earth and Planetary Science Letters*, **70**, 267-279.

Hellman, P.L.,*et al.*, 1979. The mobility of the Rare Earth Elements: Evidence and implications from selected terrains affected by burial metamorphism. *Contributions to Mineralogy and Petrology*, **71**, 23-44.

Herzberg, C.T., 1987. Magma density at high pressure Part 2: A test of the olivine flotation hypothesis. *in* Mysen, B. (ed.) Magmatic Processes: Physiochemical Principles. *Geochemical Society Special Publication*, **1**, 47-58.

Herzberg, C.T., 1992. Depth and degree of melting of Komatiites. *Journal of Geophysical Research*, **97 B4**, 4521-4540.

Herzberg, C.T., and O'Hara, M.J., 1985. Origin of mantle peridotite and komatiite by partial melting. *Geophysical Research Letters*, **12**, 541-544.

Herzberg, C.T., and Ohtani, E., 1988. Origin of komatiite at high pressures. *Earth and Planetary Science Letters*, **88**, 321-329.

Hess, H.H., 1938. A primary peridotite magma. *American Journal of Science, Series 5*, **35**, 321-344.

Hickman, M.H., 1974. 3500 m.y. old granite in southern Africa, *Nature*, **251**, 295-296.

Hickman, M.H., 1978. Isotopic evidence for crustal reworking in the Rhodesian Archaean craton, southern Africa, *Geology*, **6**, 214-216.

Hughes, C.J., 1977. Archaean variolites - quenched immiscible liquids: Discussion. *Canadian Journal of Earth Science*, **14**, 2945-2958.

Humphris, S.E., and Thompson, G., 1978a. Hydrothermal alteration of oceanic basalts by sea-water. *Geochimica et Cosmochimica Acta*, **42**, 127-136.

Humphris, S.E., and Thompson, G., 1978b. Trace element mobility during hydrothermal alteration of oceanic basalts. *Geochimica et Cosmochimica Acta*, **42**, 107-125.

Huppert, H.E., and Sparks R.S.J., 1985. Cooling and contamination of mafic and ultramafic magmas during ascent through continental crust. *Earth and Planetary Science Letters*, **74**, 371-386.

Jackson, J., and McKenzie, D.P., 1983. The geometrical evolution of normal fault systems. *Journal of Structural Geology*, **5**, 471-482.

Jahn, B.M., and Condie, K.C., 1976. On the age of the Rhodesian greenstone belts. *Contributions to Mineralogy and Petrology*, **57**, 317-330.

Jahn, B.M., Gruau, G., and Glikson, A.Y., 1982. Komatiites of the Onverwacht Group, South Africa: REE Geochemistry, Sm/Nd age and mantle evolution. *Contributions to Mineralogy and Petrology*, **80**, 25-40.

Jensen, L.S., 1976. A new cation plot for classifying subalkalic volcanic rocks. *Ontario Division of Mines, Miscellaneous Paper*, **66**.

Jochum, K.P., Seufert, H.M., and Thirlwall, M.F., 1990. High-sensitivity Nb analysis by spark-source mass spectrometry (SSMS) and calibration of XRF Nb and Zr, *Chem. Geol.*, **81**, 1–16.

Jolly, W.T., 1980. Development and degradation of Archaean lavas, Abitibi area, Canada, in light of major element geochemistry. *Journal of Petrology*, *21*, 323-363.

Keep, F.E., 1929. *The Geology of the Shabani Mineral Belt, Belingwe District.* Southern Rhodesia Geological Survey, Bulletin No.12.

Krough, and Hurley, 1968. *Journal of Geophysical Research*, **73**, 7107-7125.

Kusky, T.M., and Kidd, W.S.F., 1992. Remnants of an Archean *(sic.)* oceanic plateau, Belingwe greenstone belt, Zimbabwe. *Geology*, **20,** 43-46.

Kusky, T.M., Winsky, P.A., and Kidd, W.S.F. 1994. Comment *on* 'Blenkinsop, T.G., Fedo, C.M., Bickle, M.J., Eriksson, K.A., Martin, A., Nisbet, E.G., Wilson, J.F., 1993. Ensialic origin for the Ngezi Group, Belingwe greenstone belt, Zimbabwe.', *Geology* **22**, 766.

Langmuir, C.H., Bender, J.F., Bence, A.E., and Hanson, G.N., 1977. Petrogenesis of basalts from the FAMOUS area, Mid-Atlantic Ridge. *Earth and Planetary Science Letters*, **36**, 133-156.

Laubscher, D.H., 1963. *The origin and occurence of chrysotile asbestos and associated rocks in the Shabani and Mashaba area, Southern Rhodesia.* Unpublished PhD thesis, University of Witwatersrand, Johannesburg.

Luais, B., and Hawkeworth, C.J., 1994. The generation of continental crust: An integrated study of crust-forming processes in the Archaean of Zimbabwe. *Journal of Petrology*, **35**, 43-93.

Ludden, J.N., and Gélinas, L., 1982. Trace element characteristics of komatiites and komatiitic basalts from the Abitibi metavolcanic belt of Quebec, *in* Arndt, N.T., and Nisbet, E.G. (eds.), *Komatiites*. London: George Allen & Unwin, 331-346.

Ludden, J.N., and Thompson, G., 1978. An evaluation of the behaviour of the rare earth elements during the weathering of sea-floor basalt. *Earth and Planetary Science Letters*, **43**, 85-92.

Macgregor, A.M., 1951. Some milestones in the Precambrian of Southern Rhodesia. *Transactions of the Geological Society of South Africa*, **54**, xxvii-lxxi.

MacGeehan, P.J., and MacLean, W.H., 1980. An Archaean sub-seafloor geothermal system, 'calc alkali' trends, and massive sulphide genesis. *Nature*, **286**, 767-771.

MacKenzie, W.S., Donaldson, C.H., and Guilford, C., 1984. *Atlas of igneous rocks and their textures.* Longman, 148pp.

Martin, A., 1978. *The Geology of the Belingwe - Shabani Schist Belt.* Rhodesia Geological Survey, Bulletin No. 83, 220 pp.

Martin, A., 1980. *Belingwe - Shabani* (Map to accompany Bulletin No.83). Scale 1:100,000. Zimbabwe Geological Survey.

Martin, A., 1983. *The geology of the northern part of the Belingwe greenstone belt and surrounding granitoids.* Unpublished D.Phil thesis, University of Zimbabwe.

Martin, A., Nisbet, E.G., and Bickle, M.J., 1980. Archaean stromatolites of the Belingwe greenstone belt. *Precambrian Research*, **13**, 337-362.

Martin, A., Nisbet, E.G., Bickle, M.J., Orpen, J.L., 1993. Rock units and stratigraphy of the Belingwe Greenstone Belt: The complexity of the tectonic setting, *in* Bickle, M.J., and Nisbet, E.G., (eds). 1993. *The geology of the Belingwe Greenstone Belt, Zimbabwe.* Rotterdam: A.A.Balkema.

McDonough, W.F., and Ireland, T.R., 1993. Intraplate origin of komatiites inferred from trace elements in glass inclusions. *Nature*, **365**, 432-434.

McKenzie, D.P., 1978. Some remarks on the development of sedimentary basins. *Earth and Planetary Science Letters*, **40**, 25-32.

McKenzie, D.P., 1984. The generation and compaction of partially molten rock. *Journal of Petrology*, **25**, 713-765.

McKenzie, D.P., 1985. The extraction of magma from the crust and mantle. *Earth and Planetary Science Letters*, **74**,81-91.

McKenzie, D.P., and Bickle, M.J., 1988. The volume and composition of melt generated by extension of the lithosphere. *Journal of Petrology*, **29**, 625-679.

McKenzie, D.P., and O'Nions R.K., 1991. Partial melt distributions from inversion of rare earth element concentrations. *Journal of Petrology*, **32**, 1021-1091.

McKenzie, D.P., Nisbet E.G., and Sclater, J.G., 1980. Sedimentary basin development in the Archaean. *Earth and Planetary Science Letters*, **48**, 35-41.

Mennell, F.P., 1910. *Geological Map of Rhodesia (mining districts of Matabeleland)* Scale 1 inch = 8 miles. Ellis Allen, Bulawayo.

Moorbath, S.M., 1984. Patterns and geological significance of determinations in continental blocks, *in* Holland, H.D., and Trendall, A.F. (eds.), *Patterns of change in Earth evolution.* Dahlem Konferenzen. Berlin, Heidelberg, New York, Tokyo: Springer Verlag, 207-220.

Moorbath, S.M., Taylor, P.N., Orpen, J.L., Treloar, P.J., and Wilson, J.F., 1987. First direct dating of Archaean stromatolitic limestone. *Nature*, **326**, 865-867.

Moorbath, S.M., Wilson, J.F., Goodwin, R., Humm, M., 1977. Further Rb-Sr age and isotope data on early and late Archaean rocks from the Rhodesian craton. *Precambrian Research*, **5**, 229-239.

Moorbath, S.M., Wilson, J.F., and Cotterill, P., 1976. Early Archaean age for the Sebakwian Group at Selukwe, Rhodesia. *Nature*, **264**, 536-538.

Morris, H.S., 1969. *The Geology and Gold Mineralisation of the Shabi Shear Zone, Shabani District, Southern Rhodesia.* Unpublished PhD thesis, University of Witwatersrand, Johannesburg.

Morrison, E.R., and Wilson, J.F., 1971. Symposium on granites, gneisses and related rocks. *Excursion Guidebook, Geological Society of South Africa (Rhodesian Branch).*

Mottl M.J., 1983. Metabasalts, axial hot springs, and the structure of hydrothermal systems at mid-ocean ridges. *Geological Society of America Bulletin*, **94**, 161-180.

Nakamura, N., 1974. Determination of REE, Ba, Fe, Mg, Na and K in carbonaceous and ordinary chondrites. *Geochimica et Cosmochimica Acta*, **38**, 757-775.

Nesbitt, R.W., and Sun, S-.S., 1976. Geochemistry of Archaean spinifex-textured peridotites and magnesian and low-magnesian tholeiites. *Earth and Planetary Science Letters*, **31**, 433-453.

Nesbitt, R.W., Sun, S-.S., and Purvis, A.C., 1979. Komatiites: geochemistry and genesis. *Canadian Mineralogist*, **17**, 165-186.

Nesbitt, R.W., Walker, I.W., and Blight, D.F., 1984. Geochemistry of Archaean basaltic lavas, Diemals, Western Australia, *in* Professional Papers for 1982, *Report of the Geological Society of Western Australia*, **12**, 15-26.

Nisbet, E.G., 1982. The tectonic setting and petrogenesis of komatiites, *in* Arndt, N.T., and Nisbet, E.G. (eds.), *Komatiites*. London: George Allen & Unwin, 501-526.

Nisbet, E.G., 1985. Putting the squeeze on rocks. *Nature*, **315**, 541.

Nisbet, E.G., 1987. *The Young Earth - an introduction to Archaean geology*. Boston: Allen & Unwin, 402 pp.

Nisbet, E.G., and Walker, D., 1982. Komatiites and the structure of the Archaean mantle. *Earth and Planetary Science Letters*, **60**, 105-113.

Nisbet, E.G., Bickle, M.J., and Martin, A., 1977. The mafic and ultramafic lavas of the Belingwe greenstone belt, Rhodesia. *Journal of Petrology*, **18**, 521-566.

Nisbet, E.G., Wilson, J.F., and Bickle, M.J., 1981. The evolution of the Rhodesian craton and adjacent Archaean terrain: tectonic models, *in* Kröner, A. (ed), *Precambrian Plate Tectonics*, Amsterdam: Elsevier, 161-183.

Nisbet, E.G., Bickle, M.J., Martin, A., Orpen, J.L., Wilson, J.F., 1982. Komatiites in Zimbabwe, *in* Arndt, N.T., and Nisbet, E.G. (eds), *Komatiites*. London: George Allen & Unwin, 501-526.

Nisbet, E.G.,Arndt, N.T., Bickle, M.J., Cameron, W.E., Chauvel, C., Cheadle, M.,Hegner, E., Kyser, T.K., Martin, A., Renner, R., and Roedder, E., 1987. Uniquely fresh 2.7 Ga komatiites from the Belingwe greenstone belt, Zimbabwe. *Geology*, **15**, 1147 - 1150

Nisbet, E.G., Bickle, M.J., Martin, A., Orpen, J.L., 1993. Sedimentology of the Brooklands Formation, Zimbabwe: Development of an Archaean greenstone belt in a rifted graben, *in* Bickle, M.J., and Nisbet, E.G., (eds). 1993. *The geology of the Belingwe Greenstone Belt, Zimbabwe*. Rotterdam: A.A.Balkema.

Nisbet, E.G., Bickle, M.J., Orpen, J.L., Martin, A., 1993. Controls on the formation of the Belingwe Greenstone Belt, Zimbabwe, *in* Bickle, M.J., and Nisbet, E.G., (eds). 1993. *The geology of the Belingwe Greenstone Belt, Zimbabwe*. Rotterdam: A.A.Balkema.

Nisbet, E.G., Martin, A., Bickle, M.J., and Orpen, J.L. 1993. The Ngezi Group: Komatiites, basalts and stromatolites on continental crust. *in* Bickle, M.J., and Nisbet, E.G., (eds). 1993. *The geology of the Belingwe Greenstone Belt, Zimbabwe*. Rotterdam: A.A.Balkema.

Norrish, K., and Hutton, J.T., 1969. An accurate X-ray spectrographic method for the analysis of a wide range of geological samples, *Geochim. Cosmochim. Acta* **33**, 431-453.

Ohtani, E., Nagata, Y., Suzuki, A., Kato, T., 1995. Melting relations of peridotite and the density crossover in planetary mantles. *Chemical Geology*, **120**, 207-221.

Oldham, J.W., 1968. A short note on recent geological mapping in the Shabani area, *in* Visser, D.J.L. (ed.), Symposium on the Rhodesian Basement Complex. *Transactions of the Geological Society of South Africa, Annex,* **71**, 189-194.

Oldham, J.W., 1970. *A structural interpretation of the geology of the Shabani area, Rhodesia.* Unpublished D.Phil. thesis, University of Zimbabwe.

Orpen, J.L., 1978. *The geology of the southwestern part of the Belingwe greenstone belt and the adjacent country - the Belingwe Peak area.* Unpublished D.Phil. thesis, University of Zimbabwe.

Orpen, J.L., Bickle, M.J., Nisbet, E.G., Martin, A., 1986. Belingwe Peak (Map to accompany Short Report 51). Scale 1:100,000. Zimbabwe Geological Survey.

Orpen, J.L., Martin, A., Bickle, M.J., Nisbet, E.G., 1993. The Mtshingwe Group in the west: Andesites, basalts, komatiites and sediments of the Hokonui, Bend and Koodoovale Formations, *in* Bickle, M.J., and Nisbet, E.G., (eds). 1993. *The geology of the Belingwe Greenstone Belt, Zimbabwe.* Rotterdam: A.A.Balkema.

Pearce, J.A., 1976. Statistical analysis of major element patterns in basalts. *Journal of Petrology,* **17**, 15-43.

Phillips, W.J., 1973. Interpretation of crystalline spheroidal structures in igneous rocks. *Lithos,* **6**, 235-244.

Philpotts, A.R., 1976. Silicate liquid immiscibility: its probable extent and petrogenetic significance. *American Journal of Science,* **276**, 1147-1177.

Philpotts, A.R., 1977. Archaean variolites - quenched immiscible liquids: Discussion. *Canadian Journal of Earth Sciences,* **14**, 2945-2958.

Poldevaart, A., and Hess, H.H., 1951. Pyroxenes in the crystallization of basaltic magma. *Journal of Geology,* **59**, 472.

Renner, R., 1989. *Cooling and crystallisation of komatiite flows from Zimbabwe.* Unpublished PhD thesis, University of Cambridge, 162pp

Renner, R., Nisbet, E.G., Cheadle, M.J., Arndt, N.T., Bickle, M.J., and Cameron, W.E., 1994. Komatiite flows from the Reliance Formation, Belingwe belt, Zimbabwe: I. Petrography and Mineralogy. *Journal of Petrology,* **35**, 361-400.

Reynolds, R.C., 1963. Matrix corrections in trace element analysis by X-ray fluorescence: estimation of the mass absorption coefficient by Compton scattering. Am. Miner. **48**, 1133-1143.

Rollinson, H.R., 1993. *Using Geochemical Data: Evaluation, Presentation, Interpretation.* London. Longman.

Scholey, S.P., 1992. *The Geology and Geochemistry of the Ngezi group volcanics, Belingwe greenstone belt, Zimbabwe.* Unpublished Ph.D. thesis, Southampton University.

Smith, H.S., and Erlank, A.J., 1982. Geochemistry and petrogenesis of komatiites from the Barberton greenstone belt, South Africa. *in* Arndt, N.T., and Nisbet, E.G. (eds.), *Komatiites.* London: George Allen & Unwin, 347-397.

Stagman, J.G., 1978. *An outline of the Geology of Rhodesia.* Rhodesia Geological Survey, Bulletin No.80, 126 pp.

Sun, S-.S., and Nesbitt R.W., 1978. Petrogenesis of Archaean ultrabasic and basic volcanics: evidence from the rare earth elements. *Contributions to Mineralogy and Petrology,* **65**, 301-325.

Sun, S-.S., and McDonough, W.F., 1989. Chemical and isotopic systematics of oceanic basalts: implications for mantle composition and evolution, *in*, Saunders, A.D., and Norry, M.J. (eds.), *Magmatism in the Ocean Basins*, Special paper of the Geological Society of America, **42**, 313-345.

Takahashi, E., and Scarfe, C.M., 1985. Melting of peridotite to 14 GPa and the the genesis of komatiite. *Nature*, **315**, 566-568.

Taylor, P.N., Jones, N.W., and Moorbath, S., 1984. Isotopic assessment of relative contributions from crust and mantle sources to the magma genesis of Precambrian granitoid rocks, *Philosophical Transactions of the Royal Society of London.* **A310**, 605-625.

Taylor, P.N., Kramers, J.D., Moorbath, S., Wilson, J.F., Orpen, J.L., Martin, A., 1991. Pb/Pb, Nd-Sm and Rb-Sr geochronology in the Archaean craton of Zimbabwe. *Chemical Geology (Isotope Geosciences Section)*, **86**, 175-196.

Taylor, S.R., and McLennan, S.M., 1985. *The continental crust: its composition and evolution.* Blackwell Scientific Publications, 312pp.

Thompson, R.N., 1983. Book Review. *Journal of Petrology*, **24**, 319-320.

Thompson, R.N., 1987. Phase-equilibria constraints on the genesis and magmatic evolution of oceanic basalts. *Earth-Science Reviews*, **24**, 161-210.

Tyndale-Biscoe, R., 1958. *Geological Map of an area north of Belingwe.* Scale 1:50,000. Unpublished, Rhodesia Geological Survey.

Van Wagoner, J.C., Posamentier, H.W., Mitchum, R.M., Vail, P.R., Sarg, J.F., Loutit, T.S., and Hardenbol, J., 1988. An overview of the fundamentals of sequence stratigraphy and key definitions, *in* Wilgus, C.K., et al. (eds), Sea-level changes - An integrated approach. *Society of Economic Paleontologists and Mineralogists Special Publication,* **42,** 39-45.

Viljoen, M.J., and Viljoen, R.P., 1969a. The geology and geochemistry of the lower ultramafic unit of the Onverwacht Group and a proposed new class of igneous rock, *in* Upper Mantle Project, *Special publication of the Geological Society of South Africa*, **2**, 55-85.

Viljoen, M.J., and Viljoen, R.P., 1969b. Evidence for the existence of a mobile extrusive peridotitic magma from the Komati Formation of the Onverwacht Group, *in* Upper Mantle Project, *Special publication of the Geological Society of South Africa*, **2**, 87-112.

Weaver, B.L., and Tarney, J., 1979. Thermal aspects of komatiitic generation and greenstone belt models. *Nature*, **79**, 689-692.

Walsh, *et al.*, 1981. *Chemical Geology*, **33**, 141-153

Wilson, J.F., 1973. The Rhodesian Archaean Craton - an essay in cratonic evolution. *Philosophical Transactions of the Royal Society of London,* **A 273**, 389-411.

Wilson, J.F., 1979. A preliminary appraisal of the Rhodesian Basement Complex. *Special Publication of the Geological Society of South Africa,* **5**, 1-23.

Wilson, J.F., 1981. The granitic-gneiss greenstone shield, B. Zimbabwe, *in* Hunter, D.R. (ed.), *Precambrian of the Southern Hemisphere.* Amsterdam: Elsevier, 454-88.

Wilson, J.F., 1990. A craton and its cracks: some of the behaviour of the Zimbabwe block from the late Archaean to the Mesozoic in response to horizontal movements, and the significance of its mafic dyke fracture patterns. *Journal of African Earth Sciences*, **10**, 483-501.

Wilson, J.F., and Nutt, T.H.C., 1990. The nature and occurance of mineralisation in the Early Precambrian crust of Zimbabwe, *in* Naqvi, S.M. (ed.), *Precambrian continental crust and its economic resources.* Amsterdam: Elsevier, 555-591.

Wilson, J.F., Baglow,N., Orpen, J.L., and Tsomondo, J.M., 1990. A reassesment of some regional correlations of greenstone belt rosks in Zimbabwe and their significance in the development of the Archaean craton, *in* Glover, J.E., and Ho, S.E. (compilers), Abstract, *Third International Archaean Symposium.* Perth: Geoconferences (WA) Inc., pp.43-44.

Wilson, J.F., Bickle, M.J., Hawkesworth, C.J., Martin, A., Nisbet, E.G., and Orpen, J.L., 1978. Granite - greenstone terrains of the Rhodesian Archaean craton. *Nature*, **271**, 23-27.

Wilson, J.F., Jones, D.L., and Kramers, J.D., 1987. Mafic dyke swarms in Zimbabwe, *in* Halls, H.C., and Fahrig, W.F., (eds.), *Mafic Dyke Swarms.* Special paper of the Geological Association of Canada, 33 pp.

Worst, B.G., 1956. *The geology of the country between Belingwe and West Nicholson.* Rhodesia Geological Survey, Bulletin No.43.

APPENDIX 1

SAMPLE LOCALITY LOG FOR THE NGEZI RIVER SECTION

See Figure 3.1 for location of section.

See Figure 3.3 for a full key.

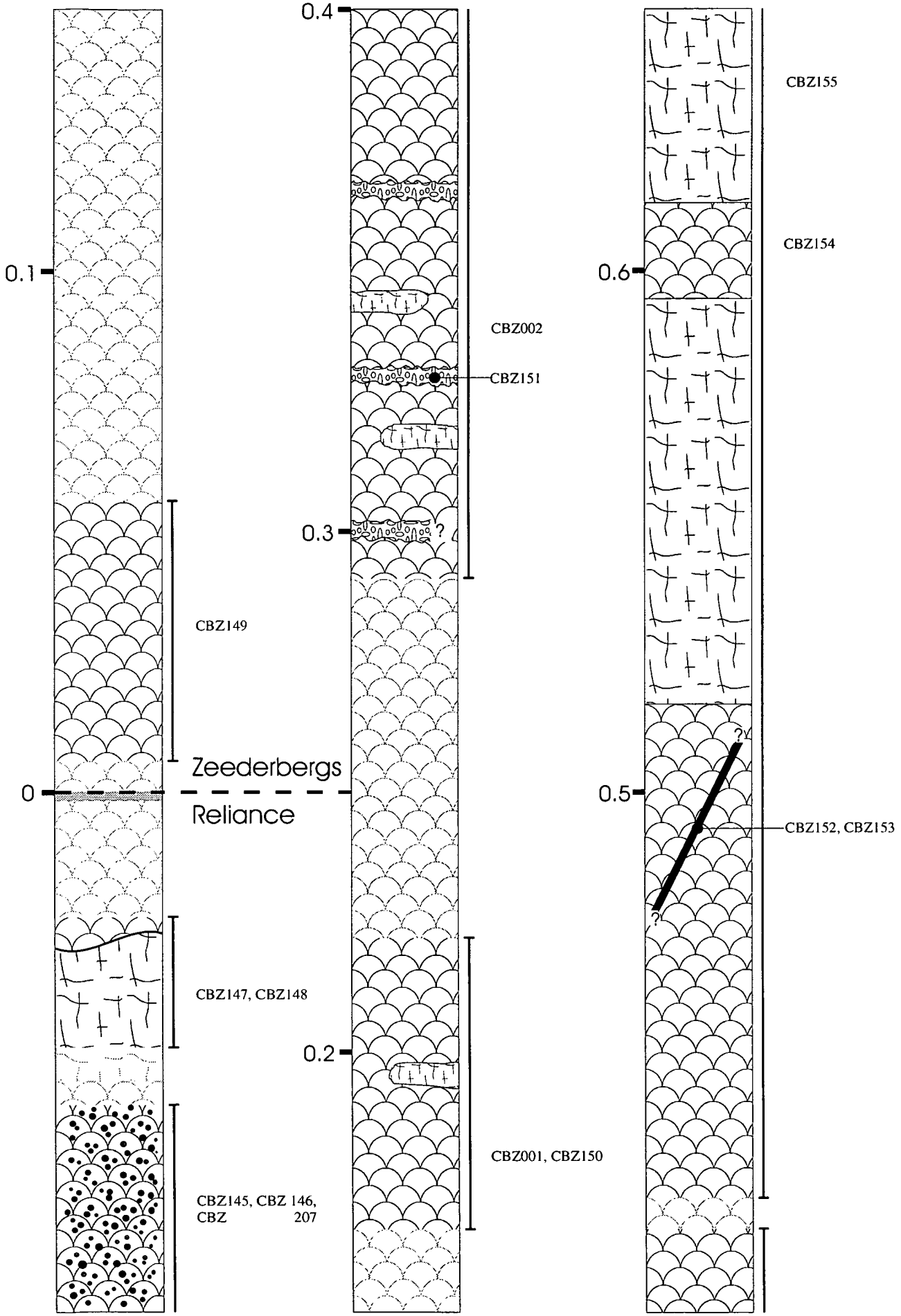
0.4
0.1
0.6
CBZ155
CBZ154
CBZ002
CBZ151
0.3
?
CBZ149
Zeederbergs
0
Reliance
0.5
?
?
CBZ152, CBZ153
CBZ147, CBZ148
0.2
CBZ001, CBZ150
CBZ145, CBZ 146,
CBZ 207

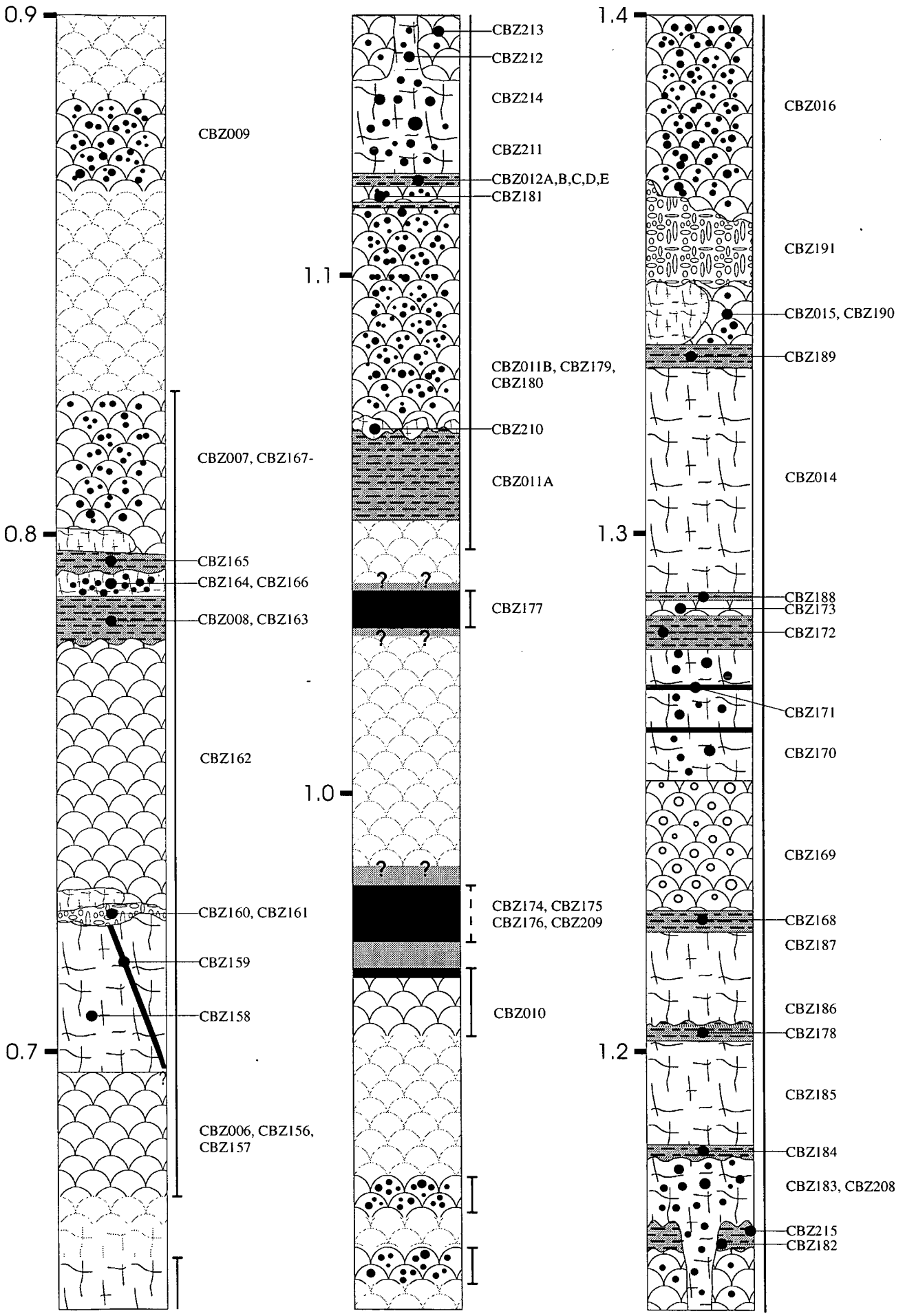
0.9
CBZ009
CBZ007, CBZ167-
0.8
CBZ165
CBZ164, CBZ166
CBZ008, CBZ163
CBZ162
CBZ160, CBZ161
CBZ159
CBZ158
0.7
CBZ006, CBZ156,
CBZ157
CBZ213
CBZ212
CBZ214
CBZ211
CBZ012A,B,C,D,E
CBZ181
1.1
CBZ011B, CBZ179,
CBZ180
CBZ210
CBZ011A
CBZ177
1.0
CBZ174, CBZ175
CBZ176, CBZ209
CBZ010
1.4
CBZ016
CBZ191
CBZ015, CBZ190
CBZ189
CBZ014
1.3
CBZ188
CBZ173
CBZ172
CBZ171
CBZ170
CBZ169
CBZ168
CBZ187
CBZ186
CBZ178
1.2
CBZ185
CBZ184
CBZ183, CBZ208
CBZ215
CBZ182

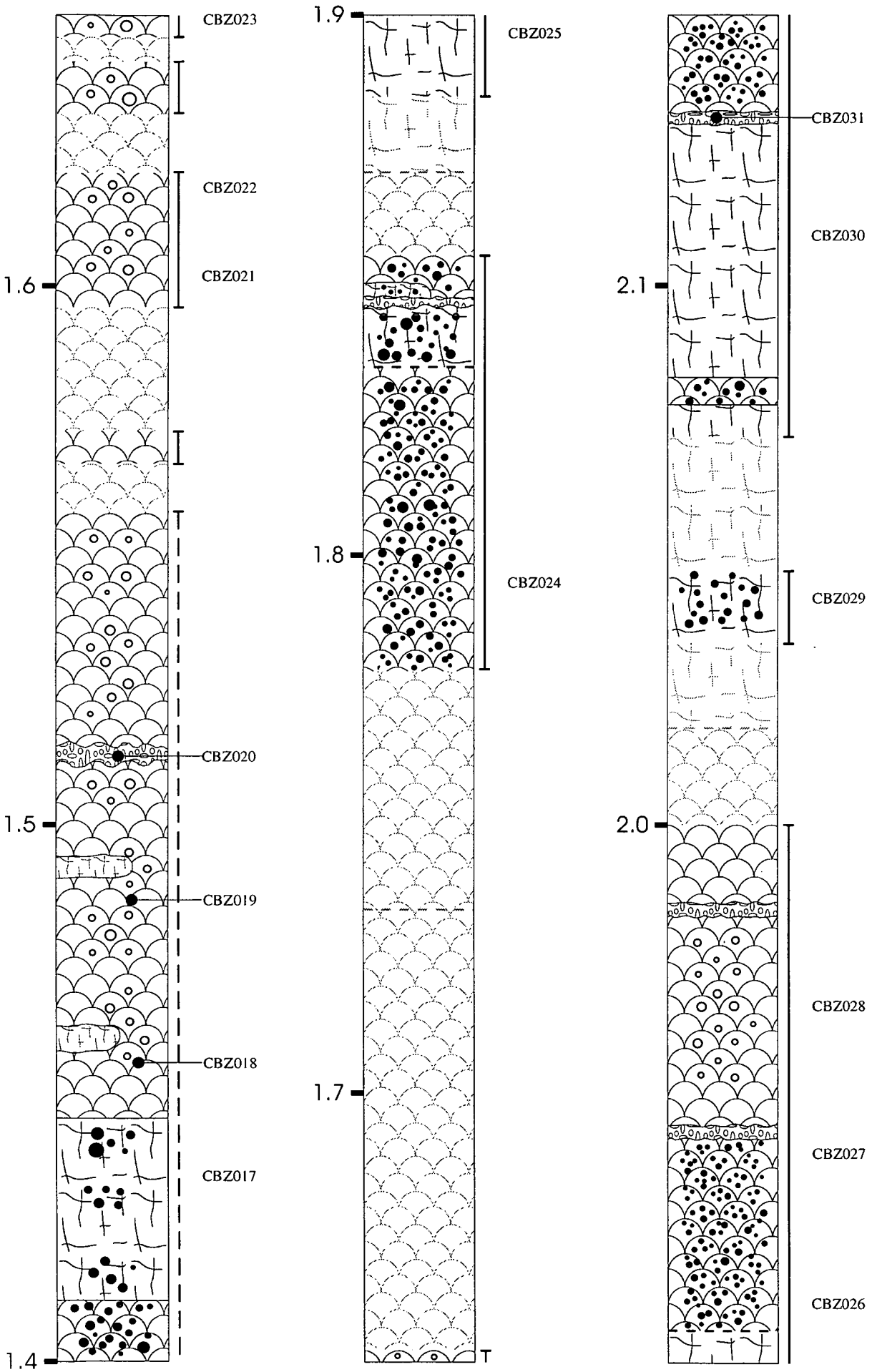
CBZ023
CBZ022
CBZ021
1.6
CBZ020
1.5
CBZ019
CBZ018
CBZ017
1.4
1.9
CBZ025
1.8
CBZ024
1.7
T
CBZ031
CBZ030
2.1
CBZ029
2.0
CBZ028
CBZ027
CBZ026

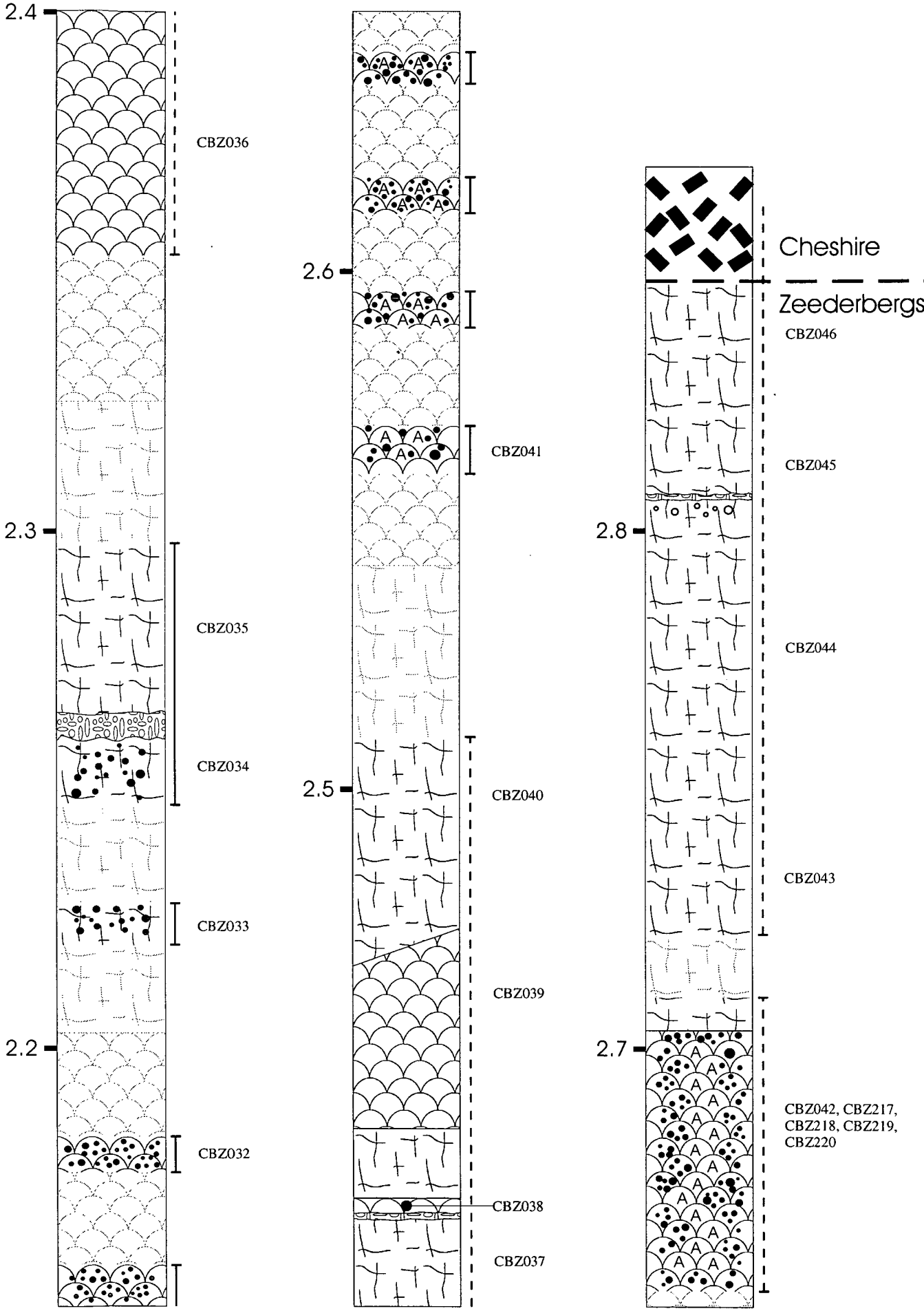
2.4
CBZ036
2.3
CBZ035
CBZ034
CBZ033
2.2
CBZ032
2.6
CBZ041
2.5
CBZ040
CBZ039
CBZ038
CBZ037
Cheshire
Zeederbergs
CBZ046
CBZ045
2.8
CBZ044
CBZ043
2.7
CBZ042, CBZ217,
CBZ218, CBZ219,
CBZ220

APPENDIX 2

BULK ROCK ANALYSES BY XRF

Adapted from:
Fitton, J.G., A.D. Saunders, L.M. Larsen, B.S. Hardarson and M.J. Norry. Volcanic rocks from the East Greenland margin at 63°N: composition, petrogenesis and mantle sources. *Proc. ODP, Sci. Results,* 152: College Station, TX (Ocean Drilling Program), in press.

Major-element concentrations were determined after fusion with a lithium borate flux containing La_2O_3 as a heavy absorber, by a method similar to that developed by Norrish and Hutton (1969). Rock powder was dried at 110° C for at least 1 hour and a nominal but precisely-weighed 1 gram aliquot ignited at 1100° C to determine loss on ignition (LOI). The residue was then mixed with Johnson Matthey Spectroflux 105 in a sample:flux ratio of 1:5, based on the *unignited* sample mass, and fused in a muffle furnace in a Pt5%Au crucible. After the initial fusion the crucible was reweighed and any flux weight loss made up with extra flux. After a second fusion over a Meker burner, the molten mixture was swirled several times to ensure homogeneity, cast onto a graphite mold and formed into a flat bead with an aluminium plunger. The mold and plunger were maintained at a temperature of 220° C on a hotplate.

Trace-element concentrations were determined on pressed-powder samples. Six grams of rock powder were mixed thoroughly with four drops of a 2% aqueous solution of polyvinyl alcohol. The mixture was formed into a 38 mm disc on a 40 mm diameter polished tungsten carbide disc, backed and surrounded by boric acid, and compressed in a hydraulic press at 0.6 tonnes cm^{-2}.

The fused and pressed samples were analysed using a Philips PW 1480 automatic X-ray fluorescence spectrometer with a Rh-anode X-ray tube. Because XRF analyses showed that many of the volcanic rocks had extremely low concentrations of incompatible trace elements, the analytical conditions and calibrations for these elements were optimised for low concentrations where appropriate. Background positions were placed as close as possible to peaks and long count times were used at both peak and background positions. Where background count rates were measured on either side of the peak, as in most trace-

element determinations, the count time was divided equally between the two positions. Analytical conditions are summarised in Table A2.1.

Corrections for matrix effects on the intensities of major-element lines were made using theoretical alpha coefficients calculated on-line using the Philips software. The coefficients were calculated to allow for the amount of extra flux replacing volatile components in the sample so that analytical totals should be 100% less the measured LOI. Intensities of the longer wavelength trace-element lines (La, Ce, Nd, Cu, Ni, Co, Cr, V, Ba, and Sc) were corrected for matrix effects using alpha coefficients based on major-element concentrations measured at the same time on the powder samples. Matrix corrections were applied to the intensities of the other trace-element lines by using the count rate from the RhK_{α} Compton scatter line as an internal standard (Reynolds, 1963). Line-overlap corrections were applied using synthetic standards.

The spectrometer was calibrated with USGS and CRPG standards, using the values given by Jochum et al. (1990) for Nb and Zr, and Govindaraju (1994) for the other elements. Excellent calibration lines were obtained using these standards. Trace-element analytical precision was estimated by analysing several standards repeatedly during the analysis of the samples. The results are given in Table A2.2. Some elements (Nb at <1 ppm, Pb and Th) were determined at least three times, and the results averaged. The averages are believed to be precise to ±0.1 ppm for Nb and ±0.5 ppm for Pb and Th. Accuracy is more difficult to quantify but may be assessed by comparing average standard concentrations reported in Table A2.2 with those given by Govindaraju (1994). Major-element precision is governed more by reproducibility in making the fused beads than by counting statistics. Calibration lines are excellent for all major elements so accuracy and precision are closely similar. Typical major-element precision estimates are given in Table A2.1.

Abbreviations used in data tables

Section (see Figure 3.1 for locations)
NR Ngezi River
VR Vanguard Road
SV Spring Valley

See §3.5.2 for explanation of 'level'

Sample	CBZ145	CBZ147	CBZ149	CBZ001	CBZ150	CBZ002	CBZ003	CBZ004	CBZ152	CBZ153	CBZ005	CBZ154	CBZ155	CBZ006	CBZ156	CBZ157	CBZ158
Rock Type	basalt	basalt	basalt	basalt	basalt	basalt	basalt	basalt	basalt	basalt	basalt	basalt	basalt	basalt	basalt	basalt	basalt
Section	NR	NR	NR	NR	NR	NR	NR	NR	NR	NR	NR	NR	NR	NR	NR	NR	NR
level	0.0	0.0	1.1	6.5	6.5	11.8	14.4	15.6	17.2	17.2	19.6	21.2	22.5	23.9	24.1	24.1	24.9
wt%																	
SiO2	59.35	52.10	54.92	52.28	55.23	51.55	50.35	51.43	52.07	49.36	51.67	50.21	49.88	49.94	51.75	52.52	50.86
Al2O3	12.23	15.43	14.96	15.61	14.79	15.38	15.14	14.78	15.03	15.23	15.58	15.30	14.76	15.64	14.60	15.56	15.50
FeO	7.69	9.00	8.77	10.38	9.13	10.66	10.79	10.31	10.82	11.04	10.26	11.38	11.46	12.24	9.85	9.73	10.80
MgO	7.56	8.76	6.80	7.72	6.76	8.56	7.69	7.03	7.94	9.74	8.34	8.29	8.07	8.16	7.22	8.02	7.63
CaO	6.70	11.54	9.68	9.18	8.59	9.70	13.84	14.23	12.10	11.62	11.58	11.18	13.06	10.88	14.75	10.15	11.92
Na2O	5.76	1.87	3.95	3.77	4.53	3.21	1.19	1.26	1.07	1.99	1.37	2.57	1.66	1.78	0.87	3.00	2.23
K2O	0.01	0.46	0.02	0.01	0.02	0.01	0.01	0.00	0.02	0.02	0.14	0.04	0.03	0.26	0.02	0.03	0.07
TiO2	0.50	0.62	0.66	0.79	0.72	0.70	0.74	0.73	0.72	0.75	0.72	0.78	0.84	0.84	0.72	0.74	0.75
MnO	0.14	0.19	0.18	0.19	0.18	0.17	0.18	0.17	0.18	0.19	0.17	0.20	0.19	0.21	0.17	0.19	0.19
P2O5	0.05	0.05	0.04	0.06	0.05	0.05	0.06	0.06	0.05	0.05	0.06	0.06	0.06	0.07	0.06	0.05	0.06
Total(witout LOI)	98.50	97.35	97.66	97.58	97.36	97.28	97.51	97.88	97.19	97.17	97.41	97.08	97.10	97.03	97.74	97.63	97.67
LOI	1.24	2.67	1.92	2.16	2.28	2.45	2.59	2.01	3.02	2.39	2.86	2.42	2.61	2.67	1.84	2.19	2.23
Total (+LOI)	99.74	100.02	99.58	99.74	99.64	99.73	100.1	99.89	100.21	99.56	100.27	99.5	99.71	99.7	99.58	99.82	99.9
ppm																	
Nb	2.9	1.3	1.5	2.7	1.7	2.4	2.2	1.7	1.6	1.7	2.2	2.0	1.9	2.6	2.0	1.9	1.8
Zr	59.5	31.3	32.5	42.2	36.0	37.9	39.4	39.4	37.0	38.0	38.3	39.6	43.1	44.5	36.5	38.1	37.9
Y	15.2	14.8	16.7	17.2	15.9	16.1	16.8	16.4	17.9	17.4	16.4	18.9	20.4	18.5	18.2	18.1	18.0
Sr	58.8	83.2	118.7	141.9	116.9	170.9	130.1	153.5	176.5	91.6	108.9	100.0	114.9	129.1	170.8	71.2	130.7
Rb	0.1	9.8	0.4	0.1	0.5	0.1	0.2	0.2	0.7	0.4	3.9	0.8	0.7	5.8	0.2	0.8	1.6
Th	3.8	2.7	1.4	1.0	3.0	0.6	2.0	1.4	3.9	3.1	1.3	3.2	3.0	2.8	3.1	2.5	3.0
Pb	1.8	2.0	1.0	1.9	2.1	1.2	1.7	0.4	3.0	3.3	0.7	1.6	1.2	1.3	2.7	1.7	1.4
Zn	90.6	63.4	73.2	88.8	72.1	78.2	80.6	72.6	80.5	83.9	81.5	83.2	87.1	97.4	73.1	75.4	82.4
Cu	75.4	49.9	128.7	79.1	125.0	131.7	148.7	131.4	138.7	125.5	147.3	132.4	112.4	148.9	129.3	87.7	126.6
Ni	165.1	161.7	151.6	182.8	160.0	186.4	178.4	171.9	168.1	180.0	221.3	184.4	148.8	163.7	167.0	175.4	163.6
Cr	597.5	359.6	410.3	439.6	434.0	429.4	419.3	410.7	433.6	452.0	465.1	455.0	433.3	263.7	438.5	445.5	444.7
Ce	15.3	4.1	4.1	4.7	6.4	4.0	5.8	4.7	8.1	1.1	7.2	5.0	8.1	5.8	6.1	3.9	4.1
Nd	6.7	4.6	4.4	4.2	4.9	4.0	3.8	4.3	4.9	3.9	4.9	4.1	6.4	3.4	6.3	4.3	5.5
La	5.7	0.1	0.1	0.1	0.1	0.1	0.1	0.1	0.1	1.6	0.1	0.1	0.1	0.1	0.1	0.1	0.1
V	187.6	241.6	249.9	256.5	247.6	231.2	247.1	241.8	238.2	245.5	231.0	255.2	267.1	271.1	250.5	255.2	252.2
Ba	46.4	108.2	23.4	13.3	19.2	0.7	2.2	4.7	10.7	17.0	16.5	17.8	17.4	48.5	1.2	24.8	29.6
Sc	36.7	39.2	43.3	50.8	39.9	45.8	44.8	39.8	38.0	40.7	43.9	43.1	41.7	51.6	43.5	42.9	39.3
ratios																	
Al2O3/TiO2	24.37	24.74	22.61	19.66	20.55	21.94	20.38	20.14	20.76	20.22	21.55	19.69	17.62	18.57	20.26	20.90	20.63
CaO/Al2O3	0.55	0.75	0.65	0.59	0.58	0.63	0.91	0.96	0.81	0.76	0.74	0.73	0.88	0.70	1.01	0.65	0.77
Zr/Nb	20.52	24.08	21.67	15.63	21.18	15.79	17.91	23.18	23.13	22.35	17.41	19.80	22.68	17.12	18.25	20.05	21.06
Ce/Y	1.00	0.28	0.25	0.28	0.40	0.25	0.35	0.29	0.45	0.06	0.44	0.26	0.40	0.32	0.33	0.22	0.23
Ce/Zr	0.26	0.13	0.13	0.11	0.18	0.11	0.15	0.12	0.22	0.03	0.19	0.13	0.19	0.13	0.17	0.10	0.11
Nb/Y	0.19	0.09	0.09	0.16	0.11	0.15	0.13	0.10	0.09	0.10	0.13	0.11	0.09	0.14	0.11	0.10	0.10
Zr/Y	3.91	2.11	1.95	2.45	2.26	2.35	2.35	2.40	2.07	2.18	2.34	2.10	2.11	2.41	2.01	2.10	2.11
Type I																	

Sample	CBZ159	CBZ162	CBZ185	CBZ186	CBZ187	CBZ169	CBZ170	CBZ171L	CBZ173	CBZ014	CBZ015	CBZ191	CBZ016	CBZ017	CBZ018A	CBZ020A	CBZ022
Rock Type	basalt	basalt	basalt	basalt	basalt	basalt	basalt	basalt	basalt	basalt	basalt	basalt	basalt	basalt	basalt	basalt	basalt
Section	NR	NR	NR	NR	NR	NR	NR	NR	NR	NR	NR	NR	NR	NR	NR	NR	NR
level	25.0	26.4	41.8	42.4	42.8	43.5	44.2	44.6	45.1	46.1	47.2	47.5	48.6	50.5	51.3	53.1	56.8
wt%																	
SiO2	56.10	52.08	52.96	49.62	53.30	57.75	52.70	60.47	53.57	55.23	50.94	52.06	50.38	53.92	52.12	52.81	54.95
Al2O3	15.33	14.68	14.74	13.45	14.27	13.11	13.86	10.20	12.99	13.47	14.52	13.63	15.87	14.31	14.75	13.44	14.37
FeO	9.12	11.67	11.63	11.67	11.71	7.67	10.51	6.96	9.86	9.08	10.36	10.18	10.94	8.68	9.32	9.00	9.35
MgO	6.58	7.26	6.44	10.13	5.89	6.19	8.41	6.10	11.30	7.47	9.65	12.27	8.51	10.82	11.51	11.30	8.12
CaO	11.10	9.40	7.38	10.38	9.29	9.77	10.34	15.19	7.11	11.88	10.01	7.77	12.31	10.19	9.84	11.59	10.25
Na2O	1.26	3.70	4.57	2.95	3.65	4.20	2.74	0.14	3.38	1.89	0.67	3.05	0.74	0.99	1.67	0.90	2.37
K2O	0.12	0.14	0.46	0.22	0.15	0.09	0.20	0.07	0.77	0.15	2.66	0.13	0.33	0.34	0.03	0.09	0.02
TiO2	0.67	0.83	1.50	1.26	1.43	0.97	0.96	0.64	0.78	0.61	0.91	0.67	0.66	0.54	0.54	0.64	0.63
MnO	0.15	0.20	0.18	0.19	0.17	0.16	0.19	0.16	0.17	0.17	0.17	0.17	0.18	0.16	0.17	0.20	0.17
P2O5	0.07	0.06	0.14	0.12	0.15	0.09	0.09	0.06	0.07	0.06	0.10	0.07	0.07	0.05	0.05	0.05	0.06
Total(witout LOI)	96.86	98.01	97.50	96.69	97.74	98.45	96.74	97.79	97.14	97.52	94.96	96.21	96.55	96.54	96.19	95.67	96.84
LOI	2.76	1.64	2.27	0.06	2.19	1.45	2.98	2.02	2.93	2.64	4.87	3.53	3.45	3.36	3.66	4.23	2.85
Total (+LOI)	99.63	99.65	99.77	96.75	99.93	99.9	99.72	99.81	100.07	100.16	99.83	99.74	100	99.9	99.85	99.9	99.69
ppm																	
Nb	3.6	2.0	4.8	3.9	4.8	2.8	2.6	1.9	2.1	2.1	3.8	1.8	2.9	1.6	1.6	2.1	1.7
Zr	74.7	42.3	106.3	85.6	110.0	70.1	66.3	41.7	53.6	39.8	72.2	49.3	54.3	37.6	36.8	42.2	40.0
Y	22.2	19.7	29.3	26.0	31.1	21.3	21.7	16.3	16.3	15.0	22.7	18.2	22.9	16.9	15.2	19.5	17.8
Sr	199.4	126.2	196.3	115.6	166.8	45.2	37.1	315.1	65.0	41.3	80.2	53.0	179.1	87.3	36.5	16.4	64.3
Rb	3.1	1.6	7.8	5.6	1.9	1.2	2.2	1.6	11.2	2.4	36.1	2.3	5.7	10.7	1.3	1.7	0.1
Th	6.1	3.3	3.7	4.8	4.3	2.0	3.4	1.3	3.0	2.1	3.9	2.4	3.0	3.6	3.5	3.8	1.4
Pb	15.7	2.2	1.1	1.9	2.0	2.3	0.5	3.3	1.1	1.0	2.1	0.2	2.7	0.3	0.2	0.2	0.2
Zn	105.6	87.8	93.7	92.4	74.4	55.2	77.3	40.3	88.9	62.6	80.2	70.9	83.7	64.6	73.4	68.8	73.8
Cu	81.6	110.2	114.5	55.7	200.1	79.4	115.3	140.5	58.2	51.2	114.7	49.8	66.6	75.2	40.7	30.7	75.0
Ni	98.8	152.6	97.3	235.6	66.2	74.5	84.9	66.6	103.3	77.1	177.8	251.8	81.7	226.9	234.9	163.0	174.0
Cr	161.3	266.7	235.4	789.6	29.1	159.0	460.8	380.0	218.3	426.2	613.8	905.0	302.3	586.0	583.3	447.6	443.1
Ce	16.6	2.6	16.1	9.6	16.0	14.5	10.1	4.5	1.6	5.0	7.2	8.4	12.7	3.8	4.1	7.7	4.6
Nd	9.8	4.5	10.6	9.0	12.6	10.1	7.4	5.9	2.3	4.5	5.4	6.0	6.1	1.9	2.7	2.2	2.4
La	3.5	0.1	4.7	4.3	4.6	2.8	1.4	0.1	0.1	0.1	0.1	0.5	1.0	0.1	0.1	0.1	0.1
V	225.5	270.0	295.0	286.6	301.8	258.0	275.6	215.3	272.8	223.1	261.6	244.5	283.4	216.1	203.5	265.7	246.0
Ba	30.5	39.1	90.8	40.1	38.4	29.5	48.4	35.0	321.1	63.5	896.0	41.8	106.4	61.7	14.8	36.5	22.5
Sc	39.6	43.7	34.2	44.7	31.1	33.5	48.0	38.3	38.6	40.3	42.2	44.4	39.5	44.8	30.5	46.0	43.3
ratios																	
Al2O3/TiO2	22.73	17.77	9.83	10.66	10.00	13.56	14.39	15.94	16.64	22.07	15.92	20.27	24.07	26.41	27.53	21.08	22.74
CaO/Al2O3	0.72	0.64	0.50	0.77	0.65	0.75	0.75	1.49	0.55	0.88	0.69	0.57	0.78	0.71	0.67	0.86	0.71
Zr/Nb	20.75	21.15	22.15	21.95	22.92	25.04	25.50	21.95	25.52	18.95	19.00	27.39	18.72	23.50	23.00	20.10	23.53
Ce/Y	0.75	0.13	0.55	0.37	0.51	0.68	0.46	0.28	0.10	0.34	0.32	0.46	0.56	0.23	0.27	0.40	0.26
Ce/Zr	0.22	0.06	0.15	0.11	0.15	0.21	0.15	0.11	0.03	0.13	0.10	0.17	0.23	0.10	0.11	0.18	0.12
Nb/Y	0.16	0.10	0.16	0.15	0.15	0.13	0.12	0.12	0.13	0.14	0.17	0.10	0.13	0.09	0.11	0.11	0.10
Zr/Y	3.36	2.15	3.63	3.29	3.54	3.29	3.06	2.56	3.29	2.65	3.18	2.71	2.37	2.22	2.42	2.16	2.25
Type I																	

Sample	CBZ023	CBZ024	CBZ025	CBZ026	CBZ027	CBZ029	CBZ030	CBZ032	CBZ033	CBZ034	CBZ035A	CBZ035B	CBZ036	CBZ037	CBZ038	CBZ039	CBZ040
Rock Type	basalt	basalt	basalt	basalt	basalt	basalt	basalt	basalt	basalt	basalt	basalt	basalt	basalt	basalt	basalt	basalt	basalt
Section	NR	NR	NR	NR	NR	NR	NR	NR	NR	NR	NR	NR	NR	NR	NR	NR	NR
level	57.9	63.1	66.7	67.0	68.1	71.5	74.0	76.5	78.1	79.1	80.0	80.0	83.5	84.6	84.9	86.5	87.8
wt%																	
SiO2	57.15	52.19	54.50	59.16	59.44	56.19	56.59	58.36	55.83	57.37	53.10	54.73	52.76	51.92	51.04	55.87	51.79
Al2O3	14.60	16.23	12.14	14.73	13.79	14.27	11.89	14.00	14.26	13.36	16.19	16.73	15.08	14.61	15.20	14.95	14.47
FeO	7.90	9.38	9.22	7.04	7.26	9.96	8.62	7.85	8.71	8.49	10.33	7.17	10.33	10.91	11.21	8.26	10.25
MgO	7.32	9.49	14.07	5.93	7.01	8.06	9.41	7.97	8.42	8.13	8.90	5.40	7.08	8.66	8.14	6.26	8.44
CaO	10.05	11.34	9.21	10.14	8.77	8.45	11.47	8.64	10.62	9.64	8.73	13.55	11.52	10.72	11.82	11.36	12.16
Na2O	2.61	0.44	0.04	2.63	2.98	2.37	1.24	2.55	1.51	2.28	1.93	1.42	2.10	1.95	1.54	2.28	1.79
K2O	0.02	0.12	0.59	0.03	0.05	0.08	0.12	0.10	0.04	0.04	0.10	0.32	0.09	0.22	0.04	0.03	0.18
TiO2	0.63	0.59	0.41	0.48	0.49	0.64	0.45	0.47	0.51	0.47	0.50	0.47	0.80	0.77	0.77	0.78	0.71
MnO	0.15	0.17	0.16	0.15	0.16	0.20	0.15	0.12	0.15	0.19	0.18	0.17	0.19	0.18	0.19	0.16	0.17
P2O5	0.06	0.06	0.04	0.05	0.05	0.07	0.05	0.05	0.04	0.04	0.04	0.04	0.05	0.05	0.05	0.05	0.04
Total(witout LOI)	97.11	96.08	95.62	97.62	97.49	97.06	97.65	97.27	96.83	97.06	96.24	97.40	96.24	96.55	97.22	97.37	97.55
LOI	2.52	3.66	3.98	2.05	2.09	2.57	2.00	2.27	2.74	2.63	3.52	2.29	3.50	3.25	2.93	2.65	2.49
Total (+LOI)	99.64	99.74	99.60	99.67	99.58	99.63	99.65	99.54	99.57	99.69	99.76	99.69	99.74	99.8	100.15	100.02	100.04
ppm																	
Nb	1.8	2.1	1.9	2.2	1.9	3.1	2.6	2.2	2.2	1.9	2.4	2.4	2.6	2.5	2.6	2.4	2.5
Zr	39.6	40.1	30.0	36.7	36.5	54.5	44.7	36.8	38.6	36.0	43.5	41.3	40.7	40.2	41.3	41.7	36.9
Y	17.7	15.0	11.7	13.4	13.8	18.6	16.2	13.3	15.9	15.0	15.6	15.7	18.3	16.2	16.5	14.0	14.5
Sr	87.5	112.5	97.9	81.2	73.4	53.9	58.2	36.8	44.9	56.1	44.8	47.6	152.5	122.2	200.6	193.5	173.2
Rb	0.4	3.7	20.4	0.8	0.8	1.1	2.4	2.6	1.2	0.0	2.4	9.2	2.1	6.8	0.9	0.6	4.7
Th	0.8	1.3	2.2	1.2	1.5	3.0	2.6	1.2	1.8	1.9	2.2	1.9	1.7	1.6	2.5	1.2	2.0
Pb	0.4	0.4	0.4	2.1	1.5	1.9	1.8	1.3	2.5	2.0	1.3	4.8	0.2	0.2	0.0	3.3	0.2
Zn	67.1	82.4	68.1	65.2	63.5	97.1	81.4	63.9	74.6	74.7	89.2	56.5	97.3	94.3	98.1	73.7	80.0
Cu	97.2	74.3	68.0	76.9	66.1	76.5	68.4	63.0	86.3	57.1	71.3	56.8	148.5	153.8	151.2	127.8	135.2
Ni	180.2	106.4	268.9	133.5	144.4	88.8	161.2	129.7	150.4	134.6	137.0	109.7	160.5	135.6	167.3	154.8	155.3
Cr	446.2	435.2	1092.9	443.0	441.1	337.6	599.8	352.5	383.0	373.5	228.2	176.4	399.8	390.6	387.6	395.5	479.5
Ce	4.5	1.4	5.3	3.6	4.3	10.4	12.1	6.0	8.6	7.4	6.4	3.8	5.4	5.1	5.1	4.2	1.3
Nd	3.1	2.5	2.9	3.0	5.2	4.7	5.3	2.1	4.8	3.1	3.9	2.9	4.9	5.1	3.6	4.2	3.3
La	0.1	0.1	0.8	0.1	0.9	2.1	4.7	0.1	0.1	0.1	1.0	0.1	0.1	0.1	0.1	0.1	0.1
V	243.4	238.6	175.5	195.2	200.7	230.6	180.4	192.0	213.6	213.1	206.8	216.3	260.3	253.7	242.5	253.8	232.9
Ba	6.3	29.1	114.2	11.1	23.1	44.2	24.1	44.1	16.5	108.3	31.2	112.3	33.3	51.7	4.3	3.9	52.6
Sc	45.6	48.1	36.7	44.6	43.7	45.0	36.3	37.8	44.4	38.3	39.4	42.4	44.6	45.5	44.0	47.4	40.6
ratios																	
Al2O3/TiO2	23.12	27.65	29.59	30.41	28.32	22.22	26.14	29.80	28.09	28.62	32.49	35.77	18.83	19.02	19.70	19.25	20.41
CaO/Al2O3	0.69	0.70	0.76	0.69	0.64	0.59	0.96	0.62	0.74	0.72	0.54	0.81	0.76	0.73	0.78	0.76	0.84
Zr/Nb	22.00	19.10	15.79	16.68	19.21	17.58	17.19	16.73	17.55	18.95	18.13	17.21	15.65	16.08	15.88	17.38	14.76
Ce/Y	0.26	0.10	0.46	0.27	0.31	0.56	0.75	0.45	0.54	0.50	0.41	0.24	0.30	0.32	0.31	0.30	0.09
Ce/Zr	0.11	0.04	0.18	0.10	0.12	0.19	0.27	0.16	0.22	0.21	0.15	0.09	0.13	0.13	0.12	0.10	0.04
Nb/Y	0.10	0.14	0.16	0.16	0.14	0.17	0.16	0.17	0.14	0.13	0.15	0.15	0.14	0.15	0.16	0.17	0.17
Zr/Y	2.24	2.67	2.56	2.74	2.64	2.93	2.76	2.77	2.43	2.40	2.79	2.63	2.22	2.48	2.50	2.98	2.54
Type I																	

Sample	CBZ043	CBZ044	CBZ045	CBZ046	CBZ126	CBZ127	CBZ071	CBZ072	CBZ128	CBZ129	CBZ073	CBZ074	CBZ130	CBZ132	CBZ134	CBZ135	CBZ076
Rock Type	basalt	basalt	basalt	basalt	basalt	basalt	basalt	basalt	basalt	basalt	basalt	basalt	basalt	basalt	basalt	basalt	basalt
Section	NR	NR	NR	NR	VR	VR	VR	VR	VR	VR	VR	VR	VR	VR	VR	VR	VR
level	95.9	97.3	98.7	99.6	4.6	7.9	9.9	13.7	14.6	18.4	21.3	23.2	23.9	25.5	34.2	36.1	37.9
wt%																	
SiO2	54.58	60.69	58.11	59.86	51.64	51.47	50.98	50.99	51.60	51.18	49.45	49.68	49.89	51.11	54.54	55.99	53.36
Al2O3	14.20	13.61	14.52	14.97	16.72	14.35	15.10	14.89	14.54	14.86	16.10	15.08	15.18	14.83	13.75	14.16	13.81
FeO	9.33	7.66	7.10	6.40	7.14	12.72	11.47	11.64	12.87	10.92	13.60	13.75	11.01	10.85	11.42	9.10	10.76
MgO	9.15	5.69	6.58	6.19	8.16	7.33	8.19	8.15	7.65	7.65	6.38	8.85	7.66	7.05	5.27	6.88	8.74
CaO	9.95	9.85	9.91	8.41	14.69	11.21	11.22	11.46	10.51	12.00	9.43	7.85	12.83	13.86	10.13	7.04	9.00
Na2O	1.65	1.56	2.23	3.03	1.41	1.64	1.93	1.71	1.79	2.55	3.60	3.52	2.34	1.45	2.82	5.38	3.25
K2O	0.33	0.04	0.56	0.02	0.06	0.05	0.04	0.10	0.05	0.08	0.02	0.03	0.09	0.01	0.22	0.08	0.06
TiO2	0.55	0.68	0.71	0.88	0.40	0.97	0.82	0.81	1.00	0.72	1.13	0.94	0.75	0.72	1.52	1.10	0.77
MnO	0.21	0.16	0.22	0.15	0.15	0.19	0.19	0.20	0.21	0.20	0.22	0.24	0.19	0.18	0.17	0.16	0.20
P2O5	0.05	0.06	0.07	0.09	0.02	0.07	0.05	0.05	0.08	0.05	0.07	0.06	0.06	0.05	0.15	0.10	0.06
Total(witout LOI)	96.76	95.65	95.33	95.10	97.34	97.59	97.38	97.25	97.05	97.40	97.61	96.66	97.82	97.40	97.59	97.73	97.08
LOI	3.46	4.35	4.42	4.87	2.36	2.48	2.53	2.75	2.63	2.22	2.40	3.06	2.08	2.12	2.00	1.88	2.63
Total (+LOI)	100.22	100	99.75	99.97	99.70	100.07	99.91	100	99.68	99.63	100.01	99.72	99.9	99.52	99.59	99.61	99.71
ppm																	
Nb	3.9	4.6	5.4	6.2	1.0	2.3	2.9	2.4	2.1	1.7	3.4	2.6	2.0	1.9	5.4	3.6	2.5
Zr	60.9	77.8	87.7	107.8	17.8	50.3	44.7	44.2	52.7	37.6	61.3	49.4	37.7	35.6	118.3	79.4	50.0
Y	17.4	19.2	20.6	24.5	10.6	22.9	19.2	19.4	23.1	17.3	25.5	20.7	18.5	17.8	31.3	24.0	19.3
Sr	120.6	36.3	157.1	130.3	92.5	92.6	121.7	146.1	131.9	83.7	119.0	54.5	140.2	282.1	311.7	66.2	43.8
Rb	9.3	0.2	14.9	0.4	1.1	0.8	0.9	2.5	1.1	1.4	0.5	0.2	1.4	0.3	3.0	1.2	1.5
Th	2.5	1.3	2.7	2.4	1.2	4.5	2.2	1.3	3.6	3.7	3.5	2.9	2.4	1.7	6.2	2.8	2.1
Pb	1.7	1.2	2.8	6.1	1.2	1.9	0.5	1.3	0.7	2.3	0.0	0.4	0.4	0.5	4.7	2.0	2.4
Zn	69.9	83.8	67.0	78.9	40.8	101.8	87.0	89.6	106.2	83.8	130.5	119.0	85.4	74.4	90.0	76.1	76.6
Cu	88.5	87.8	98.7	115.9	100.2	137.8	125.6	144.4	145.6	87.8	142.0	103.6	121.7	150.6	212.1	176.3	103.4
Ni	133.5	86.3	90.0	75.6	132.9	125.4	161.0	148.1	116.5	174.2	135.3	180.7	183.5	173.9	88.2	88.7	78.1
Cr	290.9	70.8	141.1	77.8	83.2	174.5	266.7	242.7	185.7	429.7	212.4	291.3	445.1	442.9	172.5	177.7	390.9
Ce	9.8	15.0	15.3	19.7	2.3	5.0	4.5	2.8	5.7	2.8	5.3	3.3	5.4	5.4	18.4	7.1	4.4
Nd	4.9	8.2	9.0	11.5	2.1	5.6	4.0	4.3	4.8	4.2	5.3	3.8	5.5	3.6	12.5	7.5	4.3
La	1.2	2.7	3.8	6.0	0.1	0.1	0.1	0.1	0.1	0.1	0.1	0.1	0.1	0.1	5.2	0.4	0.1
V	189.1	231.2	220.2	232.1	183.3	290.5	268.9	258.4	284.1	244.6	330.0	283.3	247.3	244.3	306.8	275.7	243.6
Ba	93.5	15.7	200.5	18.0	17.5	13.5	22.6	17.6	21.3	37.4	7.9	4.4	27.8	4.8	75.9	39.6	15.3
Sc	33.8	36.0	39.7	32.6	37.8	37.2	49.8	45.0	43.1	39.9	54.0	51.5	37.2	45.6	31.4	37.9	43.6
ratios																	
Al2O3/TiO2	25.81	19.92	20.46	16.98	41.61	14.79	18.38	18.36	14.57	20.64	14.29	16.10	20.38	20.70	9.04	12.89	17.93
CaO/Al2O3	0.70	0.72	0.68	0.56	0.88	0.78	0.74	0.77	0.72	0.81	0.59	0.52	0.85	0.93	0.74	0.50	0.65
Zr/Nb	15.62	16.91	16.24	17.39	17.80	21.87	15.41	18.42	25.10	22.12	18.03	19.00	18.85	18.74	21.91	22.06	20.00
Ce/Y	0.56	0.78	0.74	0.80	0.22	0.22	0.24	0.15	0.25	0.16	0.21	0.16	0.29	0.31	0.59	0.30	0.23
Ce/Zr	0.16	0.19	0.17	0.18	0.13	0.10	0.10	0.06	0.11	0.08	0.09	0.07	0.14	0.15	0.16	0.09	0.09
Nb/Y	0.22	0.24	0.26	0.25	0.09	0.10	0.15	0.12	0.09	0.10	0.13	0.13	0.11	0.11	0.17	0.15	0.13
Zr/Y	3.50	4.05	4.26	4.40	1.68	2.20	2.33	2.28	2.28	2.17	2.40	2.39	2.04	2.00	3.78	3.31	2.59
Type 1																	

Sample	CBZ077	CBZ136	CBZ078	CBZ093	CBZ094	CBZ137	CBZ096	CBZ139	CBZ138	CBZ140	CBZ098	CBZ099	CBZ142	CBZ106	CBZ107	CBZ108	CBZ109
Rock Type	basalt	basalt	basalt	basalt	basalt	basalt	basalt	basalt	basalt	basalt	basalt	basalt	basalt	basalt	basalt	basalt	basalt
Section	VR	VR	VR	VR	VR	VR	VR	VR	VR	VR	VR	VR	VR	SV	SV	SV	SV
level	41.8	46.3	47.9	57.4	63.4	67.9	72.4	75.8	76.3	78.2	82.9	88.2	96.6	13.2	14.7	16.8	17.9
wt%																	
SiO2	51.81	53.64	52.81	58.69	53.99	52.67	55.70	57.76	54.58	56.78	51.35	51.93	56.93	57.95	50.38	51.25	52.42
Al2O3	14.53	14.13	14.73	12.59	13.76	13.60	13.95	14.22	15.41	14.12	14.63	15.74	14.65	14.63	14.96	15.67	14.89
FeO	9.10	10.64	9.62	7.13	9.18	10.38	8.59	12.35	14.43	11.82	10.06	10.03	7.81	8.72	10.56	11.68	11.16
MgO	11.16	8.87	9.26	6.20	10.92	9.28	7.21	6.69	7.01	5.13	10.14	6.57	6.46	6.11	8.40	7.79	8.19
CaO	9.49	10.16	10.88	13.01	10.26	11.33	12.08	5.58	2.90	4.62	9.97	12.96	11.21	7.10	13.14	10.30	8.79
Na2O	3.03	1.66	1.67	1.69	1.13	1.79	1.72	0.75	0.02	0.06	2.73	1.63	1.81	3.93	1.64	2.26	3.54
K2O	0.08	0.09	0.07	0.05	0.10	0.17	0.06	1.95	4.73	7.00	0.21	0.01	0.51	0.88	0.01	0.01	0.01
TiO2	0.57	0.62	0.73	0.47	0.48	0.49	0.51	0.90	1.05	0.89	0.68	0.85	0.66	0.64	0.68	0.77	0.74
MnO	0.18	0.20	0.17	0.12	0.14	0.24	0.14	0.18	0.25	0.15	0.19	0.24	0.19	0.17	0.19	0.20	0.19
P2O5	0.04	0.07	0.06	0.03	0.03	0.05	0.04	0.11	0.12	0.12	0.04	0.05	0.07	0.07	0.05	0.06	0.06
Total(witout LOI)	95.89	95.41	96.95	98.45	95.35	95.70	97.76	94.73	95.70	96.84	96.97	94.54	95.19	97.60	97.49	96.35	97.12
LOI	3.74	4.12	3.22	1.36	4.49	3.85	2.17	4.99	4.02	2.93	2.98	5.42	4.47	1.99	2.24	3.40	2.57
Total (+LOI)	99.63	99.53	100.17	99.81	99.84	99.55	99.93	99.73	99.72	99.77	99.95	99.96	99.67	99.60	99.73	99.75	99.69
ppm																	
Nb	1.8	3.8	2.1	2.0	1.9	1.8	2.3	4.2	4.8	3.9	2.2	2.7	3.6	4.5	1.4	1.7	2.0
Zr	37.5	77.3	46.7	36.9	35.1	40.0	40.5	92.0	109.9	96.2	35.7	42.7	69.6	90.5	32.9	35.8	37.6
Y	16.5	22.5	20.4	13.3	13.2	17.0	14.3	30.0	31.6	28.2	15.2	16.7	19.6	20.1	16.8	19.0	16.3
Sr	33.9	75.9	156.5	216.1	12.1	41.2	134.5	56.6	31.4	24.8	131.5	129.3	155.5	123.4	182.6	395.9	155.0
Rb	1.5	2.5	1.6	1.3	2.5	4.4	1.6	33.6	79.8	133.2	7.0	0.4	12.6	16.2	0.3	0.1	0.7
Th	1.2	5.2	1.3	1.2	1.2	2.8	1.8	6.6	9.1	5.9	1.1	0.9	4.0	7.5	2.1	3.7	2.9
Pb	2.3	3.1	0.9	3.1	2.2	3.5	1.8	6.4	6.0	5.5	0.3	0.9	2.5	3.6	0.5	3.5	1.3
Zn	70.4	84.2	78.9	46.9	66.8	76.9	68.9	100.5	121.8	100.6	85.4	87.1	63.0	63.5	69.8	77.3	87.5
Cu	66.0	62.1	91.9	57.8	60.3	54.5	51.7	99.6	124.2	96.6	121.8	139.2	88.3	56.5	112.1	111.1	106.4
Ni	222.6	100.5	111.4	178.8	150.3	101.0	151.5	65.3	74.8	61.2	315.8	168.9	101.7	114.4	165.9	179.5	172.7
Cr	594.9	341.8	333.0	619.0	539.4	533.2	378.8	34.8	37.4	46.8	373.2	418.2	153.4	74.8	424.4	460.9	440.7
Ce	1.6	14.4	3.5	5.4	6.4	4.9	2.5	16.4	19.8	20.3	4.5	6.8	12.7	25.6	4.6	4.5	6.2
Nd	1.5	8.7	4.2	3.9	3.9	1.8	2.0	8.8	8.1	10.7	3.7	5.3	7.0	9.1	2.4	3.2	5.2
La	0.1	3.8	0.1	0.1	0.1	1.6	0.1	7.8	5.9	6.5	0.1	0.1	2.7	10.0	0.1	0.1	0.1
V	237.4	197.2	266.0	187.8	200.7	216.8	218.1	286.2	305.2	290.8	213.5	264.1	205.4	186.4	256.0	254.2	246.7
Ba	20.7	37.7	47.2	6.4	49.9	52.3	17.9	708.4	654.7	709.7	85.5	1.0	252.2	395.7	5.8	42.4	25.9
Sc	45.1	29.8	49.0	34.5	41.0	37.6	38.8	30.6	38.1	38.8	37.1	48.5	32.9	28.6	43.3	41.7	40.7
ratios																	
Al2O3/TiO2	25.35	22.74	20.30	26.74	28.49	27.50	27.24	15.84	14.63	15.79	21.39	18.52	22.34	22.84	22.10	20.22	20.08
CaO/Al2O3	0.65	0.72	0.74	1.03	0.75	0.83	0.87	0.39	0.19	0.33	0.68	0.82	0.77	0.49	0.88	0.66	0.59
Zr/Nb	20.83	20.34	22.24	18.45	18.47	22.22	17.61	21.90	22.90	24.67	16.23	15.81	19.33	20.11	23.50	21.06	18.80
Ce/Y	0.10	0.64	0.17	0.41	0.49	0.29	0.18	0.55	0.63	0.72	0.30	0.41	0.65	1.27	0.28	0.24	0.38
Ce/Zr	0.04	0.19	0.08	0.15	0.18	0.12	0.06	0.18	0.18	0.21	0.13	0.16	0.18	0.28	0.14	0.13	0.16
Nb/Y	0.11	0.17	0.10	0.15	0.14	0.11	0.16	0.14	0.15	0.14	0.14	0.16	0.18	0.22	0.08	0.09	0.12
Zr/Y	2.27	3.44	2.29	2.77	2.66	2.35	2.83	3.07	3.48	3.41	2.35	2.56	3.55	4.50	1.96	1.88	2.31
Type I																	

Sample	CBZ110	CBZ111	CBZ112	CBZ115	CBZ118	CBZ121	CBZ122	CBZ125	CBZ192	CBZ193	CBZ195	CBZ196	CBZ197	CBZ198	CBZ199	CBZ200	CBZ201
Rock Type	basalt	basalt	basalt	basalt	basalt	basalt	basalt	basalt	basalt	basalt	basalt	basalt	basalt	basalt	basalt	basalt	basalt
Section	SV	SV	SV	SV	SV	SV	SV	SV	SV	SV	SV	SV	SV	SV	SV	SV	SV
level	20.0	23.7	26.3	32.1	37.4	44.2	44.7	51.6	54.7	58.9	66.3	70.0	71.1	72.1	76.3	78.9	86.3
wt%																	
SiO2	50.07	49.32	50.56	54.45	52.35	54.42	55.40	54.01	53.82	54.05	54.66	56.29	57.21	57.75	53.70	54.13	51.11
Al2O3	15.26	14.96	15.07	13.87	16.03	14.20	14.67	15.52	15.09	12.77	15.50	15.10	14.66	14.83	14.66	15.21	14.65
FeO	11.55	11.60	11.33	10.42	8.26	9.31	8.61	9.43	10.21	10.13	9.17	9.21	8.94	8.62	9.80	10.18	11.11
MgO	8.67	8.99	8.81	8.17	10.47	10.28	7.69	7.90	8.36	11.90	8.41	6.91	6.01	6.66	7.61	8.39	8.34
CaO	11.02	11.87	9.91	6.81	9.89	8.93	11.60	9.82	7.01	7.75	9.66	9.02	10.08	8.31	11.05	8.72	12.27
Na2O	2.41	2.23	3.18	4.72	2.33	2.01	1.18	2.57	4.61	2.63	1.26	2.14	2.29	2.85	2.34	2.50	1.33
K2O	0.01	0.01	0.13	0.14	0.08	0.01	0.01	0.07	0.08	0.03	0.60	0.40	0.06	0.22	0.06	0.03	0.08
TiO2	0.76	0.77	0.75	1.14	0.43	0.61	0.57	0.56	0.58	0.50	0.54	0.67	0.52	0.52	0.52	0.56	0.78
MnO	0.19	0.20	0.20	0.18	0.12	0.17	0.23	0.16	0.18	0.19	0.14	0.19	0.18	0.19	0.21	0.22	0.28
P2O5	0.06	0.05	0.06	0.11	0.04	0.05	0.05	0.06	0.06	0.05	0.05	0.07	0.05	0.05	0.05	0.05	0.06
Total(witout LOI)	97.47	96.75	97.19	97.06	95.78	95.59	96.23	96.06	96.71	96.10	96.18	95.89	96.08	95.22	95.89	95.91	95.17
LOI	2.21	2.81	2.47	2.55	3.75	4.33	3.30	3.52	2.98	3.69	3.53	3.76	3.60	4.45	3.85	4.04	4.49
Total (+LOI)	99.68	99.56	99.66	99.61	99.53	99.92	99.53	99.58	99.69	99.79	99.71	99.65	99.68	99.67	99.74	99.95	99.66
ppm																	
Nb	1.8	1.6	1.8	3.3	1.1	1.5	0.9	2.1	2.3	2.0	2.0	2.3	1.4	1.4	1.8	1.7	1.4
Zr	38.0	38.1	37.8	80.7	26.7	36.7	33.6	48.6	51.0	48.5	46.1	55.4	38.8	38.1	39.6	41.5	24.1
Y	18.5	18.6	17.9	23.8	14.1	17.4	14.3	13.8	18.4	16.1	16.8	15.8	16.7	15.7	16.8	16.5	11.6
Sr	173.5	197.8	213.8	137.7	189.5	64.8	149.5	62.3	28.5	42.7	153.5	66.5	110.8	59.8	28.1	126.5	81.0
Rb	0.0	0.2	3.0	2.1	2.4	0.3	0.0	1.2	1.0	0.4	17.9	8.7	0.9	6.1	0.5	0.7	7.3
Th	3.4	2.6	4.1	3.9	2.0	2.0	2.0	4.7	4.4	4.6	3.5	4.0	2.4	1.3	3.7	4.0	2.0
Pb	0.2	1.4	0.9	2.8	1.9	1.7	2.3	1.1	2.2	2.4	4.6	2.7	3.3	1.7	1.9	1.9	1.9
Zn	92.6	90.7	89.2	83.7	40.1	66.6	57.3	79.4	91.7	71.5	72.9	67.6	64.9	63.2	71.8	80.4	80.6
Cu	138.7	139.1	141.3	146.4	57.7	80.4	55.7	49.4	78.2	50.5	65.7	85.6	53.8	53.9	56.5	46.1	93.7
Ni	195.6	188.2	179.7	117.2	175.7	204.2	122.3	91.2	94.1	263.9	93.8	111.8	151.0	151.3	136.9	159.2	489.3
Cr	456.3	447.1	432.4	295.0	772.1	478.2	410.1	349.3	322.8	947.9	368.7	227.9	416.0	435.2	382.7	432.3	425.9
Ce	5.6	2.8	2.3	12.4	3.5	6.1	5.8	4.6	7.8	11.5	11.4	10.4	5.2	0.0	6.4	4.2	1.8
Nd	5.4	4.4	3.3	7.7	3.0	5.4	1.1	3.5	5.3	6.9	7.2	7.2	4.3	0.0	3.1	1.9	2.6
La	0.1	0.1	0.1	0.8	0.1	1.3	0.1	0.1	2.9	2.1	1.5	0.9	0.1	0.0	0.1	0.6	0.1
V	247.4	255.0	246.1	283.1	198.1	226.5	234.7	220.7	238.7	198.0	197.6	241.4	224.6	237.0	226.2	230.0	176.0
Ba	14.9	37.2	45.3	68.8	34.6	19.5	9.4	54.5	49.2	79.4	85.6	135.0	117.0	101.3	52.2	30.6	46.0
Sc	38.6	40.8	39.5	36.4	36.9	38.1	39.9	38.6	39.6	34.1	33.4	41.3	38.4	38.5	40.4	41.2	26.4
ratios																	
Al2O3/TiO2	20.12	19.44	20.01	12.21	37.49	23.28	25.70	27.57	26.05	25.59	28.81	22.53	28.28	28.79	28.16	27.31	18.84
CaO/Al2O3	0.72	0.79	0.66	0.49	0.62	0.63	0.79	0.63	0.46	0.61	0.62	0.60	0.69	0.56	0.75	0.57	0.84
Zr/Nb	21.11	23.81	21.00	24.45	24.27	24.47	37.33	23.14	22.17	24.25	23.05	24.09	27.71	27.21	22.00	24.41	17.21
Ce/Y	0.30	0.15	0.13	0.52	0.25	0.35	0.41	0.34	0.43	0.71	0.68	0.66	0.31	0.00	0.38	0.26	0.16
Ce/Zr	0.15	0.07	0.06	0.15	0.13	0.17	0.17	0.10	0.15	0.24	0.25	0.19	0.13	0.00	0.16	0.10	0.08
Nb/Y	0.10	0.09	0.10	0.14	0.08	0.09	0.06	0.15	0.13	0.12	0.12	0.15	0.08	0.09	0.11	0.10	0.12
Zr/Y	2.05	2.05	2.11	3.39	1.89	2.11	2.35	3.52	2.77	3.01	2.74	3.51	2.32	2.43	2.36	2.52	2.08
Type I																	

TYPE II

Sample	CBZ164	CBZ166	CBZ007	CBZ167	CBZ009	CBZ010	CBZ210	CBZ011B	CBZ012A	CBZ214	CBZ213	CBZ212	CBZ183	CBZ131	CBZ133
Rock Type	basalt	basalt	basalt	basalt	basalt	basalt	basalt	basalt	basalt	basalt	basalt	basalt	basalt	basalt	basalt
Section	NR	NR	NR	NR	NR	NR	NR	NR	NR	NR	NR	NR	NR	VR	VR
level	27.7	27.7	28.4	28.4	30.8	33.7	33.9	37.6	39.3	39.8	40.4	40.4	41.3	28.2	31.1
wt%															
SiO2	52.86	54.08	51.88	51.68	52.94	54.41	52.22	52.19	48.38	55.32	51.67	51.41	50.56	55.27	53.77
Al2O3	9.38	9.27	9.02	9.62	9.38	7.04	11.04	11.00	10.58	8.12	8.61	8.37	8.85	8.34	9.89
FeO	11.99	11.73	14.23	13.74	13.51	12.41	13.10	11.83	16.90	12.77	15.88	15.72	14.76	12.98	12.11
MgO	9.62	9.52	9.13	7.53	8.33	13.21	8.66	9.31	10.16	8.33	8.90	8.80	10.80	8.42	8.49
CaO	13.03	12.17	11.15	13.64	10.99	9.15	9.58	11.09	9.53	9.99	11.17	12.66	10.75	10.13	11.06
Na2O	1.12	1.78	1.35	1.79	2.70	2.10	3.79	3.04	1.85	3.35	0.53	0.27	1.26	3.28	3.16
K2O	0.68	0.41	1.61	0.51	0.58	0.36	0.09	0.11	0.70	0.33	1.45	0.86	1.15	0.19	0.31
TiO2	1.02	0.93	1.27	1.17	1.23	1.01	1.21	1.10	1.42	1.41	1.53	1.48	1.50	1.05	0.99
MnO	0.20	0.20	0.24	0.23	0.23	0.19	0.16	0.19	0.29	0.18	0.22	0.23	0.21	0.22	0.20
P2O5	0.12	0.11	0.12	0.11	0.12	0.10	0.14	0.14	0.17	0.20	0.22	0.21	0.16	0.12	0.12
Total (without LOI)	98.13	98.10	96.50	98.80	99.14	97.15	98.42	98.35	97.44	98.08	97.78	97.61	97.41	98.59	98.44
LOI	1.45	1.51	3.38	1.04	1.07	2.37	1.54	1.43	2.65	0.91	1.78	1.92	2.09	0.93	1.07
Total (+LOI)	99.58	99.61	99.88	99.84	100.21	99.52	99.96	99.78	100.09	98.99	99.56	99.53	99.50	99.52	99.51
ppm															
Nb	6.8	6.1	9.1	8.5	9.2	8.3	4.2	4.6	5.6	12.0	13.0	12.5	12.0	9.3	5.8
Zr	75.9	68.2	112.3	98.1	112.9	94.5	58.2	60.6	70.2	186.7	194.6	183.1	137.8	153.4	60.5
Y	17.6	16.2	22.1	23.0	22.9	21.1	15.4	13.0	16.4	43.3	44.1	42.2	27.7	33.2	14.9
Sr	287.1	532.9	153.1	1122.9	252.6	49.5	220.8	659.6	61.2	78.9	454.0	902.3	81.2	67.0	322.8
Rb	6.9	3.1	17.2	4.0	20.2	17.6	1.1	3.5	8.8	4.5	22.3	11.7	18.7	1.5	2.7
Th	6.1	5.9	5.9	8.4	5.3	4.4	4.1	3.2	5.6	9.0	10.8	9.0	8.7	7.6	7.0
Pb	5.8	6.3	5.1	9.2	4.9	1.0	1.3	2.9	1.9	5.5	5.5	4.2	4.0	2.9	5.5
Zn	89.5	82.2	118.3	99.3	117.3	99.9	87.9	86.6	138.4	101.1	117.8	110.5	131.5	98.3	91.1
Cu	204.2	190.9	233.1	193.3	235.2	201.7	203.5	230.2	242.2	143.0	177.3	144.0	229.7	189.3	229.8
Ni	232.4	221.4	156.2	134.2	148.2	472.8	167.8	145.3	217.7	106.1	118.8	121.1	346.1	142.6	192.4
Cr	949.3	923.3	298.1	265.8	307.4	1440.0	361.0	295.2	444.0	486.1	534.2	569.7	876.5	553.0	611.3
Ce	28.5	26.4	28.1	31.8	30.4	19.9	13.4	15.0	15.2	39.4	42.0	41.3	32.1	33.2	21.8
Nd	16.2	15.7	15.7	18.2	18.0	15.0	10.5	10.9	12.4	26.6	25.5	25.8	22.1	20.6	12.6
La	10.0	7.9	8.2	10.2	10.0	6.3	1.0	2.6	3.4	13.4	14.8	14.5	9.8	9.8	6.4
V	184.5	171.5	202.0	217.8	198.7	169.6	201.1	178.9	225.8	231.7	261.1	261.0	193.7	181.6	186.4
Ba	245.6	183.0	571.3	150.3	111.7	31.3	34.0	78.8	335.4	244.6	464.3	209.9	406.1	67.7	106.2
Sc	20.5	20.6	26.1	19.6	24.8	30.9	21.8	20.9	28.1	27.3	22.1	25.2	20.6	22.0	21.1
ratios															
Al2O3/TiO2	9.23	9.92	7.11	8.25	7.63	6.95	9.11	9.98	7.43	5.75	5.62	5.67	5.91	7.93	10.02
CaO/Al2O3	1.39	1.31	1.24	1.42	1.17	1.30	0.87	1.01	0.90	1.23	1.30	1.51	1.21	1.21	1.12
Zr/Nb	11.16	11.18	12.34	11.54	12.27	11.39	13.86	13.17	12.54	15.56	14.97	14.65	11.48	16.49	10.43
Ce/Y	1.62	1.63	1.27	1.38	1.33	0.94	0.87	1.16	0.93	0.91	0.95	0.98	1.16	1.00	1.46
Ce/Zr	0.38	0.39	0.25	0.32	0.27	0.21	0.23	0.25	0.22	0.21	0.22	0.23	0.23	0.22	0.36
Nb/Y	0.39	0.38	0.41	0.37	0.40	0.39	0.27	0.35	0.34	0.28	0.29	0.30	0.43	0.28	0.39
Zr/Y	4.31	4.21	5.08	4.27	4.93	4.48	3.78	4.66	4.28	4.31	4.41	4.34	4.97	4.62	4.06
Type II															

Sample	CBZ075	CBZ143	CBZ114
Rock Type	basalt	basalt	basalt
Section	VR	VR	SV
level	31.8	31.8	29.5
wt%			
SiO2	55.44	49.94	53.41
Al2O3	8.85	10.50	8.48
FeO	11.14	14.39	12.21
MgO	8.98	10.12	11.23
CaO	11.04	10.87	10.71
Na2O	1.58	1.46	1.09
K2O	1.28	0.64	1.64
TiO2	1.38	1.67	0.94
MnO	0.18	0.23	0.21
P2O5	0.13	0.17	0.09
Total (without LOI)	98.01	97.24	96.89
LOI	1.74	2.36	2.68
Total (+LOI)	99.75	99.60	99.57
ppm			
Nb	9.2	10.1	6.3
Zr	123.2	144.9	72.6
Y	27.5	32.1	17.8
Sr	443.5	488.7	254.1
Rb	12.1	5.0	24.7
Th	4.6	9.9	5.5
Pb	3.8	4.7	4.4
Zn	86.9	121.4	92.2
Cu	188.1	210.8	229.7
Ni	296.0	467.3	325.2
Cr	529.1	707.1	1131.7
Ce	30.3	33.8	18.3
Nd	18.2	20.5	11.5
La	7.6	8.0	6.8
V	204.4	257.7	169.6
Ba	320.7	139.8	944.5
Sc	18.0	22.4	23.1
ratios			
Al2O3/TiO2	6.41	6.28	9.05
CaO/Al2O3	1.25	1.03	1.26
Zr/Nb	13.39	14.35	11.52
Ce/Y	1.10	1.05	1.03
Ce/Zr	0.25	0.23	0.25
Nb/Y	0.33	0.31	0.35
Zr/Y	4.48	4.51	4.08

Type II

Evolved

Sample	CBZ041	CBZ042	CBZ204	CBZ123	CBZ124	CBZ202
Rock Type	andesite	andesite	andesite	andesite	andesite	andesite
Section	NR	NR	SV	SV	SV	SV
level	90.1	94.6	93.7	47.9	49.5	89.5
wt%						
SiO2	58.78	60.37	67.58	58.67	60.45	57.90
Al2O3	13.13	14.32	13.88	13.29	13.41	15.32
FeO	11.94	8.40	5.70	8.25	7.16	8.47
MgO	3.14	3.82	1.32	4.13	4.05	3.77
CaO	6.97	5.04	3.77	15.13	14.17	12.08
Na2O	1.96	5.95	5.01	0.07	0.04	1.41
K2O	2.55	0.90	1.02	0.01	0.00	0.01
TiO2	1.22	0.94	1.36	0.50	0.50	0.82
MnO	0.17	0.14	0.17	0.20	0.16	0.16
P2O5	0.14	0.12	0.19	0.05	0.05	0.06
Total(without LOI)	97.77	98.73	95.13	95.64	95.39	95.77
LOI	1.88	1.36	4.44	3.99	4.18	3.88
Total (+LOI)	99.65	100.09	99.57	99.63	99.57	99.65
ppm						
Nb	9.1	9.5	10.4	1.6	1.5	2.1
Zr	163.6	170.4	199.5	36.0	36.6	37.1
Y	40.7	41.9	38.0	14.1	14.6	17.3
Sr	232.6	53.4	75.4	17.6	8.4	102.2
Rb	40.6	14.6	33.9	0.1	0.3	2.4
Th	9.0	6.1	8.7	2.0	1.9	3.1
Pb	6.6	1.7	6.5	1.6	2.7	2.5
Zn	97.9	80.1	49.6	43.6	42.2	82.3
Cu	69.9	128.5	220.2	58.7	52.6	124.4
Ni	19.9	33.6	21.1	127.4	107.4	144.9
Cr	19.5	45.0	13.1	481.4	485.2	406.6
Ce	32.6	45.6	27.8	5.1	4.4	3.8
Nd	16.1	21.8	14.1	3.2	4.0	4.6
La	10.6	18.0	9.6	0.1	0.1	0.1
V	329.9	209.4	382.7	187.0	183.4	251.2
Ba	1012.3	192.5	304.3	24.7	123.9	45.8
Sc	34.8	31.2	40.7	39.4	41.9	41.9
ratios						
Al2O3/TiO2	10.76	15.16	10.20	26.53	26.72	18.75
CaO/Al2O3	0.53	0.35	0.27	1.14	1.06	0.79
Zr/Nb	17.98	17.94	19.18	22.50	24.40	17.67
Ce/Y	0.80	1.09	0.73	0.36	0.30	0.22
Ce/Zr	0.20	0.27	0.14	0.14	0.12	0.10
Nb/Y	0.22	0.23	0.27	0.11	0.10	0.12
Zr/Y	4.02	4.07	5.25	2.55	2.51	2.14

Evolved

Excluded

Sample	CBZ008	CBZ011A	CBZ012B	CBZ012C	CBZ012D	CBZ012E	CBZ031A	CBZ031B	CBZ151M	CBZ151B	CBZ160	CBZ161	CBZ163	CBZ165	CBZ168
Rock Type	tuff	tuff	vb	tuff	vb	basalt	basalt	ftb	hc	hc	hc	hc	tuff	tuff	tuff
Section	NR	NR	NR	NR	NR	NR	NR	NR	NR	NR	NR	NR	NR	NR	NR
level	27.5	37.4	39.3	39.3	39.3	39.3	74.8	74.8	11.6	11.6	25.5	25.5	27.5	27.9	43.0
wt%															
SiO2	51.88	51.81	52.69	52.69	51.15	52.53	59.24	51.32	51.22	54.47	53.30	56.89	49.77	51.57	50.02
Al2O3	9.02	5.84	8.66	7.68	8.88	7.65	13.84	17.51	17.81	15.36	16.82	13.99	6.27	11.55	14.68
FeO	14.23	13.85	12.97	14.50	15.40	13.92	8.22	11.46	12.58	8.38	11.35	7.13	14.44	13.77	12.44
MgO	9.13	12.68	9.86	10.76	11.30	10.36	7.16	8.99	8.63	6.51	8.98	5.87	17.34	9.21	10.29
CaO	11.15	12.88	11.25	10.32	9.36	11.04	8.79	8.67	7.74	10.22	8.23	11.75	11.16	10.11	8.55
Na2O	1.35	1.34	3.02	2.27	2.15	2.49	1.91	1.52	0.88	4.14	0.06	3.56	0.02	2.09	1.69
K2O	1.61	0.10	0.10	0.12	0.10	0.12	0.15	0.05	0.00	0.01	0.15	0.13	0.02	0.24	0.73
TiO2	1.27	1.17	1.08	1.30	1.27	1.47	0.53	0.55	0.89	0.69	0.88	0.60	0.97	1.11	1.29
MnO	0.24	0.24	0.27	0.23	0.25	0.21	0.13	0.17	0.18	0.17	0.16	0.14	0.24	0.22	0.20
P2O5	0.12	0.09	0.11	0.12	0.13	0.21	0.04	0.06	0.07	0.05	0.07	0.04	0.08	0.12	0.12
Total (without LOI)	96.50	98.39	97.14	98.14	97.46	98.79	96.93	93.64	95.26	97.74	93.94	96.93	96.39	97.46	96.17
LOI	3.38	1.25	2.61	1.68	2.39	1.19	2.75	5.93	4.92	1.92	5.74	2.65	3.19	2.22	3.64
Total (+LOI)	99.88	99.64	99.75	99.82	99.85	99.98	99.68	99.56781	100.18	99.66	99.68	99.57948	99.57784	99.68	99.81
ppm															
Nb	7.1	6.2	5.4	6.8	7.0	13.1	2.2	2.1	2.0	1.8	1.9	1.4	6.2	6.8	4.2
Zr	76.6	70.6	67.4	89.8	82.7	189.6	40.8	40.8	42.9	35.7	44.1	30.4	70.6	84.7	93.9
Y	18.1	15.2	14.3	17.8	17.3	43.1	16.6	17.2	21.1	17.1	20.0	14.9	17.1	20.3	26.8
Sr	5.3	94.5	76.3	63.3	54.1	68.5	76.0	34.4	215.1	116.3	24.5	102.3	11.7	121.5	81.5
Rb	0.0	2.6	1.4	2.1	2.5	1.6	4.5	0.9	0.2	0.4	2.6	1.6	1.0	2.3	10.6
Th	6.1	4.5	4.3	4.7	7.9	8.5	1.2	2.9	3.0	3.2	2.5	0.8	6.3	6.6	5.5
Pb	3.3	3.5	4.3	8.2	4.1	1.2	2.5	2.0	1.6	2.6	1.0	2.8	2.4	3.7	2.5
Zn	111.3	113.1	106.5	129.8	132.7	102.0	66.2	86.3	104.8	70.9	95.4	50.4	103.6	104.6	105.8
Cu	163.1	252.7	207.4	326.5	289.2	130.9	71.4	92.8	192.6	79.3	230.8	104.1	127.4	181.1	175.3
Ni	613.4	485.2	242.3	303.3	251.3	121.8	122.1	149.7	217.8	143.4	257.9	132.6	595.7	236.4	332.7
Cr	1514.9	930.2	590.0	754.4	590.7	623.0	277.5	303.0	530.7	416.9	519.4	345.2	1696.5	732.9	902.3
Ce	11.2	16.1	16.0	21.3	19.8	47.9	8.2	3.3	4.0	4.1	5.0	3.8	21.4	24.1	12.9
Nd	8.7	13.5	12.0	15.1	13.7	28.8	5.0	3.7	5.2	4.5	4.3	4.4	14.0	14.6	10.4
La	0.6	1.7	2.7	2.6	7.4	15.2	0.9	1.5	0.1	0.1	0.1	0.1	6.0	9.9	3.7
V	179.6	182.2	174.8	200.8	183.8	230.0	228.7	247.0	268.8	265.0	287.2	213.0	174.2	212.1	303.5
Ba	3.3	6.4	104.3	114.8	166.3	126.2	36.4	34.8	6.7	12.1	55.7	61.2	3.9	77.6	200.6
Sc	28.9	24.4	20.5	25.6	25.9	26.5	41.4	38.8	37.3	37.4	38.7	31.7	25.5	32.4	37.5
ratios															
Al2O3/TiO2	7.11	5.00	8.02	5.90	7.00	5.20	26.32	31.67	19.99	22.26	19.07	23.28	6.49	10.38	11.38
CaO/Al2O3	1.24	2.20	1.30	1.34	1.05	1.44	0.64	0.50	0.43	0.67	0.49	0.84	1.78	0.88	0.58
Zr/Nb	10.79	11.39	12.48	13.21	11.81	14.47	18.55	19.43	21.45	19.83	23.21	21.71	11.39	12.46	22.36
Ce/Y	0.62	1.06	1.12	1.20	1.15	1.11	0.50	0.19	0.19	0.24	0.25	0.26	1.25	1.19	0.48
Ce/Zr	0.15	0.23	0.24	0.24	0.24	0.25	0.20	0.08	0.09	0.12	0.11	0.13	0.30	0.28	0.14
Nb/Y	0.39	0.41	0.38	0.38	0.40	0.30	0.13	0.12	0.09	0.11	0.10	0.09	0.36	0.33	0.16
Zr/Y	4.23	4.64	4.71	5.04	4.78	4.40	2.46	2.37	2.03	2.09	2.21	2.04	4.13	4.17	3.50
Excluded															

Sample	CBZ172	CBZ176	CBZ174	CBZ175	CBZ177	CBZ178	CBZ180	CBZ113	CBZ116	CBZ117	CBZ119	CBZ120	CBZ194	CBZ203	CBZ092	CBZ097	CBZ188
Rock Type	tuff	tuff	cum	cum	cum	tuff	tuff	basalt	basalt	basalt	basalt	basalt	basalt	basalt	basalt	tuff	tuff
Section	NR	NR	NR	NR	NR	NR	NR	SV	SV	SV	SV	SV	SV	SV	VR	VR	NR
level	44.9	34.1	34.4	34.4	37.6	42.3	37.6	27.4	34.2	36.3	41.1	43.7	64.2	91.1	53.9	76.3	45.2
wt%																	
SiO2	50.72	47.45	50.28	49.25	44.62	51.77	58.56	46.18	56.56	55.48	55.60	52.26	52.99	53.84	56.04	62.81	50.91
Al2O3	11.83	11.06	4.77	4.35	4.52	14.19	11.82	6.77	13.46	12.77	15.13	14.47	15.89	16.57	12.20	12.53	10.49
FeO	12.26	17.82	14.42	14.59	18.14	12.98	8.83	13.68	10.53	10.10	9.16	8.26	9.19	9.94	8.48	10.08	10.72
MgO	17.71	12.46	24.11	29.73	26.45	7.84	3.39	14.68	7.99	8.49	9.36	4.28	4.43	4.17	10.12	5.25	16.70
CaO	6.17	6.73	5.44	1.42	4.79	6.42	9.92	17.62	10.31	10.85	7.80	17.80	16.42	9.54	10.11	2.98	8.57
Na2O	0.11	1.87	0.05	0.00	0.02	3.02	6.28	0.03	0.07	0.91	1.75	0.05	0.12	3.11	2.32	0.01	0.43
K2O	0.20	0.49	0.01	0.00	0.01	1.60	0.07	0.00	0.40	0.49	0.52	2.35	0.00	1.42	0.03	5.28	1.29
TiO2	0.82	1.65	0.68	0.59	0.70	1.81	0.89	1.03	0.97	0.66	0.54	0.64	0.65	1.05	0.48	0.80	0.62
MnO	0.22	0.32	0.18	0.10	0.68	0.19	0.13	0.19	0.10	0.19	0.10	0.14	0.24	0.37	0.19	0.18	0.21
P2O5	0.07	0.14	0.06	0.06	0.07	0.18	0.11	0.08	0.10	0.06	0.05	0.06	0.06	0.09	0.03	0.08	0.06
Total (without LOI)	93.73	96.23	94.76	91.69	92.71	96.71	99.34	77.04	88.06	83.58	90.15	84.75	94.08	89.55	97.65	96.31	95.51
LOI	5.84	3.95	5.18	7.84	6.84	2.97	0.37	22.53	11.59	16.06	9.38	14.80	5.47	10.03	2.28	3.30	4.25
Total (+LOI)	99.56947	100.18	99.94	99.52943	99.55	99.68	99.71	99.57876	99.64575	99.64	99.53	99.55778	99.55	99.57948	99.93	99.61	99.76
ppm																	
Nb	2.3	9.4	2.6	2.3	2.7	7.6	4.8	5.3	2.9	1.9	1.1	1.2	2.1	2.3	2.0	4.3	1.6
Zr	56.2	125.2	34.4	34.3	38.5	152.6	72.9	57.3	67.2	42.0	32.4	34.2	54.8	49.7	35.4	83.1	42.9
Y	18.2	25.6	8.9	7.0	8.8	34.6	16.4	14.8	17.6	13.8	15.8	13.8	21.4	21.0	13.5	26.0	15.8
Sr	8.6	44.9	10.8	33.7	23.1	97.4	121.5	44.7	44.7	117.8	28.7	39.2	14.1	68.2	158.1	23.3	11.5
Rb	6.3	11.6	0.2	0.3	0.5	24.3	0.8	0.4	13.5	16.9	15.4	63.1	0.3	45.1	0.1	89.3	35.0
Th	5.2	11.9	4.5	3.2	5.6	8.4	3.9	4.8	2.3	2.7	0.9	1.5	3.2	1.8	1.2	7.0	3.6
Pb	2.3	2.8	2.2	1.6	1.8	5.0	1.4	2.3	1.8	2.7	0.5	1.9	2.5	1.9	2.5	4.9	1.5
Zn	92.7	162.9	96.2	101.0	93.2	112.7	57.0	70.9	78.9	60.2	20.9	57.8	53.2	77.9	63.3	85.0	75.4
Cu	85.8	407.3	99.7	70.9	76.6	182.9	89.8	41.4	20.2	62.4	33.0	104.8	90.0	96.0	54.9	96.6	118.1
Ni	580.9	473.5	2002.0	2171.7	1941.6	226.6	335.0	674.7	161.9	57.9	112.6	171.8	102.4	171.3	182.0	57.9	446.3
Cr	2219.0	764.9	810.7	941.4	1273.7	418.3	608.7	1431.4	495.7	239.9	467.3	594.1	294.4	379.1	648.8	35.8	1706.6
Ce	4.8	31.0	6.2	6.4	8.0	23.1	17.2	22.3	12.2	5.6	3.6	2.2	7.0	5.5	3.1	10.1	1.8
Nd	6.2	21.4	4.4	4.7	5.8	15.2	12.4	15.3	8.3	2.8	2.5	0.2	7.3	6.4	1.9	6.6	4.6
La	0.1	8.1	0.1	0.1	1.0	6.5	4.1	4.2	0.4	0.3	0.1	0.1	3.9	0.1	1.4	5.5	0.2
V	247.6	252.9	114.9	93.4	134.0	302.2	164.2	171.5	271.1	240.4	229.3	265.4	225.5	318.5	187.3	238.8	221.2
Ba	21.8	90.4	27.9	10.7	102.3	567.8	23.8	3.5	42.9	168.7	63.1	233.6	189.3	248.1	9.4	872.5	377.4
Sc	35.8	27.9	11.7	12.2	15.2	31.3	18.0	24.3	36.6	40.2	39.6	42.7	53.6	47.0	37.8	40.9	34.4
ratios																	
Al2O3/TiO2	14.39	6.69	7.04	7.42	6.43	7.85	13.32	6.59	13.94	19.46	27.84	22.58	24.38	15.80	25.43	15.72	16.81
CaO/Al2O3	0.52	0.61	1.14	0.33	1.06	0.45	0.84	2.60	0.77	0.85	0.52	1.23	1.03	0.58	0.83	0.24	0.82
Zr/Nb	24.43	13.32	13.23	14.91	14.26	20.08	15.19	10.81	23.17	22.11	29.45	28.50	26.10	21.61	17.70	19.33	26.81
Ce/Y	0.26	1.21	0.70	0.92	0.91	0.67	1.05	1.51	0.69	0.41	0.23	0.16	0.32	0.26	0.23	0.39	0.11
Ce/Zr	0.09	0.25	0.18	0.19	0.21	0.15	0.24	0.39	0.18	0.13	0.11	0.07	0.13	0.11	0.09	0.12	0.04
Nb/Y	0.13	0.37	0.29	0.33	0.31	0.22	0.29	0.36	0.16	0.14	0.07	0.09	0.10	0.11	0.15	0.17	0.10
Zr/Y	3.09	4.89	3.87	4.90	4.38	4.41	4.45	3.87	3.82	3.04	2.05	2.48	2.56	2.37	2.62	3.20	2.72
Excluded																	

Sample	CBZ189	CBZ144	CBZ182	CBZ020B	CBZ020C	CBZ184	CBZ141	CBZ206	CBZ205
Rock Type	tuff	tuff	tuff	hc	HC	tuff	tuff	basalt	basalt
Section	NR	VR	NR	NR	NR	NR	VR	SV	SV
level	46.8	30.0	40.9	53.1	53.1	41.5	79.7	83.7	98.4
wt%									
SiO2	52.56	50.00	47.64	46.46	51.51	52.99	62.04	49.10	56.89
Al2O3	11.49	6.01	6.31	19.86	18.84	10.25	15.02	13.53	14.86
FeO	12.59	14.28	18.76	8.19	10.66	12.40	14.18	10.99	8.64
MgO	17.76	17.24	12.27	6.84	9.75	12.02	3.10	14.14	6.54
CaO	4.60	11.23	12.67	17.43	5.60	7.74	0.54	10.51	8.48
Na2O	0.07	0.12	0.18	0.12	2.50	3.05	3.04	0.77	3.15
K2O	0.00	0.16	0.04	0.04	0.08	0.13	0.54	0.19	0.23
TiO2	0.79	0.84	1.59	0.71	0.81	1.12	1.24	0.54	0.73
MnO	0.16	0.24	0.30	0.18	0.18	0.21	0.20	0.18	0.39
P2O5	0.07	0.08	0.24	0.07	0.07	0.10	0.09	0.04	0.09
Total (without LOI)	93.59	96.17	97.72	93.84	94.17	97.20	94.25	95.73	93.17
LOI	5.99	3.37	2.08	6.45	5.42	2.70	5.30	3.97	6.47
Total (+LOI)	99.57948	99.54	99.80	100.2896	99.59	99.90	99.55	99.70	99.64
ppm									
Nb	2.2	5.5	13.3	2.0	2.1	3.3	6.1	1.4	3.9
Zr	52.3	65.4	204.9	46.8	50.1	72.3	123.5	24.1	78.9
Y	18.6	16.7	46.8	21.4	19.2	21.3	24.9	11.6	22.0
Sr	3.5	44.4	50.7	9.9	41.9	25.3	23.6	81.0	71.2
Rb	0.2	2.6	1.5	0.9	1.3	1.7	9.5	7.3	5.9
Th	4.6	6.3	11.7	3.5	4.4	5.6	9.4	2.0	3.9
Pb	2.3	3.4	3.0	0.8	0.7	3.1	4.5	1.9	3.0
Zn	158.1	97.7	150.2	53.6	82.6	182.4	83.2	80.6	74.1
Cu	79.7	167.8	289.4	74.5	123.4	121.8	118.1	93.7	81.3
Ni	530.7	703.2	170.3	173.4	193.9	500.4	59.3	489.3	104.7
Cr	2105.1	1499.8	546.6	481.2	563.8	1381.8	52.7	425.9	149.9
Ce	6.7	15.1	45.1	8.2	5.0	11.4	12.8	2.9	15.7
Nd	5.7	9.2	31.7	4.6	5.0	8.1	10.2	2.7	7.9
La	1.4	6.2	13.9	0.9	0.1	1.3	3.8	0.1	3.6
V	228.1	162.1	303.6	278.9	274.3	273.3	325.1	176.0	199.1
Ba	5.7	125.5	2.5	52.5	13.7	84.9	340.7	46.0	102.0
Sc	39.9	22.3	24.2	45.3	37.3	34.9	45.2	26.4	30.7
ratios									
Al2O3/TiO2	14.51	7.12	3.96	27.90	23.28	9.12	12.12	25.05	
CaO/Al2O3	0.40	1.87	2.01	0.88	0.30	0.75	0.04	0.78	0.57
Zr/Nb	23.77	11.89	15.41	23.40	23.86	21.91	20.25	17.21	20.23
Ce/Y	0.36	0.91	0.96	0.38	0.26	0.53	0.51	0.25	0.71
Ce/Zr	0.13	0.23	0.22	0.18	0.10	0.16	0.10	0.12	0.20
Nb/Y	0.12	0.33	0.28	0.09	0.11	0.15	0.24	0.12	0.18
Zr/Y	2.81	3.92	4.38	2.19	2.61	3.39	4.96	2.08	3.59
Excluded									

APPENDIX 3

REE ANALYSIS BY ICP-AES

24 samples were analysed by ICP-AES to determine their REE contents. The preparation and analysis was conducted at the RHBNC lab in Egham.

The full procedure is documented in Walsh *et al.* (1981).

The data are presented in ppm, and are divided into type I, type II, evolved and excluded samples (see Chapter 6).

Type I

Sample	CBZ003	CBZ005	CBZ169	CBZ016	CBZ022	CBZ027	CBZ034	CBZ044	CBZ128	CBZ094	CBZ110	CBZ122	CBZ196
La	1.91	1.65	4.62	7.24	2.41	3.13	3.07	6.64	2.28	2.77	1.95	1.83	4.4
Ce	6.08	5.26	11.95	16.03	6.91	7.27	6.77	16.13	7.74	6.36	6.2	4.79	10.31
Pr	0.8	0.69	1.58	1.82	0.9	0.83	0.77	1.89	1.31	0.65	0.86	0.63	1.37
Nd	5.1	4.6	7.7	8.4	4.4	4.4	3.9	8.6	6.6	4	5.2	3.6	6
Sm	1.6	1.51	2.38	2.21	1.39	1.24	1.18	2.24	2.08	1.12	1.66	1.04	1.56
Eu	0.65	0.56	0.73	1.37	0.53	0.42	0.47	0.72	0.72	0.53	0.68	0.51	0.55
Gd	2.13	1.96	3.02	2.79	2.05	1.69	1.63	2.66	2.82	1.55	2.2	1.56	1.93
Dy	2.58	2.45	3.32	3.15	2.69	2.11	2.08	2.95	3.34	1.99	2.66	1.93	2.25
Ho	0.56	0.51	0.67	0.66	0.6	0.47	0.45	0.61	0.72	0.42	0.58	0.41	0.48
Er	1.61	1.49	1.83	1.88	1.8	1.34	1.29	1.69	2.08	1.23	1.62	1.25	1.4
Yb	1.61	1.53	1.69	1.84	1.9	1.33	1.3	1.69	2.05	1.33	1.67	1.29	1.44
Lu	0.27	0.24	0.25	0.28	0.3	0.23	0.2	0.27	0.33	0.21	0.28	0.2	0.23

Type II

Sample	CBZ166	CBZ009	CBZ010	CBZ213	CBZ214	CBZ143	CBZ114
La	11.03	13.93	8.88	19.75	16.71	21.81	10.34
Ce	27.07	35.02	23.45	48.85	43.6	49.49	24.31
Pr	3.61	4.39	2.98	6.16	5.91	6.04	3.28
Nd	13.9	18.6	14	26.4	25.7	24.9	13.4
Sm	3.16	4.47	3.8	6.81	6.78	5.99	3.25
Eu	1.27	1.3	1.1	2.09	1.28	2.13	0.88
Gd	3.12	4.29	3.8	7.04	7.04	5.89	3.15
Dy	2.62	3.88	3.58	6.99	7.02	5.21	2.87
Ho	0.52	0.74	0.69	1.42	1.42	1.02	0.56
Er	1.33	1.94	1.78	3.68	3.69	2.52	1.44
Yb	1.11	1.74	1.66	3.37	3.39	2.04	1.26
Lu	0.18	0.26	0.25	0.52	0.53	0.29	0.19

(all in ppm)

	Evolved		Excluded	
Sample	CBZ042	CBZ204	CBZ106	CBZ134
La	22.47	12.14	13.33	8.26
Ce	49.25	29.92	28.83	21.17
Pr	5.42	3.57	3.08	2.73
Nd	21.5	15.4	11.8	13.1
Sm	5.15	3.98	2.64	3.99
Eu	1.27	1.08	0.61	1.36
Gd	5.63	4.79	2.76	4.79
Dy	6.29	5.63	2.96	4.95
Ho	1.33	1.21	0.61	0.99
Er	3.64	3.4	1.67	2.57
Yb	3.76	3.42	1.66	2.36
Lu	0.61	0.55	0.26	0.36

REE analyses by ICP-AES

APPENDIX 4

ISOTOPE ANALYSIS BY MASS SPECTROMETRY

24 samples were analysed to determine their Nd isotope ratios, and their Nd and Sm concentrations by isotope dilution. The preparation and analyses were carried out at the SURRC, East Kilbride. The full procedure is described below.

SURRC Procedures for Sm-Nd Analysis

Analytical techniques

Samples were accurately weighed into in PFA teflon screw-top beakers (Savillex). Samples were then dissolved using ultra-pure reagents in a HF-HNO_3-HCl digestion. The dissolved sample was accurately aliquoted (by mass) and the smaller (one third) fraction spiked with 145Nd and 149Sm spikes which were quantitatively added by mass. Rb and Sr were removed in 2.5 N HCl using Bio-Rad AG50W X8 200–400 mesh cation exchange resin. A rare-earth element (REE) concentrate was collected by elution of 3N HNO_3. Ba was then removed from the REE concentrate using elution of 1.5N HNO_3 through Eichrom Industries Sr Spec resin. Nd and Sm were separated in a "cocktail" of acetic acid (CH_3COOH), methanol (CH_3OH) and nitric acid (HNO_3) using Bio-Rad AG1x8 200–400 mesh anion exchange resin. Total procedure blanks for Sm and Nd were less than 0.5 ng.

In preparation for mass spectrometry, Sm and Nd samples were loaded directly onto triple Ta-Re-Ta filaments. Sm and Nd samples were analysed on the VG Sector 54-30 instrument. 143Nd/144Nd ratios were measured with a 144Nd beam of 1V ($1x10^{-11}$A). 12 blocks of 10 ratios were collected in the peak-jumping mode and corrected for mass fractionation using an exponential law and 146Nd/144Nd = 0.7219. Repeat analyses of the internal laboratory standard (JM) gave 143Nd/144Nd = 0.511501 1 6 (1 s.d., n = 35). Nd and Sm concentration (ID) runs were analysed as 3 blocks of 10 ratios with ion intensities of 5 x 10^{-13}A for 143Nd and 149Sm respectively. Nd and Sm isotope ratios are adjusted for mass fractionation and spike contribution and concentrations calculated using adaptations of the standard algorithms of Krough & Hurley (1968).

The initial values corrected to 2.7Ga are based on the best available Pb-Pb age for the rocks of the Reliance Formation (Chauvel *et al.*, 1993) of 2692 ± 9 Ma

The data are divided into type I, type II and evolved samples (see Chapter 6).

Type I

Sample	CBZ002	CBZ169	CBZ022	CBZ034	CBZ 044	CBZ128	CBZ094	CBZ106	CBZ110	CBZ122	CBZ196	CBZ027	CBZ134	CBZ016	CBZ005
Isotope Dilution Results															
Sm (ppm)	1.84	2.27	1.24	1.11	2.204	2.06	1.02	2.57	1.51	0.92	1.5	1.15		2.13	1.06
Nd (ppm)	6.36	7.6	3.76	3.84	8.75	6.48	3.78	12.054	5.64	2.87	5.87	4.19	14.19		3.3
147Sm/144Nd	0.17585	0.18154	0.20046	0.17569	0.15308	0.19323	0.16401	0.12955	0.16274	0.19485	0.15530	0.16682	0.17090	0.15410	0.19525
Isotope Ratio Results															
143Nd/144Nd (measured)	0.51285	0.51254	0.51290	0.51243	0.51197	0.51285	0.51245	0.51130	0.51289	0.51290	0.51206	0.51250	0.51236	0.51202	0.51292
143Nd/144Nd error (2 sigma)	0.0007	0.0008	0.002	0.0006	0.0006	0.0009	0.0006	0.0006	0.0021	0.0002	0.0024	0.0018	0.0008	0.0006	0.0036
Number of analyses accepted	115/120	144/150	48/51	114/120	116/120	94/100	116/120	114/120	85/91	49/51	50/51	79/81	124/130	115/120	20/21
Initial values at 2.7Ga															
Initial 143/144 Nd	0.50972	0.50932	0.50934	0.50931	0.50925	0.50942	0.50954	0.50900	0.51000	0.50944	0.50930	0.50953	0.50932	0.50929	0.50945
Epsilon Nd	11.38	3.40	3.81	3.32	2.16	5.43	7.77	-2.81	16.78	5.77	3.15	7.64	3.48	2.78	6.01

Type II **Evolved**

Sample	CBZ166	CBZ009	CBZ010	CBZ214	CBZ213	CBZ114	CBZ143	CBZ042	CBZ204
Isotope Dilution Results									
Sm (ppm)	3.12	4.45	3.59	6.68	6.85	3.217	5.66	6.03	4
Nd (ppm)	14.4	20.19	14.49	27.51	28.95	14.73	24.15	27.16	16.28
147Sm/144Nd	0.13166	0.13393	0.15056	0.14756	0.14379	0.13271	0.14242	0.13491	0.14931
Isotope Ratio Results									
143Nd/144Nd (measured)	0.51146	0.51159	0.51184	0.51183	0.51175	0.51164	0.51181	0.51160	0.51182
143Nd/144Nd error (2 sigma)	0.0006	0.0006	0.0007	0.0007	0.0007	0.0006	0.0021	0.0006	0.0008
Number of analyses accepted	117/120	115/120	116/120	115/120	114/120	115/120	90/91	113/120	144/150
Initial values at 2.7Ga									
Initial 143/144 Nd	0.50912	0.50921	0.50916	0.50921	0.50920	0.50928	0.50928	0.50920	0.50917
Epsilon Nd	-0.39	1.27	0.32	1.33	1.00	2.74	2.75	1.15	0.52

APPENDIX 5

ELECTRON PROBE ANALYSIS OF MINERAL PHASES

Mineral phases in representative sections were analysed using a Microscan V electron probe. The results are presented in Tables A5.1 - A5.5.

The analysis numbers refer to the number of the mineral grain *within* each sample, and the letters (C, R or N) in Table A5.1 describe the area analysed as 'core', 'rim' or 'needle'.

Table A5.1 Pyroxenes

Sample	CBZ005	CBZ005	CBZ005	CBZ005	CBZ005	CBZ005	CBZ005	CBZ005	CBZ005	CBZ005	CBZ005	CBZ005	CBZ005	CBZ005	CBZ185	CBZ185	CBZ185
Analysis	1C	2C	3C	3R	3C	3I	3I	3R	4C	4R	5C	5R	6C	6R	1N	2N	3N
SiO2	51.75	50.72	51.58	51.39	51.61	52.03	51.86	50.87	51.17	51.42	53.18	51.75	52.23	51.27	51	51.09	52.75
TiO2	0.37	0.48	0.37	0.41	0.4	0.36	0.43	0.44	0.43	0.43	0.25	0.42	0.37	0.46	0	0.23	0
Al2O3	2.24	1.86	2.95	1.81	2.9	2.5	2.06	1.77	2.95	2.39	1.17	1.8	2.5	3.09	2.52	2.16	1.8
FeO	11.8	14.95	7.96	13.27	7.9	7.58	7.21	14.28	7.92	9.52	11.07	13.2	8.4	8.2	17.26	11.15	16.5
MnO	0.29	0.33	0.2	0.29	0.19	0.18	0.19	0.33	0.2	0.26	0.31	0.33	0.21	0.24	0.24	0.29	0.25
MgO	16.38	14.59	17.21	14.86	17.09	16.85	16.2	14.53	16.24	16.59	20.05	16.78	17.54	16.68	13.66	15.08	12.99
CaO	16.53	16.17	18.19	16.94	18.52	19.66	20.39	16.49	19.77	17.81	13.33	15.26	17.9	18.79	11.49	19.01	12.77
Na2O	0.18	0.21	0.2	0.2	0.18	0.19	0.17	0.2	0.2	0.18	0.13	0.17	0.17	0.19	0.11	0.22	0.16
Cr	0.17	0.04	0.59	0.07	0.57	0.26	0.16	0.04	0.33	0.27	0.22	0.08	0.25	0.41	0.05	0.16	0.03

Sample	CBZ034	CBZ034	CBZ011B	CBZ011B	CBZ011B	CBZ011B	CBZ011B	CBZ011B	CBZ011B	CBZ011B	CBZ011B	CBZ011B	CBZ011B	CBZ011B	CBZ011B	CBZ011B	CBZ011B
Analysis	1N	2N	1C	1R	2C	2R	3C	3R	4C	4R	4C	5C	5R	6C	6R	6R	7C
SiO2	56.45	54.53	53.04	49.17	51.72	50.78	50.44	53.12	51.99	52.82	52.97	50.57	51.06	51.96	52.7	52.43	52.66
TiO2	0.01	0.02	0.24	1.02	0.35	0.6	0.94	0.47	0.24	0.35	0.27	0.93	0.61	0.37	0.67	0.27	0.3
Al2O3	1.92	1.74	1.37	4.05	1.8	2.89	3.8	1.96	2.07	1.4	1.84	2.68	3.14	1.91	5.3	1.75	1.92
FeO	10.29	11.07	5.71	14.13	7.01	8.83	9.61	8.15	6.32	7.89	5.82	11.1	9.07	7.48	10.6	7.45	6.99
MnO	0.27	0.28	0.15	0.28	0.19	0.22	0.21	0.21	0.16	0.21	0.15	0.29	0.18	0.19	0.24	0.19	0.16
MgO	16.11	16.68	18.32	12.94	16.87	14.96	15.47	16.59	17.57	16.76	17.73	14.95	15.18	17.02	12.63	17.09	17.39
CaO	12.44	12.82	20	17.73	20.53	20.77	18.98	20.42	18.79	20.11	19.9	18.13	20.02	19.86	17.41	20.08	20.48
Na2O	0.47	0.1	0.29	0.3	0.32	0.35	0.4	0.29	0.34	0.29	0.33	0.3	0.34	0.34	1.56	0.28	0.3
Cr	0.03	0.07	0.62	0.01	0.38	0.07	0.32	0.18	0.93	0.13	1.04	0.17	0.08	0.64	0.03	0.31	0.36

Sample	CBZ011B	CBZ011B	CBZ011B	CBZ011B	CBZ011B	CBZ011B	CBZ011B	CBZ011B	CBZ149	CBZ040	CBZ040	CBZ040	CBZ040	CBZ040	CBZ040	CBZ040	CBZ040
Analysis	7R	8C	8R	9C	9R	9R	10C	10R	1N	1C	1R	1C	2C	2R	3C	3R	4C
SiO2	50.91	52.89	52.31	53.58	53.6	51.17	52.61	52.69	61.37	50.26	49.06	49.96	53.17	53.17	52.72	51.9	52.85
TiO2	0.66	0.31	0.64	0.18	0.87	0.78	0.47	0.39	1.17	0.49	0.7	0.47	0.17	0.17	0.28	0.35	0.25
Al2O3	2.85	1.52	1.63	1	6.45	2.99	2.38	1.94	10.15	2.12	1.93	2.19	1.69	1.62	2.22	1.69	2.11
FeO	9.1	6.67	9.98	6.62	8.46	9.67	7.56	7.87	7.44	11.26	18.06	11.19	6.49	6.56	7.39	13.02	7.32
MnO	0.22	0.17	0.26	0.2	0.17	0.24	0.2	0.18	0.18	0.26	0.38	0.27	0.23	0.21	0.22	0.36	0.24
MgO	14.9	16.87	15.28	19.59	12.06	15.01	17.44	16.56	6.27	15.37	12.03	15.48	18.23	18.44	17.29	16.49	17.85
CaO	20.44	21.28	20.21	17.79	17.38	19.66	18.74	20.37	12.42	17.91	16.24	18.07	18.92	18.42	18.91	15.42	18.25
Na2O	0.35	0.27	0.25	0.26	2.12	0.35	0.31	0.3	3.5	0.19	0.21	0.21	0.18	0.16	0.18	0.16	0.17
Cr	0.12	0.21	0.07	0.7	0.03	0.14	0.57	0.15	0.12	0.02	0.01	0.01	0.61	0.59	0.3	0.02	0.4

Table A5.1 Pyroxenes contd.

Sample	CBZ040	CBZ040	CBZ040	CBZ164	CBZ164	CBZ164	CBZ164
Analysis	4R	5C	5R	1C	1C	3C	4C
SiO2	52.18	53.31	53.63	53.78	52.54	53.8	53.07
TiO2	0.39	0.19	0.17	0.22	0.52	0.25	0.38
Al2O3	1.79	2.15	1.66	0.99	1.96	1.21	1.57
FeO	11.01	5.98	7.18	6.13	8.54	6.54	7.31
MnO	0.28	0.19	0.22	0.19	0.22	0.21	0.21
MgO	15.94	17.61	18.83	17.95	15.65	17.22	17.15
CaO	17.6	19.68	17.78	19.13	19.91	19.6	19.09
Na2O	0.19	0.17	0.17	0.34	0.33	0.35	0.35
Cr	0.03	0.81	0.4	0.92	0.12	0.97	0.66

Table A5.2 Amphiboles

Sample	CBZ185	CBZ035	CBZ035	CBZ011B	CBZ011B	CBZ149	CBZ164
Analysis	3	1	2	1	3	1	1
SiO2	52.85	56.74	59.07	54.04	40.82	73.18	41.33
TiO2	0	0.14	0.07	0.15	1.15	0.5	1.24
Al2O3	1.89	2.69	1.29	0.95	8.25	7.2	22.33
FeO	15.69	10.17	10.47	15.21	19.51	4.12	8.87
MnO	0.24	0.25	0.29	0.23	0.35	0.1	0.11
MgO	13.24	14.54	15.57	14.44	12.34	3.67	0.94
CaO	12.67	12.47	12.76	12.82	12.27	6.86	22.28
Na2O	0.27	0.21	0.1	0.15	0.27	2.71	0.08
K2O	0.04	0.05	0.03	0.06	0.1	0.01	0

Table A5.3 Chlorites

Sample	CBZ005	CBZ005	CBZ185	CBZ185	CBZ035	CBZ035	CBZ011B	CBZ011B	CBZ011B	CBZ204	CBZ204	CBZ149	CBZ040	CBZ164
Analysis	1	2	1	2	1	2	1	2	3	1	2	1	1	1
SiO2	25.98	25.8	25.57	24.39	31.26	30.28	26.58	28.3	31.55	25.51	22.82	24.15	26.88	27.03
TiO2	0	0	0	0	0.05	0	0	1.76	1.05	0.04	0.2	0.03	0.01	0
Al2O3	19.22	20.2	19.37	19.61	16.85	17.91	19.32	17.07	18.64	19.8	19.85	19.43	19.37	17.76
FeO	22.69	22.53	28.29	28	19.47	20.32	27.16	24.94	22.26	32.62	33.75	24.77	23.33	27.36
MnO	0.33	0.31	0.35	0.37	0.43	0.45	0.36	0.34	0.29	0.33	0.36	0.41	0.27	0.4
MgO	17.54	17.55	13.03	12.76	17.93	17.94	14.24	13.44	11.97	7.85	7.99	14.53	17.02	14.44
CaO	0.03	0.02	0.08	0.06	2.4	1.67	0.23	2.06	0.95	0.1	0.12	0.16	0.08	0.07
Na2O	0.02	0.02	0.01	0.02	0.01	0.02	0.04	0.04	1.44	0.06	0.03	0.03	0.04	0
K2O	0	0	0	0	0.02	0	0.06	0.09	0.21	0.48	0.06	0.01	0	0

Table A5.4 Epidote and Clinozoisite

Sample	CBZ005	CBZ005	CBZ185	CBZ185	CBZ035	CBZ035	CBZ011B	CBZ011B	CBZ011B	CBZ040	CBZ040	CBZ164
Analysis	1	2	1	2	1	2	1	2	3	1	2	1
SiO2	37.4	37.4	52.49	37.39	38.67	37.22	37.83	39.26	39.94	38.51	39.3	38.56
TiO2	0.04	0.05	0.02	0.01	0.06	0.05	0.8	1.52	0.48	0.1	0.04	0.11
Al2O3	22.97	25.5	1.55	22.41	28.64	27.77	23.33	21.58	22.26	28.3	28.75	26.43
FeO	13.28	8.54	22.31	13.3	6.47	8.83	12.02	11.66	11.85	6.75	6.69	9.94
MnO	0.13	0.1	0.24	0.21	0.05	0.12	0.1	0.07	0.04	0.06	0.04	0.07
MgO	0.05	1.18	10.26	0.02	0.13	1.73	0.02	0.04	0.04	0.03	0.03	0.11
CaO	23.3	22.54	12.32	23.08	24.14	21.87	22.69	22.11	20.68	23.79	23.87	23.27
Na2O	0.04	0.03	0.18	0	0.01	0.01	0.06	0.28	0.55	0.02	0.03	0.01
K2O	97.21	95.34	99.37	96.42	98.17	97.6	96.85	96.52	95.84	97.56	98.75	98.5

Table A5.5 Plagioclase

Sample	CBZ005	CBZ005	CBZ005	CBZ005	CBZ035
Analysis	1	2	3	4	1
SiO2	52.72	51.85	53.52	53.01	78
TiO2	0.04	0.03	0.06	0.05	0
Al2O3	28.56	27.79	27.74	28.19	9.79
FeO	1.19	1.75	1.31	1.13	2.17
MnO	0.16	0.88	0.25	0.16	0.2
MgO	13.12	13.59	11.24	12.59	8.94
CaO	4.14	3.84	4.8	4.39	0.01
Na2O	0.03	0.03	0.6	0.05	0
K2O	99.96	99.76	99.52	99.57	99.11